BIOPHYSICAL AND BIOCHEMICAL EFFECTS AND DISTRIBUTION OF FATTY ACIDS IN PANCREATIC BETA CELLS AND MICROVASCULAR ENDOTHELIAL CELLS

ANAIS MARGUERITE SOPHIE KAHVE

DOCTOR OF PHILOSOPHY

MEDICAL STUDIES

SEPTEMBER 2018

BIOPHYSICAL AND BIOCHEMICAL EFFECTS AND DISTRIBUTION OF FATTY ACIDS IN PANCREATIC BETA CELLS AND MICROVASCULAR ENDOTHELIAL CELLS

Submitted by Anais Marguerite Sophie Kahve, to the University of Exeter for the degree of Doctor of Philosophy in Medical Studies, September 2018.

This thesis is available for Library use on the understanding that it is copyright material and that no quotation from this thesis may be published without proper acknowledgement.

I certify that all material in this thesis which is not my own work has been identified and that no material has previously been submitted and approved for the award of a degree by this or any other University.

………………...

Acknowledgements

Abstract

The incidences of obesity and type 2 diabetes and their complications are increasing globally. The presence of elevated circulating free fatty acids has been associated with the initial dysfunction of pancreatic beta cells and microvascular endothelial cells followed later by their demise. The aim of this thesis was to investigate the mechanisms by which demise occurs, and how it may be prevented.

Palmitate, a saturated fatty acid, caused cell death in both INS-1 beta cells and HCMec/D3 microvascular cells, whereas the unsaturated fatty acid oleic acid did not cause cell death, and also protected against palmitate-induced toxicity. Etomoxir, the mitochondrial CPT1 inhibitor did not rescue INS-1 or HCMec/D3 cells from palmitate-induced toxicity suggesting that palmitate-induced toxicity does not occur via entry into the mitochondria. Cells were exposed to 2-bromopalmitate, a non-metabolisable fatty acid used to reduce the pool of cytoplasmic CoA, to determine whether palmitate-induced toxicity might be mediated by its ability to be activated. Pre-incubation with 2-bromopalmitate in INS-1 cells significantly prevented palmitate-induced cell death. These data suggest that the activation of palmitate with CoA might mediate cell death.

Cell cycle analysis found that neither oleic acid nor palmitate caused an increase or decrease in cell proliferation in both INS-1 and HCMec/D3 cells. The data suggest that the mechanism of oleic acid-induced cytoprotection might not be via a pro-proliferative mechanism.

INS-1 cells were imaged using spontaneous Raman microspectroscopy after 24-hour exposure to esterified and non-esterified fatty acids. Uni- and multi-variate analysis and spectral decomposition were carried out using a methodology optimised and validated which is presented in this thesis. The aim

was to quantify changes, if any, in lipid disposition: distribution, intensity (as a measure of concentration) and composition after exogenous exposure to these fatty acids. Exposure to 0.125 mM palmitate showed a significant decrease in the percentage of lipid within the cells and a corresponding increase in the intensity of this lipid. This suggests that palmitate, alone, might be shuttled into lipid droplets. This was not observed when the cells were exposed to oleic acid, whereby an increase in the intensity of lipid was observed even though no significant change was observed in the percentage of lipid within the cells. When palmitate and oleic acid were combined, the composition of the lipid droplets changed such that the levels of palmitate decreased and the levels of oleic acid increased. These data suggest that oleic acid does not shuttle palmitate into lipid droplets. These data do not support the hypothesis that oleic acid protects against palmitate-induced cytotoxicity by shuttling palmitate into lipid droplets.

The methyl esters of palmitate and oleic acid were employed to determine whether they would affect lipid disposition. No change in lipid distribution or intensity was observed when the cells were exposed to these fatty acids, validating the requirement for the free carboxyl oxygen for the covalent binding to glycerol for the formation of lipid droplets. These data also suggest that INS-1 cells cannot de-esterify esterified fatty acids.

Table of contents

8

List of figures

Chapter 4.   Evaluation of the effects of fatty acids on the cell cycle

List of equations

List of tables

Abbreviations

2-BrPA	2-bromopalmitic acid
2-BrPA-CoA	2-bromopalmitoyl-CoA
ACS	Acetyl-CoA synthetase
AUC	Area under the curve
BODIPY-PA	BODIPY-palmitic acid
BSA	Bovine serum albumin
CARS	Coherent anti-Stokes Raman scattering microscopy
CCD	Charge-coupled device
CHO	Chinese hamster ovary
CMC	Complete medium control
CoA/ HS-CoA	Coenzyme A
CPT1	Carnitine palmitoyltransferase I
Cyt C	Cytochrome C
ddH$_2$O	Double distilled H$_2$O
Et-CoA	Etomoxyl-CoA
EtOH	Ethanol
FA	Fatty acid
FACS	Fluorescence activated cell sorting
FAO	Fatty acid oxidation
FBS	Fetal bovine serum
FSC-A	Forward scatter
HAEC	Human aortic endothelial cell
HCAEC	Human coronary artery endothelial cell
HUVEC	Human umbilical vein endothelial cell

HVSMC	Human vascular smooth muscle cell
IMM	Inner mitochondrial membrane
LCFA	Long-chain fatty acid
MeOA	Methyl oleate *or* oleate methyl ester
MePA	Methyl palmitate *or* palmitate methyl ester
NLD	Neutral lipid droplet
OA	Oleic acid
OMM	Outer mitochondrial membrane
PA	Sodium palmitate
PA-CoA	Palmitoyl-CoA
PFA	Paraformaldehyde
PBS	Phosphate buffered saline
PI	Propidium iodide
QC	Quality control
RA	Ricinoleic acid
REDOX	Reduction-oxidation
SEM	Standard error of the mean
SFA	Saturated fatty acid
SSC-A	Side scatter
T2D	Type 2 diabetes
TAG	Triacylglycerol
UFA	Unsaturated fatty acid
VC	Vehicle control

Chapter 1

Introduction

1 Introduction

This thesis is concerned with the mechanisms of fatty acid (FA) interactions within cells that may be relevant to the development of type 2 diabetes (T2D) and any associated complications. The precise causes of T2D and its complications are not known, however the presence of elevated levels of free FAs and glucose in the circulation, coupled with insulin resistance, are implicated in the death and dysfunction of both beta cells and endothelial cells.

In this Chapter I shall review some of the literature regarding the mechanisms of saturated fatty acid (SFA)-induced cytotoxicity (cell death) and the mechanisms of unsaturated fatty acid (UFA)-induced cytoprotection (when coupled with SFAs) in various cell types *in vitro* and *in vivo.* It should be noted that research on the dysfunction of beta cells, i.e. the inability for beta cells to synthesise and secrete insulin, will not be presented in this thesis. Further, the justifications for the work undertaken for this thesis will be explained throughout this Chapter and additionally at the end of this Chapter.

Each research-chapter begins with a detailed introductory section outlining the literature for that specific area of research. Rather than including this material in Chapter 1, I decided to describe the relevant literature for each area of research within its corresponding Chapter. I anticipate this approach to be of benefit as it contextualises the results and discussion sections of those Chapters, thus aiding the flow of arguments.

1.1 Diabetes Mellitus

Beta cells are one of the three principal types of endocrine cells present in the islets of Langerhans in the pancreas. Beta cells synthesise and secrete the hormone insulin which is one of the hormones responsible for regulating blood glucose levels. T2D is a metabolic syndrome characterised by beta-cell death

and dysfunction and impaired glucose-stimulated insulin secretion (Reaven 1988; Morgan 2009; Cerf 2013). In addition, peripheral cells can become insulin resistant, reducing their ability to take up glucose for normal cellular function. The relationship is complex between glucose and insulin, beta cell dysfunction and death and insulin resistance. Obesity is a risk factor for T2D as the exposure to certain SFAs can induce beta cell death and dysfunction (Cerf 2013). The onset of beta cell death is also associated with elevated levels of circulating glucose. In this instance, beta cells become exhausted from the continuous synthesis and secretion of insulin, resulting in them losing functionality which leads to beta cell death (Cerf 2013). In addition, glucose recipient organs become desensitised to the elevated circulating glucose which increases insulin demand. This demand for insulin also leads to the hyperfunction and subsequent exhaustion of beta cells which leads to further loss of beta cell function and beta cell death (Cerf 2013). It is clear that exposing beta cells and peripheral cells to chronic levels of glucose and SFAs can have detrimental effects, effects which are linked to one another and perpetuated by one another. In addition to the loss of viability of beta cells implicated in T2D, complications from diabetes can arise such as retinopathy, nephropathy and neuropathy (Horani & Mooradian 2003; Prasad *et. al.* 2014). These secondary complications are probably caused by altered functional properties of microvascular endothelial cells. These cells line micro-vessels and therefore come into contact with hormones, metabolites, cytokines and fatty acids present in the blood.

The prevalence of T2D currently accounts for approximately 90 % of all diagnosed cases of diabetes in the UK which equates to about 3.3 million people (Diabetes UK: facts and figures 2018). The cost of diabetes to the UK is estimated to have been £23.7bn in 2010/11 (Hex *et al.* 2012), similar to the cost of cancer

(Featherstone & Whitham 2010), and is expected to rise to £39.8bn in 2035/36 as a result of the expected, increasing prevalence of T2D (Hex *et al.* 2012). It is clear that the study of both beta and endothelial cells is of great importance. Understanding the mechanisms by which these detrimental effects occur to beta and endothelial cells can enable researchers to determine how to reverse or prevent these effects, which in turn may lead to improved patient care, thus relieving the burden of this disease.

1.2 Fatty acids and diabetes

The consumption of certain FAs, most notably SFAs, have been found to be implicated in the dysfunction and death of beta cells. However, it must be clarified that not all SFAs cause detrimental effects to these cells *in vitro* (Harvey *et al.* 2009; Welters *et al.* 2004) or *in vivo* (Legrand & Rioux 2015) (and will be further described in Chapter 3). Therefore, it cannot be said that all SFAs are detrimental to human health or that some FAs should be avoided in the diet. However, since detrimental effects have been observed *in vitro* with some SFAs, such as PA, at chronic, elevated concentrations, these observations warrant further investigation. By contrast, UFAs, have been shown to be non-toxic at chronic, elevated concentrations, and have also shown to be cytoprotective against the cytotoxic effects of some FAs. How these two classes of chemically similar compounds can exert such profoundly different effects in biological systems is astounding and has led many researchers to investigate these differences. The following sections will outline the chemical differences between these two classes of compounds and will be begin to describe the differential effects observed *in vitro* and *in vivo*.

1.3 Fatty acid biochemistry

FAs are organic compounds that consist of a hydrocarbon (alkyl) chain with a carboxylic acid functional group at one end. FAs are classified depending on the number of carbon atoms in the alkyl chain, whereby short-chain FAs consist of ≥ 6 carbon atoms (Schönfeld & Wojtczak 2016), medium-chain FAs consist of between 7 and 13 carbon atoms (Schönfeld & Wojtczak 2016), long-chain FAs consist of between 14 and 20 carbon atoms (Harvey *et al* 2009), and very long-chain FAs consist of ≥ 21 carbon atoms (Sassa & Kihara 2014).

An UFA is one that contains at least one carbon-carbon double bond, whereby the double bond is oriented in one of two possible conformations (1) *cis*, whereby the alkyl chains on either side of the double bond are orientated such that they are on the same side. This orientation is written in shorthand as *Z* isomerisation, or (2) *trans* whereby the alkyl chains on either side of the double bond are orientated such that that they either are on either side of the double bond. This orientation is written in shorthand as *E* isomerisation. The free rotation about a carbon-carbon double bond is zero because of the π-orbitals which overlap. Single bonds consist of σ-orbitals which have a degree of free-rotation, unlike double bonds which have none. SFAs, however, do not contain any double bonds and therefore have greater degrees of rotation than their unsaturated counterparts. In addition, the orientation of the double bond determines the space which all other bonds within the molecules can occupy.

The diet is the only exogenous source of FAs. Lipids, such as triacylglycerol (TAG)/ neutral lipid droplets (NLDs), are degraded in the small intestine by lipases, secreted from the exocrine tissue of the pancreas, into their constituent FAs (Wang *et al.* 2013). In the circulation, some FAs bind to serum albumin, some remain unbound (and are therefore termed 'free') and some are re-esterified to form TAG contained in very low density lipoproteins and chylomicrons (Balaban

et al. 2014). FAs must be in their 'free' form to enter cells. This occurs via the dissociation of FA from albumin or via the hydrolysis of chylomicrons via lipoprotein lipases (Goodman 1958). Since minute concentrations of free FAs exist in the circulation (between nM and μM) (Paris *et al*. 1978), the dissociation of FAs from FA-albumin follows Le Chatelier's principle, whereby the equilibrium shifts to counter the decrease in [FA-albumin].

Long-chain FAs (LCFAs) are degraded (catabolised), via mitochondrial beta-oxidation for the production of ATP. The entry of LCFAs into mitochondria occurs via a series of reduction-oxidation (REDOX)-coupled reactions. Firstly, LCFAs must be activated in the cytoplasm by forming a thioester with Co-enzyme A (CoA/ HS-CoA), via the enzyme acetyl-CoA synthetase (ACS), forming FA-CoA (Voet *et al*. 2000). FA-CoA then reacts with carnitine in the presence of the enzyme carnitine palmitoyltransferase I (CPT1). CPT1 resides in the outer mitochondrial membrane (OMM) and catalyses this reaction to produce FA-carnitine (Voet *et al*. 2000). FA-carnitine subsequently enters the intermembrane space of the mitochondria from where a series of steps transports the FA-carnitine complex into the inner mitochondrial membrane (IMM), generates FA-CoA and then releases the original FA. The enzymes involved in this process are essential for the influx and degradation of LCFAs in the mitochondria. Once inside the matrix of the mitochondria, FAs are beta-oxidised. Unlike LCFAs, short- and medium-chain FAs can pass through the mitochondrial membrane via passive diffusion, while very long-chain and branched chain FAs are initially degraded in the peroxisomes via alpha- and beta-oxidation prior to entry into the mitochondria (Waterham *et al*. 2016).

1.4 Cellular effects of long-chain saturated and unsaturated fatty acids

All mammalian cells require the uptake of FAs to maintain physiological health. For example, FAs are essential for the maintenance of plasma membrane integrity (Ibarguren, López & Escribá 2014), intracellular signalling and as an energy source when glucose levels are insufficient. Palmitate (PA), a long-chain SFA (C16:0), and oleic acid (OA), a long-chain *cis* (Z) mono-UFA (C18:1), are the predominant FAs present in serum of both non-obese (Yli-Jama 2002) and obese individuals (Ubhayasekera *et al*. 2013). At low concentrations (nM range), PA has acutely beneficial effects within cells. The fates of PA include: (1) degradation for energy production via mitochondrial fatty acid oxidation (FAO), (2) protein S-palmitoylation on the cytoplasmic face of the Golgi apparatus, (Aicart-Ramos *et al*. 2011), (3) incorporation into phospholipids and other lipid species for maintaining plasma- and organelle-membrane stability (Ibarguren, López & Escribá 2014), and (4) conversion to palmitoleic acid (16:1) via Δ-9-desaturase enzymes in the endoplasmic reticulum (Eynard 1997).

Chronic, elevated levels of some FAs, such as PA, have been shown to induce cell death *in vitro*. As stated by Paracelsus (1493 – 1541) "the dose makes the poison" (Gilbert 2012, p. 42). However, the mechanism by which cytotoxicity is induced is unclear. 'Lipotoxicity' refers to the phenomenon of increased cell death caused by the presence of certain FAs. The process of cell death may be via apoptosis or necrosis. Programmed cell death includes apoptosis, autophagy and necroptosis, and is triggered either through intracellular or extracellular signals (Voet *et al*. 2000). For example, the induction of the intrinsic pathway, induced by some chemical compounds, results in the disruption of the mitochondrial membrane potential and the release of cytochrome C (Cyt C) from the IMM. This then activates a downstream signalling cascade of caspase

enzymes, the result of which is cell death (Voet *et al.* 2000). By contrast, many mono-UFAs have been shown to be non-toxic to cells *in vitro* at chronic, elevated concentrations. Further, OA, and other UFA species such as palmitoleic acid, have been shown to exhibit cytoprotective effects when added exogenously to cells *in vitro*, in combination with PA (Çimen *et al.* 2016; Diakogiannaki *et al.* 2007; Maedler *et al.* 2001; Morgan *et al.* 2008; Sargsyan *et al.* 2016). However, the mechanism of cytoprotection has been debated. The following sections provide a more detailed insight into the cellular effects induced by both long-chain SFAs and long-chain UFAs.

1.4.1 Enzyme release, activation and regulation

Many studies have shown that the caspase cascade is induced by SFAs, clearly showing that the mitochondrion is implicated in cell death (Hardy *et al.* 2003; Johnson *et al.* 2012). However, evidence suggests that the mitochondrion may not be the principal driver of cell death and that the induction of cell death may be as a result of a caspase-independent process (Mishra & Simonson 2005; Patková *et al.* 2014; Ulloth *et al.* 2003). For example, this has been implied by Patková *et al.* (2014) who exposed myoblasts and myotubes to PA co-incubated with specific mitochondrial antioxidants. They measured cell viability, mitochondrial DNA damage and reactive oxygen species levels. Although they found that the antioxidants prevented both mitochondrial DNA damage and the rise of reactive oxygen species levels, there was no improvement in viability compared to PA on its own.

The study of the mitochondrion in beta cells and its possible role in mediating FA-induced cell death has attracted much attention over the years. This is particularly true for the study of diabetes due to the close interplay between FA metabolism and glucose metabolism. Malonyl-CoA is a substrate of

FA synthesis, produced via the metabolism of glucose, and acts as an inhibitor of FAO by inhibiting CPT1 (Wakil & Abu-Elheiga 2009). This enables the cell to signal to itself to stop breaking down FAs so that the cell can continue to synthesise FAs, otherwise there would be no net change in the concentration of FAs in the cell – a futile use of energy. Inhibiting CPT1, via the use of a chemical inhibitor for example, and thus inhibiting mitochondrial FA transport, results in increased glucose metabolism. This ensures the cell is still able to generate energy to continue its cellular processes. The reverse is also true, whereby an increase in FAO results in a decrease in glucose metabolism. This interplay between FAs and glucose is important because some FAs are essential for glucose-stimulated insulin secretion (Nolan *et al.* 2006). This coaction is presented schematically in figure 1.1.
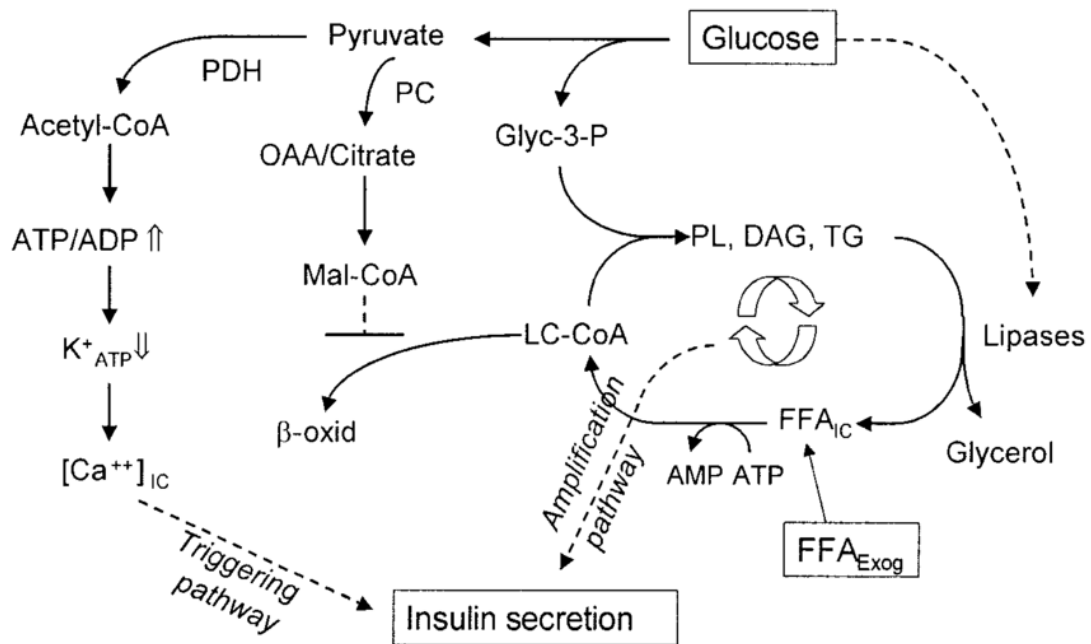
Figure 1.1 Interplay between fatty acid oxidation and glucose metabolism

The diagram shows the complex interplay between fatty acid oxidation and glucose metabolism. The breakdown of glucose produces the substrate malonyl-CoA which inhibits beta-oxidation of fatty acids (image taken directly from Nolan *et al*. 2006, Interactions between glucose and fatty acid metabolism in nutrient-secretion coupling, figure 1).

As previously stated, PA can be converted to palmitoleic acid via Δ-9-desaturase enzymes in the Golgi apparatus of beta cells (Eynard 1997), however, at elevated concentrations of PA, these enzymes become saturated. Busch *et al.* (2005) upregulated Δ-9-desaturases in MIN6 beta cells and found this to protect against PA-induced toxicity. Although this work suggests that these enzymes may become saturated and may induce cytotoxicity, the mechanism of PA-induced toxicity remains unclear.

Studies have shown that elevated levels of PA disrupt endoplasmic reticulum function, induce the unfolded protein response (a response driven by the accumulation of misfolded or unfolded proteins in the lumen of the endoplasmic reticulum) and induces cell death in INS-1 and primary beta cells (Cunha *et al.* 2008; Volmer & Ron 2015). By contrast, it has been shown that OA activates the pro-survival pathways of the endoplasmic reticulum stress response when in combination with PA (Diakogiannaki *et al.* 2008; Sargsyan *et al.* 2016).

It is clear from the literature described above that SFAs have been shown to induce multiple negative effects on organelles within different cell types. It has been argued that certain pharmacological compounds can target organelles, such as the mitochondria, and can improve the viability of cells *in vitro*. I decided to further investigate these claims to: (1) understand how these agents exert their effects on cells, and (2) better understand the structural requirements for PA-induced toxicity via the mitochondria. A review of the literature and also research I have conducted is presented in Chapter 3.

1.4.2 Cell cycle progression

A eukaryotic organism's or organ's ability to duplicate its cells accurately is an essential function. This enables it to continue to grow and function. Upon cell division, the cell grows, and its DNA, protein and organelle content doubles.

The cell then goes through a series of steps to ensure the process of cell division does not incur mistakes, and where it can it eliminates those mistakes. This process of cell division in eukaryotic cells is shown in figure 1.2 and is further explained in Chapter 4.
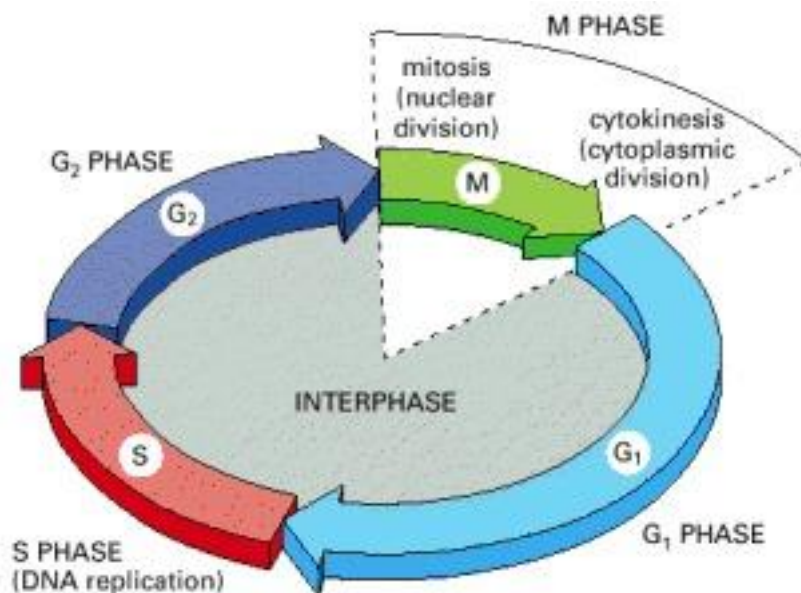
Figure 1.2 Cell cycle progression

The diagram shows the various stages of the cell cycle: G0+G1, S, G2 and M. The phases between G0+G1 and G2 are known as interphase. During this time, the cell prepares itself for cell division, including duplicating the DNA, protein and organelle content with the cell. The M phase is where mitosis (nuclear division) occurs and is when the cell divides into two identical daughter cells (image taken directly from Alberts *et al*. 2002, An overview of the cell cycle, figure 17.3).

As previously discussed, FAs play important roles in maintaining cell health and can have various effects on cellular processes. Therefore, studying the effects of FAs on the cell cycle, a fundamental cellular process, would only seem fitting. Furthermore, the effects on the cell cycle could help elucidate whether these effects are related to the mechanisms by which some FAs may cause harm and others may not.

Upon reading the literature regarding the effects which FAs have on cell cycle progression, it was clear that many contradictions were apparent. Studies *in vitro* have shown that some physiological molecules, such as incretins (Friedrichsen *et al.* 2006), can stimulate beta cell proliferation. LCFAs have also been found to affect cell proliferation, but in the reverse direction; thus, SFAs cause cell death and this may be mediated, in part, by inhibition of DNA replication or cell cycle progression (Artwohl *et al.* 2003; Ben-Harosh *et al.* 2017; Diakogiannaki *et al.* 2007; Lamers *et al.* 2011; Pascoe *et al.* 2012). The effects of UFAs may be different since OA can be pro-proliferative in human vascular smooth muscle cells (HVSMCs) (Lamers *et al.* 2011), BRIN-BD11 rat beta cells (Diakogiannaki *et al.* 2007) and rat islets (Brelje *et al.* 2017). However, this is contentious as others have shown no significant difference between OA-treated and untreated cells in human umbilical vein endothelial cells (HUVECs) (Artwohl *et al.* 2003), murine islets (Pascoe *et al.* 2012) and pancreatic stellate cells (Ben-Harosh *et al.* 2017).

I therefore decided to further investigate the contentious issue of whether PA affects cell cycle progression *in vitro*. I also decided to investigate the effects of OA, alone and in combination with PA, to determine whether the mechanism of OA-induced cytoprotection might be induced via a pro-proliferative mechanism.

I further address these contradictions in Chapter 4 by critically reviewing the literature with a focus on beta and endothelial cells.

1.4.3 Lipid composition

FAs are incorporated into phospholipids – these are lipid structures, composed of SFAs and UFAs, which are essential for the synthesis of the plasma and organelle membranes of cells. Membranes are composed of different types of phospholipids depending on their function, e.g. some membranes may need to be more permeable or flexible than others. Since the functionality of biological membranes is dependent upon its composition, it can be said that phospholipids and the FAs they are composed of are considerably important for maintaining cellular health.

The 'Membrane Theory of Diabetes', by Pilon (2016), hypothesises that changes in phospholipid composition and thus membrane structure, due to excess SFAs, alters the function of the beta cell. Pilon (2016) suggests that SFAs reduce the degree of membrane curvature and subsequently decrease membrane permeability due to their close packing in space. In addition, studies in human erythrocytes suggest that the phospholipids in the outer membrane of the plasma membrane are more saturated than the inner membrane, making the outer membrane less fluid and less permeable than the inner membrane (Emmelot & Van Hoeven 1974). It could, therefore, be hypothesised that the rigidification of the outer membrane of the plasma membrane of beta cells, via the incorporation of SFAs, could impair insulin signalling and glucose uptake (Pilon 2016). By contrast, unsaturated *cis* FAs, such as OA, increase the degree of membrane curvature and increase membrane permeability (Rawicz *et al*. 2000). Thus, it is important to be exposed to healthy levels of FA to maintain the appropriate composition of biological membranes to maintain cell health.

Cyt C is normally bound to the IMM via cardiolipin, a phospholipid embedded within the IMM containing four (predominantly unsaturated) FA chains (Paradies *et al.* 2014). It has been suggested that the incorporation of SFAs within cardiolipin, or other phospholipids within the membrane may facilitate the partial unfolding and release of Cyt C from the IMM, resulting in the induction of the caspase cascade (Paradies *et al.* 2014).

Sphingolipids are a class of lipid which comprise a sphingosine and FA moiety. Other components can be incorporated onto sphingolipids such as phosphocholine (an intermediary product in the formation of phosphatidylcholine) and sugar residues. Ceramide is a sphingolipid which contains a single sphingosine molecule and a FA, e.g. PA (Galadari *et al.* 2013). Sphingolipids are important components of membranes and influence their stability. However, they can also play a role in signalling (Bartke & Hannun 2009), cellular differentiation and proliferation (Ohanian & Ohanian 2001). The presence of ceramide is clearly vital for maintaining normal physiological health, however, elevated levels of ceramide can have detrimental cellular consequences. The mechanism remains unclear. The study by Robblee *et al.* (2016) has shown that elevated levels of ceramide can cause endoplasmic reticulum stress, activate the unfolded protein response and mediate apoptosis in macrophage cells. Similarly, Gjoni *et al.* (2014) hypothesise that PA-induced toxicity in INS-1 cells is mediated via the accumulation of ceramide and the dysregulation of ceramide metabolism in the endoplasmic reticulum. Further, the study by Guo *et al.* (2009) shows that elevated levels of ceramide induce INS-1-cell apoptosis via the extrinsic death receptor, the intrinsic mitochondrial pathways and the intrinsic endoplasmic reticulum pathway. Guo *et al.* (2009) went further and showed that inhibiting ceramide metabolism rescued cells from PA-induced toxicity in INS-1 cells,

showing the important role that ceramide synthesis plays in the mediation of beta-cell toxicity. Since PA is required for the synthesis of ceramide, it has been hypothesised that exposure of cells to elevated FA levels mediates beta-cell toxicity through the increased production of ceramide. The mechanism of ceramide-induced toxicity has been further explored. Studies have shown that pro-inflammatory cytokines, such as interleukin-1β and interferon-γ, may mediate beta-cell toxicity as a consequence of the formation of ceramide, however, differential responses have been observed between different beta-cell lines (Galadari *et al.* 2013). It has also been hypothesised that ceramide-enriched membrane microdomains alter the spatial distribution of plasma membrane-bound proteins, and that these microdomains may rigidify the plasma membrane. It has also been suggested that enhanced clustering of certain proteins, such as receptors, in the plasma membrane, could promote beta-cell apoptosis, however, the full role that receptor clustering plays in diabetes is not clear (Galadari *et al.* 2013).

By contrast, the study by Listenberger *et al.* (2001) has suggested that FA-induced apoptosis can also be mediated through a ceramide-independent mechanism. The study employed the use of Chinese hamster ovary (CHO) cells (a cell line widely used in cell biology as it can be readily genetically manipulated to study differential effects in disease states) showed that PA-mediated apoptosis was not prevented when *de novo* ceramide synthesis was prevented (Listenberger *et al.* 2001). These data suggest that there are either species- or cell-specific mechanisms of PA-induced toxicity, or that there are varying effects of ceramide formation in cells.

Interestingly, Listenberger *et al.* (2003) has proposed that when CHO cells are exposed to PA and OA in combination, OA enables the storage of PA in the

form of TAG/ NLDs within these cells, therefore preventing PA from exerting its detrimental effects on the cell. Whether this is the case in other cell types has prompted other researchers to investigate this effect and the mechanism by which this occurs in more detail. This effect inspired me to investigate this hypothesis further in beta cells. Research presented in Chapter 5 describes a methodology using spontaneous Raman microspectroscopy, a label-less technique, to quantify the distribution and composition of lipid within beta cells treated with PA and OA alone and in combination, the results of which are presented in Chapter 6.

In conclusion, not all long-chain SFA are toxic to cells *in vitro*. However, PA, the most abundant SFA in the diet is toxic to many cell types during chronic, elevated concentrations (µM range) *in vitro*, including beta cells (Dhayal *et al.* 2008; Maedler *et al.* 2001), vascular endothelial cells (Artwohl *et al.* 2003; Harvey *et al.* 2009), osteoblasts (Gunaratnam *et al.* 2013) and smooth muscle cells (Rho *et al.* 2007). Many effects have been measured upon SFA exposure, such as cell viability, changes in cytoplasmic caspase levels, reactive oxygen species production (Gehrmann *et al.* 2015; Newsholme *et al.* 2007) and endoplasmic reticulum stress (Cazanave *et al.* 2010). These data suggest that the mechanism of toxicity may not be limited to the demise of one organelle, indicating that the mechanism of action may be extremely complex. By contrast, mono-UFAs, such as OA, has been shown to not only be non-toxic to cells at chronic levels *in vitro*, but it has also been shown to prevent the toxic effects induced by some SFAs, when combined, most notably with PA (Çimen *et al.* 2016; Diakogiannaki *et al.* 2007; Maedler *et al.* 2001; Morgan *et al.* 2008; Sargsyan *et al.* 2016).

1.5 Synopsis of the work presented in this thesis

The research presented in this thesis focuses on the following three areas: (1) the structural requirements for FA-mediated effects on beta cell and microvascular endothelial cell viability, and the requirement for SFAs to enter mitochondria to mediate cytotoxicity, (2) the effects of SFAs and UFAs on beta cell and microvascular endothelial cell cycle progression, and (3) the changes in lipid disposition (distribution, intensity and composition) of beta cells exposed to exogenously supplied SFAs and UFAs. A methodology was developed to study these cellular changes using spontaneous Raman microspectroscopy. The robustness of this method was validated using the equivalent esterified FAs to the parent FAs. Finally, the results of these experiments are presented, the technical limitations are discussed, and further work is described.

Chapter 2

Routine materials and methods

2 Routine materials and methods

2.1 Cell culture

All cell culture procedures were carried out in a Class 2 microbiological safety cabinet. All cells were grown in an incubator with 95 % air and 5 % CO_2 in a humidified atmosphere at 37 °C. Aseptic technique was followed whereby all instruments and reagents were autoclaved prior to use and all relevant materials were disinfected thoroughly with 70 % (v/v) EtOH (Fisher Chemical).

2.1.1 Rat-derived beta-cell line

The INS-1 beta-cell line was derived from a rat insulinoma by methods reported by Asfari *et al.* (1992). The approximate doubling time of the INS-1 cells was 48 hours in my hands. The INS-1 cells were cultured in RPMI-1640 medium containing 11 mM glucose, supplemented with 10 % (v/v) fetal bovine serum (FBS) (Sigma), 2 mM L-glutamine (Gibco), 100 U/ ml penicillin (Gibco), 100 µg/ ml streptomycin (Gibco) and 50 µM β-mercaptoethanol (Fisher Chemical). Culture medium containing the above components will be known herein as 'beta cell complete medium'. Any deviations from the composition of this medium will be made explicit.

2.1.1.1 Culture of cryopreserved beta cells

Prior to the thawing of beta cells, beta cell complete medium was pre-warmed to 37 °C. Cells were defrosted by incubating at 37 °C in a water bath for 1 – 2 minutes. Once the cells were defrosted, 10 ml beta cell complete medium pre-warmed to 37 °C was added to the flask. The cells from the cryogenic vial were added to a T75 flask (Sarstedt, 75 cm^2). The vial was washed thoroughly with beta cell complete medium to ensure all cells were transferred to the flask.

The medium was then removed and replaced with fresh beta cell complete medium every 48 hours.

2.1.1.2 Sub-culture of proliferating beta cells

The cells were sub-cultured when they had reached 80 – 90 % confluency. The medium was removed and discarded. The cells were dissociated from the T75 flask by incubating with 2 ml trypsin-EDTA solution (0.05 % (w/v) trypsin, 0.53 mM EDTA•4Na) (ThermoFischer Scientific) pre-warmed for 3 minutes at 37 °C. 10 ml beta cell complete medium pre-warmed to 37 °C was then added to the flask to neutralise the trypsin. The cell-solution was then transferred to a 50 ml centrifuge tube (Sarstedt). The dissociated cells were pelleted by centrifugation at 188 g for 5 minutes. The supernatant was removed and discarded and the pellet was re-suspended in maximum 4 ml beta cell complete medium pre-warmed to 37 °C. 1 ml cell suspension and 10 ml beta cell complete medium was added to a T75 flask. Cells were used up to passage 40.

2.1.1.3 Cryopreserving beta cells

Cells that were not immediately needed for experimentation were cryopreserved. When cells had reached 90 – 100 % confluency, the medium was removed from the flask and discarded. The method for sub-culturing was followed, as described in section 2.1.1.2, however, instead of re-suspending the pellet in beta cell complete medium, the pellet was re-suspended (1:2) in freezing medium DMSO:FBS (16.6 %/ 83.3 %; v/v) (Sigma) pre-warmed to 37 °C. The cells were stored at - 80 °C for 24 hours before being transferred to liquid nitrogen and stored at - 175 °C until required.

2.1.1.4 Seeding of beta cells for fatty acid treatment

Flasks that were fully confluent were sub-cultured into 6-well plates (Sarstedt). The method for sub-culturing was followed, as described in section

2.1.1.2. The cell pellet was re-suspended in 1 ml beta cell complete medium pre-warmed to 37 °C. 20 µl of the cell-suspension was removed and placed in a haemocytometer with a 1 µl counting-chamber (figure 2.1). The cells were counted under a light microscope at a magnification of 100x. The number of live cells was counted in each corner square and averaged.
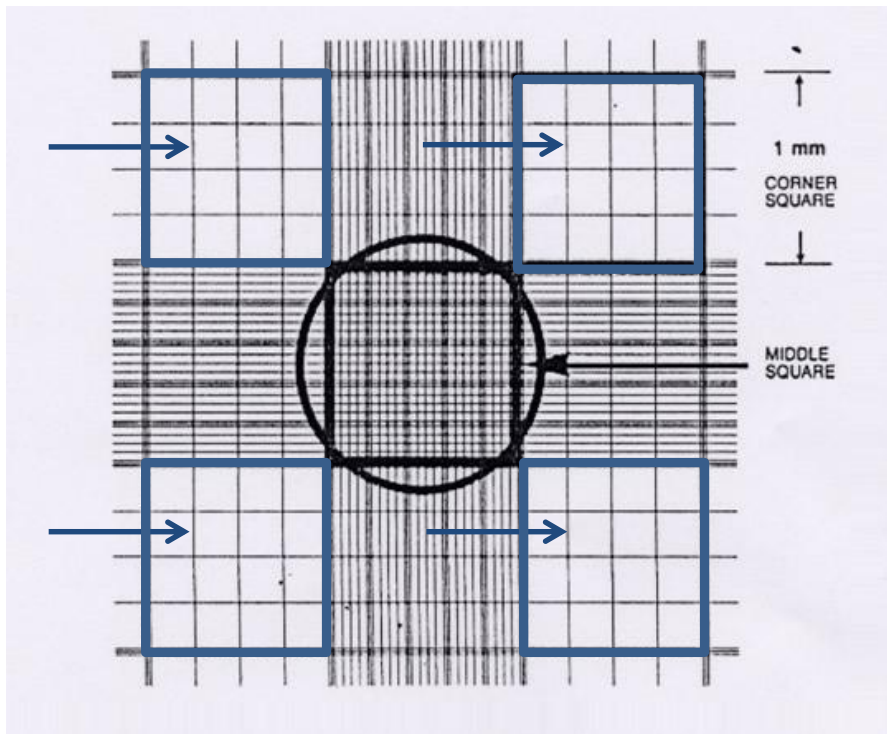
Figure 2.1 Counting of cells on a haemocytometer

Trypan blue (Sigma) made up in phosphate buffered saline (PBS) (Lonza) was used as the vital dye stain because of its ability to cross the plasma membrane and be retained within non-viable cells. A haemocytometer was used to count the number of viable cells to ensure accurate seeding of plates for treatment with fatty acids. Cells in all four chambers (indicated by the dark blue arrows) outlined in blue were counted and averaged. Viable cells appeared yellow in colour, and dead cells appeared dark blue/ black. The number of viable cells represented the number of cells/ μl fluid. Based on the average number of viable cells, the desired number of cells required for seeding could be calculated. This method was also adapted to calculate cell viability and the total average cell number.

For example, an average of 150 viable cells in all four corner-squares of the haemocytometer constitutes 1.5 x10^6 cells/ ml in 10 ml beta cell complete medium. For beta-cell experiments, 0.4 x10^6 cells were added to each well of a 6-well plate, 0.2 x10^6 cells/ well in a 12-well plate, and 0.1 x10^6 cells/ well in a 24-well plate. To obtain the correct seeding density, the cell suspension was diluted. See equation 2.1 and subsequent calculations below.

Equation 2.1 Calculating the correct seeding density for cells for experimentation

$$C1 \; X \; V1 = C2 \; X \; V2$$

Whereby:

C1 = number of viable cells x10^6/ ml;

V1 = initial volume of complete medium added to cells to create cell suspension;

C2 = desired number of cells/ ml in final cell suspension;

V2 = final volume of complete medium added to cells.

Example:

$$V2 = \frac{C1 \; X \; V1}{C2}$$

$$V2 = \left(\frac{1.5 \; x10^6 X \; 10 \; ml \; complete \; media}{0.4 \; x10^6 \; cells/ \; ml} \right)$$

$$V2 = 37.5 \; ml$$

2.1.2 Human-derived endothelial-cell line

The HCMec/D3 microvascular endothelial-cell line was derived from microvessels constituting the human blood brain barrier by methods reported by Weksler *et al.* (2005). The HCMec/D3 cells were cultured in endothelial cell basal

medium MV-2 containing 5.55 mM glucose and 10 mM L-glutamine (PromoCell) supplemented with 5 % (v/v) foetal calf serum (PromoCell), 0.01 mg/ ml gentamicin (Sigma), 1.25 ng/ ml epidermal growth factor (recombinant human), 2.5 ng/ ml basic fibroblast growth factor (recombinant human) (PromoCell), 5 ng/ ml insulin-like growth factor LR3 (PromoCell), 0.125 ng/ ml vascular endothelial growth factor 165 (recombinant human) (PromoCell), 0.25 µg/ ml ascorbic acid (PromoCell) and 0.05 µg/ ml hydrocortisone (PromoCell). Culture medium containing the above components will be known herein as 'endothelial cell complete medium'. Any deviations from the composition of this medium will be made explicit.

2.1.2.1 Culture of cryopreserved endothelial cells

Prior to thawing of endothelial cells, endothelial cell complete medium was pre-warmed to 37 °C and a T75 flask was incubated with 3 ml collagen stock solution (1:29, rat tail collagen (Sigma) in PBS (Lonza, without Ca + Mg, 0.0067 M PO4, sterile filtered) (v/v)). Cells were defrosted by incubating at 37 °C in a water bath for 1 – 2 minutes. Once the cells were defrosted, the collagen solution was removed from the T75 flask and retained for future use. 10 ml endothelial cell complete medium pre-warmed to 37 °C was added to the flask. The cells from the cryogen vial were added to the flask. The vial was washed thoroughly with endothelial cell complete medium to ensure all cells were transferred to the flask. The endothelial cell complete medium was removed and replaced with fresh medium every 48 hours and sub-cultured when they reached 80 – 90 % confluency.

2.1.2.2 Subculture of proliferating endothelial cells

The monolayer was rinsed once with pre-warmed 5 ml PBS (Lonza), then the PBS was removed and discarded. The cells were dissociated from the T75

flask by incubating with 3 ml trypsin-EDTA solution (0.25 % (w/v) trypsin, 0.02 % (w/v) EDTA) (Sigma) for 3 minutes at 37 °C. 10 ml PBS (Lonza) was added to the flask to neutralise the trypsin. The cell-solution was then transferred to a 50 ml centrifuge tube (Sarstedt). The flask was washed twice with 5 ml PBS (Lonza) and the cell-suspension was added to the centrifuge tube. The dissociated cells were pelleted by centrifugation at 423 g for 3 minutes. The supernatant was removed and discarded and the pellet was re-suspended in 30 ml pre-warmed endothelial cell complete medium. 10 ml cell-suspension was added to 3x T75 flasks pre-coated with collagen. Cells were used between passages 31 and 35.

2.1.2.3 Cryopreserving endothelial cells

Cells that were not immediately needed for experimentation were cryopreserved. When cells had reached 90 – 100 % confluency, the medium was removed from the flask and discarded. The method for sub-culturing was followed, as described in section 2.1.2.2, however, instead of re-suspending the pellet in endothelial cell complete medium, the pellet was re-suspended (1:1 or 1:3) in freezing medium DMSO:FBS (5 %/ 95 %; v/v) (Sigma) pre-warmed to 37 °C. The cells were stored at - 80 °C for 24 hours before being transferred to liquid nitrogen and stored at - 175 °C until required.

2.1.2.4 Seeding of endothelial cells for fatty acid treatment

Flasks that were fully confluent were sub-cultured into 6-well plates (Sarstedt). The method for sub-culturing was followed, as described in section 2.1.2.2. The pellet was re-suspended in 1 ml endothelial cell complete medium pre-warmed to 37 °C. 20 µl of the cell-suspension was removed and added to a haemocytometer, as described in section 2.1.1.4. The live cells were counted in each of the four corner squares and averaged. Initial experiments employed a seeding density of 1.0 x10^6 cells/ well in a 6-well plate. However, after 48 hours

of incubation, a high proportion of the cells had died, probably because they had reached confluency. Therefore, it was decided to optimise the seeding density of these cells to allow for the relative comparison of the beta and endothelial cells. Endothelial cells were plated in 6-well plates and exposed to endothelial cell complete medium for 24, 48, 72 and 96 hours. Cell viability and the total average cell number (number of live and dead cells) were examined at varying seeding densities (0.25×10^6, 0.5×10^6 and 0.75×10^6 cells/ ml, corresponding to 25, 50 or 75 cells/ µl). The experimental design is shown in table 2.1, whereby endothelial cell complete medium was added to the cells on Day 0 and was not replaced during the entire duration of the experiment.

Day				
0	1	2	3	4
Growth (hours)				
0	24	48	72	96

Table 2.1 Day versus growth of endothelial cells

The number of days where cells are exposed to endothelial cell complete medium and the corresponding number of hours of growth are shown.

Figure 2.2 shows how percent viability changed over time when endothelial cells were seeded at increasing densities. Percent viability was calculated using vital dye staining whereby the average number of viable and non-viable cells were calculated (section 2.2). It can be seen that a seeding density of 0.75 x10^6 cells/ ml resulted in a consistent loss of viability over time. However, when seeded at 0.25 x10^6 cells/ ml and 0.5x10^6 cells/ ml, the proportions of dead cells were reduced and comparable. Based on these data, it was deemed appropriate to select 0.25 x10^6 cells/ ml as the optimal seeding density for the endothelial cells when these were to be incubated in 6-well plates. This decision was strengthened with the notion that the fewer the number of cells used per treatment per experiment, the more experiments could be conducted.
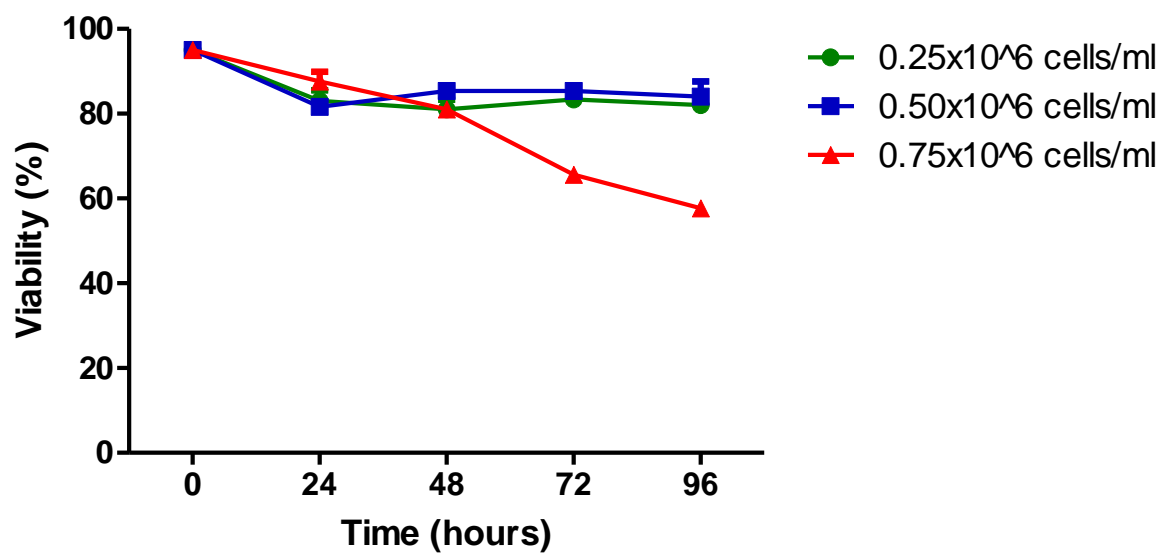
Figure 2.2 The influence of initial seeding density on endothelial cell viability
Cells were seeded at one of three densities as shown, and their viability monitored over time. The data represent a single experiment conducted in triplicate. Cells were analysed using vital dye staining. Mean ± SEM, n=3.

Percent viability was also compared to the total cell number. Figure 2.3 shows the rate of growth represented as the total cell number/ μl. It can be seen that, when seeded at a density of 0.75 x10^6 cells/ ml, the total cell number increased steadily over the initial 72 hours, but then decreased by 96 hours. This corresponded with the changes in cell viability (figure 2.2) to demonstrate that the number of dead cells increased as the number of live cells decreased. In addition, it can be seen that the growth-rate of the endothelial cells increased steadily yet at a slower rate when the cells were seeded at 0.25 x10^6 cells/ ml and 0.5 x10^6 cells/ ml than when they were seeded at 0.75 x10^6 cells/ ml. As the growth-rate at 0.25 x10^6 cells/ ml and 0.5 x10^6 cells/ ml were comparable, it was decided to conduct experiments with endothelial cells seeded at 0.25 x10^6 cells/ ml in 6-well plates. The seeding density was halved when employing 12-well plates (0.125 x10^6 cells/ well), and halved again for use in 24-well plates (0.065 x10^6 cells/ well).
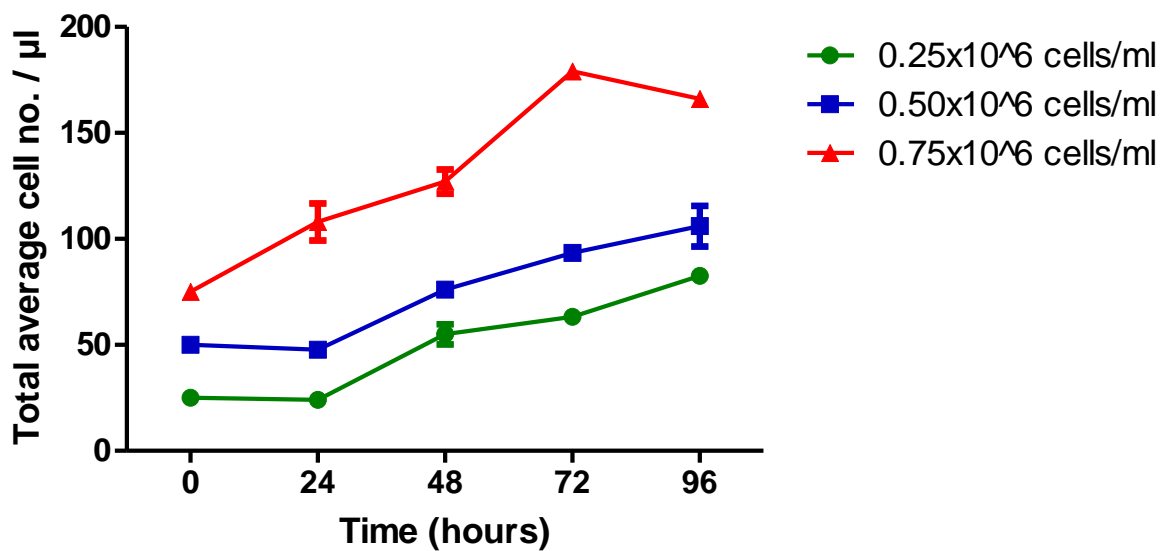
Figure 2.3 Influence of seeding density on total average cell number during the growth of endothelial cells

Total average cell number (number of live and dead cells) over time was measured at three seeding densities: 0.25 x10^6 cells/ ml, 0.50 x10^6 cells/ ml and 0.75 x10^6 cells/ ml. The data represent a single experiment conducted in triplicate. Cells were analysed using vital dye staining. Mean ±SEM, n=3.

2.1.3 Preparation of fatty acid stock solutions

The following fatty acid stock solutions were prepared at 90 mM in 90 % (v/v) EtOH: oleic acid (OA) (Sigma); methyl palmitate (MePA) (Sigma); methyl oleate (MeOA) (Sigma); ricinoleic acid (RA) (Sigma) and 2-bromopalmitic acid (2-BrPA) (Sigma). Sodium palmitate (PA) (sodium salt derivative of palmitic acid) (Sigma) was prepared at 50 mM in 50 % (v/v) EtOH (table 2.2) (Welters *et al*. 2004). The EtOH was prepared using absolute EtOH and autoclaved distilled water which was subsequently filter-sterilised. The fatty acid stock solutions were heated to 70 °C for 5 minutes and then stored at - 20 °C until required.

Sodium palmitate	$CH_3(CH_2)_{13}CH_2$ — C(=O) — ONa
Oleic acid	$CH_3(CH_2)_5$ —(cis double bond)— $(CH_2)_7$ — C(=O) — OH
Methyl palmitate	$CH_3(CH_2)_{13}CH_2$ — C(=O) — OCH_3
Methyl oleate	$CH_3(CH_2)_5$ —(cis double bond)— $(CH_2)_7$ — C(=O) — OCH_3
2-bromopalmitic acid	$CH_3(CH_2)_{12}CH_2$ — CH(Br) — C(=O) — OH
Ricinoleic acid	$CH_3(CH_2)_5$ — CH(OH) — CH_2 —(cis double bond)— $(CH_2)_7$ — C(=O) — OH

Table 2.2 Chemical structures of fatty acids presented in this thesis

The chemical structures of: sodium palmitate, oleic acid, methyl palmitate, methyl oleate, 2-bromopalmitic acid and ricinoleic acid are shown here and were employed in this thesis.

2.1.4 Treatment of beta cells with fatty acids

Fatty acid stock solutions were bound to 10 % (w/v) fatty acid-free bovine serum albumin (BSA) (Sigma). The binding of fatty acids to albumin was performed to mimic the physiological situation in which circulating fatty acids are bound to plasma proteins (principally serum albumin) (Goodman 1958; van der Vusse 2009). The alkyl chain of fatty acids is hydrophobic and would precipitate out of solution if it were not bound to BSA (Oliveira *et al.* 2015). 10 % (w/v) BSA was made by dissolving the appropriate mass of BSA powder in the required volume of serum-free RPMI-1640 medium containing 11 mM glucose (Lonza), supplemented with 2 mM L-glutamine (Gibco), 100 U/ ml penicillin (Gibco), 100 µg/ ml streptomycin (Gibco) and 50 µM β-mercaptoethanol (Fisher Chemical), then incubating at 37 °C for 1 hour (Dhayal & Morgan 2011). This serum-free medium supplemented with the above constituents will be known herein as 'beta cell complete serum-free medium' and any deviations from the composition of this medium will be made explicit. The 10 % (w/v) BSA solution was then filter-sterilised. The fatty acid working solutions were made such that they contained final concentrations of 9 % (w/v) BSA and 5 % (v/v) EtOH. The fatty acid working solutions were incubated in a 95 % air and 5 % CO_2 humidified atmosphere at 37 °C for at least 1 hour (Dhayal & Morgan 2011) prior to their addition to the cells to ensure the free fatty acid/ fatty acid-albumin had reached equilibrium.

The following experimental design was employed for use in 6-well plates: Day 0: plates were seeded with 1 ml cell suspension (0.4 x10^6 cells/ ml) in beta cell complete medium pre-warmed to 37 °C. Day 1: the beta cell complete medium was removed from the wells and discarded, 1.8 ml beta cell complete serum-free medium was added and 200 µl of the appropriate fatty acid treatment was added to the appropriate well to ensure a 1/10 dilution of the fatty acid stock solution. The serum-free medium for the beta cells contained all the

supplementary components as required for the complete medium, however, FBS was omitted. All vehicle control-treated cells (VCs) were exposed to BSA and EtOH. In all treatments, the final concentration of BSA was 0.9 % (w/v) and the final concentration of EtOH was (v/v) 0.5 %, unless otherwise stated. Day 2: the cells were harvested after 24 hour exposure to fatty acids, or the cells were left for an additional 24 hours to grow. Day 3: the cells were harvested after 48 hour exposure to fatty acids. Table 2.3 shows the steps taken in order to conduct a 24 and/ or 48 hour fatty acid exposure experiment.

Day	0	1	2	3
Action	Seeding of cells	Addition of fatty acid treatment and beta cell complete serum-free medium	24 hour growth. Cells were harvested or left to grow for an additional 24 hours	48 hour growth. Cells were harvested

Table 2.3 Treating INS-1 beta cells with fatty acids
The table presents the various actions required in order to conduct a 24 and/ or 48 hour fatty acid exposure experiment with beta cells.

2.1.5 Treatment of endothelial cells with fatty acids

The method for treating endothelial cells with fatty acids was followed similarly to that for beta cells, as described in section 2.1.4. The serum-free medium for the endothelial cells contained no supplementary components, i.e. it consisted only of the medium supplied by the manufacturer. The endothelial cell serum-free medium, which did not contain any supplements, will be known herein as 'endothelial cell serum-free medium' and any deviations from the composition

of this medium will be made explicit. In all treatments, the final concentration of BSA was 0.9 % (w/v) and the final concentration of EtOH was (v/v) 0.5 %, unless otherwise stated

2.1.6 Treatment of cells with etomoxir

A 110 mM stock solution of etomoxir sodium salt hydrate (Sigma) (table 2.4), a carnitine palmitoyltransferase 1 (CPT1) inhibitor, was made up in PBS (Lonza). Etomoxir was dissolved in the appropriate volume of serum-free medium to give a concentration of 110 µM. Cells were subsequently treated with fatty acids, as described previously in sections 2.1.4 or 2.1.5 depending on the cell type. After the addition of the appropriate volume of albumin-bound fatty acids, the final concentration of etomoxir became 100 µM. It should be noted that etomoxir was not bound to BSA as it was employed as a pharmacological enzyme inhibitor.
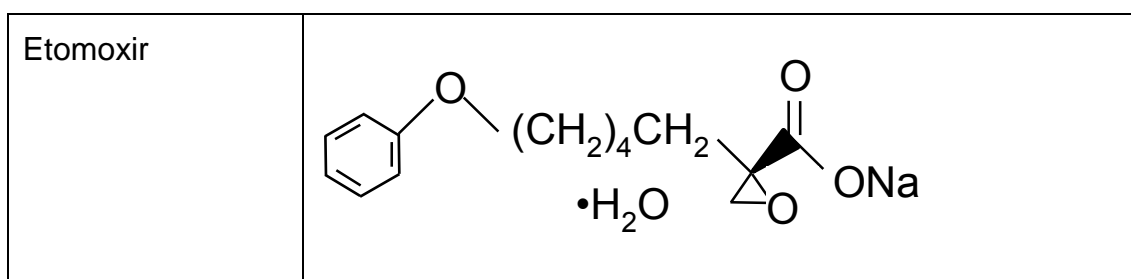
Etomoxir	

Table 2.4 Chemical structure of etomoxir sodium salt hydrate
Etomoxir was employed as a chemical inhibitor of the CPT1 protein present on the OMM. The inhibition of this protein was used to determine whether the entry of FAs into the mitochondria is essential for mediating cytotoxicity.

2.2 Vital dye staining

It is important to note that trypan blue staining was not required for the sub-culturing of cells, however, it was required for the quantification of cell viability. This is because, for sub-culturing, it is not essential to know the number of dead

cells. In addition, the live and dead/ non-viable cells can be distinguished without the use of trypan blue: live cells appear light in colour, and dead/ dying/ non-viable cells appear darker in colour when visualised under a light microscope without the use of a stain. However, when quantifying percentage cell viability, the number of live and dead cells must be accurately calculated. The use of trypan blue ensured these cells were accurately distinguishable and counted.

2.2.1 Quantification of cell viability

Using the vital dye staining method, the number of live and dead cells were counted under the light microscope to determine cell viability as a percentage. See equation 2.2 below.

Equation 2.2 Calculating percentage cell viability

$$Cell\ death\ (\%)$$

$$= \left(\frac{average\ number\ of\ dead\ cells}{average\ number\ of\ dead\ cells\ +\ average\ number\ of\ live\ cells} \right) X\ 100$$

$$Cell\ viability\ (\%) = 100 - number\ of\ dead\ cells$$

Example:

$$Cell\ death\ (\%) = \left(\frac{1\ dead\ cell}{1\ dead\ cell\ +\ 32\ live\ cells} \right) X\ 100 = 3.03$$

$$Cell\ viability\ (\%) = 100 - 3.03$$

$$Cell\ viability\ (\%) = 97$$

2.2.2 Quantification of cell growth by vital dye staining

Using the vital dye staining method, the number of live and dead cells were counted under the light microscope to determine the total average cell number. See equation 2.3 below.

Equation 2.3 Calculating total average cell number

$$Total\ average\ cell\ number$$

$$= average\ no.of\ dead\ cells + average\ no.of\ live\ cells$$

2.2.3 Preparation of beta cells for quantification

At the end of each experiment, the cells were harvested from the plates. The medium was removed from each well and added to a 15 ml centrifuge tube (Sarstedt). 0.5 ml trypsin-EDTA solution (ThermoFischer Scientific) pre-warmed to 37 °C was added to each well and incubated for 3 minutes at 37 °C. Once detached from the wells, 1 ml beta cell complete medium consisting of 11 mM glucose (Lonza) was added to wells to neutralise the trypsin. The cell-solution was then removed from the wells and added to a 15 ml centrifuge tube. The cells were centrifuged at 188 g for 5 minutes. The supernatant was removed and discarded. The pellet was resuspended in 0.5 ml beta cell complete medium consisting of 11 mM glucose (Lonza) and 0.5 ml 0.4 % (w/v) trypan blue (Sigma) made up in PBS (Lonza).

2.2.4 Preparation of endothelial cells for quantification

At the end of each experiment, the cells were harvested from the plates. The same method, as described in section 2.2.3, was used, however, the cells were washed with PBS before and after the addition of trypsin-EDTA solution (Sigma). Once the cells were detached from the wells, 1 ml endothelial cell complete medium containing 5.55 mM glucose (PromoCell) was added to wells

to neutralise the trypsin. The cell-solution was then removed from the wells and added to a 15 ml centrifuge tube. The cells were centrifuged at 423 g for 3 minutes. The supernatant was removed and discarded. The pellet was resuspended in 0.5 ml endothelial cell complete medium containing of 5.55 mM glucose (PromoCell) and 0.5 ml 0.4 % (w/v) trypan blue (Sigma) made up in PBS (Lonza).

2.3 Flow cytometry

Flow cytometry allows for the characterisation and measurement of cells and their intracellular constituents as they travel in a continuous stream. A beam of light from a laser light source (argon-ion laser) can either: (1) pass through the cell unobstructed, (2) bend around the outer membrane of the cell, or (3) diffract from components within the cell. The photons which pass through the cell unobstructed do not yield useful information about the status of the cell, however, the photons which bend around the cell can provide useful information such as the size of the cell. For example, a cell that is dividing and is in the G2 phase of the cell cycle would be larger in size than a non-dividing cell. Outgoing photons (photons which have come from the light source) which have bent around the cell are detected on the opposite side of the incoming photons. Where the outgoing photons are travelling in the same direction as the incoming photons, this type of light scattering is known as forward scatter (FSC-A). Photons which pass through the cell unobstructed are also detected in this way. Photons which are obstructed by cellular components, such as the nucleus, diffract to a much greater extent than those which are bent around the plasma membrane. This type of scatter, known as side scatter (SSC-A), can allow for the differentiation of healthy, live cells from dead cells. This is because a healthy cell will have its nucleus intact, whereas a dead cell will have a condensed nucleus and a disorganised cytoplasm, i.e. a dead cell will have an increased level of granularity.

Although cell death can be determined using the method described here, flow cytometry can also be coupled with fluorescent labels to yield more detailed information. For example, in fluorescence activated cell sorting (FACS) the fluorescent dye propidium iodide (PI) can be used to quantify and characterise functional aspects of the cell such as the extent of DNA fragmentation. PI is a membrane impermeant phenanthridinium dye that intercalates with DNA. PI is therefore only incorporated into the DNA of dying and dead cells as their plasma membranes are fragmented and permeable. These cells are described as 'PI positive cells'. A laser beam of wavelength 488 nm passes through the DNA-PI complex and emits light at a longer wavelength compared to the wavelength at source (615 nm) which is then measured. The results can provide information regarding cell viability (i.e. the percentage of dead and live cells) and cell cycle progression (i.e. the percentage of cells at the different stages of cell division). As PI cannot enter live cells, FACS can only indirectly detect these cells. Such cells are referred to as 'PI negative cells'.

2.3.1 Quantification of cell viability by flow cytometry

The quantification of cell death using flow cytometry was preferentially employed over trypan blue staining because flow cytometry significantly increases the output of data compared to vital dye staining and is considered to be more robust. Therefore, cell viability ('viability %') was determined using flow cytometry for the majority of experiments presented in this thesis.

2.3.1.1 Preparation of cells for quantification of cell viability

The appropriate methods for culturing both beta and endothelial cells treated with fatty acids were followed, as described in sections 2.1.4 and 2.1.2.4, respectively. Both live and dead cells were collected for each treatment in 12x75 mm tubes (BD Biosciences). The pellet was re-suspended in 200 µl of the

appropriate complete medium containing the appropriate glucose concentration. A 200 µl working solution of 20 µl/ ml PI-FACS buffer (1000 µl/ ml PI stock solution (Sigma) made up in water diluted 1:50 with FACS buffer (PBS (Lonza), 2 % FBS (Sigma)) was added to each tube. The samples were kept on ice for 10 minutes and then analysed on the BD Accuri™ C6 Plus Flow Cytometer (BD Biosciences). Before the analysis of the samples was conducted, a Quality Control (QC) run was performed. 2x drops of QC beads (BD Biosciences) were added to 0.5 ml deionised H_2O, vortexed, then analysed.

2.3.1.2 Data analysis

Both live and dead cells stained with PI were included in the analysis of cell viability (figure 2.4). Increasing FSC-A represents increasing cell size and increasing SSC-A represents increasing granularity. These two parameters, cell size and granularity, allow for the differentiation between the two populations of live and dead cells, as live cells are typically larger than dead cells and are also less granular.

Annexin 5 is a protein that binds to the phospholipid phosphatidylserine. Phosphatidylserine is transferred from its normal localisation on the inner leaflet of the plasma membrane to the outer leaflet during apoptosis (Martin *et al*. 1995). The detection of this phospholipid is also utilised to quantify percent viability. Previous work from our group has shown that Annexin 5 positive cells correspond to the cells which are PI negative after flow cytometric analysis (Russell 2010).
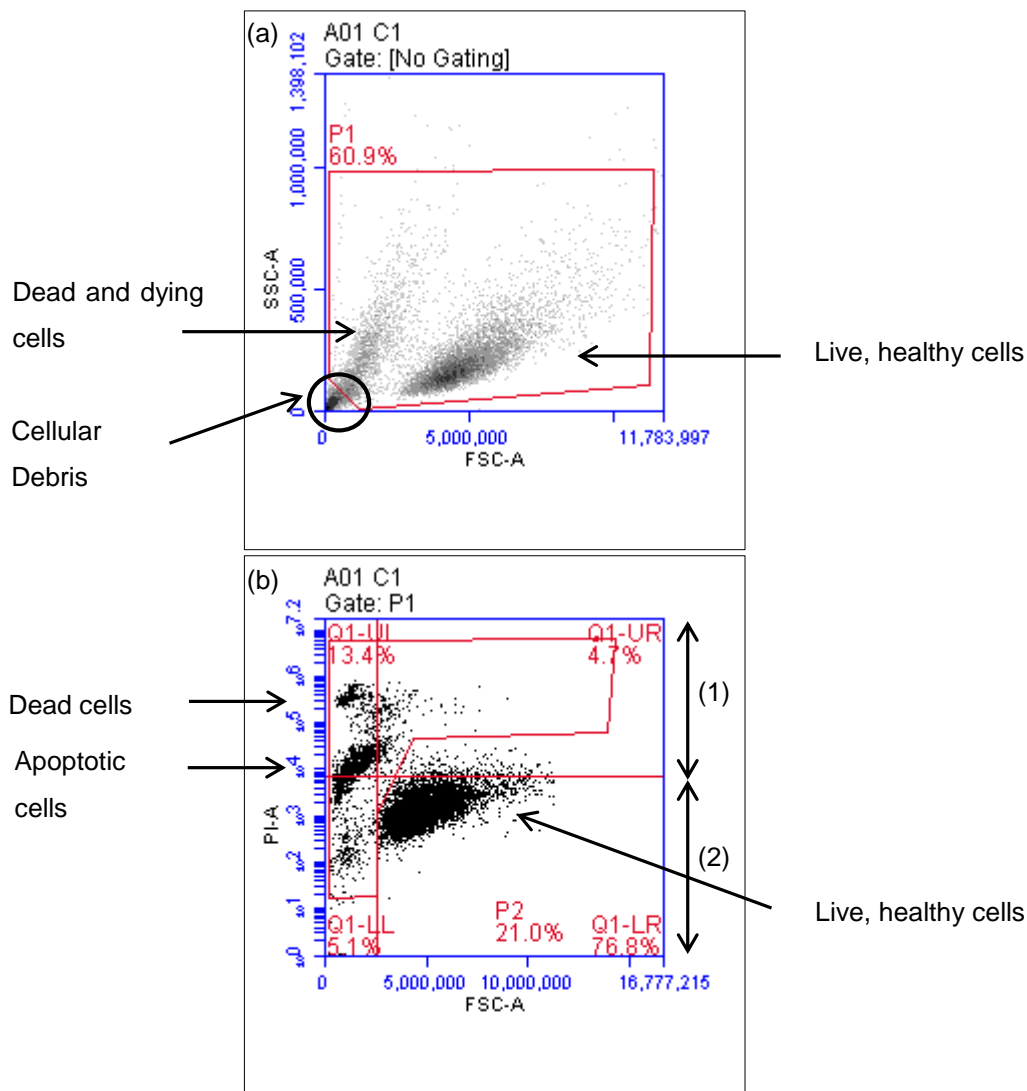
Figure 2.4 Viability analysis of INS-1 and HCMec/D3 cells

INS-1 and HCMec/D3 cells were cultured, stained with propidium iodide (PI) and analysed on the BD Accuri™ C6 Plus Flow Cytometer. The cells were pre-treated with their respective complete medium for 24 hours then exposed to their respective serum-free medium for a further 48 hours. The data presented in this figure represent untreated INS-1 cells. (a) The cells were gated [P1] to exclude cell debris on a FSC-A vs SSC-A plot. (b) Cells from P1 were gated [P2] to exclude live cells on a FSC-A vs PI/E-A plot. (1) PI positive cells (Q1-UL & Q1-UR) in this gate are dead. (2) PI negative cells (Q1-LL & Q1-LR) outside gate P2 are live. The percentage of live cells (21.0 %) is given based on the percentage of dead cells in P2.

Chapter 3

Structural requirements for fatty acid-mediated effects on cell viability

3 Structural requirements for fatty acid-mediated effects on cell viability

3.1 Introduction

LCFAs are metabolised principally via mitochondrial beta-oxidation in a series of REDOX-coupled reactions. LCFAs must first be activated via the enzyme acetyl-CoA synthetase (ACS) which generates a thioester bond between the FA and cytoplasmic CoA. CoA becomes covalently bound via the carboxyl oxygen allowing the FA to dock onto the OMM where CoA is subsequently recycled, allowing: (1) the FA to enter the mitochondria via the enzyme carnitine palmitoyltransferase I (CPT1), and (2) for other FAs to become activated for entry into the mitochondria. Data show that the upregulation of CPT1 rescues myotubes from PA-induced cell death (Henique *et al.* 2010), indicating the potential importance of CPT1 for FA disposal and metabolism. Other data, however, show that PA and OA, alone, upregulate the expression of CPT1 mRNA in MIN6 beta cells (6.2- and 5.4-fold, respectively) (Busch *et al.* 2002). Since both FAs upregulate CPT1, but only PA induced loss of viability, the data suggest that increased CPT1 is not a means by which PA-induces toxicity. Interestingly, the inhibition of mitochondrial FAO has been shown to induce the hyperpermeability of endothelial-cell plasma membranes, *in vitro*, indicating that FAO is an important regulator of endothelial-cell function (Patella *et al.* 2015) and growth (Schoors *et al.* 2015). Patella *et al.* (2015) found a significant decrease in the viability of HUVECs upon silencing CPT1 with small interfering RNA, suggesting that endothelial cells undergo a basal level of FAO required for maintaining normal cell health. Chemical inhibition of CPT1 with etomoxir, a known inhibitor of CPT1, has been found to attenuate PA-induced cell death in rat islets, *ex vivo*

(Chen *et al.* 1994), and in BRIN-BD11 beta cells, *in vitro* (Diakogiannaki *et al.* 2007). However, this effect was not observed by the study conducted by Patella *et al.* (2015), suggesting that the method of gene silencing may be a more robust method for cell-manipulation. Similarly, Staiger *et al.* (2006), found no effect on the viability of human coronary artery endothelial cells (HCAECs) during exposure to etomoxir. By contrast, the same group exposed HCAECs to Triacsin C, an ACS inhibitor, and found a decrease in cell viability in the presence of PA. Their work suggests that the conversion of PA to palmitoyl-CoA (PA-CoA) is essential for PA to mediate toxicity. These data therefore suggest that other processes downstream of PA-CoA production, such as protein palmitoylation or incorporation of PA into lipid droplets, may be responsible for the induction of PA-induced cell death. Shimabakuro *et al.* (1998) also suggest that the formation of alkyl-CoA is the toxic metabolite which is responsible for cytotoxicity. They came to this conclusion by exposing rat islets, *ex vivo*, to alkyl-CoA synthetase in the presence of Triacsin C, and found alkyl-induced toxicity was prevented.

The aims of this Chapter were to investigate the structural requirements for the induction of FA-induced cell death and cytoprotection in both INS-1 and HCMec/D3 cells. PA and OA, were employed as they are the predominant SFA and UFA, respectively, present in human serum. The use of INS-1 cells was employed as FAs have been implicated in the demise of beta cells. The effects of FAs were also compared to HCMec/D3 cells as many vascular complications arise from the development of type 2 diabetes, such as nephropathy and diabetic foot (Hex *et al.* 2012).

I sought to determine whether the entry of PA into mitochondria was inhibited using structural analogues of PA. Structural analogues can be defined as compounds with a "similar backbone and almost the same functional groups"

to their parent compound (Nikolova & Jaworshka 2003, p.1007). The PA analogues employed here were methyl palmitate (MePA) and 2-bromopalmitate (2-BrPA). Cells were also exposed to etomoxir, a pharmacological inhibitor of the mitochondrial enzyme CPT1, in the absence and presence of PA to determine whether cytoprotection could be induced. 2-BrPA was employed as it is suggested to inhibit CPT1, like etomoxir, however, this evidence is limited as only Chase & Tubbs (1972) make this suggestion. 2-BrPA was therefore primarily used to investigate whether its ability to become activated and reduce the pool of CoA might influence cytotoxicity of PA. This analogue, which is structurally more similar to PA than etomoxir, was employed as a method to limit the secondary effects afforded by etomoxir.

MePA has a methyl group covalently bound to the free carboxyl oxygen on the acid component of the alkyl chain. MePA was employed to determine whether PA-induced cytotoxicity was dependent upon this carboxyl oxygen being free. This was because it has previously been suggested that the formation of alkyl-CoA may be the toxic metabolite responsible for cytotoxicity (Shimabakuro *et al*. 1998). Thus, cytotoxicity observed in the studies presented in this Chapter may be as a result of the toxic metabolite PA-CoA.

In addition, I sought to determine the requirements for OA-induced cytoprotection using structural analogues of OA. The OA analogues were methyl oleate (MeOA) and ricinoleic acid (RA). MeOA has a methyl group covalently bound to the free carboxyl oxygen on the acid component of the chain. This was employed to determine whether OA-induced cytoprotection was dependent upon this carboxyl oxygen being free. RA possesses a hydroxyl group (-OH) on the 6th carbon atom from the terminal end of the carbon chain. This compound was

employed to determine the importance of keeping the alkyl chain free from substituents.

3.2 Methods

INS-1 and HCMec/D3 cells were cultured, as described in Chapter 2. The cells were seeded into 6- or 12-well plates in beta cell or endothelial cell complete medium, respectively, for 24 hours which was subsequently removed and replaced with serum-free medium for either 24 or 48 hours depending on the duration of the experiment. The FA stock solutions: PA, OA, MePA, MeOA, 2-BrPA and RA were dissolved in EtOH and conjugated to 10 % FA-free BSA, as described in sections 2.1.4 and 2.1.5. Etomoxir was not conjugated to BSA but dissolved in serum-free medium, as described in section 2.1.6, where the final concentration of etomoxir was 100 µM. Cells were harvested at the appropriate time point and analysed using flow cytometry and PI or vital dye staining (section 2.2.2) for the determination of cell death (section 2.3.1.1).

3.3 Results

3.3.1 Effects of palmitate and oleic acid on cell viability

Figure 3.1 shows that PA dose-dependently caused cell death after 48-hour exposure in both INS-1 and HCMec/D3 cells. By contrast, OA did not cause any loss of viability at concentrations up to 0.5 mM after 48-hour exposure in either cell type. The cytotoxic actions of PA were time-dependent (figure 3.2) in HCMec/D3 cells as has been shown previously in beta cells (Chen *et al.* 1994; Diakogiannaki *et al.* 2007; Welters *et al.* 2004).

3.3.2 Effects of etomoxir on cell viability

Cells were exposed to etomoxir in the presence of PA to determine whether the inhibition of the mitochondrial enzyme CPT1 could prevent PA-induced cytotoxicity. A final concentration of 100 µM etomoxir was chosen based

on previous studies where this concentration was employed (Chen *et al.* 1994; Staiger *et al.* 2006). Chen *et al.* (1994) utilised rat islets, *ex vivo*, to investigate whether the uptake of FAs via the mitochondria could be attenuated. They found that the enzyme CPT1 could be inhibited by at least 50 µM etomoxir. However, Staiger *et al.* (2006) found that PA-induced toxicity in HCAECs was not prevented with 100 µM etomoxir.

HCMec/D3 cells were exposed to 0.25 mM PA in the absence or presence of 100 µM etomoxir to examine whether mitochondrial FAO is required for mediating cytotoxicity (figure 3.3). Etomoxir alone did not reduce cell viability. PA markedly reduced cell viability compared to vehicle-treated cells ($p < 0.001$) but OA did not reduce cell viability. Interestingly, the combination of etomoxir with PA induced more cell death than PA alone ($p < 0.05$). However, no difference in cell viability was observed when OA was combined with etomoxir compared to cells exposed to OA alone.

A dose-response curve with increasing PA concentrations in the presence and absence of 100 µM etomoxir was then constructed (figure 3.4). The aim was to determine whether cytoprotection from etomoxir was dependent upon the dose of PA. HCMec/D3 cells were exposed to the combination of 100 µM etomoxir with increasing concentrations of PA, however, no differences were observed in viability between the two treatments. These data suggest that mitochondrial FAO does not contribute to PA-induced toxicity.

INS-1 cells were exposed to 0.25 mM PA in the absence or presence of 100 µM etomoxir to examine whether mitochondrial FAO is required for mediating cytotoxicity (figure 3.5). Unlike in the HCMec/D3 cells, etomoxir alone did worsen cell viability ($p < 0.01$) in the INS-1 cells. PA markedly reduced cell viability compared to vehicle-treated cells ($p < 0.001$) but OA did not reduce cell viability.

Contrary to the HCMec/D3 cells, the combination of etomoxir with PA had no effect on the INS-1 cells compared to PA alone. Interestingly, OA was able to improve the cell viability of cells treated with etomoxir compared to cells treated with etomoxir alone (p<0.001).
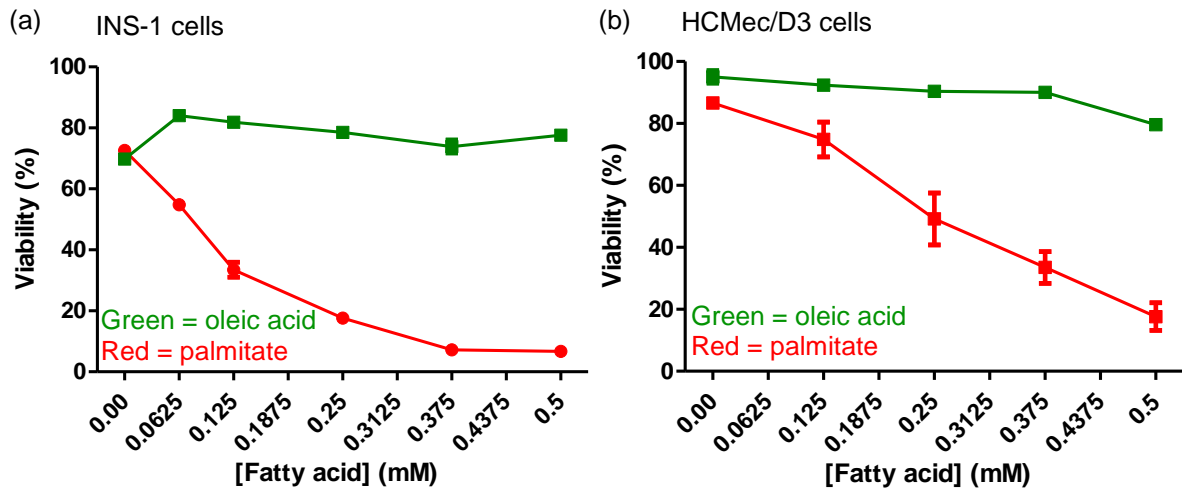
Figure 3.1 Dose-dependent effects of palmitate and oleic acid on INS-1 and HCMec/D3 cell viability after 48 hours

(a) INS-1 cells were pre-treated with complete medium for 24 hours, then for 48 hours with serum-free medium and increasing doses of palmitate (red line) and oleic acid (green line). The data are from two separate experiments each conducted in quadruplet. Cells were analysed on a BD Accuri™ C6 Plus Flow Cytometer. Mean values ± SEM, n=8. (b) HCMec/D3 cells were pre-treated with complete medium for 24 hours, then for 48 hours with serum-free medium and increasing doses of palmitate (red line) and oleic acid (green line). The palmitate data represent two experiments each conducted in triplicate. The oleic acid data are from a representative experiment conducted in triplicate. Cells were analysed using vital dye staining. Mean values ± SEM, n=6 (palmitate), n=3 (oleic acid).
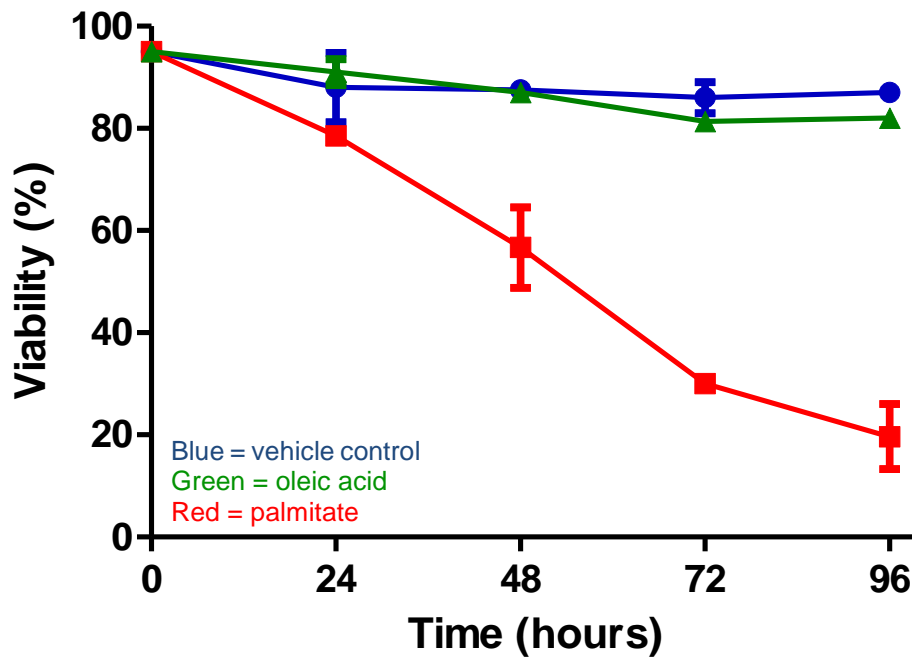
Figure 3.2 Time-dependent effects of palmitate and oleic acid exposure in HCMec/D3 cells

Time-dependent experiment showing HCMec/D3-cell responses to treatments. HCMec/D3 cells were pre-treated with complete medium for 24 hours, then for 24h, 48h, 72h or 96h with serum-free medium. Treatments: vehicle control (BSA + EtOH; blue line), 0.25 mM palmitate (red line) and 0.25 mM oleic acid (green line). The data are from a representative experiment conducted in triplicate. Cells were analysed using vital dye staining. Mean ± SEM, n=3.
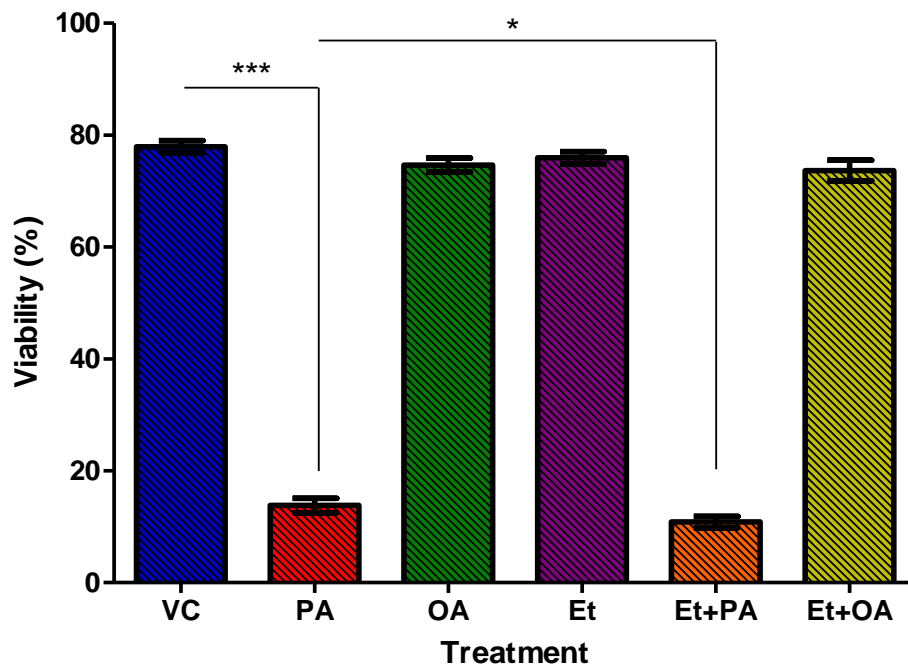
Figure 3.3 Effects of fatty acids on HCMec/D3 cells in the presence or absence of etomoxir

HCMec/D3 cells were pre-treated with complete medium for 24 hours, then for 48 hours with serum-free medium. Treatments: vehicle control (VC; BSA + EtOH; blue bar), 0.25 mM palmitate (PA; red bar), 0.25 mM oleic acid (OA; green bar), 100 µM etomoxir (Et; purple bar), 100 µM etomoxir + 0.25 mM palmitate (Et + PA; orange bar) and 100 µM etomoxir + 0.25 mM oleic acid (Et + OA; yellow bar). The data represent three experiments each conducted in quadruplet. Cells were analysed on a BD Accuri™ C6 Plus Flow Cytometer. One-way ANOVA with Tukey's multiple comparison test * ($p<0.05$), *** ($p<0.001$). Mean ± SEM, n=12.
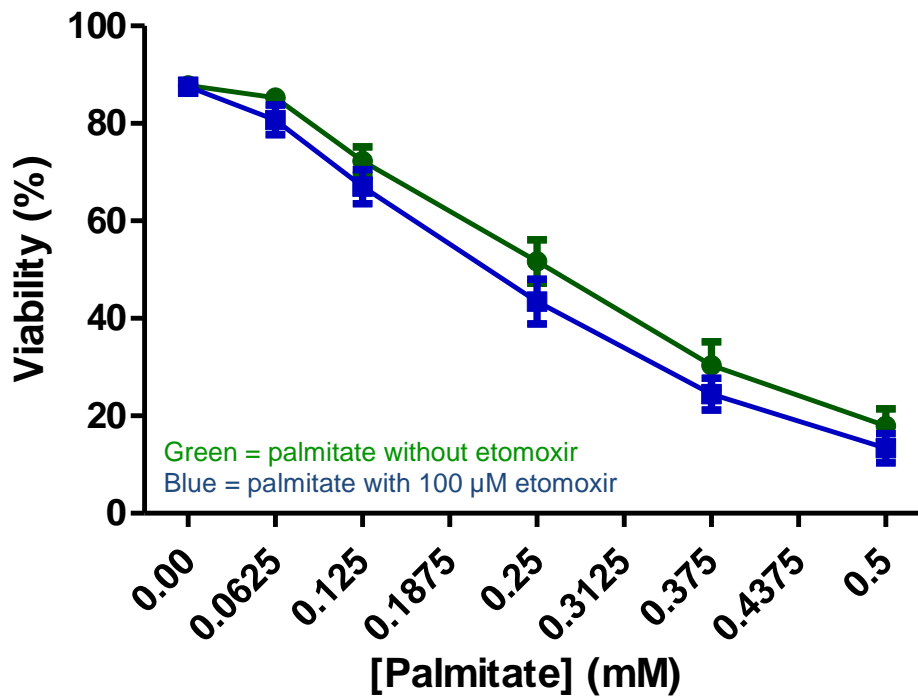
Figure 3.4 Dose-dependent effects of palmitate on HCMec/D3 cells in the presence or absence of etomoxir

HCMec/D3 cells were pre-treated with complete medium for 24 hours, then for 48 hours with serum-free medium and increasing doses of palmitate without etomoxir (green line) or with 100 µM etomoxir (blue line). The data represent three separate experiments each conducted in duplicate. Cells were analysed on a BD Accuri™ C6 Plus Flow Cytometer. Two-way ANOVA. Mean ± SEM, n=6.

Figure 3.5 Effects of fatty acids on INS-1 cells in the presence or absence of etomoxir

INS-1 cells were pre-treated with complete medium for 24 hours, then for 48 hours with serum-free medium. Treatments: vehicle control (VC; BSA + EtOH; blue bar), 0.25 mM palmitate (PA; red bar), 0.25 mM oleic acid (OA; green bar), 100 µM etomoxir (Et; purple bar), 100 µM etomoxir + 0.25 mM palmitate (Et + PA; orange bar) and 100 µM etomoxir + 0.25 mM oleic acid (Et + OA; yellow bar). The data are from two independent experiments each conducted in triplicate. Cells were analysed on a BD Accuri™ C6 Plus Flow Cytometer. One-way ANOVA with Tukey's multiple comparison test ** ($p < 0.01$), *** ($p < 0.001$). Mean ± SEM, n=6.

3.3.3 Effects of 2-bromopalmitic acid on cell viability

The effects of 2-BrPA on cell viability and its capability of improving PA-induced cytotoxicity were investigated. 2-BrPA, like etomoxir, requires activation via ACS and may improve PA-induced cytotoxicity by reducing the pool of cytoplasmic CoA. Limited evidence suggests that 2-BrPA is capable of inhibiting the mitochondrial enzyme CPT1 (Chase & Tubbs 1972). Thus, for the purposes of this thesis, it was assumed that 2-BrPA does not inhibit CPT1. Based on this, it was hypothesised that any observed cytoprotection from the co-incubation of 2-BrPA with PA may be, in part, due to the ability for 2-BrPA to reduce the pool of CoA and prevent the toxic formation of PA-CoA.

PA and 2-BrPA each caused a dose-dependent decrease in the viability of INS-1 cells after 24-hour exposure (figure 3.6), whereby statistical significance was observed at 0.125 mM and above between both PA and 2-BrPA ($p<0.01$, $p<0.001$ and $p<0.0001$). Statistical significance was observed between the VC treatments from both PA and 2-BrPA treatments ($p<0.001$), however, this difference is unlikely to have any biological significance as it can be clearly seen that the INS-1 cells respond very similarly to both PA and 2-BrPA. Surprisingly, the combination of these two FAs resulted in the abrogation of the toxicity seen with either FA alone ($p<0.001$) (figure 3.7). By contrast, with its actions in INS-1 cells, increasing concentrations of 2-BrPA caused only a less dramatic decrease in the viability of HCMec/D3 cells over 24 hours (figure 3.8). However, PA caused significant cell death in this time. When used in combination, 2-BrPA protected INS-1 cells against PA-induced toxicity ($p<0.001$) (figure 3.9).

INS-1 cells were again treated with PA and 2-BrPA alone and in combination for 24 hours, however, two further treatments were added to the experiment (figure 3.10). I wanted to further explore the idea that when PA and 2-BrPA were co-incubated they might compete against each other for the

availability of the substrate CoA. This experiment sought to determine whether chelation of CoA by either FA affected toxicity upon addition of the second FA. By reducing the pool of CoA with 0.25 mM of a FA for 4 hours, then subsequently co-incubating with 0.25 mM of a second FA for 20 hours, the toxicity of the second FA could be determined. The toxicity of both PA and 2-BrPA was significantly reduced by the period of pre-incubation with 2-BrPA or PA, respectively. ($p<0.001$). These data suggest that the primary FA chelated CoA and may have prevented the formation of the toxic metabolite, either PA-CoA or 2-bromopalmitoyl-CoA (2-BrPA-CoA).
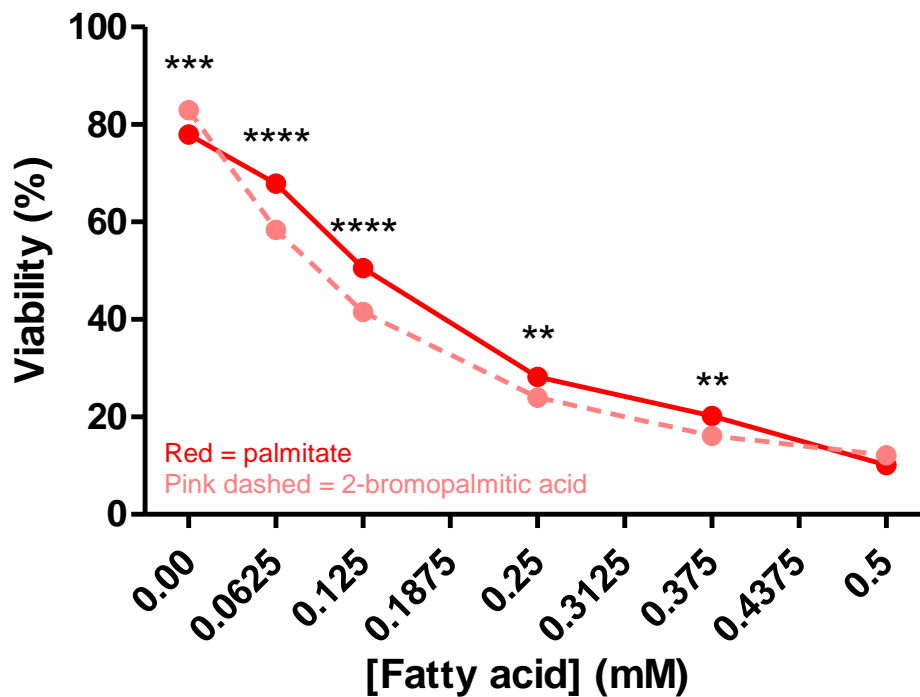
Figure 3.6 Dose-dependent effects of palmitate and 2-bromopalmitic acid on INS-1 cells after 24 hours

INS-1 cells were pre-treated with complete medium for 24 hours, then for 24 hours with serum-free medium and increasing doses of palmitate (red line) or 2-bromopalmitic acid (pink dashed line). The data represent three experiments each conducted in triplicate. Cells were analysed on a BD Accuri™ C6 Plus Flow Cytometer. Two-way ANOVA with Bonferroni multiple comparison test ** ($p < 0.01$), *** ($p < 0.001$), **** ($p < 0.0001$). Mean ± SEM, n=9.
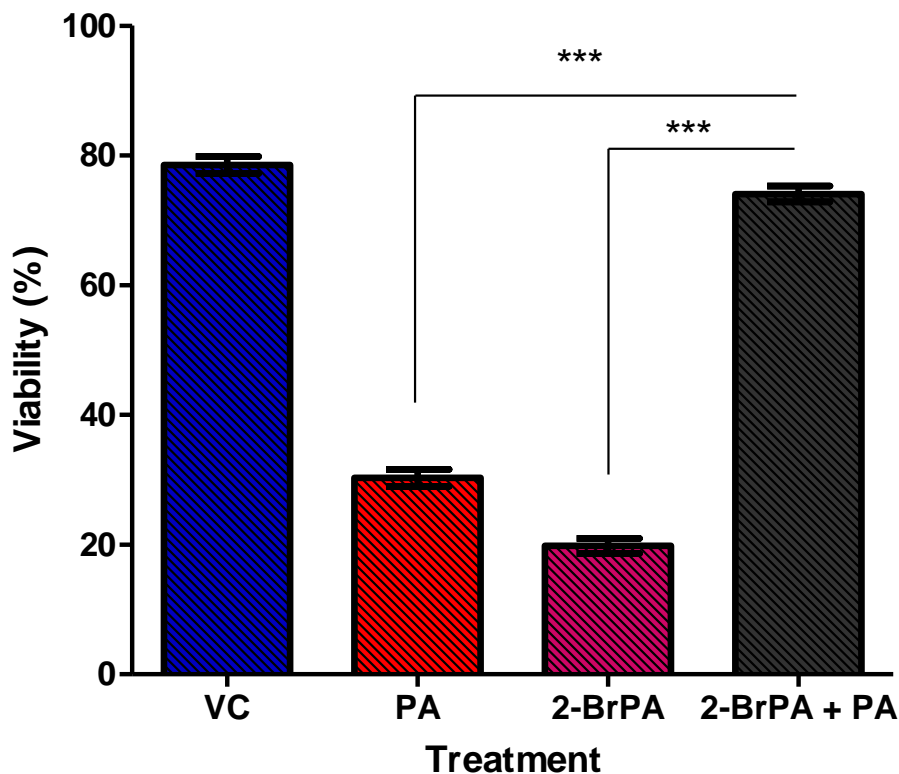
Figure 3.7 Effects of palmitate and 2-bromopalmitic acid on INS-1 cells after 24 hours

INS-1 cells were pre-treated with complete medium for 24 hours, then for 24 hours with serum-free medium. Treatments: vehicle control (VC; BSA + EtOH; blue bar), 0.25 mM palmitate (PA; red bar), 0.25 mM 2-bromopalmitic acid (2-BrPA; pink bar) and co-incubation of 0.25 mM palmitate + 0.25 mM 2-bromopalmitic acid (2-BrPA + PA; black bar). The data are from three separate experiments each conducted in triplicate. Cells were analysed on a BD Accuri™ C6 Plus Flow Cytometer. One-way ANOVA with Tukey's multiple comparison test *** ($p < 0.001$). Mean ± SEM, n=9.
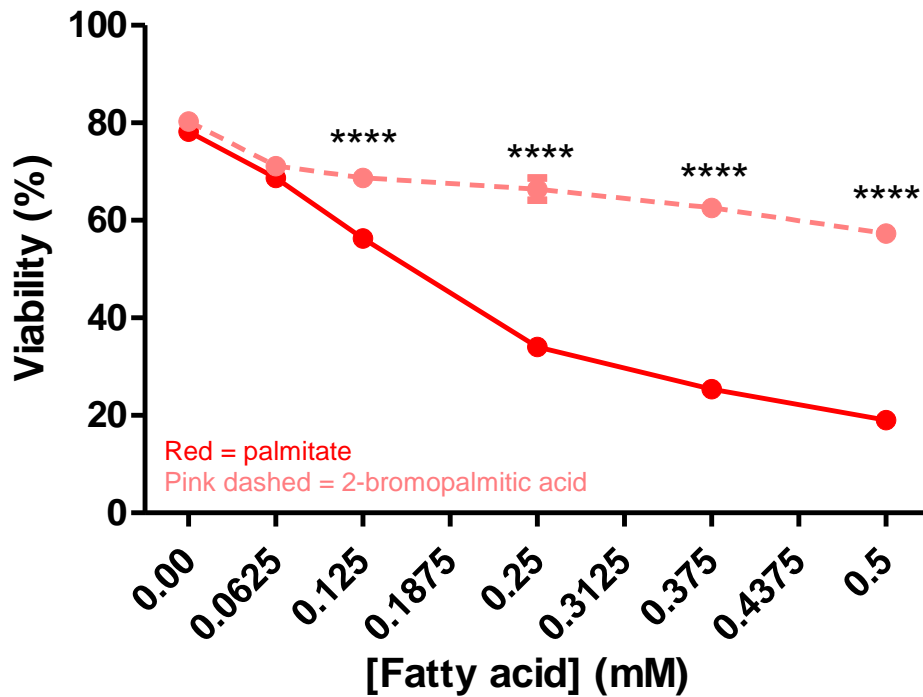
Figure 3.8 Dose-dependent effects of palmitate and 2-bromopalmitic acid on HCMec/D3 cells after 24 hours

HCMec/D3 cells were pre-treated with complete medium for 24 hours, then treated for 24 hours with serum-free medium and increasing doses of palmitate (red line) or 2-bromopalmitic acid (pink dashed line). The data represent three experiments each conducted in triplicate. Cells were analysed on a BD Accuri™ C6 Plus Flow Cytometer. Two-way ANOVA with Bonferroni multiple comparison test **** ($<p0.0001$). Mean ± SEM, n=9.
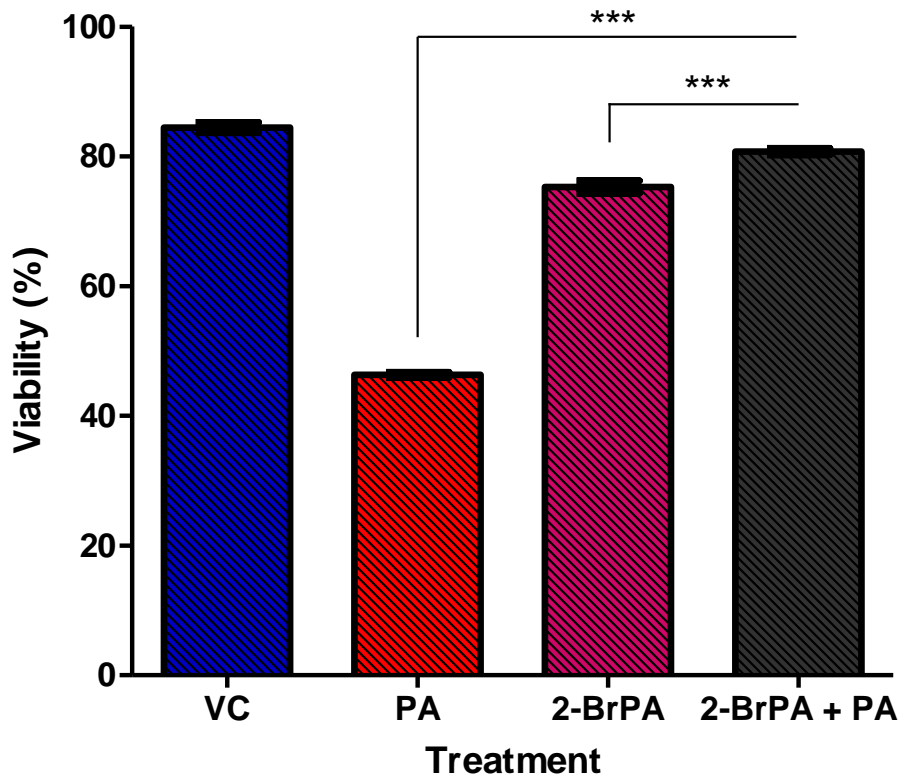
Figure 3.9 Effects of palmitate and 2-bromopalmitic acid on HCMec/D3 cells after 24 hours

HCMec/D3 cells were pre-treated with complete medium for 24 hours, then for 24 hours with serum-free medium. Treatments: vehicle control (VC; BSA + EtOH; blue bar), 0.25 mM palmitate (PA; red bar), 0.25 mM 2-bromopalmitic acid (2-BrPA; pink bar) and co-incubation of 0.25 mM palmitate + 0.25 mM 2-bromopalmitic acid (2-BrPA + PA; black bar). The data represent three experiments each conducted in triplicate. Cells were analysed on a BD Accuri™ C6 Plus Flow Cytometer. One-way ANOVA with Tukey's multiple comparison test *** ($p < 0.001$). Mean ± SEM, n=9.
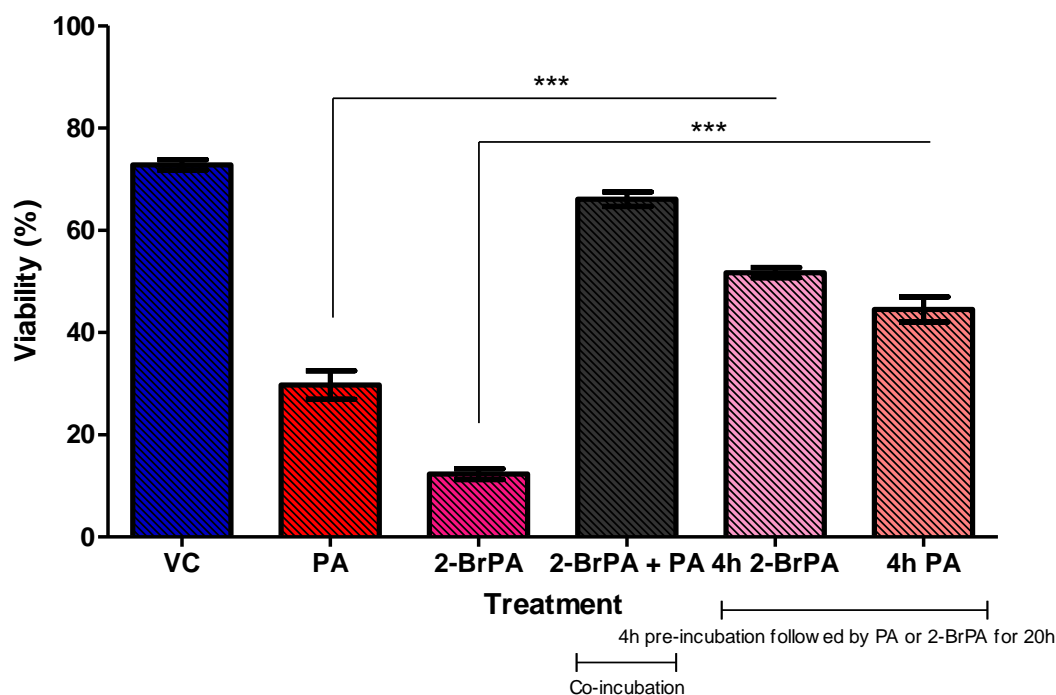
Figure 3.10 Effects of pre-incubation with palmitate and 2-bromopalmitic acid prior to addition of a second fatty acid in INS-1 cells

INS-1 cells were pre-treated with complete medium for 24 hours, then for 24 hours with serum-free medium. Treatments: vehicle control (VC; BSA + EtOH; blue bar), 0.25 mM palmitate (PA; red bar), 0.25 mM 2-bromopalmitic acid (2-BrPA; dark pink bar), co-incubation of 0.25 mM palmitate + 0.25 mM 2-bromopalmitic acid (2-BrPA + PA; black bar), 4 hours with 0.25 mM 2-bromopalmitic acid then co-incubation with 0.25 mM palmitate (4h 2-BrPA; light pink bar) and 4 hours with 0.25 mM palmitate then co-incubation with 0.25 mM 2-bromopalmitate (4h PA; light orange bar). The data represent three experiments each conducted in triplicate. Cells were analysed on a BD Accuri™ C6 Plus Flow Cytometer. One-way ANOVA with Tukey's multiple comparison test *** ($p < 0.001$). Mean ± SEM, n=9.

3.3.4 Effects of esterified fatty acids on cell viability

INS-1 and HCMec/D3 cells were exposed to 0.25 mM of the methyl esters of either PA or OA for 48 hours (figures 3.11 and 3.12, respectively). Cells were exposed to these FAs to investigate the requirement for the carboxyl oxygen atom to be free to induce cytotoxicity and cytoprotection. In both cell types, MePA alone was not toxic and it failed to prevent the loss of viability caused by PA, indicating that MePA does not have cytoprotective effects. The data suggest that the free carboxyl group of PA is essential for inducing toxicity under these conditions. The data also reveal that MeOA is cytoprotective to both cell types, albeit less than the parent FA, OA, when provided to the cells in combination with PA, implying that the free carboxyl group of OA is not an absolute requirement for cytoprotection.
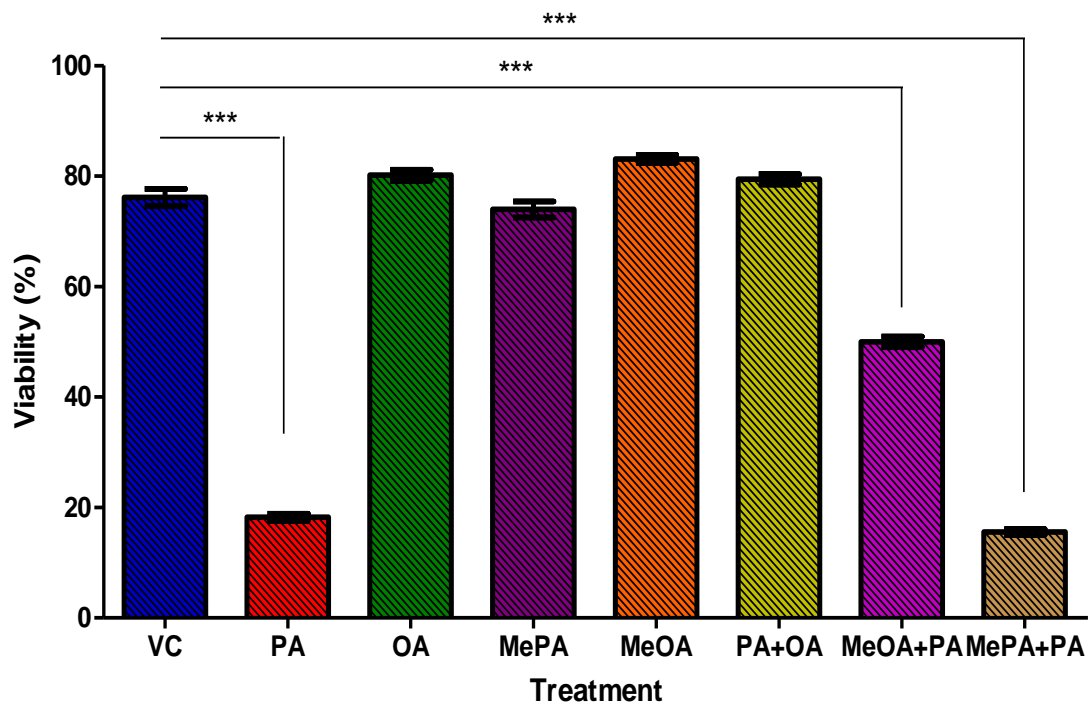
Figure 3.11 Effects of fatty acids and fatty acid analogues on INS-1 cell viability

INS-1 cells were pre-treated with complete medium for 24 hours, then for 48 hours with serum-free medium and 0.25 mM fatty acid treatment: vehicle control (VC; BSA + EtOH; blue bar), palmitate (PA; red bar), oleic acid (OA; green bar), methyl palmitate (MePA; dark purple bar), methyl oleate (MeOA; orange bar), palmitate + oleic acid (PA + OA; yellow bar), methyl oleate + palmitate (MeOA + PA; light purple bar) and methyl palmitate + PA (MePA + PA; light brown bar). 0.9 % BSA and 0.5 % EtOH final percentages. The data represent three experiments each conducted in triplicate. Cells were analysed on a BD Accuri™ C6 Plus Flow Cytometer. One-way ANOVA with Tukey's multiple comparison test *** ($p<0.001$). Mean ± SEM, n=6.

Figure 3.12 Effects of fatty acids and fatty acid analogues on HCMec/D3 cell viability

HCMec/D3 cells were pre-treated with complete medium for 24 hours, then for 48 hours with serum-free medium and 0.25 mM fatty acid treatment: vehicle control (VC; BSA + EtOH; blue bar), palmitate (PA; red bar), oleic acid (OA; green bar), methyl palmitate (MePA; dark purple bar), methyl oleate (MeOA; orange bar), palmitate + oleic acid (PA + OA; yellow bar), methyl oleate + palmitate (MeOA + PA; light purple bar) and methyl palmitate + PA (MePA + PA; light brown bar). 0.9 % BSA and 0.5 % EtOH final percentages. The data represent three experiments each conducted in duplicate. Cells were analysed on a BD Accuri™ C6 Plus Flow Cytometer. One-way ANOVA with Tukey's multiple comparison test *** ($p < 0.001$). Mean ± SEM, n=6.

3.3.5 Effects of ricinoleic acid on cell viability

INS-1 and HCMec/D3 cells were exposed to 0.25 mM of RA, an analogue of OA with an alcohol functional group on the 6th carbon atom from the end of the alkyl chain, for 48 hours (figures 3.13 and 3.14, respectively). Cells were exposed to RA to investigate the requirement for the alkyl chain of an UFA to be free to induce cytoprotection. RA was toxic ($p < 0.001$ vs VC), yet RA was much less toxic in HCMec/D3 cells, although still significantly toxic compared to the VC ($p < 0.001$) whereby RA also failed to prevent the loss of viability caused by PA. In subsequent experiments, RA was also added in combination with both OA and PA to investigate whether it might be antagonistic, i.e. whether RA might prevent OA from exerting its protective effect against PA. Interestingly, RA did not prevent OA from inducing its cytoprotective effects, suggesting that RA is not antagonistic against OA. The data imply that the 6th carbon atom from the end of the alkyl chain must be free as a requirement for OA-induced cytoprotection.

INS-1 cells were exposed to increasing doses of PA and RA for 48 hours to compare the toxicities of RA and PA to determine whether RA, an UFA, is more toxic than PA, a SFA. Figure 3.15 shows PA caused less cell death than RA at all doses tested, up to and including 0.25 mM, whereby statistical significance was observed at all concentrations above and including 0.0625 mM between both PA and RA ($p < 0.0001$). INS-1 cells were subsequently exposed to increasing concentrations of OA in the presence of either 0.25 mM PA or 0.125 mM RA for 48 hours. The aim was to determine the extent to which OA could protect against PA- and RA-induced toxicity. Figure 3.16 shows that concentrations of OA greater than 0.0625 mM were able to prevent both PA- and RA-induced toxicity. No statistical difference was observed between PA and RA at any concentration.
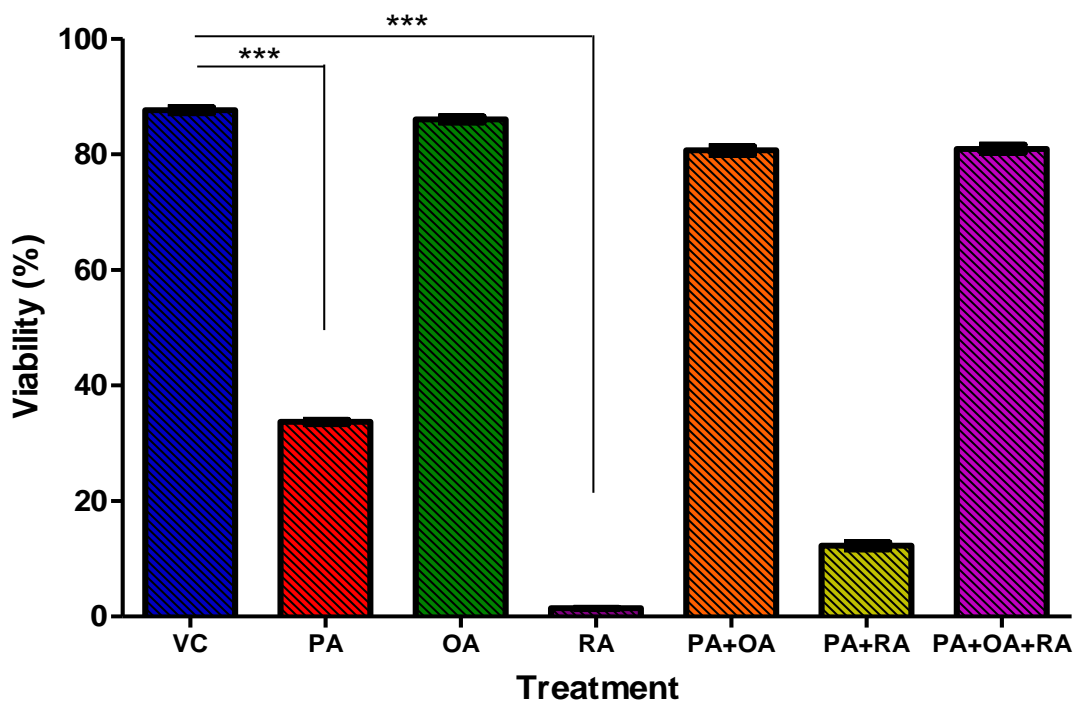
Figure 3.13 Effects of fatty acids and fatty acid analogues on INS-1 cell viability
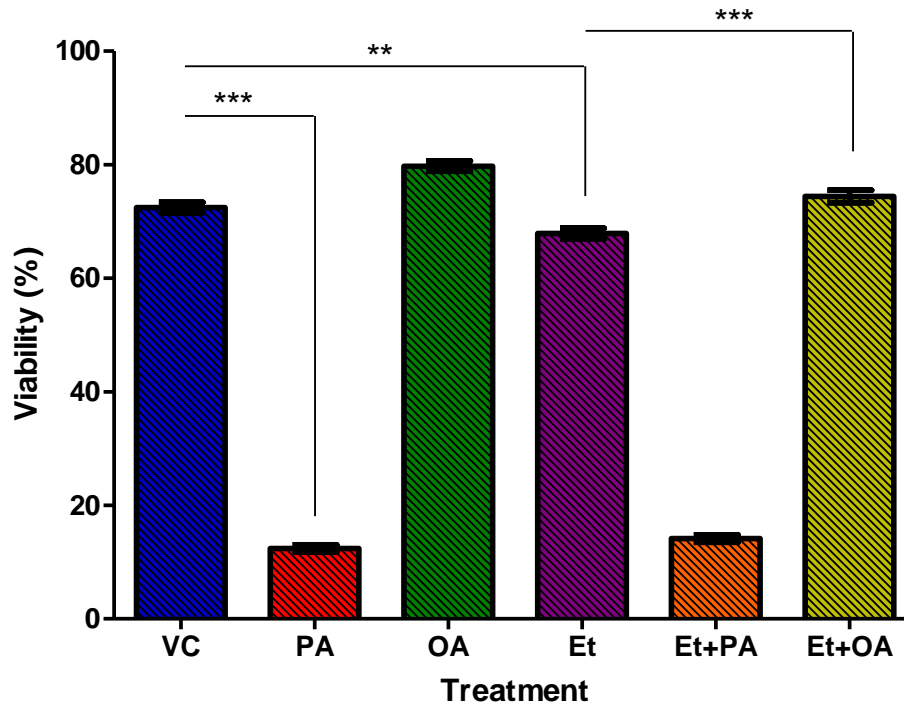
INS-1 cells were pre-treated with complete medium for 24 hours, then for 48 hours with serum-free medium and 0.25 mM fatty acid treatment: vehicle control (VC; BSA + EtOH; blue bar), palmitate (PA; red bar), oleic acid (OA; green bar), ricinoleic acid (RA; brown bar), palmitate + oleic acid (PA + OA), palmitate + ricinoleic acid (PA+RA; yellow bar) and palmitate + oleic acid + ricinoleic acid (PA + OA + RA; purple bar). 0.85 % BSA and 0.75 % EtOH final percentages. The data represent three experiments each conducted in triplicate. Cells were analysed on a BD Accuri™ C6 Plus Flow Cytometer. One-way ANOVA with Tukey's multiple comparison test *** ($p < 0.001$). Mean ± SEM, n=9.

Figure 3.14 Effects of fatty acids and fatty acid analogues on HCMec/D3 cell viability after 48 hours

HCMec/D3 cells were pre-treated with complete medium for 24 hours, then for 48 hours with serum-free medium and 0.25 mM fatty acid treatment: vehicle control (VC; BSA + EtOH; blue bar), palmitate (PA; red bar), oleic acid (OA; green bar), ricinoleic acid (RA; brown bar), palmitate + oleic acid (PA + OA), palmitate + ricinoleic acid (PA+RA; yellow bar) and palmitate + oleic acid + ricinoleic acid (PA + OA + RA; purple bar). 0.85 % BSA and 0.75 % EtOH final percentages. The data represent two experiments each conducted in quadruplet. Cells were analysed on a BD Accuri™ C6 Plus Flow Cytometer. One-way ANOVA with Tukey's multiple comparison test *** (p<0.001). Mean ± SEM, n=8.

Figure 3.15 Dose-dependent effects of palmitate and ricinoleic acid on INS-1 cell viability after 48 hours

INS-1 cells were pre-treated with complete medium for 24 hours, then for 48 hours with serum-free medium and increasing doses of palmitate (PA; red line) or ricinoleic acid (RA; green line). The data represent three experiments each conducted in triplicate. Cells were analysed on a BD Accuri™ C6 Plus Flow Cytometer. Two-way ANOVA with Bonferroni multiple comparison test **** ($p < 0.0001$). Mean ± SEM, n=9.
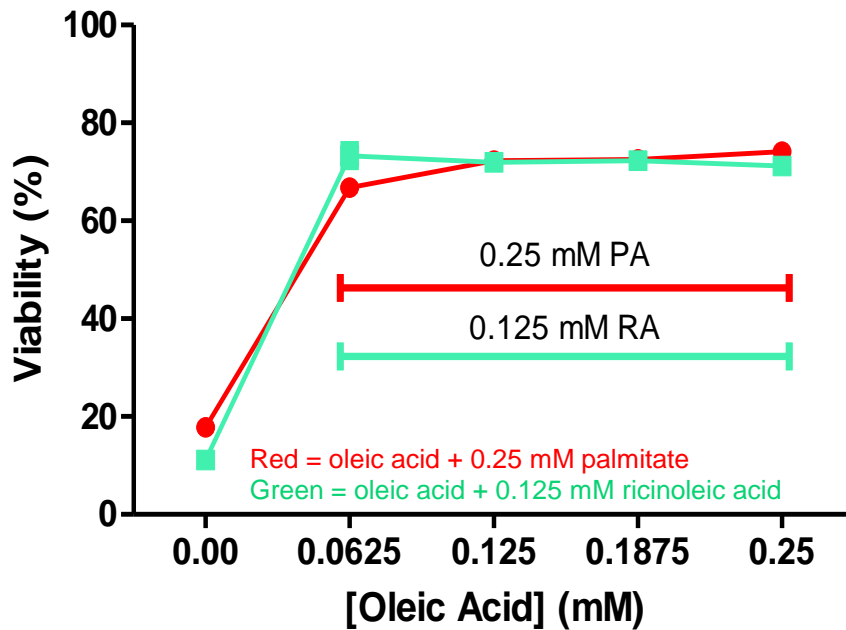
Figure 3.16 Effects of palmitate and ricinoleic acid and increasing concentrations of oleic acid on INS-1 cell viability after 48 hours

INS-1 cells were pre-treated with complete medium for 24 hours, then for 48 hours with serum-free medium and increasing doses of oleic acid in the presence of 0.25 mM palmitate (PA; red line) or 0.125 mM ricinoleic acid (RA; green line). The data represent three experiments each conducted in singlet. Cells were analysed on a BD Accuri™ C6 Plus Flow Cytometer. Two-way ANOVA with Bonferroni multiple comparison test. No sig diff. Mean ± SEM, n=3.

3.4 Discussion

3.4.1 Investigating the structural requirements for fatty acid activation and the role of CPT1 in mediating cytotoxicity

INS-1 and HCMec/D3 cells were exposed to increasing concentrations of PA and OA, alone, over 48 hours to investigate their responses. Figure 3.1 shows that PA induced dose-dependent cell death in both cell types, whereas OA was not toxic. Further, HCMec/D3 cells were exposed to 0.25 mM PA and 0.25 mM OA, alone, up to 96 hours to investigate their time-dependent effects, thus demonstrating that PA has both dose- and time-dependent effects on cell viability, yet OA does not (figure 3.2). In order to study the effects of various combinations of FAs on cell viability, and determine whether cytotoxicity could be alleviated, a PA concentration of 0.25 mM was chosen.

To investigate whether the entry of LCFAs, such as PA, into mitochondria is a requirement for cytotoxicity, I sought to block the entry of PA into mitochondria using the chemical inhibitor etomoxir. This compound is activated via ACS such that it can subsequently bind to CPT1; the enzyme responsible for the entry of LCFAs from the cytoplasm into the mitochondria via the OMM. Both HCMec/D3 and INS-1 cells were co-incubated with etomoxir and PA for 48 hours (figures 3.3 and 3.5, respectively). Etomoxir alone had no effect on cell viability in HCMec/D3 cells, however, etomoxir did worsen cell viability in INS-1 cells. In HCMec/D3 cells the combination of etomoxir with PA worsened toxicity compared with PA alone. Since cell viability was not improved in HCMec/D3 cells, these data suggest that PA entry into the mitochondrion via CPT1 is not a requirement for cytotoxicity. In INS-1 cells no difference in cell viability was observed between cells treated with PA alone and cells treated in combination with etomoxir and PA. It can therefore also be suggested that PA entry into the mitochondrion via CPT1 is not a requirement for cytotoxicity in INS-1 cells.

Etomoxir has been used by many researchers to investigate the effects of SFAs in mammalian cells. In some cell types, etomoxir has been shown to improve the viability of cells treated with LCFAs, such as in rat islets (Chen *et al.* 1994), however, in other studies, etomoxir has not only been unable to rescue cells from PA-induced toxicity (Staiger *et al.* 2006), but it has itself caused cell death (Schoors *et al.* 2015). The study by Staiger *et al.* (2006) set out to determine whether etomoxir would be able to rescue HCAECs from PA-induced apoptosis. PA-induced apoptosis was observed, yet no effect was observed when cells were exposed to 100 µM etomoxir. HCAECs were subsequently treated with both PA and etomoxir. Cells were exposed to etomoxir for 30 minutes before 1 mM PA was added for 24 hours. The researchers concluded that since etomoxir did not affect PA-induced apoptosis, beta oxidation is not involved in the mechanism by which SFAs induce apoptosis in HCAECs. The work by Schoors *et al.* (2015) sought to determine whether etomoxir would affect angiogenesis in HUVECs, with the aim of utilising etomoxir as a pharmacological agent to prevent PA-induced cell death. However, they found that etomoxir alone reduced FAO and cell proliferation. Because of this effect, etomoxir was not combined with PA. Whether the observed differences in responses are due to species differences is not clear.

Etomoxir is an analogue of SFAs, consisting of a free carboxyl oxygen, (allowing for activation via ACS) an epoxide and an o-linked-1,4-para-chloro-benzene ring (table 2.4). Activation via ACS involves the covalent binding of the free carboxyl oxygen to CoA, irreversibly forming etomoxyl-CoA (Et-CoA). Based on this mechanism, the interpretation of data, whereby cells have been exposed to etomoxir, can be difficult and indeed misleading since the agent is not simply an inhibitor of CPT1. Rather, the precise mechanism by which etomoxir acts

within the cell is unclear. Since etomoxir requires activation (as do LCFAs), any observed etomoxir-induced cytoprotection may either be due to: (1) etomoxir's ability to reduce the intracellular pool of CoA required for PA-activation, thus preventing PA-CoA-induced cytoplasmic toxicity, or (2) due to etomoxir's ability to inhibit CPT1 and prevent the entry of PA into the mitochondria. If etomoxir-induced cytoprotection were mediated by a reduction in the pool of cytoplasmic CoA, the mechanism of toxicity could equally be related to responses operating in the cytoplasm (and, for example, actions on other cellular organelles, such as lipid droplets), as on the mitochondria. Hence, it may be an over-interpretation of the data to suggest that sensitivity to etomoxir necessarily reflects a requirement for entry of FA into the mitochondria.

It is important to note though that etomoxir is not cytotoxic to HCMec/D3 cells. This is an interesting observation as compounds containing an epoxide group can become transformed to form diols which can result in cell death (Greene *et al.* 2000). Alternatively, etomoxir might not induce cell death as a result of the presence of the benzene ring acting as an electron sink, thus rendering the free carboxyl oxygen less nucleophilic and possibly less likely to react and bind covalently with CoA. Nevertheless, why etomoxir would have differential effects in some cell types is unclear.

Since etomoxir has multiple effects on the cell, it was deemed important to investigate other compounds which might also deplete the intracellular pool of CoA as a means to influence cell viability. To investigate this, I made use of the FA analogues 2-BrPA and MePA. 2-BrPA is an analogue of PA with a bromine atom covalently bound to the carbon atom in the alpha (C_2) position from the carboxyl carbon. It has been suggested that this compound can bind to CoA forming 2-BrPA-CoA and can inhibit CPT1 (Chase & Tubbs 1972). Even though

beta oxidation occurs at the third carbon atom from the carboxyl carbon, the presence of the bromine atom may cause steric hindrance, especially since beta oxidation involves the sigma (single) bond between the second and third carbon atoms from the carboxyl oxygen to become converted to a pi (double) bond. Hence, the bromine atom may prevent this process from occurring.

2-BrPA is thought to act primarily by reducing the pool of intracellular CoA, however, evidence suggests that 2-BrPA inhibits protein palmitoylation, particularly S-palmitoylation (Webb *et al.* 2000). This effect may therefore have detrimental effects on the cell. In INS-1 cells, co-incubation of etomoxir with PA did not prevent PA-induced toxicity (figure 3.5), yet co-incubation of 2-BrPA with PA did prevent PA-induced cell death (figure 3.7). Similar responses were observed in HCMec/D3 cells (figures 3.3 and 3.9, respectively).

In the INS-1 cells, 2-BrPA was found to cause cell death, as observed with PA (figure 3.6). This suggests that INS-1 cells are not able to tolerate a reduction in the pool of CoA and/ or the formation of 2-BrPA-CoA. Of course, however, 2-BrPA may have other effects on the cell which may not be tolerated, such as being an inhibitor of protein S-palmitoylation (Webb *et al.* 2000). This may result in some PA which is endogenously present within the cell being unable to bind to cysteine residues on proteins in the Golgi apparatus, possibly preventing lipoproteins from being exocytosed from the cell, and possibly inducing cytotoxicity. This inhibition of S-palmitoylation might be why toxicity is observed in INS-1 cells. Interestingly, when 2-BrPA was combined with PA, the cell viability of INS-1 cells was found to be comparable to the VC (figure 3.7). This difference in response was wholly unexpected and implies that the combined actions of the FAs are mutually antagonistic. There is no obvious explanation, however, one possibility implies some kind of competition between the two FAs, possibly for

CoA, resulting in both FAs being diverted to a pathway where their presence does not elicit a toxic response. As suggested by Chase & Tubbs (1972), it may be possible that 2-BrPA-CoA affects the equilibrium of the formation of palmitoyl-carnitine (the PA analogue required for the transfer of PA across the OMM via CPT1) from PA-CoA. In other words, 2-BrPA-CoA might be able to prevent the formation of palmitoyl-carnitine, suggesting that palmitoyl-carnitine might be responsible for cytotoxicity. This may be the case in the HCMec/D3 cells. However, this hypothesis would not be able to justify the observation in INS-1 cells because the presence of 2-BrPA-CoA would likely cause some toxicity, as observed when INS-1 cells were treated with 2-BrPA alone (figure 3.6). The method for detecting palmitoyl-carnitine, presented by Hulme *et al.* (2017), might be utilised to further investigate this hypothesis.

In contrast, 2-BrPA, unlike PA, was found to be non-toxic to HCMec/D3 cells (figure 3.8), whereby statistical significance was observed at 0.125 mM and above between both PA and 2-BrPA ($p < 0.0001$). This suggests that HCMec/D3 cells are able to tolerate a reduction in the pool of CoA, possibly because these cells have greater levels of cytoplasmic CoA. The results also suggest that HCMec/D3 cells are able to tolerate the formation of 2-BrPA-CoA. Further, the formation of 2-BrPA-CoA might not have any biological effects on these cells and may be inert. Interestingly, when 2-BrPA was combined with PA, toxicity was comparable to the VC (figure 3.9). This may be due to 2-BrPA's ability to reduce the pool of CoA, thus preventing the formation of toxic PA-CoA. However, why INS-1 and HCMec/D3 cells would respond differentially is unclear since the activation of LCFAs via CoA is essential for their entry into mitochondria. The data presented here were obtained after exposure to FAs for 24 hours. It is possible that the observed heightened sensitivity of INS-1 cells to 2-BrPA and the

lessened sensitivity of HCMec/D3 cells to 2-BrPA might be a temporal effect. In other words, toxicity in HCMec/D3 cells might be observed above 24 hours of exposure. Over time, the accumulation of 2-BrPA might have physical effects on the cell possibly affecting cytoplasmic processes and leading to cell death, such as: (1) the accumulation of diacylglycerol (Hagve & Christophersen 1987) or (2) the insertion into membranes, disrupting membrane integrity (McMahon & Boucrot 2015)

To further investigate the requirements for FA activation for the induction of cell death, INS-1 cells were pre-treated with either 2-BrPA or PA for 4 hours and then with 2-BrPA or PA for a further 20 hours (figure 3.10). This experiment sought to determine whether the direct reduction of the pool of CoA might improve cellular viability. Interestingly, when PA was added to INS-1 cells for 4 hours and the cells were subsequently exposed to 2-BrPA for 20 hours, cell viability improved compared to cells exposed to PA alone for 24 hours. Since 2-BrPA can undergo activation via CoA, it may be possible that 2-BrPA is able to bind to CPT1 and prevent the entry of PA into the mitochondria, as suggested by Chase & Tubbs (1972). It is possible that PA may also prevent 2-BrPA-induced cytotoxicity via a similar mechanism. The data show that incubating cells with either PA or 2-BrPA for 4 hours is not as effective at preventing cytotoxicity versus their co-incubation. Once the second FA is added, however, toxicity improves versus exposure to PA or 2-BrPA for 24 hours. From this we can conclude that cytotoxicity can be prevented, possibly via the prevention of FA activation, however, this mechanism is unclear. It can be suggested, however, that some kind of competition may be occurring within the cell which prevents both PA and 2-BrPA from inducing cell death.

MePA was employed to further investigate the importance of a FA consisting of a free carboxyl oxygen atom on cell viability. It is chemically impossible for MePA to bind with CoA, due to the carboxyl oxygen atom being covalently esterified to a methyl group. Thus, since MePA cannot reduce the pool of cytoplasmic CoA, it was hypothesised that this compound, when combined with PA, would not improve PA-induced cell death. In support of this, viability data revealed no improvement following the addition of MePA compared to PA alone, in both cell types (figures 3.11 and 3.12). Interestingly, unlike its parent FA, PA, MePA alone was non-toxic. This observation shows that neither INS-1 nor HCMec/D3 cells de-esterify MePA, otherwise toxicity would be observed. From these data we can conclude that a free carboxyl oxygen atom is required (possibly for cytotoxicity for the formation of the toxic metabolite PA-CoA). Thus, it can be suggested that the activation of PA is a requirement for cytotoxicity. When MePA was combined with PA, cell viability was lost to the same extent as seen with PA alone. Interestingly, this was not observed when PA was combined with 2-BrPA, suggesting that cytoprotection might be a result of the chelation of CoA via the presence of a free carboxyl oxygen atom on the alkyl chain of the FA. Overall, the data suggest that entry of PA into the mitochondria or the availability of the pool of CoA could be responsible for the ability of PA to cause cell death.

3.4.2 Investigating the structural requirements for unsaturated fatty acids to mediate cytoprotection

The ability for OA to protect against PA-induced cytotoxicity was further investigated using its methyl ester analogue MeOA. In both INS-1 and HCMec/D3 cells, the viability of MeOA was found to be comparable to the VC (figures 3.11 and 3.12, respectively). Interestingly when MeOA was combined with PA, MeOA was shown to be cytoprotective, but to a lesser extent that its parent FA, OA. Since, by contrast with OA, MeOA is cytoprotective in cells exposed to PA, these

data suggest that: (1) the mechanisms of protection do not require a free carboxyl oxygen, (2) the unsaturation of the carbon chain may be responsible for cytoprotection, and that (3) the mechanism of PA-induced toxicity might be due to the presence of a free carboxyl oxygen. However, other studies introduce caveats to these arguments. For example, a study by Harvey *et al.* (2009) sought to investigate the effects of SFAs and UFAs on Human aortic endothelial cell (HAECs). They showed that myristic acid, a SFA consisting of 14 carbon atoms in the alkyl chain, is not toxic to HAECs. Additionally, the study by Welters *et al.* (2004) shows that myristate (C14) (sodium salt of myristic acid) is not cytotoxic to BRIN-BD11 beta cells. Further, work has shown that phytanic acid, a branched chain UFA, consisting of 16 carbon atoms in the alkyl chain, is not toxic to BRIN-BD11 beta cells up to 100 µM after 17 hour incubation (Dhayal, unpublished work). These observations suggest that the length of the alkyl chain might be an irrelevant aspect when considering the mechanism of toxicity of PA, and also show that the presence of a free carboxyl oxygen atom is not the sole requirement for cytotoxicity.

In addition to understanding the importance of keeping the carboxyl oxygen free from substituents to mediate cytoprotection, the importance of keeping the alkyl chain free from substituents was studied. Previous experiments have shown that elaidic acid (an analogue of OA containing a *trans* carbon-carbon double bond between the 9th and 10th carbon atoms of the alkyl chain) is not toxic to BRIN-BD11 beta cells and that it is protective when combined with PA (Dhayal *et al.* 2008). Additional studies have shown that the precise position of the carbon-carbon double bond within the FA chain is not an absolute determinant of cytoprotective activity since petroselinic acid, a mono-UFA with

the carbon-carbon double bond between the 12th and 13th carbon atoms, prevents PA-induced death in BRIN-BD11 cells (Dhayal & Morgan 2011).

Interestingly, unlike a whole raft of other UFA derivatives, RA induced significant cell death in both the INS-1 and HCMec/D3 cells (figures 3.13 and 3.14, respectively). This was unexpected and the mechanism by which RA induces cell death is unclear. However, it may be possible for hydroxyl-FAs to react with one another via their hydroxyl groups on the alkyl chain to form polyesters via the carboxyl oxygen; yielding either large polymer structures or ring-like structures, as described by Slivniak & Domb (2005) and Hayes *et al*. (2012). The formation of these higher order compounds may, perhaps, cause the cell death reported in this Chapter. However, evidence suggests that other hydroxyl-FAs can be non-toxic or even cytoprotective since Kunda *et al*. (2018) noted that hydroxyl-PA is not toxic in murine models, unlike its parent FA, PA, and may even ameliorate insulin sensitivity.

The data illustrating the effects of RA on INS-1 and HCMec/D3 cells add weight to the argument advocating that a change in the chemical composition of the alkyl chain, such as the addition of an -OH group, and the structure of the chain in space, affects the ability of OA not only to regulate toxicity but also to mediate cytoprotection when combined with a SFA. These data highlight the importance of maintaining the structure and composition of the UFA carbon chain for exerting its non-toxic and/ or cytoprotective effect(s).

To conclude, the work presented in this Chapter has shown the differential responses which INS-1 and HCMec/D3 cells have towards PA and analogues of PA. Whether the entry of PA into the mitochondrion is a requirement for PA-induced toxicity is yet unclear. In addition, the methods which are employed to study FA-entry into the mitochondrion require careful consideration and

interpretation. This work has also shown how small chemical changes to the structure of UFAs can affect cell viability, yet the mechanism by which these effects occur is yet unclear.

Chapter 4

Evaluation of the effects of fatty acids

on the cell cycle

4 Evaluation of the effects of fatty acids on the cell cycle

Data presented in Chapter 3 showed that PA was cytotoxic in both INS-1 beta cells and HCMec/D3 microvascular endothelial cells. In addition, OA was found to not only be non-toxic in both cell types but was also shown to prevent PA-induced cell death. The literature suggests that these FAs might be able to effect the cell cycle. The purpose of this Chapter therefore sought to further investigate whether the mechanism of PA-induced cytotoxicity and OA-induced cytoprotection was as a result of their ability to affect cell cycle progression.

4.1 Introduction

Many types of eukaryotic cells can replicate for the purposes of regeneration, repair and restoration, as well as for growth and asexual reproduction. Beta cells of the pancreas are strongly proliferative in young children (up to the age of 2 years) but the rate of proliferation then declines dramatically and is almost absent in adults (Tschen *et al.* 2009). However, this situation can change in response to physiological circumstances including during pregnancy and, possibly in obesity (Bonner-Weir *et al.* 2010; Nir *et al.* 2007; Wang *et al.* 2015b). Mature beta cells are therefore known to be relatively stable, poorly-proliferative cells as they will only replicate in response to very specific stimuli. Similarly, microvascular endothelial cells have very low basal rates of turnover, and only replicate when they are stimulated after damage (Tannock & Hayashi 1972).

Cell division occurs by mitosis in all somatic cells and is sub-divided into four distinct phases which, collectively, comprise the cell cycle. The stages are as follows: G0+G1, S, G2 and M. The G0+G1 phase is considered to be the cell's resting state, a state where the cell is prepared for DNA synthesis, when required

(Voet *et al.* 2000). The G0+G1 phase is followed by the S phase, the only period in the cell cycle where DNA is synthesised. The S phase leads into the G2 phase where the cell prepares for cell division by doubling all other cellular components. The final phase, M, involves the physical processes of cell division and the formation of daughter cells (Voet *et al.* 2000).

Each phase of the cell cycle is preceded by a checkpoint to ensure that the cell is adequately prepared for cell division and that mistakes in the DNA replication process are corrected before the next phase is embarked upon. These checkpoints, regulated by cyclin-dependent kinases, are essential because they ensure that only cells with correctly copied DNA divide (Voet *et al.* 2000). Incorrectly copied DNA or uncontrolled replication can be dangerous and may lead to the formation of tumours (Voet *et al.* 2000). It is therefore important to determine whether exogenous or endogenous molecules can inhibit or enhance the efficiency of the checkpoint control mechanisms during the cell cycle.

In the context of diabetes, it is important to learn whether relevant exogenous compounds can stimulate beta cell growth to maintain beta cell mass and glucose homeostasis as this might be of therapeutic value. For example, work conducted by Wang *et al.* (2015a) show, using three different mouse and human islet *in vivo*-based models, that harmine, a small molecule, is capable of inducing beta cell proliferation. Therefore, understanding how otherwise quiescent cells may be induced to replicate in adult life could improve the lives of those living with diabetes.

Various methods exist to monitor cell proliferation *in vitro* or *ex vivo*, and, in many of these, cells are treated with agents which become incorporated into newly formed DNA such that they can be detected immunologically. Examples include BrdU and EdU, two nucleotide analogues which are incorporated into

replicating DNA. In addition, proteins, e.g. Ki-67 (Kim & Sederstrom 2015), and mcm-2 (Yousef *et al.* 2017) can also be used as these are synthesised only at specific points during the cell cycle. The rate of DNA replication is assessed as the extent of incorporation of the surrogate molecules which are then quantified and compared to untreated cells. These studies can inform us as to whether certain compounds are pro-proliferative or even able to inhibit proliferation.

The aims of this Chapter were to determine whether SFAs or UFAs influence progression through the cell cycle of INS-1 beta cells and HCMec/D3 microvascular endothelial cells using an intercalating dye, PI, and flow cytometry. Particularly, I sought to determine whether: (1) PA was able to inhibit cell proliferation as a contributory factor to its mechanism of cell death, (2) OA was able to induce a pro-proliferative response alone, and (3) OA was able to prevent PA-induced cell death by inducing a pro-proliferative response as a compensatory mechanism for PA-induced cell death.

Although neither beta cells nor endothelial cells normally proliferate *in vivo*, the use of cell lines were employed here as a model to investigate the effects of FAs on the cell cycle. The use of cell lines, although not directly translatable to cells *in vivo*, may help to further our understanding of beta cell and endothelial cell biology and slowly bridge the gap between the effects of FAs observed *in vitro* and *in vivo*.

4.2 Methods

INS-1 and HCMec/D3 cells were cultured, as described in Chapter 2. Cells were prepared for cell cycle quantification using flow cytometry.

4.2.1 Preparation of cells for quantification of cell cycle progression

Live and dead cells were harvested after 24-hour pre-treatment with complete medium and then after exposure for 48 hours to complete serum-free medium and FAs complexed to albumin, as described in Chapter 2.

A group of positive control HCMec/D3 cells were also employed. These cells were treated with endothelial cell complete medium for 72 hours (complete medium control: CMC).

All the cells were collected after each treatment in 12x75 mm tubes (BD Biosciences) and centrifuged. The cell pellet was resuspended in 250 µl cold saline GM and 750 µl cold 95 % (v/v) EtOH for 30 minutes to achieve plasma membrane permeabilisation and simultaneous fixation (table 4.1).

Saline GM/ fixative solution

Stock solutions were made up in double distilled water (ddH$_2$O) and stored at 5 °C (table 4.1).

G-(+)-glucose (Sigma)	110 mg/ ml (0.61 M)
KCl (Sigma)	40 mg/ ml (0.54 M)
Na$_2$HPO$_4$ (Sigma)	39 mg/ ml (0.28 M)
KH$_2$PO$_4$ (Sigma)	15 mg/ ml (0.11 M)

Table 4.1 Stock solutions of components for saline GM/ fixative solution
Stock solutions of the components in this table were made up in double distilled water. These solutions were added to other components to make saline GM.

500 µl of the stock solutions (table 4.1) were added to the following solution: 25 ml ddH$_2$O consisting of 0.4 g NaCl (Sigma) + 50 µl 0.5 M EDTA (Sigma). This solution (now ~ 27 ml) was made up to 50 ml with ddH$_2$O. This final solution is known as saline GM.

Cells that were not immediately analysed on the flow cytometer were stored at - 20 °C for up to 2 weeks (in falcon tubes suitable for freezing). Frozen cells were defrosted then centrifuged at 188 g for 5 minutes or 423 g for 3 minutes for INS-1 or HCMec/D3 cells, respectively. Each pellet was resuspended in 1 ml staining solution consisting of PI:RNase A, (50 µg/ ml PI (Sigma), 100 µg/ ml RNase A (ThermoFischer Scientific) in PBS) for 1.5 hours and then analysed on the BD Accuri™ C6 Plus Flow Cytometer (BD Biosciences).

4.2.2 Data analysis

Live and dead cells were harvested after the appropriate time point, the cell membranes permeabilised then fixed and the DNA subsequently stained with PI. The live cell population was gated on a FSC-A vs SSC-A plot, as shown in figure

4.1. While in a viability assay the PI stain binds DNA of non-viable cells (as their plasma membranes are no longer intact) in the cell cycle assay the plasma membranes of viable cells are deliberately permeabilised. Since only viable cells are able to proliferate, it was imperative that only live cells were included in the analysis. The FSC-A-axis depicts cells of increasing size and the SSC-A-axis depicts cells with increasing granularity. The live cell population was selected (gated) for analysis, whereas cellular debris and swollen cells were excluded. The live cell population was subsequently gated for single cells on a PI-Height vs PI-Area plot, whereby cellular aggregates, e.g. doublets (two cells joined together), were excluded to ensure accurate determination of the percentage of single cells in each phase of the cell cycle, as shown in figure 4.1. The final stage of the analysis involved the separation of the desired cell population into each stage of the cell cycle: G0+G1, S and G2+M. All single cells which had their plasma membranes permeabilised were plotted on a Count vs PI-Area plot where the cells in the different phases of the cell cycle were quantified, as shown in figure 4.1. Although the gating process aims to exclude any non-viable cells (those with disrupted plasma membranes and doublets), some cells with fragmented DNA are present in the viable cell population as these cells have intact plasma membranes. These cells, the M6 population, therefore represent cells which have fragmented DNA yet have intact plasma membranes. Thus, the cells in the G0+G1, S and G2+M phases have both intact plasma membranes and intact DNA. The cells which have an intact plasma membrane and fragmented DNA will be known herein as 'non-viable'.
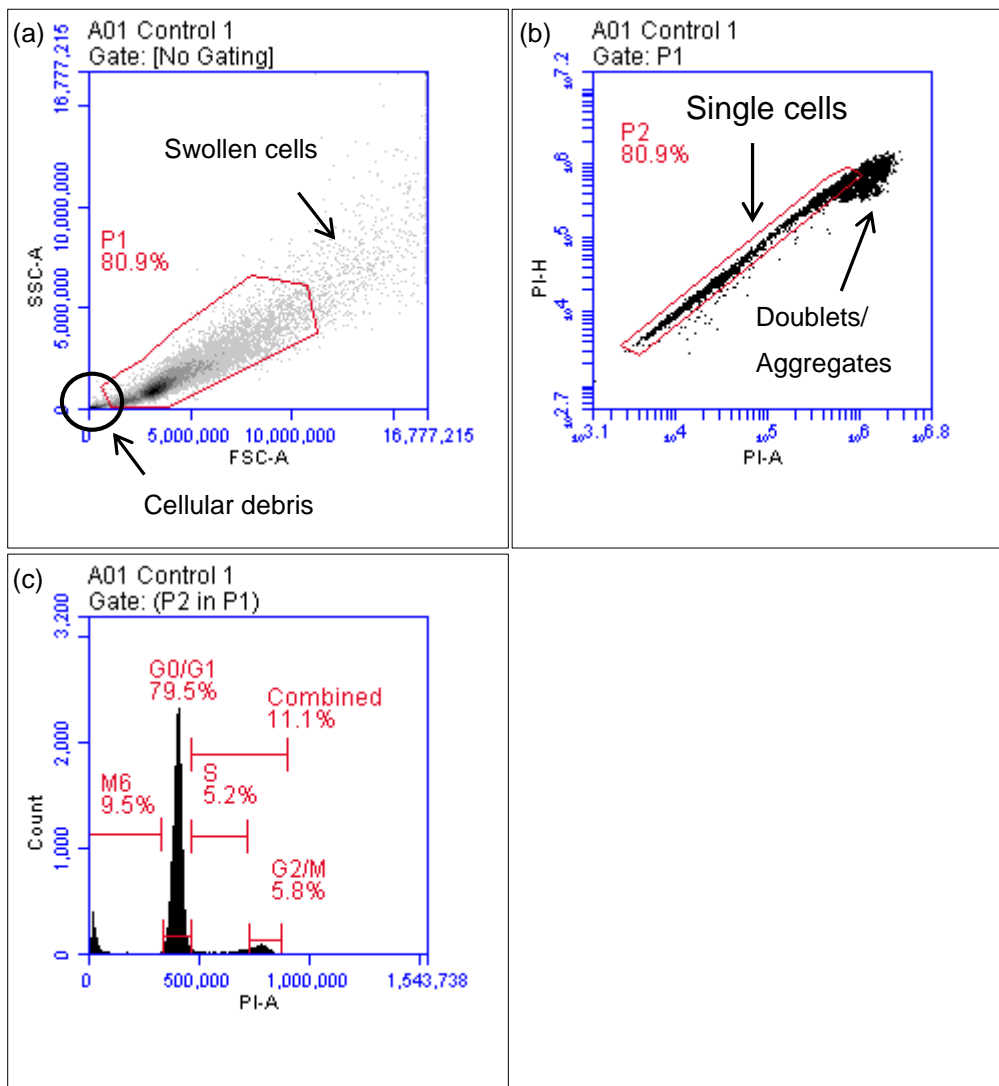
Figure 4.1 Cell cycle analysis using flow cytometry

INS-1 cells were cultured, stained with PI and analysed on the BD Accuri™ C6 Plus Flow Cytometer. (a) Cells were pre-treated with complete medium for 24 hours, then with serum-free medium, fatty acid-albumin complex and vehicle (BSA + EtOH) for 48 hours. The cells were gated [P1] to exclude cell debris and swollen cells on a FSC-A vs SSC-A plot. (b) Cells from P1 were gated [P2] to exclude for doublets/aggregates on a PI-A (area) vs PI-H (height) plot. (c) A PI histogram of cells (gated on single cells from P2 gate) distinguishes the percentage of cells at the G0+G1, S and G2+M cycle phases. M6 indicates the percentage of cells which are non-viable.

4.3 Results

4.3.1 Percentage calculations

To investigate whether FAs influence proliferation in INS-1 and HCMec/D3 cells, cells were analysed using flow cytometry after staining with PI. The percentage of cells in the different phases of the cell cycle were calculated and expressed in the following categories: non-viable, G0+G1 phase, S phase and G2+M phase (figures 4.2 and 4.4). Since only dividing cells are considered to be proliferating, cells in the S and G2+M phases were combined (figures 4.2 and 4.4). The INS-1 cells treated with the VC were exposed to BSA and EtOH. The HCMec/D3 control cells were treated with either: (1) complete medium, without BSA or EtOH (CMC: positive control), or (2) serum-free medium, with BSA and EtOH (VC: vehicle control).

4.3.2 Data normalisation

In order to eliminate the possibility of the non-viable cell population influencing the relative percentages of viable cells, each viable cell population was normalised against the non-viable cell population and the values were re-plotted (figures 4.3 and 4.5). The coefficient was calculated for each sample and the percentage of diving cells recalculated. See equation 4.1 and subsequent calculations below.

Equation 4.1 Calculation of coefficient for data normalisation

$$Coefficient = \frac{Percentage\ of\ all\ live\ +\ dead\ cells}{Percentage\ of\ all\ live\ cells}$$

Example:

$$Percentage\ of\ all\ live + dead\ cells\ = (G0 + G1 + S + G2 + M + non - viable)$$

$$= 98.93\ \%$$

$$Percentage\ of\ all\ live\ cells = (G0 + G1 + S + G2 + M) = 78.85\ \%$$

Calculation of coefficient:

$$Coefficient = \frac{98.93}{78.85} = 1.26$$

Calculation of percentage of cells in G0+G1 phase with coefficient:

$$Percentage\ of\ cells\ in\ G0 + G1\ phase = 54.28\ \%$$

$$Coefficient\ X\ percentage\ of\ cells\ in\ G0 + G1\ phase$$
$$1.26\ X\ 54.28 = 68.4\ \%$$

4.3.3 Effects of fatty acids on INS-1 and HCMec/D3 cells

Figures 4.2 and 4.4 show the effects of FAs on cell cycle progression in INS-1 and HCMec/D3 cells. Exposure of INS-1 cells to the VC resulted in approximately 19 % non-viable cells, 67 % of cells in the G0+G1 phase, 8 % of cells in the S phase and 6 % of cells in the G2+M phase. Exposure of HCMec/D3 cells to the VC resulted in approximately 15 % non-viable cells, 56 % of cells in the G0+G1 phase, 11 % of cells in the S phase and 18 % of cells in the G2+M phase. The percentage of non-viable cells is consistent with the data presented in Chapter 3. Some HCMec/D3 cells were also exposed to complete medium for 72 hours. This positive control (CMC) shows that a pro-proliferative response can be elicited in these cells. On average, fewer non-viable cells (9 %) were observed and a greater proportion of cells in the G0+G1 (60 %) phase was detected in the CMC compared to the VC (non-viable: 15 %; G0+G1: 56 %).

In both cell types, exposure to 0.25 mM PA for 48 hours resulted in an absolute increase in the percentage of non-viable cells and a decrease in the proportion of cells in the G0+G1 phase (figures 4.2 and 4.4). However, the exposure of these cells to MePA, the esterified analogue of PA, was comparable to the VC, indicating the requirement of the free carboxyl group for PA to induce cell death. When MePA was combined with PA, the percentage of non-viable cells was comparable to that of PA alone indicating that MePA is not able to protect against PA-induced toxicity. Exposure of both cell types to 0.25 mM OA resulted in the percentage of cells in each phase of the cell cycle comparable to the VC. Interestingly, OA in combination with PA was comparable to OA on its own, indicating the ability of OA to protect against PA-induced toxicity, as also shown in the viability data in figures 3.11 and 3.12.

Figures 4.2 and 4.4 show the percentage of cells in the S and G2+M phases of the cell cycle combined. The data show that 0.25 mM PA on its own (or in combination with MePA) caused a significant decrease in the percentage of cells in the S and G2+M phases ($p < 0.001$). 0.25 mM OA in combination with 0.25 mM PA was able to prevent the cell death caused by PA alone. When used in combination with PA, OA did not cause an increase in the percentage of cells in the S and G2+M phases. These data suggest that OA does not induce a strong pro-proliferative response as part of its mechanism of cytoprotection.

Figures 4.3 and 4.5 show the percentage of cells in the G0+G1, S and G2+M phases after normalisation to account for the non-viable cell population. The percentage of cells in each phase of the cell cycle was comparable to untreated cells, whereby the majority of cells were in the G0+G1 phase and the remaining cells were divided relatively equally between the S and G2+M phases.

Figures 4.3 and 4.5 show the normalised percentages of cells in the S and G2+M phases of the cell cycle combined. These two phases were combined because they represent the dividing cell populations. The data show no significant difference between the VC and any FA-treated cells, alone or in combination. The data suggest that neither SFAs nor UFAs induce a pro-proliferative response or inhibit proliferation in INS-1 and HCMec/D3 cells.

Since both INS-1 and HCMec/D3 cells responded in the same way using the method presented in this Chapter, the evidence from the literature to discuss the effects of different techniques on beta cells and endothelial cells will be combined in the discussion section of this Chapter.
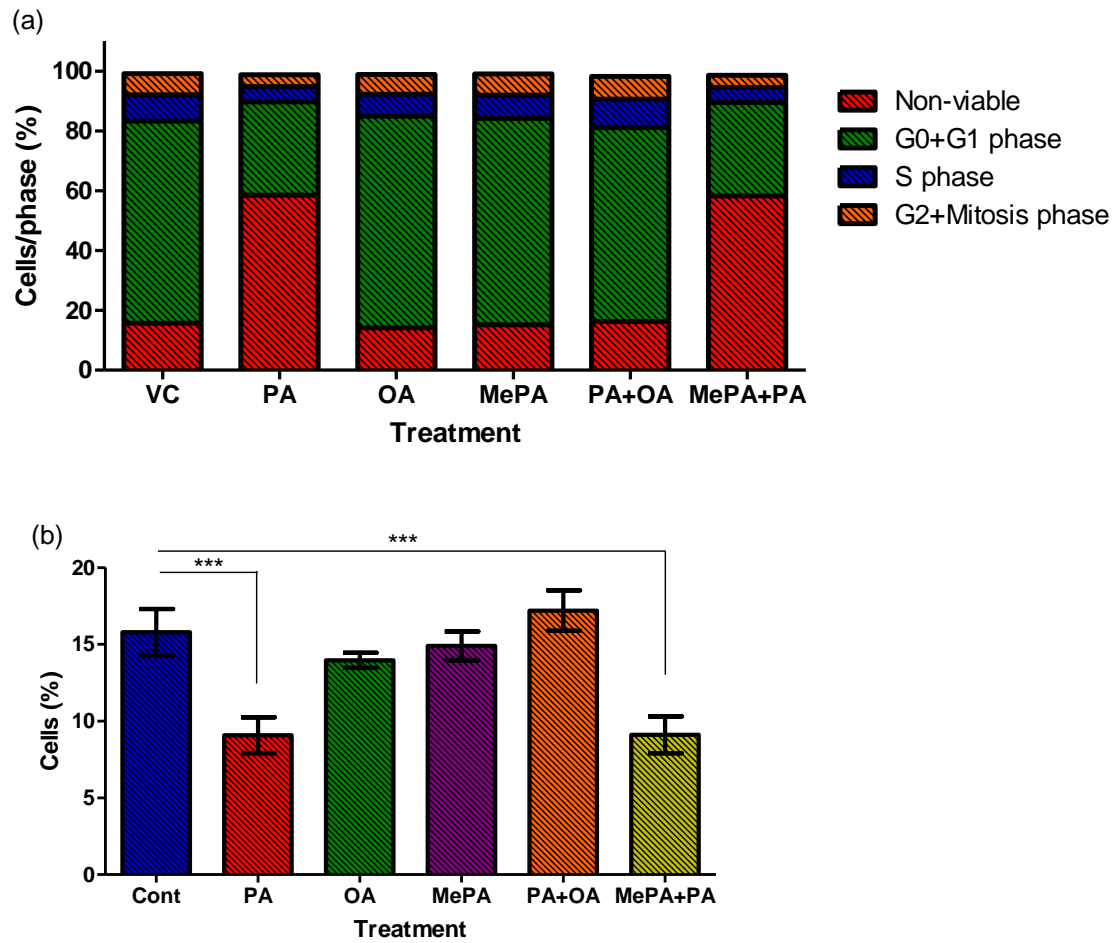
Figure 4.2 Effects of fatty acids and fatty acid analogues on INS-1 cell cycle progression after 48 hours

INS-1 cells were pre-treated with complete medium for 24 hours, then for 48 hours with serum-free medium and 0.25 mM fatty acid treatment: vehicle control (VC) (BSA + EtOH), palmitate (PA), oleate (OA), methyl palmitate (MePA), palmitate + oleate (PA + OA) and methyl palmitate + palmitate (MePA + PA). The data represent four experiments each conducted in triplicate. Cells analysed on BD Accuri™ C6 Plus Flow Cytometer. (a) Percentage of: non-viable cells (red bar); cells in G0+G1 phase (green bar); cells in S phase (blue); cells in G2+M phase (orange). (b) S and G2+M phase data from graph 1 combined. One-way ANOVA with Tukey's multiple comparison test *** ($p<0.001$) n=12. Mean ± SEM.

(a)

(b)
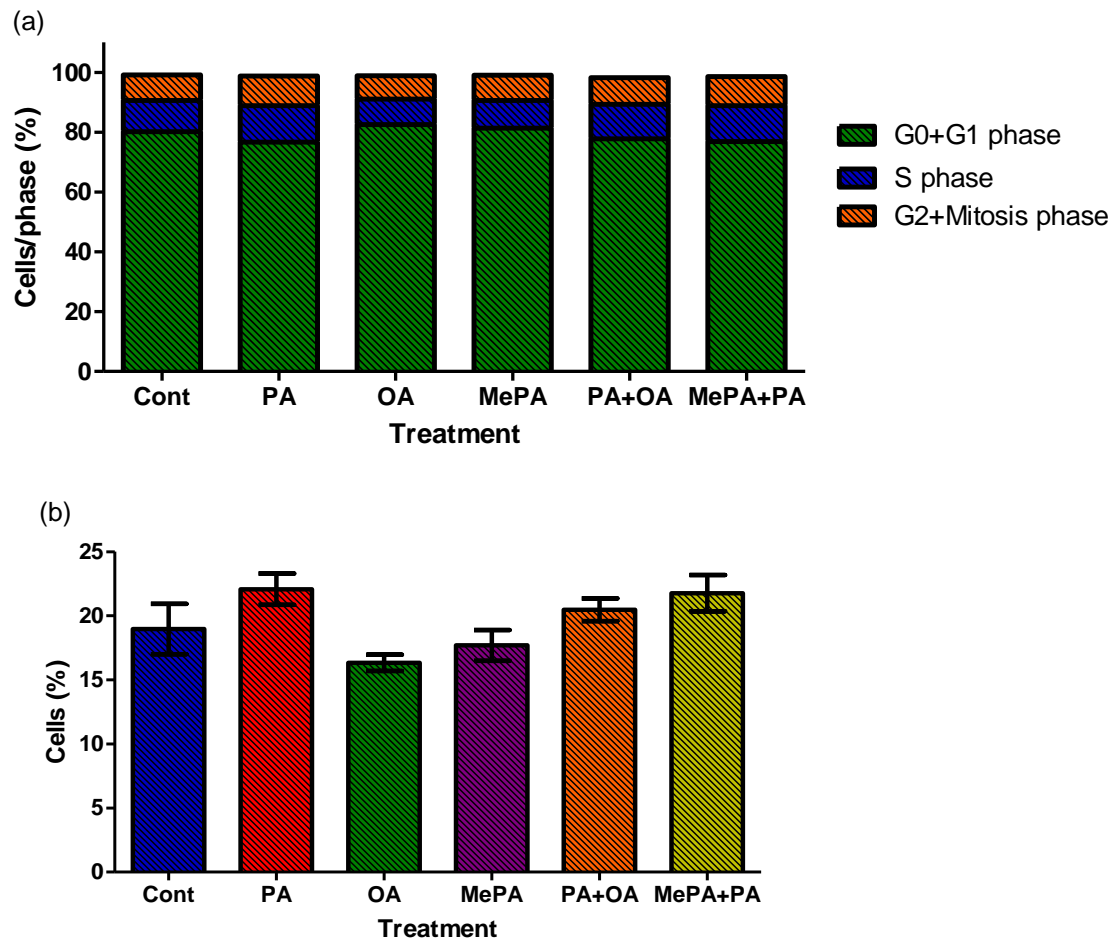
Figure 4.3 Effects of fatty acids and fatty acid analogues on INS-1 cell cycle progression after 48 hours post-normalisation

INS-1 cells were pre-treated with complete medium for 24 hours, then for 48 hours with serum-free medium and 0.25 mM fatty acid treatment: vehicle control (VC) (BSA + EtOH), palmitate (PA), oleate (OA), methyl palmitate (MePA), palmitate + oleate (PA + OA) and methyl palmitate + palmitate (MePA + PA). The data represent four experiments each conducted in triplicate. Cells analysed on BD Accuri™ C6 Plus Flow Cytometer. (a) Percentage of: cells in G0+G1 phase (green bar); cells in S phase (blue); cells in G2+M phase (orange) normalised against the percentage of non-viable cells. (b) S and G2+M phase data from graph 1 combined. One-way ANOVA with Tukey's multiple comparison test. No sig. diff. n=12. Mean ± SEM.
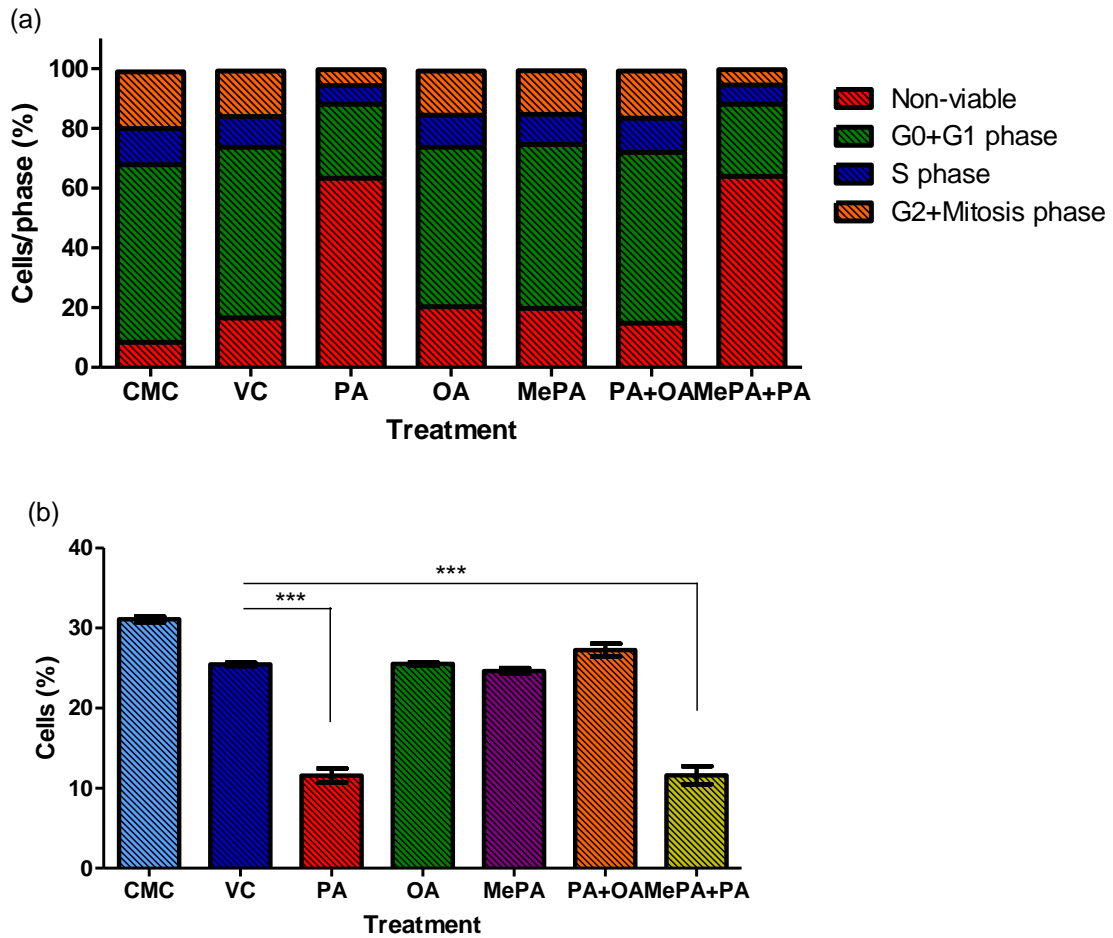
Figure 4.4 Effects of fatty acids and fatty acid analogues on HCMec/D3 cell cycle progression after 48 hours

HCMec/D3 cells were pre-treated with complete medium for 24 hours, then for 48 hours with serum-free medium and 0.25 mM fatty acid treatment: vehicle control (VC) (BSA + EtOH), palmitate (PA), oleate (OA), methyl palmitate (MePA), palmitate + oleate (PA + OA) and methyl palmitate + palmitate (MePA + PA). Cells in the CMC group were exposed to complete medium for 72 hours. The data represent three experiments each conducted in duplicate. Cells analysed on BD Accuri™ C6 Plus Flow Cytometer. (a) Percentage of: non-viable cells (red bar); cells in G0+G1 phase (green bar); cells in S phase (blue); cells in G2+M phase (orange). (b) S and G2+M phase data from graph 1 combined. One-way ANOVA with Tukey's multiple comparison test *** (p<0.001) n=6. Mean ± SEM.

(a)

(b)
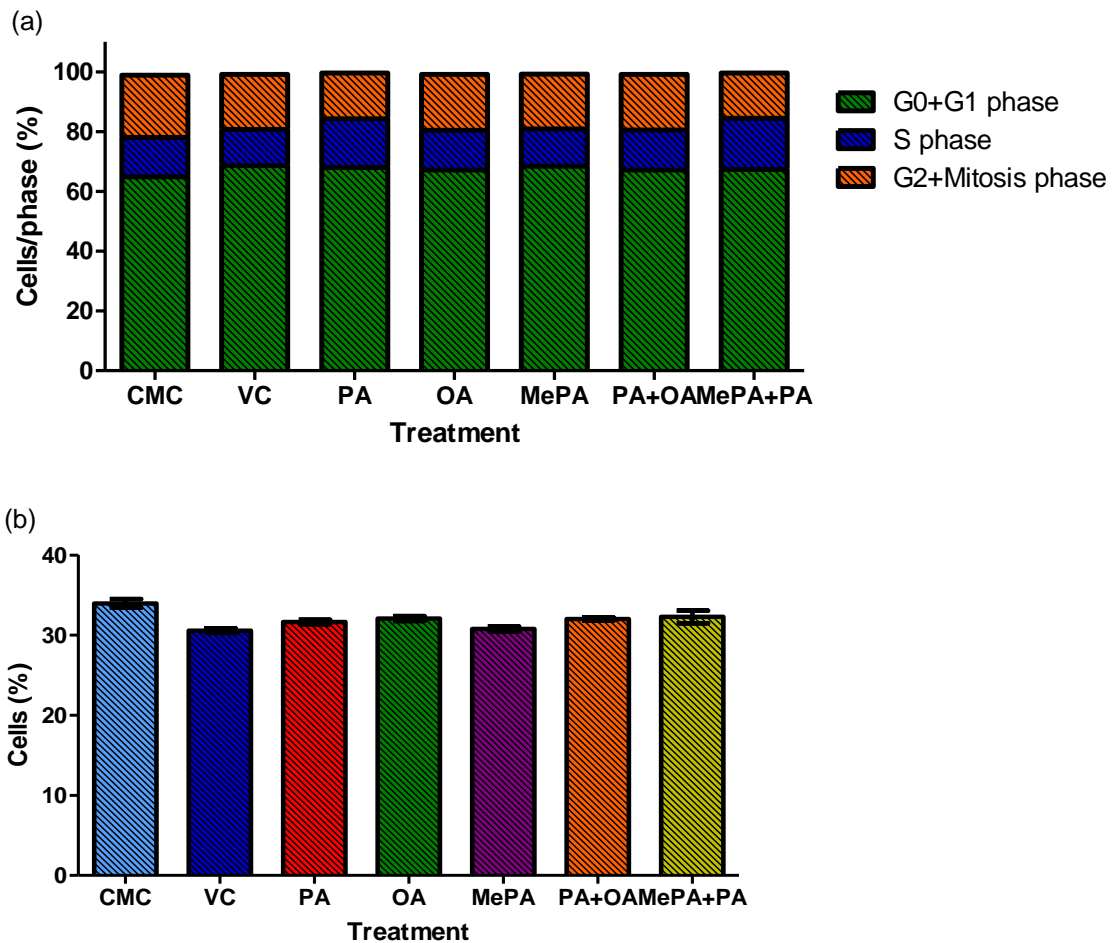
Figure 4.5 Effects of fatty acids and fatty acid analogues on HCMec/D3 cell cycle progression after 48 hours post-normalisation

HCMec/D3 cells were pre-treated with complete medium for 24 hours, then for 48 hours with serum-free medium and 0.25 mM fatty acid treatment: vehicle control (VC) (BSA + EtOH), palmitate (PA), oleate (OA), methyl palmitate (MePA), palmitate + oleate (PA + OA) and methyl palmitate + palmitate (MePA + PA). Cells in the CMC group were exposed to complete medium for 72 hours. The data represent three experiments each conducted in duplicate. Cells analysed on BD Accuri™ C6 Plus Flow Cytometer. (a) Percentage of: non-viable cells (red bar); cells in G0+G1 phase (green bar); cells in S phase (blue); cells in G2+M phase (orange) normalised against the percentage of non-viable cells. (b) S and G2+M phase data from graph 1 combined. One-way ANOVA with Tukey's multiple comparison test. No sig. diff. n=6. Mean ± SEM.

4.4 Discussion

Although BrdU is often considered as the gold standard for measuring cell proliferation (Mead & Lefebvre 2014), there are technical and temporal limitations to this technique. For example, the moment in time which the BrdU nucleotide is added to the cells, and the length of time which the cells are exposed to the nucleotide can affect the final results. BrdU may be added at the beginning, middle or end of the experiment which can result in more or less of the compound being incorporated onto DNA. For example, Pascoe *et al.* (2012) exposed mouse islets, cultured *ex vivo*, to BrdU to the final 24 hours of a 72 hour incubation and did not observe pro-proliferation upon exposure to OA. However, Brelje *et al.* (2017) exposed rat islets, also cultured *ex vivo*, to BrdU during the last 12 hours of cell culture and did observe OA-induced pro-proliferation. These technical differences could have resulted in differential BrdU incorporation into the DNA of cells upon exposure to OA.

Based on the limitations attributed to the BrdU assay, it was decided to utilise an alternative method. I consider that the method presented in this Chapter is superior to that of other cell proliferation methods for the following reasons: (1) it removes from the analysis cells with both intact plasma membranes and fragmented DNA, and cellular aggregates, (2) it separates the proportion of cells into the different phases of the cycle (non-viable, G0+G1, S and G2+M), (3) the nucleotide stain, PI, was added at the end of the experiment so as not to affect normal cellular functions, and (4) it normalises the viable cell population against the non-viable cell population.

A casual consideration of the cell cycle data presented in this Chapter might lead to the conclusion that PA inhibits cell proliferative because there was a large decrease in the percentage of cells in the S and G2+M phases following exposure

to this FA in both INS-1 and HCMec/D3 cells. However, this conclusion is challenged when the data are normalised such that viable cells are compared against the population of non-viable cells. The normalisation process removes any ambiguity that the non-viable cell population might have on the data. This is because the non-viable cells, although having intact plasma membranes, do not have intact DNA, which skews the percentage values obtained for the viable cell population. The non-viable cell population must therefore be removed for the analysis to be valid. Rather than simply removing these data and re-plotting the values, the process of normalisation allows the data to be restructured and prevents confounding factors from affecting the interpretation of the data. In this case, normalising the viable cell population to account for the non-viable cell population improves the integrity of the data.

The post-normalised data for all FAs in both cell types show no differences in proliferation compared to the VC. In the case of PA, since the data show no difference in the percentage of cells in the combined S and G2+M phases, these data suggest that the mechanism of cytotoxicity of PA observed here is probably not due to PA inhibiting cell proliferation. The cytotoxicity observed is therefore likely to be via a different mechanism. In addition, there is no statistically significant increase in the percentage of cells in the S and G2+M phases exposed to OA in combination with PA. These data suggest that OA does not protect against PA-induced toxicity via a pro-proliferative mechanism.

4.4.1 Effects of unsaturated fatty acids on cell proliferation

A study by Ben-Harosh *et al*. (2017) measured relative cell proliferation (cell number) of pancreatic stellate cells after exposure to pathophysiological (0.5 mM) levels of OA and PA. The aim of that study was to determine whether these two most frequently consumed dietary FAs could lead to cell stress. By measuring

cell proliferation, they sought to determine whether the FAs could affect cellular activation and migration. The researchers were interested in understanding whether the cells could undergo compensatory pro-proliferation upon exposure to stimuli inducing stress. Since PA has been shown in various models to induce cell stress, this FA was compared against OA, its non-toxic counterpart. They found that OA was not able to induce cell proliferation in these cells, since the rate of cell proliferation was comparable to the untreated pancreatic stellate cells. The researchers chose to count the cells under a haemocytometer, however, they failed to state whether they included both the viable and non-viable cell populations in the proliferation analysis. In addition, the steps taken to calculate cell proliferation are not described. Since OA failed to provoke a pro-proliferative response, the researchers took this response to be expected as OA does not induce cell stress. The idea that toxic stimuli might induce a pro-proliferative response is very interesting as it highlights the different perspectives when considering whether compounds can or cannot induce pro-proliferation. The researchers suggest that compounds which induce cell stress should provoke pro-proliferation, however, using the method I have presented in this Chapter, a pro-proliferative response was not observed in either the beta or the endothelial cells upon exposure to PA. However, one would not expect to observe a pro-proliferative response *in vitro* because the cells do not have the internal milieu of an organ.

Likewise, it has been shown that OA alone is not pro-proliferative in beta cells of mice (Pascoe *et al.* 2012). In that study, mice were infused with saline, Liposyn II (a fat emulsion), glucose or both Liposyn II and glucose for four days. The aim of the study was to determine whether the presence of elevated free FAs in the circulation would affect beta cell proliferation. Primary beta cells were

isolated and their rate of proliferation compared to that of INS-1 cells using a BrdU-based assay. The authors found that lipid infusion did not alter basal beta cell proliferation in either cell type, nor was significant cell death observed. The incorporation of BrdU into OA-treated cells was comparable to untreated beta cells.

Artwohl *et al.* (2003) employed a more detailed approach to study the cell cycle whereby the proportion of HUVECs in each phase of the cycle were analysed. Similar to the method presented in this Chapter, cells were fixed in ice cold ethanol (75 %), exposed to a solution of RNase A and PI, then subsequently analysed using flow cytometry. They showed that OA marginally, yet statistically significantly, decreased the percentage of cells in the S phase and increased the percentage of cells in the resting, G0+G1 phase. These data suggest that OA does not induce a pro-proliferative response in the cells, possibly because, as suggested by Ben-Harosh *et al.* (2017), OA is not toxic and therefore a compensatory response is not required.

Contrastingly, OA has been shown to induce cell proliferation in rat islets *ex vivo* (Brelje *et al.* 2017), in BRIN-BD11 rat beta cells *in vitro* (Diakogiannaki *et al.* 2007) and in HVSMCs (Lamers *et al.* 2011) using the BrdU assay. It is interesting that some studies find that OA does not affect cell proliferation, whereas others show OA to be pro-proliferative. OA may in fact be pro-proliferative and the different effects seen may be due to differences in cell lines from different species, for example, from the studies conducted by Pascoe *et al.* (2012) and Brelje *et al.* (2017), whereby mice and rats were used, respectively. In addition, the use of cells *ex vivo*, as employed by Pascoe *et al.* (2012) and Brelje *et al.* (2017), does not provide a robust representation of the effects of FAs on beta cells. This is because islets consist of various other cells, including alpha

cells, which may respond differentially to beta cells and may therefore affect the metabolism of FAs and therefore the interpretation of the data.

4.4.2 Effects of saturated fatty acids on cell proliferation

Artwohl *et al.* (2003), Ben-Harosh *et al.* (2017), Diakogiannaki *et al.* (2007), Lamers *et al.* (2011) and Pascoe *et al.* (2012) found that PA is toxic to beta cells and endothelial cells, and also concluded that PA has no effect on cell proliferation.

Work by Ben-Harosh *et al.* (2017) found that PA halted cell proliferation in pancreatic stellate cells. However, what was not clear was whether PA halted cell proliferation or whether the non-viable cell population masked proliferation. What the researchers failed to state was whether they normalised the viable cell population against the non-viable cell population.

Pascoe *et al.* (2012) showed that PA caused a significant decrease in the incorporation of BrdU into the DNA of viable INS-1 cells and hence concluded that PA is able to inhibit proliferation. The researchers concluded that this effect was caused by PA inhibiting cell proliferation, however, this effect is likely to be due to cell death induced by PA. The researchers also wanted to determine whether certain cyclin-dependent kinase inhibitors were affected as a further measure of cell-cycle progression *ex vivo* and *in vitro*. The aim of this analysis was to determine whether expression levels of these cell-cycle regulators were affected by FAs. By studying these regulators, they sought to determine whether FAs would target components upstream of cell proliferation, such as the localisation of proteins responsible for gene regulation. They found that PA did not block the nuclear localisation of cyclin D2, suggesting that if a reduction in proliferation were to be observed, it would most likely be due to an effect downstream of cyclin D2. Cyclin-dependent kinases, such as cyclin-dependent

kinase 4, are responsible for blocking the progression of the cell cycle past the G1 phase. Interestingly, upon exposure of INS-1 cells to PA, an increase in the expression of p16 and p18 inhibitors of cyclin dependent kinase 4 was observed, thus preventing cell proliferation.

Similarly, Artwohl *et al.* (2003) showed that the SFA stearic acid (C18:0), dose-dependently increased apoptosis in HUVECs. The researchers came to this conclusion after they normalised the viable cell population against the non-viable cell population. They observed stearic acid-induced G0+G1 cell cycle arrest, a decrease in the percentage of cells in the S phase, and no change in the percentage of cells in the G2+M phase. A concomitant up-regulation of the cyclin dependent kinase inhibitor p21, a negative regulator of the G0 phase of the cell cycle, was also observed. This is an interesting observation as they suggest that the stearic acid-induced G0+G1-arrest could be interpreted as being responsible for inducing apoptosis.

4.4.3 Limitations to studying cell proliferation

Su & O'Farrell (1998) suggest that when studying cell growth, attention should turn to studying the dysregulation of size (hypertrophy) rather than cell proliferation (hyperplasia). This is because it is worth noting that, although a compound might not affect the cell cycle, cells can grow without dividing; they can undergo hypertrophy, a process by which cells grow in size and where the cell cycle is not altered. In the context of diabetes, it might be worth: (1) considering the use of assays such as cellular hyperplasia, or the duplication of cellular components to study whether cells can compensate for cell death caused by toxic stimuli, or (2) determining whether compounds can affect specific processes associated with cell division, such as the localisation of cell cycle regulators, e.g. cyclin D3, which can lead to the dysregulation of growth. Although

some diabetes research does focus on identifying therapeutic compounds to induce hyperplasia, the focus might require shifting to study hypertrophy and cell-cycle deregulation. This is because cell proliferation is not directly proportional to growth – a reduction in beta cell mass does not necessarily require the induction of cell proliferation because cells can divide without getting larger. Indeed, diabetes research is shifting slightly such that the connections between cell mass and cell proliferation are being investigated. For example, the notion that pancreatic ductal and/ or acinar cells can transdifferentiate into insulin-producing beta cells, without resulting in a hyperplastic response is emerging (Kim & Lee 2016). Hence, the fact that beta cells do not proliferative during adolescence and adulthood is proving irrelevant in identifying therapeutic treatments for diabetes.

In conclusion, the data presented in this Chapter show that OA is not pro-proliferative in either INS-1 beta cells or the HCMec/D3 cells, adding to the existing body of evidence (Artwohl *et al.* 2003; Ben-Harosh *et al.* 2017; Pascoe *et al.* 2012) arguing that the mechanism of OA-induced cytoprotection is not via a pro-proliferative mechanism. The data presented in this Chapter therefore suggest that the mechanism of OA-induced cytoprotection occurs via a different mechanism.

Although the literature is divided as to whether OA is pro-proliferative in both INS-1 and HCMec/D3 cells, the literature states that PA does not inhibit cell proliferation. The data presented in this Chapter add to this body of evidence (Artwohl *et al.* 2003; Ben-Harosh *et al.* 2017; Diakogiannaki *et al.* 2007; Lamers *et al.* 2011; Pascoe *et al.* 2012) showing that PA does not inhibit cell proliferation. These data therefore suggest that the mechanism of PA-induced cytotoxicity is not via the inhibition of cell proliferation.

Lastly, further work, involving the study of the duplication of cellular components to determine whether PA stunts the growth of cells, and subsequently causes cell death, might be worth conducting.

Chapter 5

Development of a methodology using Raman microspectroscopy to study intracellular lipid disposition

5 Development of a methodology using Raman microspectroscopy to study intracellular lipid disposition

5.1 Introduction

5.1.1 Spectroscopy

Spectroscopy is an analytical technique used to analyse the electromagnetic radiation emitted, absorbed or scattered by molecules and/ or the atoms they comprise. The information obtained aids the understanding of the electronic configuration of atoms and their vibrational states.

5.1.1.1 Vibrational states

As very little energy is needed to change the rotation of a molecule, the electromagnetic radiation emitted or absorbed lies in the microwave region. However, the vibrational energy of a molecule changes greatly when exposed to radiation since the change in energy is dependent upon the bond lengths, their strengths and atomic weight. Raman microspectroscopy, for example, cannot measure microwaves, yet molecular changes in vibrational energy can be measured.

5.1.1.2 Raman scattering

Raman microspectroscopy enables the understanding of molecular energy levels by analysing the frequencies present in the radiation scattered by molecules and their constitutive atoms. A laser beam from a monochromatic light source (ω_p) is passed through a sample and the scattered radiation is measured. There are three different forms of outgoing radiation. This is because how the outgoing radiation is emitted is dependent upon whether the incoming radiation

comes into contact with the electronic field of the sample. Some of the radiation that passes through the sample is not scattered and is emitted at the same energy as the incoming radiation. This is termed Rayleigh scattering (ω_p). However, most radiation that passes through a sample is scattered, i.e. incoming photons collide with atoms of the molecule and change their energy states (Toporski, Dieing & Hollricher 2018, p. 50). This is because if the incoming radiation does come into contact with the sample, this radiation will affect the electrical charge distribution of the molecules within the sample (Toporski, Dieing & Hollricher 2018, p. 48). Thus, the outgoing radiation will be representative of the chemical composition of sample and the frequency of the incoming radiation. Since in Raman microspectroscopy the incoming radiation is in the visible spectrum, any Rayleigh scattering will be in the visible spectrum. Photons that lose some of their energy and emerge with a lower energy (and thus a lower frequency) are termed Stokes radiation (ω_s). Photons that gain energy and emerge with a higher energy, and thus a higher frequency, are termed anti-Stokes radiation (ω_{as}) (figure 5.1).
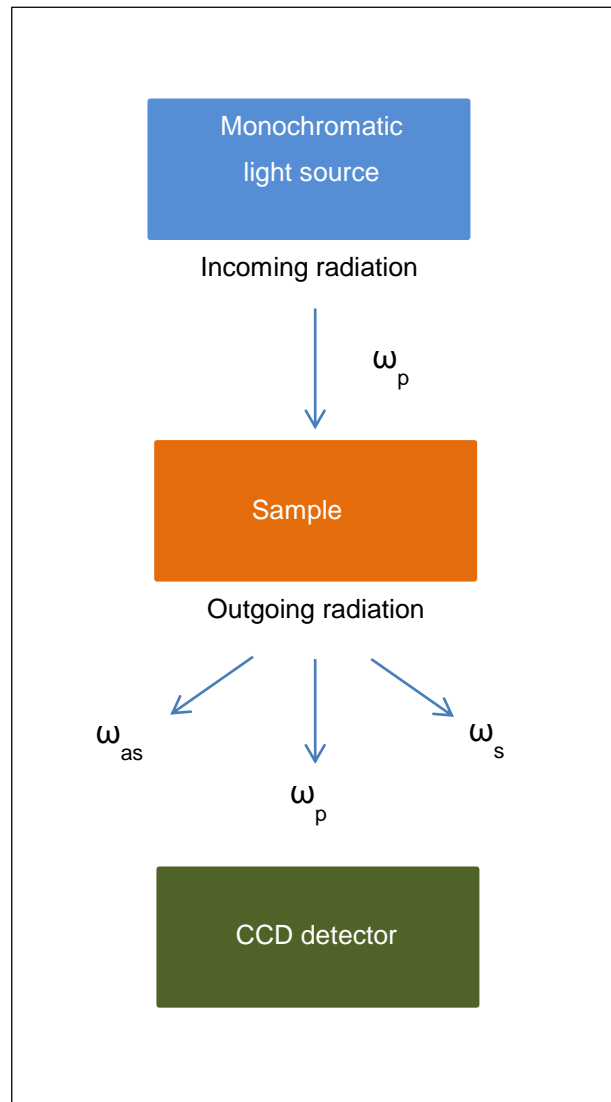
Figure 5.1 Schematic of a Raman scattering experiment

How incoming radiation is scattered is dependent upon whether it comes into contact with the electronic system of the sample: ω_{as} anti-Stokes scatter (scattering of wavelength is higher in energy than incoming radiation), ω_p Rayleigh scatter (scattering of wavelength is the same as incoming radiation), and ω_s Stokes scatter (scattering of wavelength is lower in energy than incoming radiation). Scattered light is detected using a CCD detector.

5.1.1.3 Raman microspectroscopy

Raman microspectroscopy is a label-free technique which is used to study the composition of materials, primarily those which consist of small numbers of substances; such as the pigments within paints or graphene structures. Recently, however, this technique has also been utilised to study changes in the chemical nature of components within cells such as nuclear material (Krafft *et al.* 2006), proteins (Bazylewski, Divigalpitiya & Fanchini 2017) and lipids (Bradley *et al.* 2016; Cao *et al.* 2016; Chen *et al.* 2015; Chien *et al.* 2012; Kochan *et al.* 2013a; Kochan *et al.* 2013b; Kochan *et al.* 2015; Majzner *et al.* 2014; Majzner, Chlopicki & Baranska 2016; Majzner *et al.* 2018; Mansfield & Winlove 2017; Schie *et al.* 2013; Slipchenko *et al.* 2009;Stiebing *et al.* 2014; Stiebing *et al.* 2017; van Manen *et al.* 2005; Yue *et al.* 2012).

In the study conducted by Krafft *et al.* (2006), human embryonic stem cells were exposed to a stress-inducing stimulus for 24 hours which is known to block DNA synthesis. The aim was to determine whether spontaneous Raman microspectroscopy could detect changes in nuclear composition upon cell stress. Cluster analysis identified the nuclear material in the spectral range from 980 cm^{-1} to 1600 cm^{-1}. The spectra were normalised against the phenylalanine peak at 1003 cm^{-1}. Upon exposure to the stress-inducing stimulus the cell nucleus was found to decrease in size, coupled with a decrease in the intensity of the nuclear material, indicating degradation of DNA and RNA: cellular changes which occur during the early stages of apoptosis (Krafft *et al.* 2006).

Despite the conclusions that are drawn from the study conducted by Krafft *et al.* (2006), it should firstly be noted that the cells imaged were not analysed individually. This means that some spectra were in fact representing cellular material from two cells that were imaged side by side. This would normally be acceptable if the spectra from the two cells had been collected separately, then

subsequently averaged. However, this was not the case. Based on this observation, I was determined to analyse all the INS-1 beta cells, in this thesis, individually even if two cells were imaged side by side, then subsequently average the spectra taken from each individual cell. This would ensure that the numbers of cells imaged per treatment were accurately depicted. Secondly, the conclusions drawn from the study conducted by Krafft *et al.* (2006) were based on six cells only. This did not seem adequate, in my opinion, in terms of statistical significance. I was therefore determined to image and analyse as many INS-1 cells per treatment as possible to ensure that the data could be confidently relied upon.

The aim of the study conducted by Bazylewski, Divigalpitiya & Fanchini (2017) was to determine whether spontaneous Raman microspectroscopy could distinguish between modifications to L-cysteine amino acids in proteins and enzymes. In this case, they wanted to monitor the reversible formation and cleavage of disulphide bonds. Cysteine-based samples were dissolved in deionised water and spectra were obtained. The researchers were able to identify the products obtained from chemical reactions using Raman microspectroscopy and claim that their methodology can be applied to the study of enzyme activity of sulphur containing groups.

The study conducted by Bradley *et al.* (2016) employed the use of coherent anti-Stokes Raman scattering microscopy (CARS). This technique, a Raman spectroscopy technique, involves selecting a single vibrational frequency/ wavenumber to generate uni-variate data in the form of Raman maps. This technique cannot, therefore, generate multi-variate data in the form of spectra. The aim of the study conducted by Bradley *et al.* (2016) was to measure lipid distribution in mouse oocytes and embryos. In order to visualise C-H bonds in

LDs, they used the 2850 cm^{-1} vibrational frequency as this wavenumber has been suggested to correspond to C-H bond within R-CH$_2$/ R-CH$_3$ groups within lipids, as described by Baeten *et al.* (1998) (table 5.1). Bradley *et al.* (2016) found that CARS was able to discern the degree of aggregation of LDs and observed that the aggregation of LDs changed significantly during oocyte maturation and during embryo development.

Chien *et al.* (2012) also employed CARS to measure intracellular lipids. The researchers overexpressed two lipid regulatory proteins (one to increase TAG content and another to decrease TAG content) in live Drosophila larvae under fed and starved conditions. The aim was to determine whether CARS could be used to determine changes in the size of LDs. The researchers chose to use the 2845 cm^{-1} vibrational frequency to visualise C-H bonds present in lipids and obtained uni-variate data. They found that CARS was able to identify significant differences in lipid content in oenocytes (which are analogous to hepatocytes in mammals) and body fat, and were able to conclude that the two cell types metabolise and utilise lipids differentially.

The study conducted by Schie *et al.* (2013) aimed to compare lipid composition and lipid ratios within HepG2 hepatocytes using a home-built CARS system coupled with a spontaneous Raman system. HepG2 cells were exposed to 0.25 mM OA and 0.25 mM palmitic acid, alone and in combination, for 24 hours, to determine whether the composition of LDs reflected which exogenous FAs the cells were exposed to - a similar aim to one presented in this thesis, although not executed in the same way. The research conducted by Schie *et al.* (2013) also aimed to either support or counter the research conducted by Listenberger *et al.* (2003), which suggests that OA might be able to protect cells from PA-induced cytotoxicity by shuttling PA into LDs. Schie *et al.* (2013) also coupled CARS with

gas chromatography to determine whether the results from CARS could be replicated and validated using an alternative method. These experiments involved removing the lipid from the cells and converting them to methyl ester FAs and quantifying their composition.

The HepG2 cells were exposed to up to 0.5 mM OA and up to 0.5 mM palmitic acid, alone and in combination, for 24 hours. From their data, they concluded that the FA composition was, on average, similar in all the LDs in the samples they studied. However, only three LDs were studied from one cell per treatment group, using the CARS system, which in terms of statistical analysis does not instil confidence in the data. Unfortunately, the researchers do not state which statistical analysis they used to analyse their data, and the Raman maps of the HepG2 cells are questionable as the nuclei are not clearly visible. In addition to this, the researchers noticed that many cells exposed to 0.25 mM palmitic acid had detached from their substrate after their 24 hour exposure (most likely due to them undergoing apoptosis). Although they obtained Raman maps of cells still adherent to their substrate, it is likely that the lipid within those adherent cells were not representative of healthy cells. Despite these shortcomings, Schie *et al.* (2013) concluded that when HepG2 cells were exposed to equimolar concentrations of OA and palmitic acid, the level of palmitic acid increased, suggesting that their data do support the hypothesis presented by Listenberger *et al.* (2003). However, they failed to realise that this effect was also observed when the HepG2 cells were exposed to palmitic acid alone. If OA had shuttled palmitic acid into LDs, a far greater increase in the percentage of palmitic acid would have been observed in the HepG2 cells versus those exposed to palmitic acid alone. Thus, it cannot be concluded that OA shuttles palmitic acid into LDs

meaning that the data presented by Schie *et al.* (2013) do not support the hypothesis presented by Listenberger *et al.* (2003).

The aim of the study conducted by Chen *et al.* (2015) was to investigate the function of human sweat glands in humans. The researchers did this by applying olive oil onto a sweat gland and imaging the ejection of sweat droplets from the sweat gland. Since sweat is composed of water and some electrolytes, it does not mix with the olive oil. Thus, any movement of the sweat through the gland would be detected via the movement of olive oil on the surface of the gland. The researchers employed the 2845 cm^{-1} wavenumber to image the ejection of sweat droplets from the sweat glands as this wavenumber has been suggested to correspond to C-H bond within R-CH$_2$/ R-CH$_3$ groups within lipids. Using the CARS system, Chen *et al.* (2015) were able to visualise the movement of sweat. They observed that during sweat discharge the olive oil was flushed out from the sweat pore allowing them to visualise and determine the temporal sequence of sweat discharge from the glands.

Yue *et al.* (2012) employed the use of CARS and spontaneous Raman microspectroscopy to study the cell membranes of non-neoplastic human mammary epithelial HMT-3522S1 cells. The researchers treated the cells with ethylene glycol tetraacetic acid, a disruptor of the formation of acini-cell (secretory cells of mammary glands) apical polarity. They explained that these cells must maintain both apical and basal polarity in order to prevent the disruption of mammary tissue architecture and to prevent cancer development. Thus, the aim of their research was to determine whether, using CARS, they could detect changes in lipid ordering in apical and basal membranes and subsequently characterise apical polarity in live mammary acini. Forty cells per treatment were analysed which gave confidence in the statistical analysis. The Raman spectra in

the R-CH$_2$/ R-CH$_3$ region between 2700 cm^{-1} and 3500 cm^{-1} underwent peak fitting analysis whereby the peaks within this region were separated to avoid overlapping peaks. In this case, the peaks in the spectral region described above, were fitted into seven Lorentzian bands. The area under the Curve (AUC) for each of the seven bands were calculated and compared between one another and between different treatments. From this, the researchers observed differential lipid composition between lipids in the apical and basal membranes of acini cells, suggesting differences in lipid packaging.

Cao *et al.* (2016) employed the use of stimulated Raman microspectroscopy coupled with a high-throughput microfluidics system to quantify the formation and distribution of LDs in live, adherent HeLa cells. HeLa cells are human cervical cancer cells and are used extensively in cell biology. Stimulated Raman microspectroscopy is similar to CARS, whereby it generates uni-variate data. HeLa cells were cultured directly onto the microfluidics system and were exposed to increasing concentrations of OA for 3 hours then imaged the cells using the 2850 cm^{-1} wavenumber to detect C-H bonds in CH$_2$ groups within lipids. Cao *et al.* (2016) stated that they used OA to induce lipid accumulation in the HeLa cells. However, they do not state why they specifically used OA, nor do they cite previous literature that have shown or suggested that OA induces the formation of LDs. The researchers conducted one experiment in triplicate and 3466 cells were imaged in total. The researchers found that the size of the LDs was consistent when the HeLa cells were exposed to different concentrations of OA. They also found that the intensity of the LDs did not show significant variation between the treatments. Interestingly, they found that the number of LDs in the HeLa cells increased as the concentration of exogenous OA increased, and from this they concluded that the HeLa cells store excessive lipids by increasing the

number of LDs. However, intercellular heterogeneity was observed, whereby some cells exposed to very low concentrations of OA had large amounts of LDs, whereas at high concentrations of OA, some cells had very few LDs. Cao *et al.* (2016) note the importance of detecting, measuring and characterising sub-populations of cells in order to improve our understanding of basic cell biology and how cells might respond to medications, for example.

Slipchenko *et al.* (2009) employed the use of spontaneous Raman microspectroscopy, CARS and stimulated Raman spectroscopy to investigate the formation of LDs in live cells *in vivo* and *in vitro* upon exposure to deuterated and non-deuterated FAs. Investigations were conducted in live differentiated and undifferentiated murine fibroblast-like 3T3-L1 cells, CHO cells, and subcutaneous adipocytes and sebaceous glands from an ear of a living BALB/c mouse. In order to determine whether certain FAs were present in the LDs of these cells, the Raman spectra of pure FAs were obtained to enable their comparison with spectra obtained from cells. In order to do this, the researchers obtained the spectra from methyl ester FAs: MePA, MeOA and methyl linoleic acid (C18:2).

The researchers wanted to observe how much of the exogenously supplied deuterated palmitic acid had been incorporated into endogenous LDs. Using spontaneous Raman microspectroscopy and CARS, 3T3-L1 cells were exposed to 50 µM deuterated palmitic acid for four days to study *de novo* lipid synthesis. The Raman spectra were normalised against the 1445 cm^{-1} peak as this peak corresponds to C-H bonds in CH_2 groups in lipids. They were then able to compare the relative peak heights of the band at 1654 cm^{-1} which corresponds to C=C bonds in unsaturated lipids. The 1654/ 1445 cm^{-1} ratio for FAs produced via *de novo* synthesis was 0.32 ± 0.04 (mean ± standard deviation), whereas for cells exposed to oleic acid, the ratio was 0.58 (standard deviation not provided).

From this, the researchers concluded that the LDs in untreated 3T3-L1 cells contained a significant portion of SFAs.

The researchers also compared the ratio of the peaks at 2100 cm^{-1}, as this corresponds to C-D bonds found in deuterated compounds and is used as a proxy to detect exogenous FAs, and at 2850 cm^{-1}, as this corresponds to C-H bonds found in CH$_2$ groups in lipids and is used as a proxy to detect endogenous FAs. Differentiated 3T3-L1 cells were exposed to deuterated palmitic acid and non-deuterated oleic acid in a 1:9 molar ratio. Based on the ratios of the peaks corresponding to C-D and C-H bonds, the researchers concluded that the exogenous FAs constituted 19 % of the total lipids studied. From this, they then concluded that LDs accumulate in differentiated 3T3-L1 cells in the presence of exogenous FAs due to free FA uptake as well as *de novo* lipid synthesis. Unusually, the researchers did not study the effects of non-deuterated palmitic acid and non-deuterated oleic acid separately on LD formation in this cell type. Therefore, it would be inaccurate to conclude that deuterated palmitic acid is taken up in such low quantities as instead, the presence of non-deuterated oleic acid may have altered the uptake of deuterated palmitic acid and its incorporation into LDs. A subsequent experiment involved the exposure of undifferentiated 3T3-L1 cells to 50 µM deuterated palmitic acid for four days. As undifferentiated 3T3-L1 cells do not synthesise LDs *de novo*, the aim of the experiment was to determine whether this FA would accumulate within the cell. Interestingly, the researchers observed that LDs were composed of 70 % C-D bonds, inferring that the LDs were 70 % composed of deuterated palmitic acid.

3T3-L1 cells were then analysed via the coupling of spontaneous and stimulated Raman microspectroscopy. Like with CARS, a Raman map was generated for each vibrational frequency selected. Contrast of the LDs,

cytoplasm and the nucleus were compared at 2600 cm⁻¹, 2850 cm⁻¹ and 2935 cm⁻¹. At 2850 cm⁻¹ a bright contrast was observed from LDs, a low contrast from the cytoplasm, and no contrast from the nucleus. At 2935 cm⁻¹ a higher contrast was observed from the cytoplasm and nucleus compared to 2850 cm⁻¹. Contrast nearly disappeared at 2600 cm⁻¹. This was expected as only deuterated bonds appear at this vibrational frequency, as described by van Manen *et al*. (2005) and Stiebing *et al*. (2017).

Slipchenko *et al*. (2009) then investigated the effects of exposing CHO cells to 500 µM oleic acid for 6 hours using spontaneous Raman microspectroscopy and CARS. Three LDs from one CHO cell were analysed using single point spectra and compared to the spectrum of pure MeOA. Untreated cells were found to contain no LDs. However, upon exposure to oleic acid, an increase in the number of LDs was observed, compared to the untreated cells, suggesting that the presence of oleic acid induces the formation of LDs in CHO cells. The three cell spectra were also found to be identical. In addition, upon comparison of the averaged cell spectra with the spectrum of MeOA, the researchers stated that the cell spectrum resembled the spectrum of MeOA. A higher intensity of the peak at 1265 cm⁻¹, corresponding to =C–H bonds, as described by Weng *et al*. (2003) Weng, and at 1654 cm⁻¹ were observed in the cell spectrum compared to the spectrum of pure MeOA. From this, it could be suggested that oleic acid: (1) induces the formation of LDs, (2) induces endogenous LDs to become more unsaturated, and/ or (3) itself becomes incorporated into LDs.

Next, the researchers then determined the 1654/ 1445 cm⁻¹ ratio for FAs in LDs present in subcutaneous adipocytes and sebaceous glands using CARS and second-harmonic generation, a technique which generates contrast and allows for the visualisation of intracellular structures. Similar to the study conducted by

Yue *et al.* (2012), Slipchenko and co-workers conducted peak fitting analysis of the Raman spectra between 2500 cm^{-1} and 3500 cm^{-1}. This spectral region was fitted into six Lorentzian bands and the AUC for each of the six bands were calculated and compared between the two cell types. For subcutaneous adipocytes the ratio was 0.82 ± 0.04, and for sebaceous glands the ratio was 0.29 ± 0.03, suggesting a higher level of saturated lipids in the glands. The 2850/ 2935 cm^{-1} ratio was also compared for the two cell types. A 2.1-fold increase in SFAs in the sebaceous glands was observed compared to the subcutaneous adipocytes, suggesting that lipid packing in sebaceous glands is more ordered than in the subcutaneous adipocytes.

Finally, the researchers conclude that *in vivo* fat contains more UFA than the fat formed via *de novo* synthesis in 3T3-L1 cells. This conclusion was based on the observation that the 1654/ 1445 cm^{-1} ratio for FAs in LDs in the subcutaneous adipocytes was much higher (0.82 ± 0.04) than in the 3T3-L1 cells (0.32 ± 0.04).

The study conducted by van Manen *et al.* (2005) involved using spontaneous Raman microspectroscopy to determine whether it could identify the composition of LDs in human-derived PLB-985 cells, differentiated into neutrophil cells, exposed to deuterated arachidonic acid. It has been suggested that LDs consist of a monolayer of phospholipids (Ohsaki, Suzuki & Fujimoto 2014). Arachidonic acid, an omega-6 polyunsaturated FA consisting of four carbon-carbon double bonds, is thought to be a component of phospholipids within LDs. It has been suggested that these LDs could act as a source of arachidonic acid for the synthesis of eicosanoids. Eicosanoids are signalling molecules made by the oxidation of arachidonic acid or other polyunsaturated FAs. The researchers exposed differentiated PLB-985 cells to deuterated arachidonic acid for 1 hour and obtained uni- and multi-variate data. The =C-H bond within the RHC=CHR

group at approximately 3014 cm^{-1} (Sadeghi-Jorabchi *et al.* 1970; van Manen *et al.* 2005) shifts to the silent region of the spectrum, between 1800 – 2800 cm^{-1}, due to the presence of C-D bonds, as described by van Manen *et al.* (2005), Slipchenko *et al.* (2009) and Stiebing *et al.* (2017). This occurs because deuterium, a heavier isotope of hydrogen, affects the vibrational tendencies of the sigma bond. van Manen *et al.* (2005) observed peaks in the 2220 cm^{-1} and 2249 cm^{-1} regions of the Raman spectrum which they concluded had corresponded to the presence of deuterated arachidonic acid within the cells. The researchers were then able to visualise the deuterated arachidonic acid and determine that it localised closely with LDs using the 1658 cm^{-1} wavenumber corresponding to C=C bonds within UFAs present within LDs, as suggested by Sadeghi-Jorabchi *et al.* (1970) (table 5.1). van Manen *et al.* (2005) then exposed neutrophil cells to latex beads, which were phagocytosed (engulfed) by the cells, and observed where they localised within the cells. It was observed that the membranes of the phagosomes were in close proximity of the LDs consisting of arachidonic acid. Based on this observation, the researchers suggested that arachidonic acid is released from LDs and may be important in the maturation of phagosomes.

Interestingly, van Manen *et al.* (2005) observed that the neutrophils which were inactivated did not take-up FAs or behave in the same way as those that were activated. Inactivated/ quiescent neutrophils contained little or no LDs, whereas the number of LDs appeared to increase upon exposure to deuterated arachidonic acid. Unfortunately, however, the researchers did not state how many cells were utilised per treatment group within the study, nor did the researchers quantify these observations and employ statistical analysis to justify the observations.

Stiebing *et al.* (2014) also exposed cells to deuterated FAs to determine whether spontaneous Raman microspectroscopy would determine whether they were incorporated into LDs. THP-1 monocytes were differentiated into macrophages then exposed to 400 μM deuterated arachidonic acid and deuterated palmitic acid, alone and in combination, for various lengths of time (3, 6, 8, 24 and 32 hours). The study of lipid uptake and storage behaviour in macrophages is important because these cells play a key role in the development of atherosclerotic lesions within the walls of blood vessels. The overexposure of these cells to FAs causes the formation of LDs and gives these cells a foamy appearance. Thus, Stiebing *et al.* (2014) aimed to determine whether these two deuterated FAs localised within LDs in macrophage cells by obtaining uni- and multi-variate data using spontaneous Raman microspectroscopy. Gas chromatography was also employed, similar to the study conducted by Schie *et al.* (2013), to validate the Raman data.

Spontaneous Raman microspectroscopy was able to visualise the lipid content within untreated macrophage cells, however, the vibrational frequency which was utilised to observe the lipid is not mentioned in the research paper. Of the four untreated cells presented in the paper, lipid heterogeneity was observed. The researchers suggest that this heterogeneity was due to the different stages of the cell cycle which the cells were in.

Stiebing and co-workers observed that deuterated arachidonic acid was present in macrophage cells, an observation similar to that reported by van Manen *et al.* (2005), whereby neutrophil cells were exposed to deuterated arachidonic acid. In the macrophage cells a rapid increase of deuterated arachidonic acid in LDs was observed within 3 hours, but levels plateaued at 8

hours. In addition, the area which the LDs occupied did not increase after 8 hours of exposure to deuterated arachidonic acid.

Interestingly, the formation of foam cells was not observed. This could have been because foam cells may not form upon exposure to polyunsaturated FAs. Foam cells may only form upon exposure to SFAs.

Unfortunately, Stiebing *et al.* (2014) did not present the data for the macrophage cells exposed to deuterated palmitic acid alone. They did, however, describe the data obtained. The researchers detected deuterated palmitic acid in almost all LDs within the macrophage cells at all of the time points studied. The biological significance of this observation is not considered.

Upon co-incubation with deuterated arachidonic acid and deuterated palmitic acid, Stiebing *et al.* (2014) observed heterogeneous storage of these two FAs within LDs. It cannot be inferred from these data whether these results support the hypothesis presented by Listenberger *et al.* (2003) that UFAs or polyunsaturated FAs protect cells from the cytotoxic effects of palmitic acid or PA by shuttling them into LDs.

The results from the gas chromatography studies were similar to the Raman results whereby the amount of arachidonic plateaued after 24 hours. The combined Raman and gas chromatography data suggest that arachidonic acid is first stored in LDs where saturation within LDs in reached after 8 hours. For longer incubation times, arachidonic acid is likely to be metabolised into adrenic acid (a FA consisting of two additional carbon atoms in the alkyl chain compared to adrenic acid), and/ or incorporated into phospholipids of cell membranes and organelle membranes. The researchers suggest that the conversion of arachidonic acid to adrenic acid might be more energetically favourable for the storage of arachidonic acid within cells.

The study conducted by Stiebing *et al.* (2014), where THP-1 monocyte cells were differentiated into macrophage cells, was followed up in a study published by Stiebing *et al.* (2017). The same cell type was studied using spontaneous Raman microspectroscopy, stimulated Raman microspectroscopy and CARS. The aim of the study was to expose the macrophage cells to deuterated palmitic acid and track the intracellular mobility of deuterated palmitic acid and the growth of LDs. Using spontaneous Raman microspectroscopy and the 2101 cm^{-1} wavenumber, the C-D bond present within the deuterated palmitic acid was visualised within LDs in the macrophage cells. Raman maps were obtained every 30 minutes for 5 hours. The researchers found that the intensity of deuterated palmitic acid increased over time. Although the trend of the data suggests that FA uptake plateaued after 4 hours of exposure of deuterated palmitic acid, the range of time points was not extensive enough to determine this conclusively. The distribution of the LDs observed in the Raman maps were also seen to change, whereby LDs appeared to arrange themselves in the perinuclear region.

By using the 1650 cm^{-1} wavenumber, the researchers wanted to determine whether C=C bonds, present within UFAs were localised within LDs, and hence gain a better insight into the composition of FAs within the LDs. A C=C signal was detected within LDs indicating the presence of UFAs within the LDs. However, it cannot be determined whether the presence of C=C bonds were attributed to: (1) the unsaturation of palmitic acid to palmitoleic acid, or (2) the bonds present in endogenous UFAs (before the cells were exposed to deuterated palmitic acid).

In addition, the researchers observed that the macrophage cells they imaged were able to take up the FAs because they were viable. However, the cells may have been: (1) pre-apoptotic, or (2) able to tolerate the presence of the elevated levels of deuterated palmitic acid if the cells contained sufficient desaturase

enzymes to convert palmitic acid into palmitoleic acid, as suggested by Eynard (1997).

In order to visualise the uptake of deuterated palmitic acid in real-time, the stokes lasers in the stimulated Raman microspectroscopy and CARS systems which the researchers employed were fixed at 2125 cm^{-1}. The researchers observed that the LDs were highly abundant around the nucleus. Interestingly, two populations of cells were observed. Some cells contained a high concentration of deuterated palmitic acid, whereas some cells contained very low concentrations of deuterated palmitic acid. Stiebing *et al*. (2017) suggest that this lipid heterogeneity might have been due to some cells exhausting their lipid storage capacity faster than other cells, particularly if some cells already had large numbers of LDs to begin with. The researchers suggest that this observed effect could be considered to be a mechanism which protects cells from lipotoxicity. However, why some cells would contain more LDs than others before they had been exposed to any FAs (i.e. why this heterogeneity exists and what its biological significance is) is unclear.

In addition, Stiebing *et al*. (2017) observed was that foam cells did not form when macrophage cells were exposed to deuterated palmitic acid. Similarly, the observation was made in the study by Stiebing *et al*. (2014) that foam cells were not formed upon exposure to deuterated arachidonic acid. It may be the case that foam cells only form under certain conditions, such as upon exposure to SFAs. However, since the formation of foam cells was not observed upon the exposure of macrophage cells to deuterated palmitic acid in the study conducted by Stiebing *et al*. (2017), it could be suggested that foam cells form under more biologically and/ or physically complex conditions. Unfortunately, Stiebing *et al*. (2017) did not clearly state whether the cells visualised in the spontaneous

Raman microspectroscopy studies were the same cells employed in the coherent Raman studies. In addition, it would appear that only four cells were imaged in the coherent Raman studies, which in terms of statistical analysis does not instil confidence in the data.

The aims of the study by Mansfield & Winlove (2017) were to: (1) study the distribution and composition of endogenous LDs, and (2) study the localisation of exogenous FAs in two zones of chondrocyte cells (cells which secrete the matrix of cartilage) in bovine cartilage: the deep and superficial zones. Lipids within cartilage were studied because evidence had suggested that changes in lipid content are associated with osteoarthritic degradation in humans and animal models. More specifically, it had been suggested that SFAs may increase the progression of osteoarthritis.

Spontaneous Raman microspectroscopy was employed to investigate the composition of endogenous LDs in the $2840 - 2850$ cm^{-1} spectral range. In total, cartilage joints from 19 animals were used for the study. The joints were collected from a local abattoir. Multiple samples from 11 cartilage joints were analysed for Raman analysis. Confocal microscopy was employed to investigate the localisation of exogenous LDs using 1 µM of the fluorescent marker BODIPY-palmitic acid (493/503) (BODIPY-PA), a labelled version of palmitic acid employed as a proxy for unlabelled palmitic acid, for various time points. Multiple samples from eight cartilage joints were analysed for the analysis of FA uptake.

From the Raman and confocal studies, Mansfield & Winlove (2017) found that endogenous lipid in the deep zone of the bovine cartilage were more numerous in number and were larger than in the superficial zone. In addition, the endogenous lipid was predominantly unsaturated. Interestingly, the researchers observed that the quantity of lipid within the chondrocytes increased with depth

into the tissue. Lastly, the researchers believe they were the first to have obtained Raman spectra from chondrocyte cells embedded within intact tissue.

The work published by Kochan *et al.* (2013a), Kochan *et al.* (2013b), Kochan *et al.* (2015), Majzner *et al.* (2014), and Majzner, Chlopicki and Baranska (2016), Majzner *et al.* (2018), generated from a collaborative approach to research, describe research which aimed to study the distribution and composition of LDs in liver tissue *ex vivo*, HAECs *in vitro* and HMEC-1 cells *in vitro*. The main findings of these studies are presented below.

The study by Kochan *et al.* (2013a) involved comparing the LD content of livers of 16 week-old diabetic (db/db) and 24 week-old atherosclerotic (ApoE/LDLR$^{-/-}$) mice to the livers of control mice using histochemical staining and spontaneous Raman microspectroscopy. Sections of liver were stained with Oil Red O, a lipophilic dye used to visualise lipid. More lipid was observed in the livers from atherosclerotic (ApoE/LDLR$^{-/-}$) mice compared to the control mice. However, the numbers of mice in the control group was not disclosed in the research paper, and the extent of lipid distribution in the tissues were not quantified. Next, Raman maps were generated of the livers in the 2800 – 3020 cm^{-1} spectral range. The researchers observed that in contrast to the histochemical staining, lipid content was the highest in the livers of the diabetic mice compared to the control mice. The researchers then compared the lipid content of the liver tissues from the diabetic mice with their protein content by generating Raman maps in the 1215 – 1275 cm^{-1} spectral range to identify the amide III region in proteins. From this, they observed signals from proteins in areas close to the edge of the LDs. This is an interesting observation as it has been suggested that LDs contain proteins either on the outer surface (Welte 2007; Wilfling *et al.* 2014) or inside (Ohsaki, Suzuki & Fujimoto 2014). Next, the

researchers compared Raman maps at the 1656 cm^{-1} and 1445 cm^{-1} bands corresponding to C-H bonds within saturated FAs in present within LDs to determine the degree of unsaturation of the LDs. This was done by dividing the average peak area of the band at 1656 cm^{-1} by the average peak area of the band at 1445 cm^{-1}. The researchers found no change in the degree of unsaturation of the LDs within livers from any of the groups of mice.

A similar study was published by Kochan *et al.* (2013b) where liver tissue from six month-old atherosclerotic (ApoE/LDLR$^{-/-}$) mice, who were fed a control diet, were examined via spontaneous Raman microspectroscopy, infrared spectroscopy and histochemical staining. Unfortunately, few conclusions were made regarding the lipid state of the tissue from the mice. For example, ratios of the band intensities 1656 cm^{-1} and 1444 cm^{-1} were supposedly calculated from the LDs from within the tissue, however, the results were not shown. From the infrared measurements, the presence of cholesterol was observed in small quantities in some areas, yet this was not observed in the Raman maps. Lastly, the researchers stated that the lipid-rich tissue from the livers of the atherosclerotic mice had low protein content. This is an interesting observation as the opposite phenomenon was observed in the livers of the diabetic mice in the study by Kochan *et al.* (2013a), as described previously.

A follow-up study by Kochan *et al.* (2015) involved characterising lipids in the livers of mice. Similar to the previous studies conducted by Kochan and co-workers, the aim of this study was to determine whether spontaneous Raman microspectroscopy could determine the chemical composition of lipids in the livers of mice with non-alcoholic fatty liver disease. Two mice models which exhibited macrovesicular and microvesicular steatosis were employed. Within these groups, some mice were fed a high fat diet and others were fed a low

carbohydrate, high protein diet. The researchers observed LDs in both groups of mice. The livers of mice model exhibiting macrovesicular steatosis developed large LDs, however, the mice models developed small LDs. The degree of saturation of the LDs was then investigated by comparing the ratios of the Raman bands at 1659 cm^{-1} and 1446 cm^{-1}. Interestingly, in both groups of mice, a significant decrease in the unsaturation of the LDs was observed compared to the LDs in the control cells.

The study by Majzner *et al.* (2014) involved exposing liver tissue *ex vivo* and endothelial cells *in vitro* to arachidonic acid, then characterising the composition of the LDs using spontaneous Raman microspectroscopy. Spectral characterisation was achieved by comparing cell spectra with reference lipid spectra. Three male C57BL/6J mice were fed a high fat diet (consisting of 60 % of calories from saturated fat) for six weeks, and three control mice were fed a standard diet for six weeks. In addition, primary HAECs were exposed to 25 μM arachidonic acid for 24 hours. The researchers do not state what vehicle this FA was dissolved in, however, it can be assumed it was dissolved in sterile water because they say that the control cells were exposed to sterile water in place of the FA. Many studies previous to this study state that FAs must be dissolved in BSA in order to best-replicate physiological conditions. Thus, unfortunately, the results from the study conducted by Majzner *et al.* (2014) cannot be directly compared with other studies.

Further, in order to obtain a more accurate representation of the degree of saturation of LDs in the endothelial cells, 3D Raman maps of LDs were acquired. This involved 'depth profiling' the cells, a process whereby the cells are measured in 2D layers and then combined to form a 3D image. In this case, there were nine layers in a stack for every 1.0 μM in the z-direction. From the data, the

researchers observed the formation of LDs as a result of the uptake of arachidonic acid, and the cell spectra of the LDs indicated that their main component was arachidonic acid. The HAECs were subsequently stained with Nile Red, a lipophilic dye, and were studied under confocal microscopy. Although changes in LD content within the cells were not quantified, and the numbers of cells studied per study was not disclosed in the journal paper, the researchers concluded that the cells treated with arachidonic acid contained more LDs than in the control cells, and inferred that this observation concurred with the observations from the Raman results.

Lastly, to determine the degree of LD unsaturation in liver tissue, Majzner et $al.$ (2014) compared the ratios of the 1656 cm^{-1} and the 1444 cm^{-1} Raman bands from the spectra corresponding to LDs. This analysis was conducted despite the observation by Rygula et $al.$ (2013) that the 1656 cm^{-1} wavenumber also corresponds to the Amide I stretching vibration mode, C=O which is present within proteins. From their analysis, Majzner et $al.$ (2014) concluded that the distribution of saturated versus unsaturated lipids in liver LDs was homogenous.

Similar to the study conducted by Majzner et $al.$ (2014), the study by Majzner, Chlopicki and Baranska (2016) involved exposing HAECs to 10 µM or 25 µM arachidonic acid or eicosapentaenoic acid (an omega-3 polyunsaturated FA) for 24 hours and employing spontaneous Raman microspectroscopy to investigate the uptake, distribution and size of LDs formed in these cells. In addition, the cells were exposed to various concentrations of 1-methylnicotinamide hydrochloride, a metabolite of nicotinamide, which has been implicated in inducing certain effects in the endothelium, such as anti-inflammatory effects. Previous work by Majzner et $al.$ (2014) had suggested (using spontaneous Raman microspectroscopy) that exposing HAECs to arachidonic acid and

eicosapentaenoic acid, separately, resulted in the spectra of LDs containing Raman bands similar to those found in the Raman spectra of those FAs. Thus, Majzner, Chlopicki and Baranska (2016) sought to determine whether the formation and composition of endothelial cells exposed to those two FAs in the presence of 1-methylnicotinamide hydrochloride affected the formation and composition of LDs. To determine the degree of unsaturation of the LDs within the cells, the ratio of the Raman bands at 1659 cm^{-1} and 1446 cm^{-1} were compared. For each experimental condition, at least three biological replicates were seeded and at least five cells were analysed by spontaneous Raman microspectroscopy.

Firstly, in order to determine the extent to which these two FAs were incorporated into the LDs of the HAECs, 3D Raman maps at the 3000 – 3030 cm^{-1} band were generated. Analysis of the Raman maps indicated the incorporation of these two FAs in the LDs of HAECs exposed to them. In addition, it was observed that cells exposed to 10 µM arachidonic acid/ eicosapentaenoic acid formed smaller LDs relative to the cells exposed to 25 µM arachidonic acid/ eicosapentaenoic acid, suggesting that the size of LDs is dependent upon the [FA]. The spectra corresponding to the LDs within these cells identified spectral features typically exhibited in the pure spectrum of these two FAs.

Next, the researchers studied the effect of exposing HAECs to 100 µM 1-methylnicotinamide hydrochloride in the absence and presence of arachidonic acid/ eicosapentaenoic acid. In the absence of either of these two FAs, 1-methylnicotinamide hydrochloride did not induce the formation of LDs. However, in the presence of arachidonic acid/ eicosapentaenoic acid, 1-methylnicotinamide hydrochloride seemed to potentiate the formation of LDs, suggesting that 1-methylnicotinamide hydrochloride was able to facilitate the uptake of arachidonic

acid/ eicosapentaenoic acid into LDs. This was observed despite there not being any Raman evidence indicating that 1-methylnicotinamide hydrochloride had been taken up by the cells. Therefore, the mechanism by which LD formation was potentiated remains unclear.

The researchers also employed the histochemical stain Nile Red to visualise lipids under fluorescence microscopy. For each experimental condition, three biological replicates were prepared and at least 35 images from each replicate were analysed and the standard deviation calculated. The results were quantified whereby the number of intracellular LDs were counted per treatment group. It was observed that the largest number of LDs within cells, on average, were those exposed to 25 µM arachidonic acid and 25 µM 1-methylnicotinamide hydrochloride.

Similar to the previous studies published by Majzner and co-workers in 2014 and 2016, the study by Majzner *et al.* (2018) involved employing spontaneous Raman microspectroscopy to determine the chemical composition of LDs within endothelial cells exposed to polyunsaturated FAs. Contact atomic force microscopy was also employed to investigate whether the exposure of the endothelial cells affected the stiffness of the plasma membrane.

HMEC-1 microvascular endothelial cells were exposed to 10 µM or 25 µM arachidonic acid, deuterated arachidonic acid, eicosapentaenoic acid and docosahexaenoic acid (an omega-3 polyunsaturated FA) for 24 hours. At least three biological replicates were prepared for each experiment with at least five to eight technical replicates within each biological replicate. Interestingly, the researchers observed the formation of LDs upon exposure to arachidonic acid and eicosapentaenoic acid, separately, however, no accumulation of LDs was observed upon exposure to docosahexaenoic acid. This suggests that

docosahexaenoic acid was degraded or possibly converted to a different FA which was not incorporated into LDs. Unfortunately, however, the researchers failed to quantify the changes observed which does not add confidence to their final conclusions.

The results from the atomic force microscopy experiments, which were performed on randomly selected cells, demonstrated that the presence of LDs in the endothelial cells increased the stiffness of the plasma membranes. However, whether the increased stiffness of the plasma membrane of cells was caused by: (1) a change in the chemical composition of the plasma membrane, or (2) an increase in cytoplasmic surface tension caused by an increase in the presence of cytoplasmic LDs. To be able to determine the cause of the increased stiffness of the plasma membrane of cells, I would advise researchers to measure the permeability of plasma membranes. If the permeability of the plasma membrane decreases after cellular exposure to polyunsaturated FAs, this would suggest that the composition of the plasma membrane had been altered, and could justify the observed stiffness in the plasma membranes. However, if no change in the permeability of plasma membranes is observed, then the observed stiffness of the plasma membranes could be as a result of the increase in cytoplasmic surface tension. This could make it seem like the cell is stiffer.

5.1.1.4 Measuring cellular molecules

The ability to measure the composition of intracellular FA stores in beta cells is of interest to researchers studying diabetes because some FAs are associated with the destruction of beta cells. Therefore, understanding how FAs are metabolised and distributed within cells is important. Various techniques, involving labelled and label-free FAs have attempted to address this question. Studies have shown that Raman microspectroscopy can detect not only the

composition of fatty stores but also their size, number and spatial distribution (Bradley *et al.* 2016; Chien *et al.* 2012). Although work has shown that fluorescently-labelled palmitic acid accumulates in the Golgi apparatus (Corcoran, unpublished work), it has been difficult to determine the spatial distribution of fluorescent UFAs since these are not commercially available. Raman microspectroscopy might allow us to determine the differences in the spatial distribution of SFAs and UFAs in INS-1 beta cells, thus furthering our understanding of FA-induced toxicity. It is important to note that this technique, however, cannot distinguish between changes in diacylglycerol and TAG formation as these are structurally too similar. In addition, it is not possible for this technique to distinguish between glycerol-bound FAs, the bilayer lipid structure which cell membranes are composed of, and the monolayer of lipid membranes which organelles are composed of. This could mean that the lipid structures observed in the Raman maps presented in this thesis are composed of a combination of LDs and membrane structures. However, it is unlikely that lipid structures within membranes were detected because if they were, the plasma membrane of the cells analysed would be clearly demarcated with a more intense yellow colour compared to the cytoplasm.

Using radiolabelled FAs, the study by Akoumi *et al.* (2017) showed that exposure to OA induced the formation of lipid droplets in H9C2 cardiomyocytes, whereas PA was found to poorly induce the formation of lipid droplets. This was also observed when Listenberger *et al.* (2003) exposed CHO cells to radiolabelled OA and PA. This phenomenon was also observed when Cao *et al* (2016) exposed HeLa cells to 1.2 mM non-radiolabelled OA, when Slipchenko *et al.* (2009) exposed CHO cells to 500 µM non-radiolabelled oleic acid, and when Plötz *et al.* (2016) exposed INS-1 beta cells to 100 µM non-radiolabelled oleic

acid. Further, Listenberger *et al.* (2003) suggest that OA might shuttle PA into TAG, acting as the principal mechanism by which cell death is evaded (Listenberger *et al.* 2003).

Techniques, such as Gas Chromatography – Mass Spectrometry, have shown that the exposure of BRIN-BD11 insulin-producing beta cells to SFAs and UFAs, alone and combination, results in the total lipid content changing to reflect the FA they have been exposed to (Diakogiannaki *et al.* 2007). This suggests that changes in lipid droplet-content might be dependent upon the species of FA that the cells are exposed to. In an attempt to visualise changes to lipid droplets *in situ*, studies using markers, such as Oil Red O, Nile Red and BODIPY-PA, have proven useful, yet inconclusive. In a study by Plötz *et al.* (2016) INS-1 cells were exposed to SFAs and UFAs, then subsequently stained with Oil Red O to study changes in lipid distribution. The researchers found that UFAs strongly induced the formation of lipid droplets compared to the untreated cells, whereas SFAs only induced minor lipid droplet formation. No correlation between cytoprotection and the ability of LDs to form, upon FA co-incubation, was observed. In addition, not only can it be argued that fluorescent dyes can detrimentally affect the physical processes of NLD formation, but the results from experiments emploing the use of fluorescent dyes can be misleading. This is because changes in saturation and chain length of the carbon chain of Fas cannot be inferred from the distribution and localisation of the emitted flourescence from fluorescent dyes.

Since cells consist of a plethora of different chemical entities, our ability to measure changes in chemical composition is extremely challenging. Raman microspectroscopy can quantify the disposition of lipid within cells, thus it can be considered to be superior to other techniques which aim to measure these cellular changes. Raman microspectroscopy was therefore employed in this thesis to

study lipid disposition within cells. In this Chapter, I describe a comprehensive methodology to quantitatively study changes in the distribution and composition of NLDs in INS-1 cells exposed to non-esterified and esterified FAs. This method can be adapted for use in any adherent cell type.

5.2 Instrument set-up and data acquisition

Raman maps were acquired on a WiTec alpha 300r Raman microspectrometer with a 532 nm (green) laser with 16 mW power at the sample and a 63x INA water immersion objective (Zeiss WPlan Apochromat). A few drops of water were placed on the coverslip for the water immersion objective, and maps were collected at room temperature. The maps covered the entire spectral range from 0 cm^{-1} to 3800 cm^{-1} with 4 cm^{-1} spectral resolution. An integration time of 0.1 s and a 600 g/ mm grating was found to provide a satisfactory compromise between the spatial resolution and mapping time.

5.2.1 Rationale choosing the 2845 ± 10 cm^{-1} band for analysis

In order to study global changes in the lipid disposition within INS-1 cells, it was important to select a wavenumber which could identify the presence of lipids, preferably in the form of LDs. Table 5.1 consists of the Raman band assignments of FAs within intracellular LDs. Specifically, it includes only the assignments for the alkyl chain, i.e. carbon-carbon and carbon-hydrogen bonds, and does not include carboxyl group assignments. This section highlights some concerns researchers may have when deciding which wavenumber to choose in order to best-represent the lipid content within eukaryotic cells.

The bands at 1444 cm^{-1} and 1310 cm^{-1} correspond to the scissoring (Sadeghi-Jorabchi et al. 1970) and twisting vibrations (Baeten et al. 1998) of the C-H bond within the CH$_2$ group, respectively (table 5.1). It was decided not to use these wavenumbers to measure changes in lipid disposition for this study since

it would not be possible to distinguish between the incorporation of SFAs or UFAs into LDs.

The band at the 1050 – 1150 cm^{-1} spectral range corresponds to the C-C stretching vibration mode within alkyl chains of lipids and FAs, as described by Chan *et al*. (2005) (table 5.1). This region can therefore be measured to determine changes in the saturation of the alkyl chain. However, this region was not chosen for the study presented in this thesis because the peaks in this region are very low in absolute intensity. It would, therefore, be difficult to be sure if a change in intensity were true, as a large change in intensity would need to occur to indicate a change in alkyl saturation.

The band at the 2800 – 2970 cm^{-1} spectral range corresponds to the stretching vibration mode of the C-H bond within both CH_2 and CH_3 groups. This region can be used to indicate changes in the saturation of alkyl chains as the saturation/ unsaturation of the carbon chain affects the stretching vibration mode of the C-H bond. The study of this region would serve as a proxy for measuring change in the saturation of the carbon chain, and thus would be informative. However, currently, no Raman spectroscopic system is able to differentiate between two FAs which have the same saturation content but have small changes in the length of the carbon chain.

Based on the Raman regions of lipid described above, and the observation that others (Chen *et al*. 2015; Chien *et al*. 2012; Mansfield & Winlove 2017; Nan, Potma & Xie, 2006) have used the 2845 cm^{-1} region (either alone or including an extended band width of ± 10 cm^{-1}), or the 2850 cm^{-1} region (Bradley *et al*. 2016; Cao *et al*. 2016; Slipchenko *et al*. 2009) for studying changes in lipid distribution and/ or disposition within biological material, the 2845 ± 10 cm^{-1} spectral range was chosen to determine whether exposing INS-1 cells to differential FAs affects

the disposition of intracellular lipid. This spectral range was utilised to collect uni-variate data for determining changes in lipid distribution and concentration, the method for which is further described in section 5.6.1.

Challenges were faced when determining the most suitable method to measure changes in the composition of lipid. A method was required to be able to determine whether there had been an increase or decrease in the saturation content of lipid within cells. This type of analysis is known as multi-variate analysis and is further described in section 5.6.2.1.

It should be noted that Raman microspectroscopy is particularly suited for the analysis of lipids compared to other techniques, such as infrared spectroscopy. This is because water and aqueous environments have a strong infrared scattering cross-section, whereas water has a very weak Raman scattering cross-section (Tipping *et al.* (2016). This, therefore, makes it difficult to study molecules in aqueous environments using infrared spectroscopy. In addition, the Raman band for water is above 3014 cm^{-1} (Sun 2009) which is outside the 2800 – 2970 cm^{-1} region which corresponds to C-H bonds within R-CH$_2$/ R-CH$_3$ groups. Furthermore, lipids exhibit a large Raman scattering cross-section (Stiebing *et al.* 2017). Thus, researchers can study lipids using Raman microspectroscopy: (1) without having to be concerned about the band for water obscuring the band for lipid, and (2) because this method is particularly suited for visualising the distribution and composition of lipids.

Table of assignments of the main Raman bands of lipids		
Raman shift (approx. cm^{-1})	Group (bond), vibration-type	Reference
1050 – 1150	R-$(CH_2)_n$-R (C-C), stretch	Chan *et al.* (2005)
1250 – 1300	RHC=CHR (=C–H), in-plane bend	Weng *et al.* (2003)
1310	R-CH_2 (C-H), twisting out-of-plane bend	Baeten *et al.* (1998)
1444	R-CH_2 (C-H), scissoring in-plane bend	Sadeghi-Jorabchi *et al.* (1970)
1661	RHC=CHR (C=C), *cis* stretch	Sadeghi-Jorabchi *et al.* (1970)
1670	RHC=CHR (C=C), *trans* stretch	Bailey & Horvat (1972)
2800 – 2970	R-CH_2/ R-CH_3 (C-H), symmetric stretch	Baeten *et al.* (1998)
3014	RHC=CHR (=C-H), asymmetric stretch	Sadeghi-Jorabchi *et al.* (1970)

Table 5.1 Table of assignments of the main Raman bands of the alkyl chain within lipids/ FAs

The assignments of the main Raman bands of lipids/ FAs are shown in this table. The Raman shifts listed include those that are only associated with the alkyl chain within lipids and FAs, i.e. carbon-carbon (C-C/ C=C) and carbon-hydrogen (=C-H/ C-H) bonds. The table does not include carboxyl group assignments. The Raman shifts are presented as approximate cm^{-1} values. The types of vibration shown are either stretch vibrations or bending vibrations (also known as deformations).

5.3 Cell culture

Although Raman mapping of live cells has been described in the literature by Draux *et al.* (2008), Klein *et al.* (2012), Slipchenko *et al.* (2009), Smith, Wright & Ashton (2016), I chose to fix the INS-1 cells instead of mapping them live. This was to avoid complications arising from physical movement and structural or metabolic changes occurring in the cell during the inevitably long mapping time and increased sensitivity to radiation damage.

5.3.1 Seeding of beta cells

INS-1 cells were cultured and subcultured, as described in sections 2.1.1.1 and 2.1.1.2. 1x borosilicate glass, round coverslip (Ø 13 mm, Scientific Laboratory Supplies) was added per well in a 24-well plate (Sarstedt). Coverslips were prepared as follows: wash for 1 hour in 1 M HCl, rinse with ddH$_2$O, rinse with 70 % (v/v) EtOH, and store in 100 % EtOH. Cells were seeded at 1 x 10^5 cells per well in complete medium and were incubated for 24 hours. The FA-BSA working solutions were made, as described in section 2.1.4, and incubated at 37 °C for at least 1 hour, as described by Dhayal & Morgan (2011), prior to the addition to the cells. The complete medium was removed, 450 µl serum-free medium was added per well, and 50 µl treatment was added to the appropriate well to give a final volume of 500 µl. VC–treated cells were exposed to BSA and EtOH only, with the final percentages at 0.9 % (w/v) and 0.5 % (v/v), respectively.

After 24-hour exposure to the treatment the cells were fixed. 4 % (w/v) 400 µl cold paraformaldehyde (PFA) made up in PBS was added to each well (without the removal of the medium from the wells) and the cells were incubated at 37 °C for 10 minutes. All liquid was subsequently removed from the wells before the further addition of 400 µl PFA. The wells were incubated for 15 minutes at room temperature. The PFA was removed from the wells before the cells were

subsequently washed once with 500 μl sterile PBS for 1 minute. The PBS was removed from the wells before a further 500 μl PBS was added. The coverslips were stored in PBS for up to 1 hour before being transferred onto Superfrost Plus glass slides (25 x 75 x 1.0 mm, Thermo Fischer Scientific).

5.3.2 Fixing and preparing the beta cells for Raman microspectroscopy

The coverslips were removed from the wells carefully with tweezers and a needle. The coverslip was dipped in PBS to wash residual medium or treatment from the surface of the cells. The coverslip was placed, cells facing down, onto the surface of a Superfrost Plus glass slide. Excess PBS was dried and nitrocellulose was immediately added to the rim of the coverslip and glass slide to create a seal, as described by Mansfield & Winlove (2017). The cells were analysed on the microspectrometer within nine days of sealing with nitrocellulose. Before the cells were analysed, the upward facing side of the coverslip was cleaned using a cotton bud with 70 % (v/v) EtOH to remove any adherent cells and debris.

Immunocytochemical analysis of cells grown on coverslips involves fixing coverslips onto Superfrost Plus glass slides using fluorescence mounting medium (Dako). An issue for Raman mapping was potential contributions to the spectra or to the background from the mounting medium. A comparison was therefore undertaken of mounted and unmounted cells. Borosilicate glass does not show a signal on the spectrum between 2800 cm^{-1} and 3100 cm^{-1}, thus a signal should not be observed in this region of the spectrum. Only a signal should be observed from the cell itself. The mounting medium coated both the substrate and the cell. A spectrum of the substrate was measured. It was found that the mounting medium generated a signal where there should not be one (figure 5.2). A spectrum of the cell was also measured. The spectrum was found to be the

same as that obtained from the substrate. The mounting medium therefore interfered with the spectral region of interest for the study of intracellular lipids: the C-H stretching vibration mode between 2800 cm^{-1} and 3100 cm^{-1} (compare figures 5.2 and 5.3), thereby obscuring any signal arising from the cell. This trial revealed the sensitivity of the Raman technique and highlighted the importance of optimising the method for fixed cells.
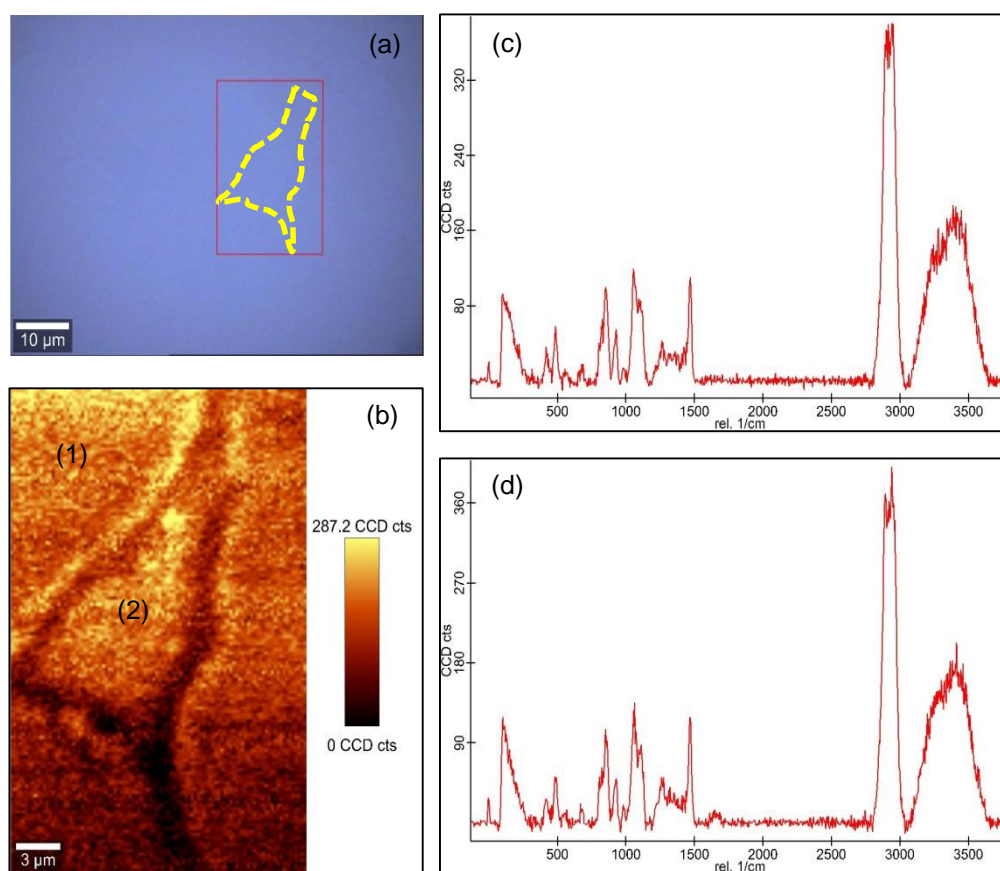
Figure 5.2 Intra- and extra-cellular spectra of a beta cell fixed with mounting medium

INS-1 beta cells were treated with complete medium for 72 hours. The cells were fixed onto a Superfrost Plus glass slide with mounting medium. The coverslip and glass slide were sealed with nitrocellulose. (a) White light image of beta cell, red box drawn around single cell (yellow dotted line). (b) Raman map using the band at 2845 ± 10 cm^{-1} with a 0.5 s integration time. Spectrum (c) corresponds to the area outside the cell (1) (the substrate coated in mounting medium). Spectrum (d) corresponds to regions within the cell (2), also coated in mounting medium. No differences were seen within the spectral region of interest (2800 – 3100 cm^{-1}) between spectra (c) and (d).
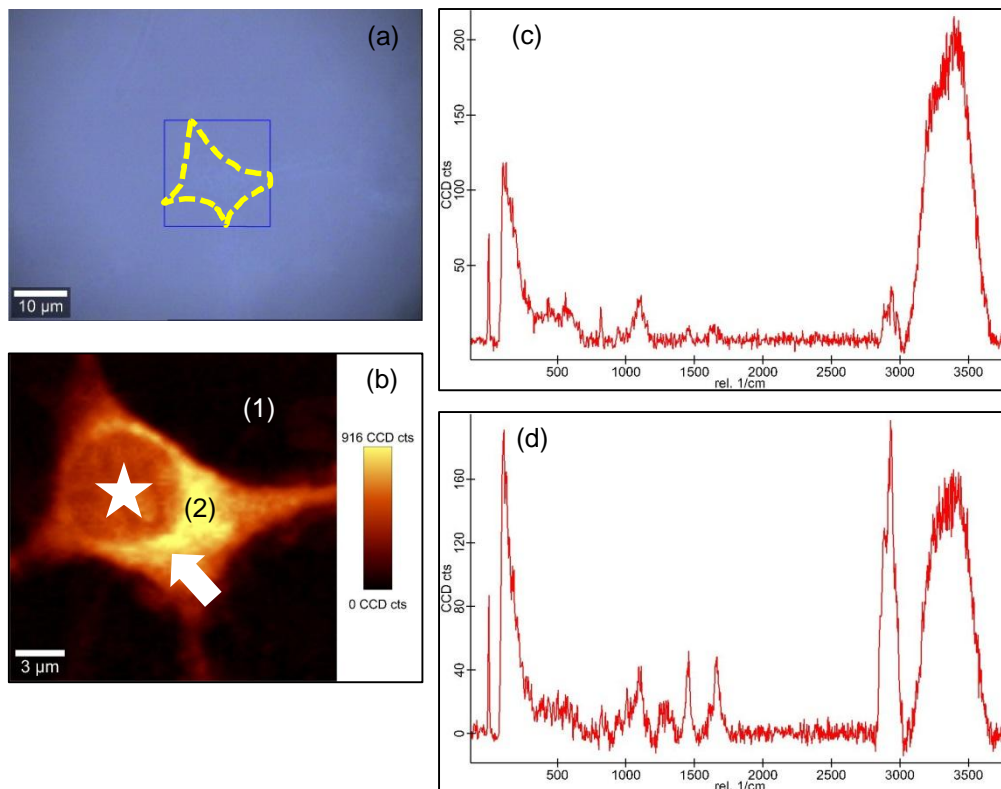
Figure 5.3 Intra- and extra-cellular spectra of a beta cell fixed without mounting medium

INS-1 beta cells were treated with complete medium for 72 hours. Mounting medium was not used to fix the coverslip onto the glass slide. The coverslip was sealed onto the glass slide using nitrocellulose. (a) White light image of beta cell, blue box drawn around single cell (yellow dotted line). (b) Raman map, using the band at 2845 ± 10 cm^{-1} with a 0.5 s integration time. Spectrum (c) corresponds to the area outside the cell (1) (the substrate). Spectrum (d) corresponds to regions within the cell (2). The spectrum corresponding to the outside of the cell (c) shows minimal intensity versus the spectrum corresponding to the inside of the cell (d) within the region of interest (2800 – 3100 cm^{-1}). The white star shows the location of the nucleus. The white arrow points to yellow pixels, all of which correspond to lipid.

5.3.3 Spectra of pure fatty acids

To assist in peak attribution, spectra were obtained for pure PA and pure OA and compared with cell spectra averaged per treatment. This method had been described and employed by Chan *et al.* (2005), Kochan *et al.* (2015), Majzner *et al.* (2014), Majzner *et al.* (2018), Slipchenko *et al.* (2009) and Stiebing *et al.* (2014).

In the study presented in this thesis, the pure FAs were deposited onto a Superfrost Plus glass slide and three single point spectra of different points of the sample, using the 20x dry lens with a 0.5 s integration time with 20 accumulations, were acquired. Figure 5.4 shows the full spectrum of pure PA after averaging three single point spectra. The three single point spectra were averaged and background subtracted. The spectra were not normalised.

Section 5.5.3 outlines the process for conducting background subtraction of a Raman map. In figure 5.4 the C-H stretching vibration mode is expanded to show the two peaks of highest intensity at 2852 cm^{-1} and 2882 cm^{-1}. This method was also employed for measuring single point spectra of pure OA.
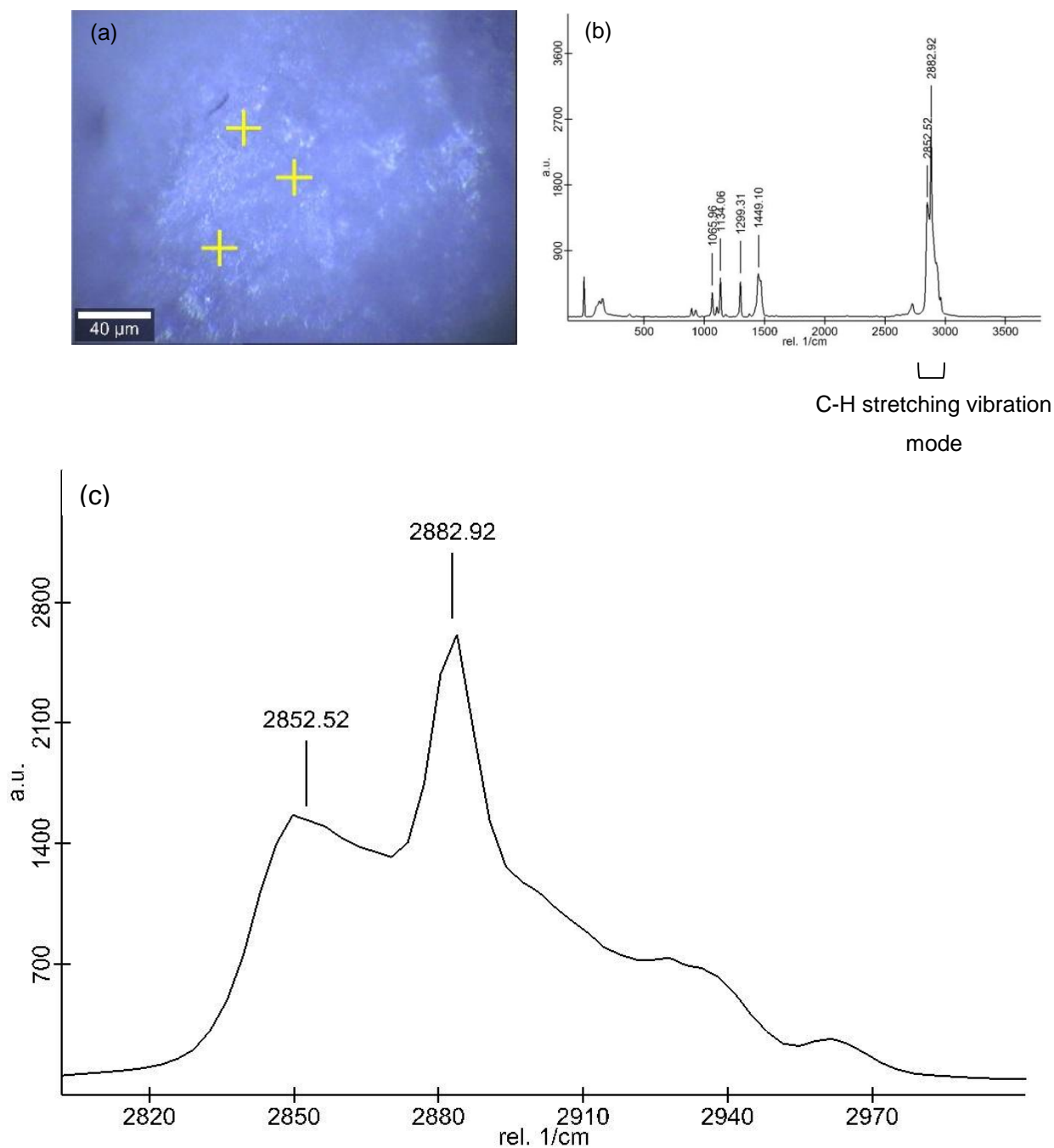
Figure 5.4 Raman spectrum of pure sodium palmitate

(a) White light image of pure sodium palmitate. Yellow cross-hairs represent the positions where 3 single point spectra were taken on the sample. (b) Spectrum of averaged single point spectra of sodium palmitate. (c) Spectral range between 2800 cm^{-1} and 3000 cm^{-1} of graph (b) showing prominent peaks at 2852 cm^{-1} and 2882 cm^{-1}.

5.4 Beta cell selection for mapping

In preliminary experiments, it was established that it was preferable to conduct the analysis on single cells rather than over a whole field due to limitations in the analysis software. Individual cells were selected for analysis on the following criteria: the cell must:

(1) Be anchored to the substrate via at least one protrusion, indicating the cell is healthy. Since dead cells detach from their substrate and remain floating in the medium they could be excluded from the analysis,

(2) Not be exhibiting signs of exocytosis. The cell in figure 5.5 shows a "bleb" on the side of the cell (as shown by the white arrow) and is probably undergoing exocytosis and does not have an intact nucleus. Therefore, it is likely that this cell is undergoing apoptosis. This cell was excluded from the analysis,

(3) Be in the G0+G1 phase of the cell cycle. This was determined by the intensity of the nuclear space of the Raman map relative to the background intensity:

   a. The Raman map at 2845 ± 10 cm^{-1} of a healthy cell was required to show a round nucleus with a continuous boundary and uniform intensity. This indicated that the nuclear DNA was intact. Figure 5.3 depicts a healthy cell. The white star shows the location of the nucleus which is clearly defined as a round, black space. The white arrow points to yellow pixels, all of which correspond to lipid,

   b. Examples of cells that might have been dividing (in the S or G2+M phases) or undergoing cell death (pre-apoptosis, apoptosis, or necrosis) are shown in figure 5.5. For example, the cell in figure 5.5 appears to be dividing as two nuclei are visible (as shown by the two white stars). None of the cells presented in figure 5.5 have clearly defined nuclei and were, therefore, excluded from the analysis.
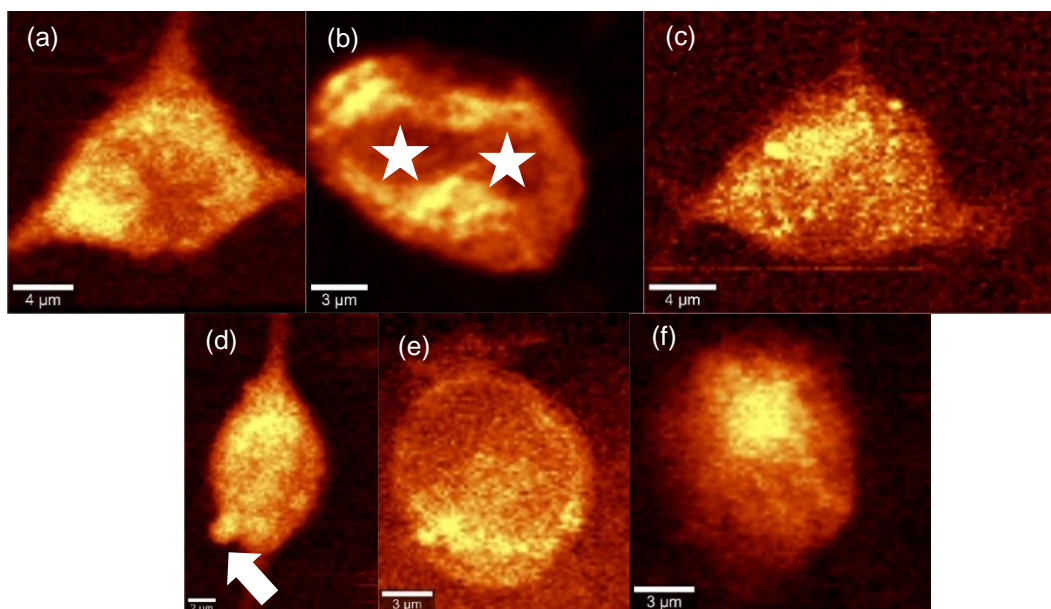
Figure 5.5 Raman maps of INS-1 beta cells excluded from analysis

Raman maps of INS-1 beta cells using the band at 2845 ± 10 cm^{-1}. The lipid distribution within these cells was not measured as their nuclei were not clearly visible, either because the cells were dividing or because the cells were undergoing cell death. (a) The cell does not have a clearly defined nucleus. (b) The cell is dividing, as shown by the two white stars which show the location of the two nuclei. (c) The cell does not have a clearly defined nucleus. (d) The cell does not have a clearly defined nucleus, and the white arrow shows the location of a bleb indicating that this cell is likely to be undergoing apoptosis. (e) The cell does not have a clearly defined nucleus. (f) The cell does not have a clearly defined nucleus.

5.5 Data pre-processing

5.5.1 Cosmic ray removal

All maps were pre-processed using the WiTec Project FOUR+ software. Cosmic rays were removed using the 'CRR & Smooth' function. The Filter Size was set at 2 and the Dynamic Factor was set between 1 and 100 for every cell analysed in this thesis. Figure 5.6 shows the colour of the cosmic ray changing from blue to red. This change of colour indicated that the ray had been removed from the data-set. It is essential to remove cosmic rays because their high intensities can skew the true data obtained from the cell. The process of cosmic ray removal did not change the highest intensity value within the cell shown in figure 5.6. This was expected since no rays were present in the 2845 ± 10 cm^{-1} spectral range of any pixel in the Raman map.

5.5.2 Intensity values

Intensity values are measures of photons which, when they hit a detector, known as a charge-coupled device (CCD), are converted into electrons. The device then measures the electric charge of the corresponding pixel and converts this energy into a visual output. The visual output of the interaction between the electron and detector corresponds to a unit of measurement, known as a CCD count, which is given to each pixel. The result is a false colour image/ map of intensity of the material/ substance being imaged/ mapped.
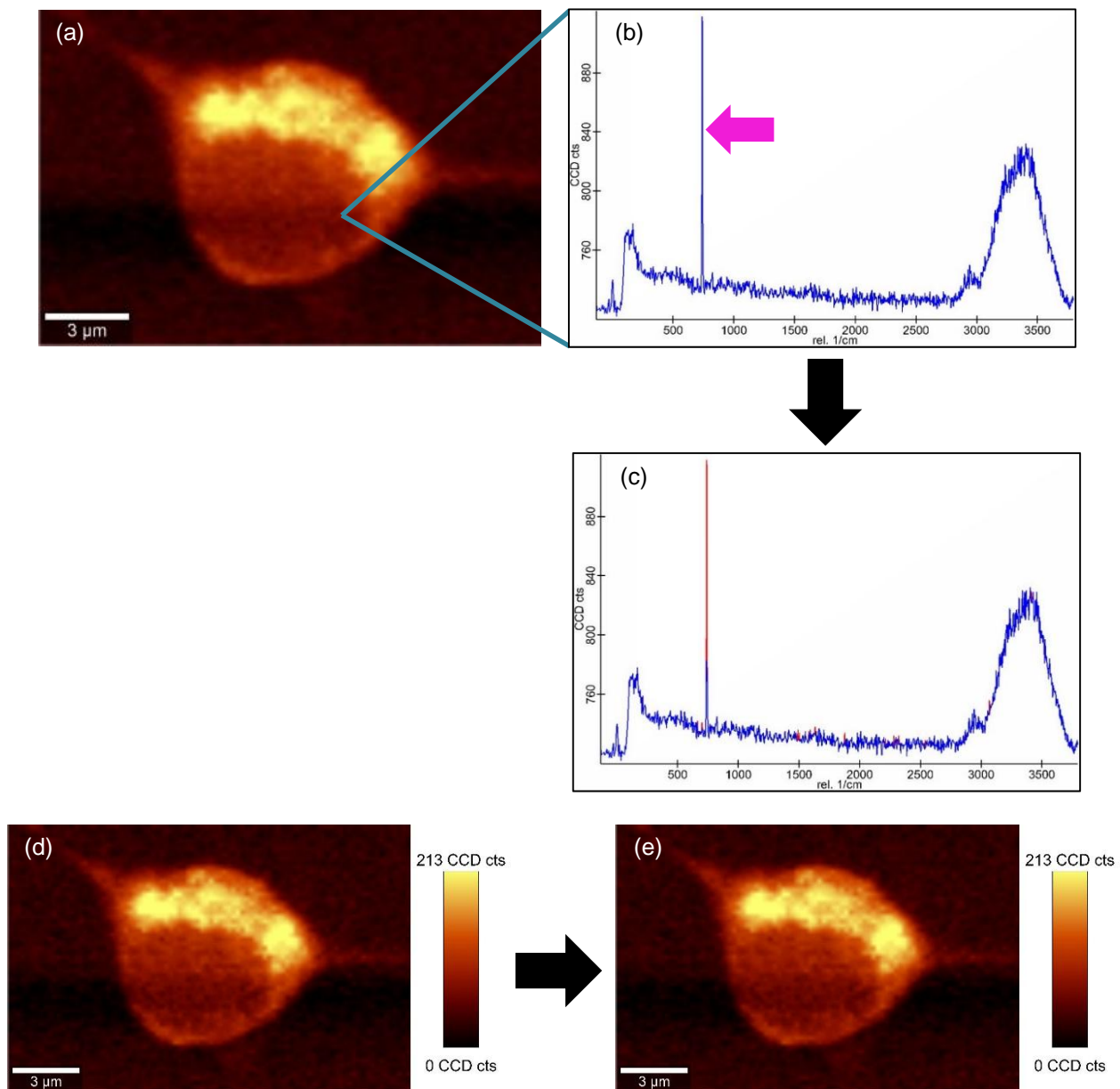
Figure 5.6 Identification and removal of cosmic rays from Raman map of INS-1 beta cell

(a) Raman map of INS-1 cell before cosmic ray removal. 2845 ± 10 cm^{-1} band chosen to visualise lipid within the cell. The map was scanned manually for cosmic rays. (b) Spectrum of a single pixel shows a single, blue, sharp peak at ~ 700 cm^{-1} (see pink arrow). This is a cosmic ray which required removal from the spectrum. The Filter Size was set at 2 and the Dynamic Factor was set between 1 and 100. (c) After cosmic ray removal the blue peak turned red in colour. (d) Raman map of INS-1 cell before cosmic ray removal using the band at 2845 ± 10 cm^{-1}. (e) Raman map of INS-1 cell after cosmic ray removal using the band at 2845 ± 10 cm^{-1}. The chosen Filter Size and Dynamic Factor values were applied globally within the Raman maps. No change in intensity value (CCD counts) was observed.

5.5.3 Background subtraction

Fluorescent background was removed using the 'Shape' function within the 'Background Subtraction' function in the WiTec Project FOUR+ software. The Shape function was employed as it is considered to be the most effective for subtracting fluorescent areas. The 'Shape Size' parameter was always set at 100 and the 'Noise Factor' parameter was always set at 2 for every cell analysed in this thesis. The process for background subtraction involves selecting regions of the spectrum which contain peaks to fit the baseline. The same regions were selected manually for every spectrum from every cell, thus ensuring consistent and replicable removal of the fluorescent background from every cell.

Conducting background subtraction in the pre-analysis of data is vital. The process of background subtraction decreased the highest intensity value from 213 to 136.9 CCD counts within the cell shown in figure 5.7. If this step is not conducted, data can be misinterpreted and conclusions drawn can be misleading.
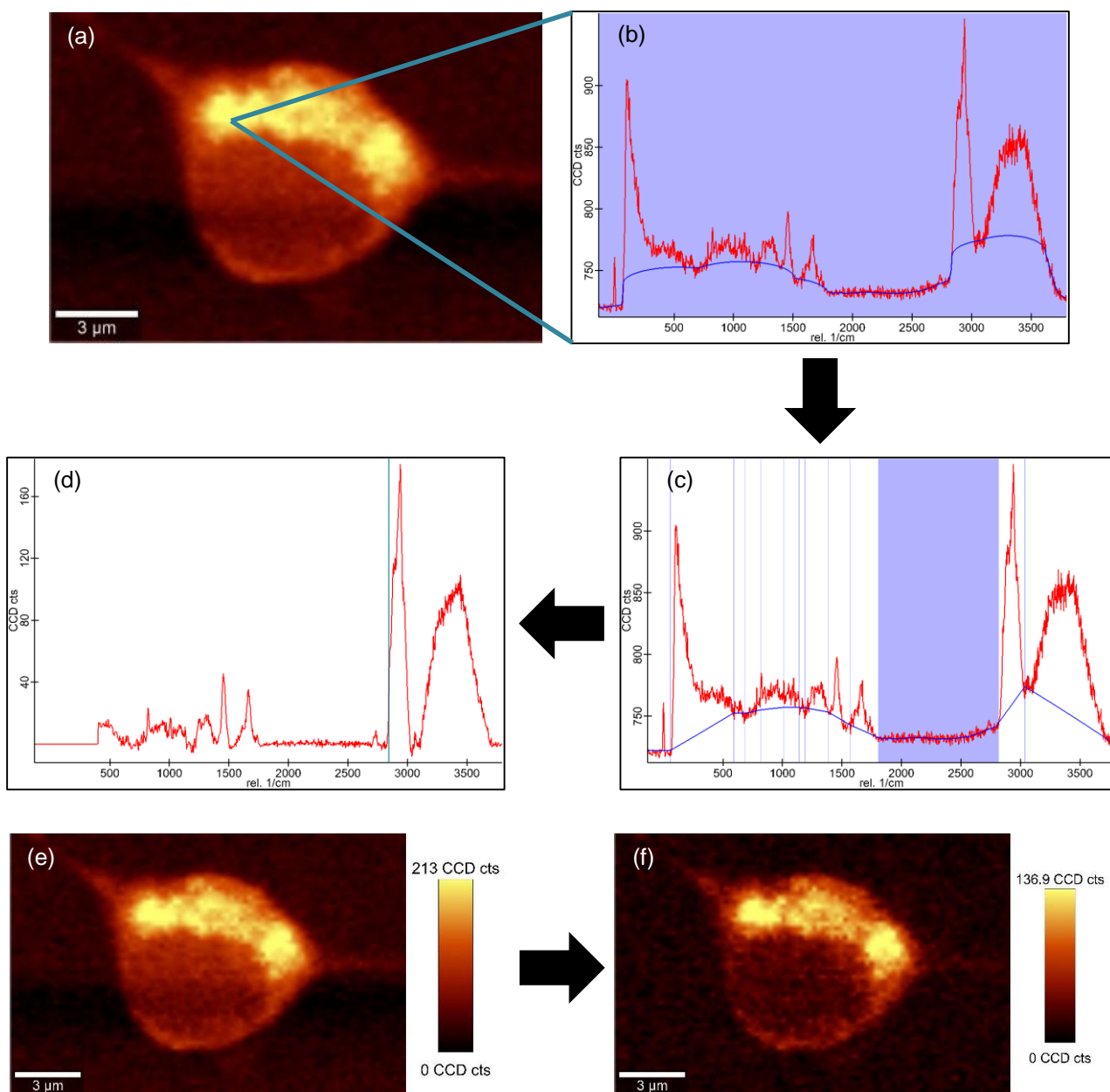
Figure 5.7 Background subtraction of Raman map of INS-1 beta cell

(a) Raman map of INS-1 cell after cosmic ray removal from figure 5.6. 2845 ± 10 cm^{-1} band chosen to visualise lipid within the cell. The spectrum of a single pixel corresponding to lipid within the cell was selected for background subtraction. (b) Shape Size was set at 100 and the Noise Factor was set at 2. (c) Sections highlighted in white were applied globally to all pixels within the Raman map, whereby the sections were baselined. (d) Spectrum of a single pixel corresponding to lipid after background subtraction. (e) Raman map of INS-1 cell before background subtraction using the band at 2845 ± 10 cm^{-1}. (f) Raman map of INS-1 cell after background subtraction using the band at 2845 ± 10 cm^{-1}. The intensity bar (CCD counts) shows the difference in intensity between the Raman map before and after background subtraction. The highest intensity value decreased from 213 to 136.9 CCD counts after background subtraction.

5.6 Data processing and analysis

5.6.1 Quantifying lipid distribution and concentration

The measured intensity of a Raman spectral line depends on the scattering cross-section of the bond in its particular chemical environment, spectrophotometer performance and pre-processing procedures such as background subtraction. All of these factors introduce uncertainties that must be borne in mind in relating spectral intensity to the actual concentration of a molecule of interest.

Uni-variate analysis involves quantifying the pixels of interest observed from a Raman map by selecting a specific wavenumber from the spectrum. It is important to note that Raman maps are 2D images and represent a cross-section in the middle of the cell (Toporski, Dieing & Hollricher 2018, p. 101). Thus, the quantification of molecules cannot be extrapolated to 3D images of cells. This is a limitation of the technique, however, as long as the same plane is selected for each cell, the cells can be compared. The middle of the cell was selected manually using the laser as a guide to select the plane of the cell with the highest area of intensity.

Figure 5.8 schematically outlines the process for generating a Raman map. Simply, a plane within the cell is selected, then a map is generated at the 2845 $\pm$ 10 cm^{-1} spectral range. The map undergoes pre-processing using WiTec Project FOUR+ software, then undergoes processing. For the purposes of this thesis, the total cell area, the percentage of lipid, and the intensity of lipid within each map was analysed using ImageJ software.
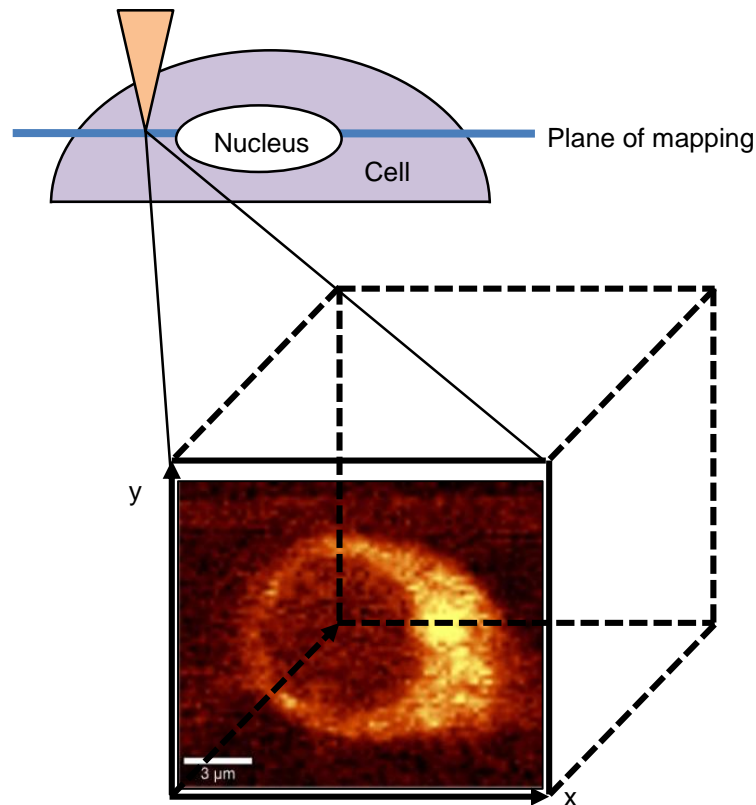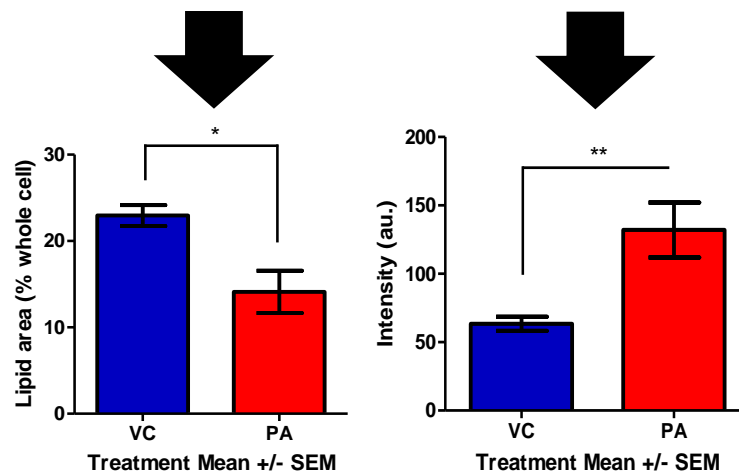
Figure 5.8 Uni-variate analysis used to measure lipid distribution and intensity

To generate a 2D Raman map, a plane within the cell must be selected. To quantify lipid distribution the 2845 ± 10 cm^{-1} band was selected. The Raman map is then: (1) pre-processed using WiTec Project FOUR+ software, then (2) imported into ImageJ to be processed. The maps are analysed to quantify all the pixels corresponding to each map, the pixels of interest within each cell and their intensity values. All of these pixels have x and y coordinates.

The Raman map in figure 5.9 shows a clear nucleus within the cell (dark brown in colouring) and a clear outline of the cell with three protrusions indicating that the cell is attached to the substrate and is healthy. The yellow pixels are indicative of the C-H bonds of interest. I sought to quantify these yellow pixels and calculate their percentage within the 2D plane/ cross-section of the cell.

ImageJ analysis of each cell was used to map and quantify the lipid distribution using the spectral band at 2845 ± 10 cm^{-1} (corresponding to the CH$_2$ symmetric stretching vibration mode). Before the lipid distribution could be quantified each Raman map underwent a process of thresholding. The process of thresholding is used to create binary images from greyscale images. This is because these components cannot be calculated using the coloured Raman maps. A binary image only contains pixels which are black and white. Figure 5.9 shows how a Raman map is converted from an image with orange and yellow colouring to a black and white image. An algorithm is used to threshold images. Many algorithms exist, and each one will calculate whether a pixel should become a binary unit (i.e. white or black pixel) depending on what the intensity value of the original Raman pixel is. Each algorithm choses a different intensity value to threshold against. By ensuring the instrument set-up is the same each time an image of a cell is taken, and by ensuring that the same algorithm is used to analyse each cell, a group of cells can be compared against one another.

| (a) Raman map of INS-1 cell at 2845 ± 10 cm^{-1} | MinError 67.7 % | Otsu 38.8 % | MaxEntropy 21.3 % |
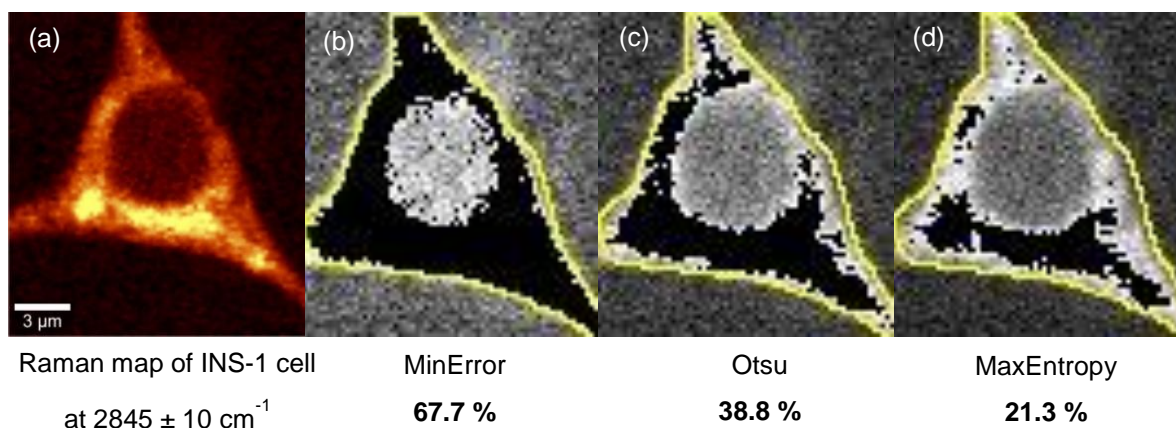
Figure 5.9 Thresholding one INS-1 beta cell

(a) Raman map of a single INS-1 cell taken using the spectral band at 2845 ± 10 cm^{-1}. The cell is healthy. It consists of: a clear nucleus which is dark brown in colour, three protrusions (indicating that the cell is attached to the substrate and is healthy), and yellow pixels which are indicative of the C-H bonds of interest (pixels which correspond to C-H bonds within lipids). (b) The same Raman map as (a) but each pixel is converted into a binary unit. The MinError threshold algorithm has been applied. 67.7 % of the cell contains the pixels of interest. (c) The same Raman map as (a) but each pixel is converted into a binary unit. The Otsu threshold algorithm has been applied. 38.8 % of the cell contains the pixels of interest. (d) The same Raman map as (a) but each pixel is converted into a binary unit. The MaxEntropy threshold algorithm has been applied. 21.3 % of the cell contains the pixels of interest.

An algorithm for the analysis of all the INS-1 cells was chosen based on whether it could best represent the number of yellow pixels shown on a Raman map. Figure 5.9 shows the differences in threshold values between three algorithms (MinError, MaxEntropy and Otsu). The percentage of black pixels which correspond to the yellow pixels in the original Raman map are shown for each of the three algorithms. Figure 5.9 shows that the MinError algorithm calculated that the cell contained 67.7. % of the pixels of interest, and hence the bond of interest. However, it can be seen that this algorithm has converted too many pixels black, i.e. the number of black pixels does not match the number yellow pixels on the original Raman map. The Otsu algorithm was also considered to be unsuitable. The coverage of black pixels from the MaxEntropy algorithm (21.3 %) best-matches the yellow pixels from the Raman map. Of the 16 algorithms trailed on the ImageJ software the MaxEntropy algorithm was deemed to be the most appropriate algorithm to use as it best represented the percentage of pixels corresponding to the yellow pixels on the original Raman map.

Using ImageJ software, the following steps were taken to calculate the number of pixels corresponding to the bond of interest within the 2D image of the INS-1 cell, and their corresponding intensity values: (1) select the pre-processed Raman map using the spectral band at 2845 ± 10 cm^{-1} and convert the image into an ASCII file, (2) import the image into the ImageJ software. The image will appear in greyscale, (3) draw a line around the cell, (4) threshold the image using the MaxEntropy algorithm with the cell boundary selected. This process converts the greyscale image into a binary image. The pixels of interest corresponding to lipid appear black, and all other pixels appear white. In order for the ImageJ software to quantify the intensity values of the pixels of interest, these pixels must

be black in colour. Thus, the colouring of the pixels is reversed, (5) reverse the colour of the background pixels with the pixels of interest so that the background pixels and pixels which are not of interest appear black and the pixels of interest appear white. This process is outlined schematically in figure 5.10.

The ImageJ software can go one step further and can quantify the intensity values of each of the pixels which have been selected for thresholding. The intensity value of the black pixels become zero and the intensity values of the pixels of interest become greater than zero. For each map/ cell the ImageJ software averages the intensity values of all the pixels within the cell boundary. The intensity values for cells within treatment groups can be averaged and then compared between treatment groups to quantify changes in the concentration of the molecules of interest.
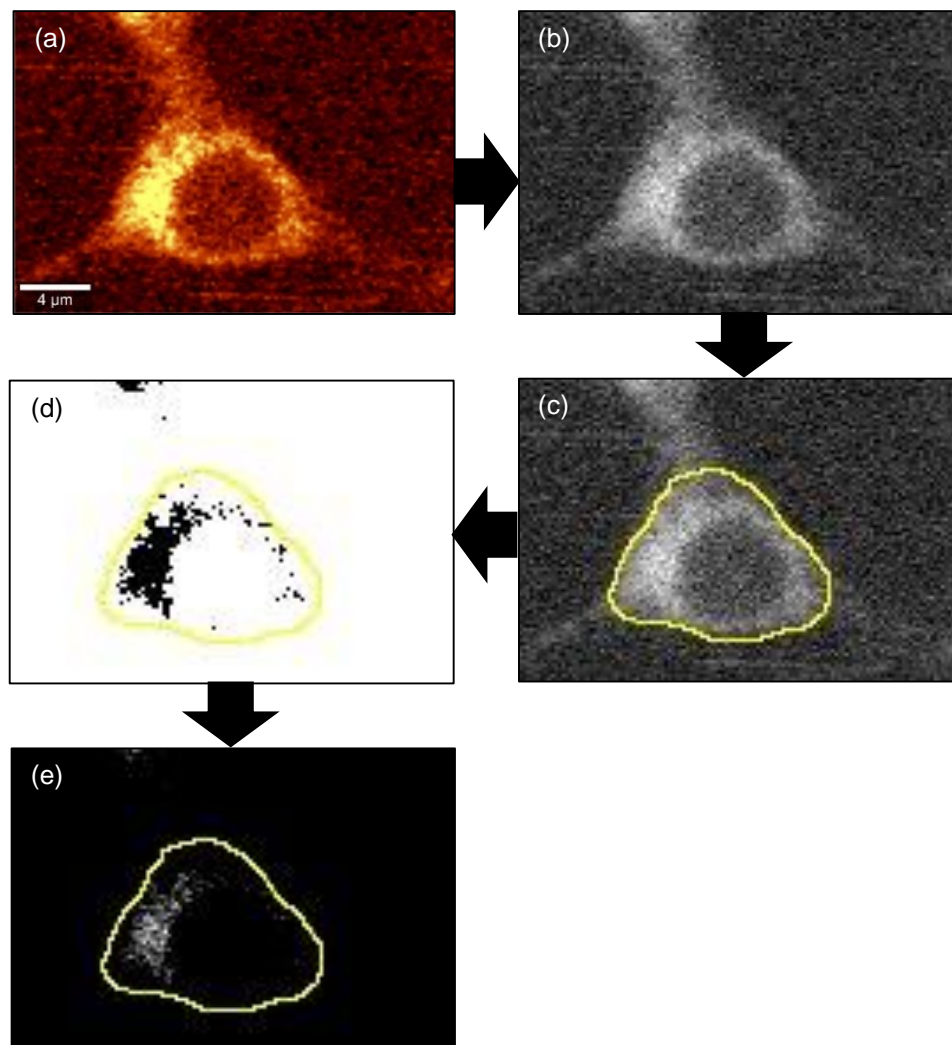
Figure 5.10 ImageJ analysis of Raman map depicting one INS-1 beta cell

(a) Raman map of INS-1 cell using the band at 2845 ± 10 cm^{-1}. (b) Greyscale image of Raman map imported into ImageJ. (c) Yellow line drawn around cell to define the cell boundary. (d) Thresholding of image using MaxEntropy algorithm with cell boundary selected. This process converts the greyscale image into a binary image. The pixels of interest corresponding to lipid, are black, and all other pixels are white. (e) The colours of the pixels have been reversed, whereby the pixels of interest are now white and all other pixels are black.

5.6.2 Quantifying lipid droplet composition

As previously described, uni-variate analysis allows for the quantification of a certain bond by selecting a specific wavenumber from the Raman spectrum. This analysis can be taken further. Much of the existing research using spontaneous Raman microspectroscopy focuses on identifying the chemical composition of cellular material, known as multi-variate analysis.

Multi-variate analysis was employed here to determine whether changes in the composition of lipid within the INS-1 cell could be detected after their exposure to exogenous FAs. This was done using the 'Cluster Analysis' function within the WiTec Project FOUR+ software. Cluster analysis collates and averages all of the spectra which correspond to the pixels of interest within a single Raman map. The spectra from cells within the same treatment group are averaged and normalised to obtain a better representation of the spectra selected, especially if the data being selected have similarities (Toporski, Dieing & Hollricher 2018, p. 109 - 113). Lastly, the spectra from different treatment groups can then be compared and further analyses on the spectra, such as peak fitting, can be carried out. Figure 5.11 shows how this process involves collating the spectra from a single Raman map.
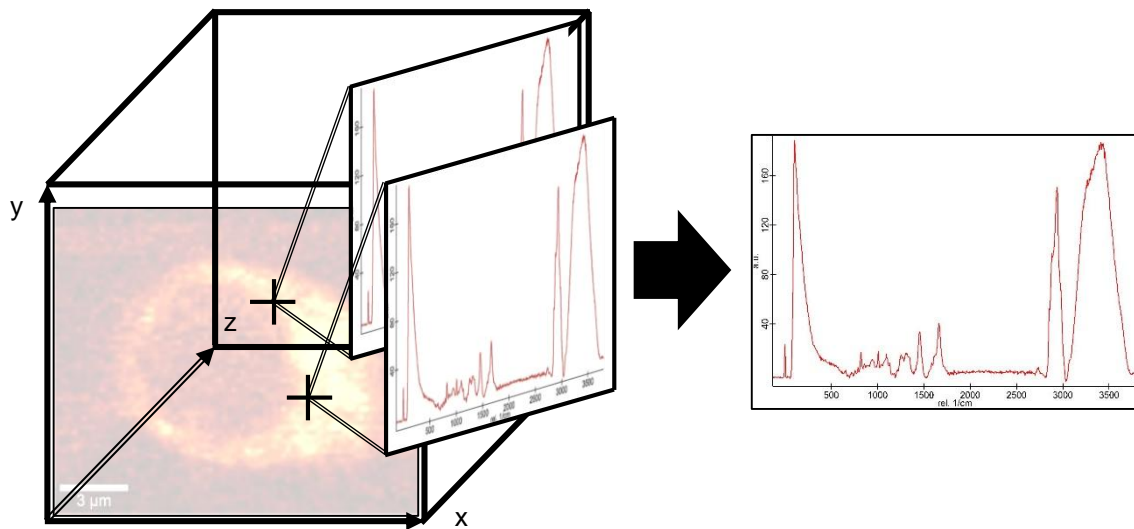
Figure 5.11 Multi-variate analysis used to measure lipid composition

Cluster analysis collates and averages all the spectra of the pixels corresponding to the molecules of interest within a single Raman map (in this case, the pixels which are coloured yellow). The black cross-hairs correspond to pixels of interest. The pixels have x and y coordinates, yet the spectra are in the z-axis. The spectra corresponding to the pixels of interest within a single Raman map are averaged. The spectra from multiple single cells within the same treatment group are averaged and normalised. The spectra from different treatment groups can then compared.

The following steps were taken to select and average the spectra of pixels corresponding to intracellular lipid using the cluster analysis function: (1) select the pre-processed Raman map using the spectral band at 2845 ± 10 cm^{-1} to visualise the pixels corresponding to lipid, (2) using the K-means cluster analysis function, select three clusters. Each cluster will highlight a separate part of the Raman map depending on the similarity of the intensity of the pixels. Pixels with very similar intensity values are collated and a false colour map of those pixels are visualised. Figure 5.12 shows a cell where every single pixel has been falsely coloured. The substrate (borosilicate glass) is coloured green, the plasma membrane is coloured blue, and the intracellular space is coloured red. The red component of the cell contains the pixels of interest which correspond to lipid, (3) a manual process of 'de-selection' involves identifying the pixels of interest within these three clusters which correspond to the pixels in the original Raman map, (4) the spectra of these pixels are then averaged. In this case, the pixels which correspond to intracellular lipid are averaged. This involves collating and averaging all of the spectra of the pixels which correspond to the population of yellow pixels, (5) each averaged spectrum from each cell within a treatment group is then collated and averaged to generate a single spectrum. Lastly, the spectra from each treatment group are then normalised against the phenylalanine peak at 1008.3 cm^{-1}, as described by Krafft *et al.* (2006). This peak was chosen as the position of this peak does not change in absolute terms on the x-axis of spectra following alterations to the intracellular environment. This entire process is outlined schematically in figure 5.12.
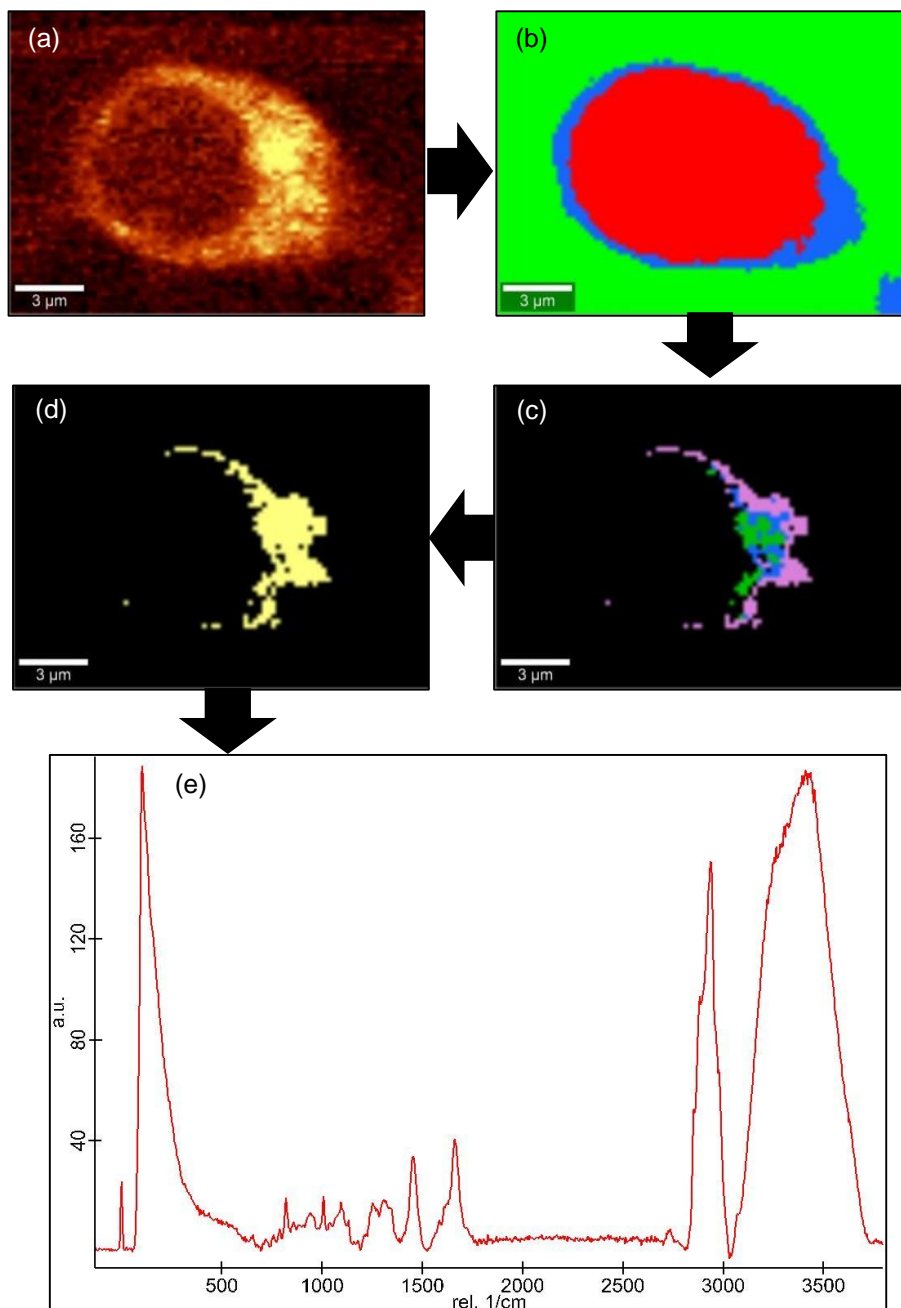
Figure 5.12 Cluster analysis of Raman map of INS-1 beta cell

(a) Raman map of INS-1 cell using the spectral band at 2845 ± 10 cm^{-1}. (b) False colouring of pixels within the cell, whereby the pixels corresponding to the: substrate are green; plasma membrane are blue; intracellular space are red. (c) The pixels corresponding to the pixels of interest have been identified. (d) All of the pixels of interest have been collated and averaged which has generated a single spectrum (e).

179

5.6.2.1 Overlaying spectra of pure fatty acids with cell spectra

In order to determine the degree of unsaturation of intracellular LDs, and determine whether changes in the unsaturation-content of lipids within cells had occurred upon exposure to exogenously supplied FAs, Kochan *et al.* (2013a), Kochan *et al.* (2013b), Kochan *et al.* (2015), Majzner *et al.* (2014), Majzner, Chlopicki & Baranska (2016) and Slipchenko *et al.* (2009) chose to compare the relative ratios of Raman peaks of lipid within cell spectra at approximately 1656 cm^{-1} and 1444 cm^{-1}. Although the study by Li-Chan *et al.* (1994) would argue that 3010 cm^{-1} is a good indicator for the identification of UFAs. This method of comparing the relative ratio of peak heights was also employed by Slipchenko *et al.* (2009). However, in addition to comparing the relative peaks corresponding to C=C bonds and C-H, Slipchenko *et al.* (2009) also compared the relative ratios of the peaks at 2100 cm^{-1} (corresponding to C-D bonds) and 2850 cm^{-1} (corresponding to C-H bonds in CH_2 groups).

The 1656 cm^{-1} peak is thought to correspond to the C=C *cis* bond in UFAs and the 1444 cm^{-1} peak is thought to correspond to C-H bonds of the R-CH_2 group in both UFAs and SFAs. Thus, if the ratio of these two spectral peaks are calculated and a higher relative peak height of 1656 cm^{-1} is observed versus the relative peak height of 1444 cm^{-1}, this might indicate that the sample is more unsaturated than saturated. The comparison of these two specific wavenumbers was first described by Sadeghi-Jorabchi *et al.* (1970) where the unsaturation content of various commercial oils, such as sunflower oil, were investigated using fourier transform Raman spectroscopy. However, Sadeghi-Jorabchi *et al.* (1970) employed the 1661 cm^{-1} peak, not the 1656 cm^{-1} peak, to determine the unsaturation content of oils. The primary aims of these Raman studies were to identify whether oils had been subject to adulteration (Li-Chan *et al.* 1994) and to determine their quality (Li-Chan *et al.* 1996). It was not until the 1990s where

Raman microspectroscopy was applied to clinical situations, such as the study by Frank *et al.* (1994) which sought to identify irregularities in healthy breast tissue biopsied from healthy individuals versus healthy breast tissue biopsied from tissue adjacent to cancerous tissue. The identification of specific FAs within single cells began much later as a result of the advancement of technology and as a result of improved software to analyse both uni- and multi-variate data. Additionally, the study of nuclear material using Raman microspectroscopy, as previously mentioned, has also recently begun. However, other methods to study nuclear damage exist that are less time-consuming than Raman microspectroscopy, and will continue to be used until: (1) the acquisition time of Raman maps can be accelerated without compromising resolution, (2) the through-put capabilities of the technology are improved, and (3) data pre-processing and processing (uni- and multi-variate analysis) can be automated without compromising quality. Nonetheless, the application of Raman microspectroscopy to study cellular changes at a single-cell level has slowly become an important endeavour as it can allow researchers to better understand the cellular mechanisms which affect human health and the mechanisms which may lead to the onset of disease.

For the purposes of the analysis presented in this thesis, the relative peak ratios of the 1656 cm^{-1} and 1444 cm^{-1} spectral regions were not compared. The reasons for this were two-fold: (1) proteins, like lipids, also contain CH_2 bonds, bonds which feature in the 1400 – 1500 cm^{-1} spectral range (Rygula *et al.* 2013). Thus, any changes in absolute or relative peak intensity would not enable us to differentiate between the presence of protein and lipid within the cell, and (2) the spectrum of pure OA has a peak at approximately 1656 cm^{-1}, which is where proteins also have a peak corresponding to the Amide I stretching vibration mode,

C=O, as described by Rygula *et al.* (2013). Therefore, any changes in absolute or relative peak intensity would not allow for the differentiation between changes in carbon chain saturation in lipids and the presence of protein.

Contrary to the method described above, the method of overlaying the spectrum of pure PA and OA with averaged cell spectra was contemplated in order to identify the presence of PA or OA (esterified or non-esterified) within the LDs of intracellular LDs. Considerations were made to determine whether this approach could detect the presence of certain FAs (e.g. the difference between SFAs and UFAs), and whether certain peaks corresponding to pure FAs could be compared with peaks found in the spectra of cells. If peaks appear in the same position on the x-axis of spectra corresponding to a pure FA and that of a cell, this could indicate the presence of that particular FA within the cell. This method could also identify changes in the relative peak heights from the cell spectra to indicate at what concentration the FA has been incorporated into the lipid structures.

It could be argued that this method of overlaying the spectra of pure FAs with cell spectra is not robust enough as the binding of FAs to glycerol may shift the position of the 2845 cm^{-1} peak on the x-axis. This could occur as a result of a change in the chemical composition of the molecule inducing a change in the stretching vibration mode of the C-H bonds within the FAs. This effect might render the use of this wavenumber obsolete as it would not be possible to detect whether PA, for example, is incorporated into lipid. However, this argument can be countered by noting that the C-H bond stretching vibration mode within FAs should not be significantly affected upon their incorporation into TAGs. This is because glycerol binds via the carboxyl group, and not via the alkyl chain. This argument is strengthened further as evidence from Czamara *et al.* (2014) shows

very similar peak positions between the 2800 – 3100 cm^{-1} region of the spectrum of PA and its corresponding TAG: tripalmitin. This suggests that the binding of PA with glycerol does not affect the vibrational stretching mode of C-H bonds in the PA. This is likely to be the case for other FAs too.

Based on the limitations and arguments presented in this Chapter, I decided that the method of overlaying the spectra of pure FAs with normalised cell spectra was the most robust method for measuring changes in the incorporation of PA and OA into lipid within INS-1 cells. This method was therefore employed for determining the composition of lipid within these cells.

5.6.2.2 Peak fitting of cell spectra

Further considerations were made to determine whether the degree of unsaturation of LDs within FA-treated cells versus untreated cells could be measured. A method of calculating the AUC of peaks corresponding to peaks in the spectra of pure PA and pure OA was considered. This approach involved conducting a process known as 'peak fitting', employed by Slipchenko *et al.* (2009) and Yue *et al.* (2012).

The peak fitting process involves conducting spectral decomposition followed by second derivative analysis of spectra. The averaged and normalised cell spectra underwent peak fitting using WiRE 2.0 software. Background subtraction was conducted for the spectrum of each cell corresponding to each treatment. The curve fitting extended over the C-H region of all the spectra analysed. Even though the individual spectra were noisy, they were not smoothed before being fitted to avoid removing data. The baseline for background subtraction was a cubic spline fitted at 2600 cm^{-1}, 2700 cm^{-1}, 2800 cm^{-1}, 3250 cm^{-1} and 3740 cm^{-1}. Cubic spline interpolation was employed preferentially over polynomial

interpolation because polynomial interpolation can delete data where the baseline points exceed the original spectrum.

Second derivative analysis identified six peaks which were fitted using the WiRE 2.0 software on each averaged spectrum between 2700 cm^{-1} and 3050 cm^{-1} (figure 5.13). The peak centres were allowed to drift during the analysis, however, no significant difference was observed between individual spectra within treatments or between treatments. Note that the cross-hairs on figure 5.13, and any other similar figures, do not represent anything, they are automatically present on the last curve during the fitting process.

Although more curves provide better fitting, I aimed to fit each spectrum with the minimum number of curves to account for the true peaks within the spectrum. Although five curves were trialled, these gave a false fitting at the 2720 cm^{-1} peak, thus six peaks were employed. The software then calculated the peak centre, peak width, peak height, gaussian % and the AUC for each peak of each spectrum analysed. The same parameters were employed for each curve fitted.

To determine whether there had been a change in the FA composition of cells exposed to exogenously exposed FAs, the AUC of the peaks of interest were compared with the AUC of the peaks of interest of the cells exposed to the corresponding VC. See equation 5.1 below.

Equation 5.1 Identifying the presence of a particular fatty acid within a Raman cell spectrum and calculating fold change of this peak

$$\textit{Presence of fatty acid} = \frac{\textit{AUC for peak of interest from cells exposed to exogenous FAs}}{\textit{AUC for peak of interest from cells exposed to the VC}}$$

The workings for this calculation are shown in the following example for 0.125 mM PA versus the VC:

(1) Identify the appropriate AUC values by identifying the appropriate peaks to interrogate:

(a) The peak for identifying PA presence in the lipid spectrum of cells exposed to PA was 2882.28 cm^{-1}. The AUC for this peak was 4378.84 ± 342 cm^{-1},

(b) The peak for identifying PA presence in the lipid spectrum of cells exposed to VC was 2885.99 cm^{-1}. The AUC for this peak was 4214.09 ± 314 cm^{-1}.

(2) Calculate fold change:

$$\frac{4378.84}{4214.09} = 1.04$$

(3) Calculate error as a percentage:

$$\left(100x\frac{342}{4378.84}\right) + \left(100x\frac{314}{4214.09}\right) = 15.26\ \%$$

(4) Calculate absolute error:

$$1.04x\left(\frac{15.26}{100}\right) = 0.158704 = 0.16$$

Fold change = 1.04 ± 0.16

Note that any conclusions or suggestions drawn from the peak fitting values have been done with only the fold change values, whereby the error values have not been taken into consideration. This is because the error values are required

to represent the statistical significance of the data. The error values do not, upon

publication of this thesis, hold any biological significance.
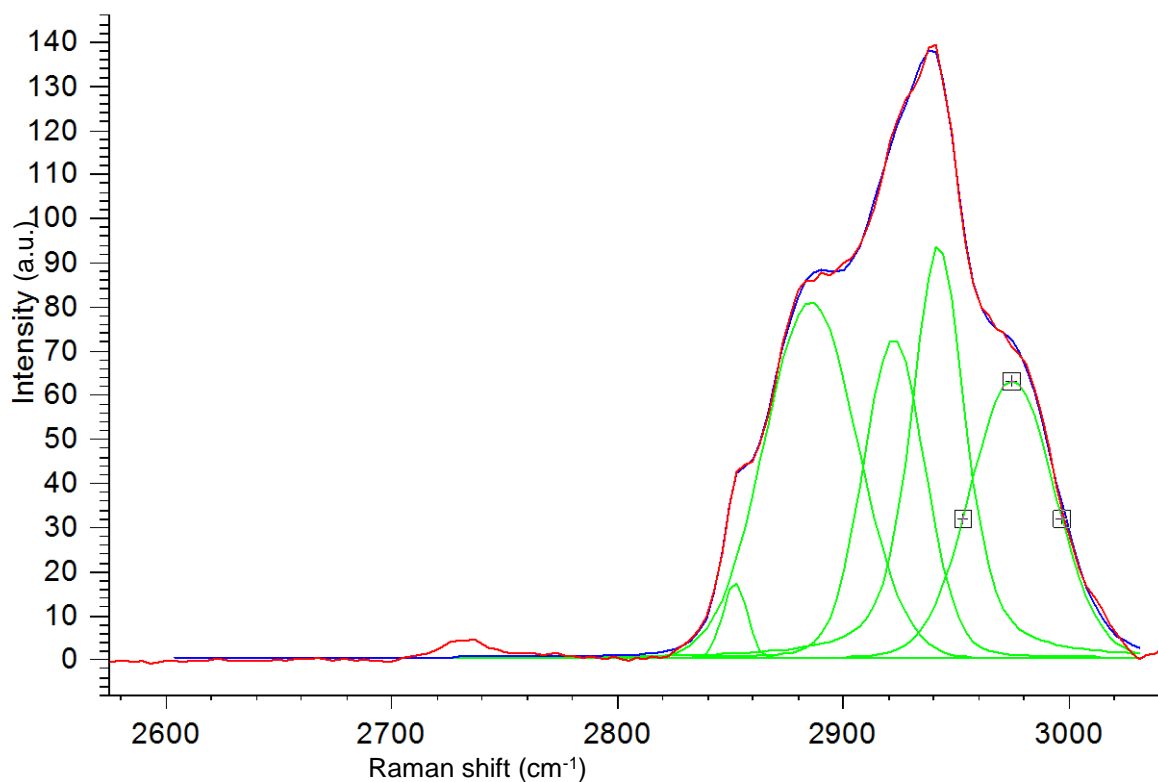
Figure 5.13 Peak fitting of spectrum corresponding to untreated INS-1 beta cells

The spectra from 16 vehicle control-treated cells from the non-esterified fatty acid data-set were averaged and normalised against the phenylalanine peak at 1008.3 cm^{-1} (red line). Baseline subtraction was conducted within the 2600 – 3740 cm^{-1} region of the spectrum, followed by peak fitting (blue line), whereby 6 curves were fitted. From each of the 6 curves (green lines) (only 5 curves shown), the peak centre and the AUC were calculated with WiRE 2.0 software.

In conclusion, I have developed a robust methodology to measure the distribution, intensity and composition of lipid within fixed INS-1 beta cells. This method has been applied to INS-1 cells exposed to exogenous FAs. The results from this work are presented in Chapter 6.

Chapter 6

Use of Raman microspectroscopy to

study the distribution and composition

of lipid in beta cells

6 Use of Raman microspectroscopy to study the distribution and composition of lipid in beta cells

6.1 Introduction

The Raman microspectroscopy methodology presented in Chapter 5 was employed to investigate the hypothesis that differential deposition of SFAs and UFAs into LDs occurs in beta cells *in vitro*. Since each FA molecule has its own vibrational signature, determined by the atoms in the molecule, the characteristics of the individual bonds and their polarisability, these frequencies can be measured. As a result, labels are not required in this technique.

The aims of the work presented in this Chapter were three-fold: to investigate whether: (1) exposing beta cells to PA causes a change in LD disposition (distribution and composition) in beta cells, whether (2) OA would be able to mitigate the effects caused by PA, by shuttling PA into LDs, and whether (3) esterified FAs affect LD disposition.

6.2 Methods

6.2.1 Seeding of beta cells and treatment with fatty acids

INS-1 cells were seeded, as described in section 5.3.1, treated with FAs, as described in section 2.1.4, and fixed, as described in section 5.3.2. The following FA stock solutions were prepared: 90 mM OA (Sigma) in 90 % (v/v) EtOH, 50 mM PA (Sigma) in 50 % (v/v), 90 mM MePA (Sigma) in 90 % (v/v) EtOH; and 90 % MeOA (Sigma) in 90 % (v/v) EtOH. 10 % FA-free BSA (Sigma) was prepared in RPMI-1640 serum-free medium. Cells were treated with 0.125 mM or 0.5 mM FAs for 24 hours before being fixed and imaged using a WiTec alpha

300r Raman microspectrometer, as described in section 5.2. Cells treated with the VC were exposed to serum-free medium, BSA and EtOH only. The final percentages of BSA and EtOH at 0.9 % (w/v) and 0.5 % (v/v), respectively for all treatments. Cells treated with the VC will also be known herein as 'untreated cells'.

6.2.2 Pre-processing of Raman maps

Three data-sets of Raman maps were collected, each from differential FA treatments. They are: (1) non-methyl ester 0.125 mM FA, (2) non-methyl ester 0.5 mM FA, and (3) methyl-ester 0.125 mM FA. Within each data-set cells were pre-processed, then processed. However, some cells which were pre-processed were not included in any further analysis. These cells and the reasons for not including them in any further analysis are described here: (1) one VC-treated cell within the 'methyl-ester 0.125 mM FA' data-set did not undergo uni- and multi-variate analysis as I deemed its percentage lipid value abnormally low compared to other data points within the data-set. Thus, this cell was considered to be an anomalous result. It must be noted that although ten VC-treated cells were imaged and pre-processed, only nine cells underwent further analysis, and (2) one methyl palmitate-treated cell within the 'methyl-ester 0.125 mM FA' data-set did not undergo uni- and multi-variate analysis as I deemed its percentage lipid value abnormally high compared to other data points within the data-set. Thus, this cell was considered to be an anomalous result. It must be noted that although nine methyl palmitate-treated cells were imaged and pre-processed, only eight cells underwent further analysis. These abnormal values could be due to one of the following reasons: (1) an incomplete removal of all cosmic rays during the pre-processing stage, or (2) a cell-specific biological anomaly concerning the size of the cell(s) and/ or the percentage of lipid within the cell(s).

6.2.3 Analysis of intracellular lipid distribution and concentration (uni-variate analysis)

The distribution of lipid was determined by mapping and quantifying the total intensity of the 2845 ± 10 cm^{-1} spectral band within individual cells. One image was taken/ cell/ treatment over a plane approximately at mid-depth through the cell. The Raman maps were pre-processed and analysed, as described in sections 5.5 and 5.6, respectively. ImageJ analysis allowed the total area fraction of each cell and the distribution of lipid within each cell, in which the peak intensity was above background, to be quantified. In all cases, the MaxEntropy algorithm was deemed most suitable for thresholding the images because the number of pixels corresponding to lipid matched most closely to the original Raman map, as described in section 5.6.1.

6.2.4 Analysis of lipid composition (multi-variate analysis) and peak fitting

Cluster analysis was applied to the pixels corresponding to lipid, as described in section 5.6.2, to quantify the contributions of individual lipid species within the INS-1 cells. From each FA treatment studied, the spectra from the INS-1 cells were averaged. Subsequently, the peaks in the C-H region of the cell spectrum between 2800 cm^{-1} and 3100 cm^{-1} were decomposed to identify peaks that were hidden by stronger signals, as described in section 5.1.6.1. In many cases, large peaks are made up of smaller peaks. The positions of these smaller peaks on the x-axis can distort the shape and size of the larger peaks, thus allowing for misinterpretation of the data. After peaks have been decomposed, the AUC of each peak can be compared between differential treatments. However, it can be difficult to identify which peaks to compare with one another. As discussed in Chapter 5, I decided to overlay cell spectra with spectra of pure FAs to determine whether the lipid within cells was composed of a particular FA.

By identifying the peaks which overlay on the x-axis, it could as to whether that particular FA was present within the lipid.

An alternative approach could have been to compare the relative peak heights of two peaks within a spectrum of one treatment and compare it with another treatment. However, this would not have been appropriate. This is because important information, such as the shape and height of the peak, would not have been taken into consideration and may have biased the data, which is why calculating the AUC is considered a more robust approach. In addition, choosing two peaks to compare would have been difficult as the process of assigning peaks to chemical bonds is already a difficult process. The interpretation and conclusions made from these data would have proven extremely complex and possibly misleading.

In order to choose the peaks which corresponded to chemical components in the spectra of both the pure FA and the intracellular lipid, both the pure FA spectra and cell spectra were overlaid. In the case of PA, the best-fitting peak was present at ~ 2882 cm^{-1} (figure 6.9). In the case of OA, the best-fitting peak was present at ~ 2853 cm^{-1} (figure 6.18). These peaks were identified within the decomposed peaks within cell spectra and compared between treatments.

Each decomposed peak from each FA treatment was compared with their respective VC. The calculation for determining whether a FA was present within the Raman maps corresponding to lipid within cells exposed to a particular FA was conducted as shown in equation 5.1. This equation can be explained in more detail as follows: (1) determine which peak of the pure FA spectrum to quantify and ensure this peak corresponds to one of the decomposed peaks within the cell spectrum, (2) identify the curve centre of the peak from the spectrum corresponding to the FA-treated cell spectrum (3) identify the curve centre of the

peak from the spectrum corresponding to the VC, (4) divide the AUC of the peak identified in step (2) with the peak identified in step (3), then calculate the error values (in this case the standard error of the mean (SEM)). The final value obtained indicates the fold change in the area of the peak of the FA-treated cell versus the VC-treated cell. A value of ~ 1 indicates that there is no change in the areas of both cell spectra, thus indicating no change in the composition of the lipid within the FA-treated cell spectrum. It should be noted, however, that other cellular components contain C-H bonds, including other FAs and protein, thus the values obtained from the multi-variate analysis presented here can merely indicate whether a change in the composition of the cell spectrum is due to the presence of the two FAs of interest here: PA or OA.

6.3 Results

6.3.1 Vehicle control-treated cells versus 0.125 mM palmitate-treated cells

6.3.1.1 Lipid distribution and concentration

The cells exposed to the VC showed a consistent distribution of lipid (bonds corresponding to the CH_2 stretch vibration) throughout the cell (figure 6.1). The Raman maps of untreated cells showed a clear distribution of yellow pixels within the cells. Lipid within beta cells had not been visualised before using Raman microspectroscopy, so it was interesting to see such vast amounts within the untreated cells. However, according to Krafft *et al.* (2006), it should not be a surprise to see so much lipid within untreated cells, as normal, healthy, cells should, apparently, be lipid-rich.

Of the 15 cells exposed to 0.125 mM PA, seven cells showed comparable lipid distribution to the untreated cells, however, in eight cells lipid accumulated in circular structures. The size and number of these circular structures have not

been quantified, they are merely visual observations. Instead, the number of pixels of interest and their intensity values have been quantified (figure 6.2).

Note that the figures representing total cell area, percentage intracellular lipid, and lipid intensity depict the data in two graphs. A bar chart shows the mean value of all the data points ± SEM. A scatter plot shows the absolute values used to calculate the mean values presented in the bar chart. The lowest (min) and highest (max) values are presented with error bars.

There was no significant change in the total area of the PA-treated cells indicating that under these incubation conditions the treated cells were not undergoing apoptosis. Furthermore, changes in lipid distribution were not a consequence of a change in the physical size of the cell (figure 6.3).

There was a significant reduction in the area of lipid within PA-treated beta cells ($p < 0.05$) (figure 6.4). Interestingly, the scatterplot shows different populations of lipid. Nine cells were comparable to the VC-treated cells, which had lipid areas between 10 and 30 %, whereas six cells had lipid areas between 0 and 10 %.

There was a significant increase in the intensity of lipid within PA-treated cells ($p < 0.01$) (figure 6.5). These data correlate with the data presented in figure 6.4 which showed that the concentration of lipid within the cell increased, probably due to the lipid occupying less space within the cells.
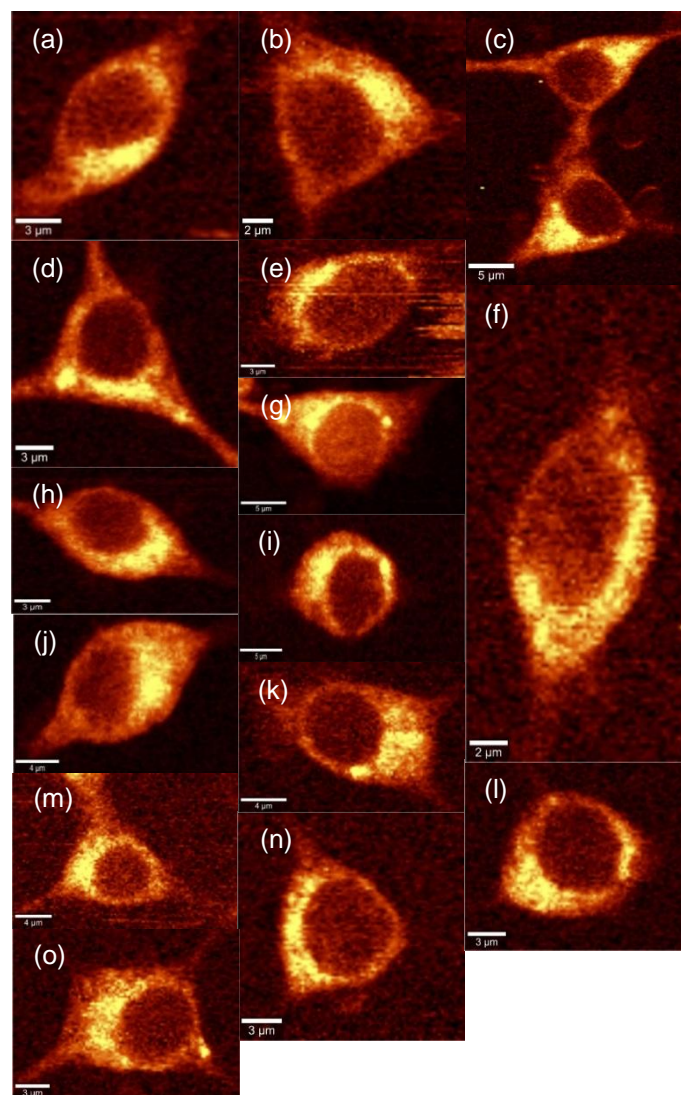
Figure 6.1 Raman maps showing distribution of lipid within untreated beta cells

INS-1 cells were treated for 24 hours with complete medium, then treated with BSA and EtOH in serum-free medium for 24 hours. (a – o) The data represent cells imaged from six experiments. Sixteen cells were imaged and pre-processed using a WiTec 300r Raman microspectrometer. The yellow pixels correspond to lipid at the CH_2 symmetric stretch vibration mode: 2845 ± 10 cm^{-1} spectral band.
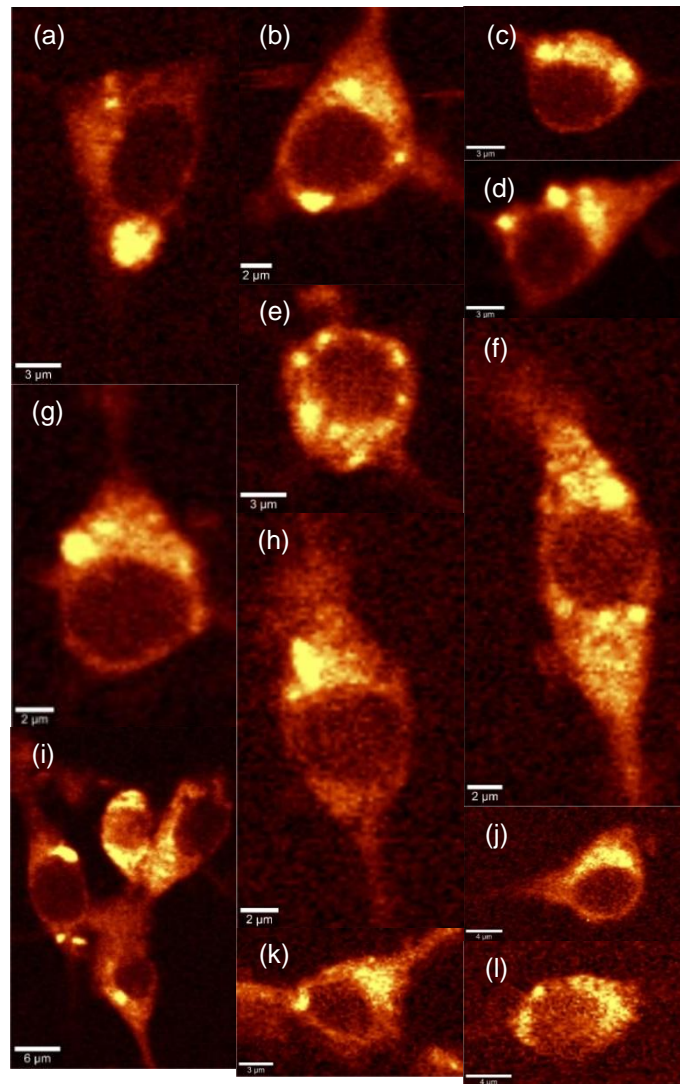
Figure 6.2 Raman maps showing distribution of lipid within palmitate-treated beta cells

INS-1 cells were treated for 24 hours with complete medium, then treated with 0.125 mM palmitate for 24 hours. (a – l) The data represent cells imaged from six experiments. Fifteen cells were imaged and pre-processed using a WiTec 300r Raman microspectrometer. The yellow pixels correspond to lipid at the CH_2 symmetric stretch vibration mode: 2845 ± 10 cm^{-1} spectral band.
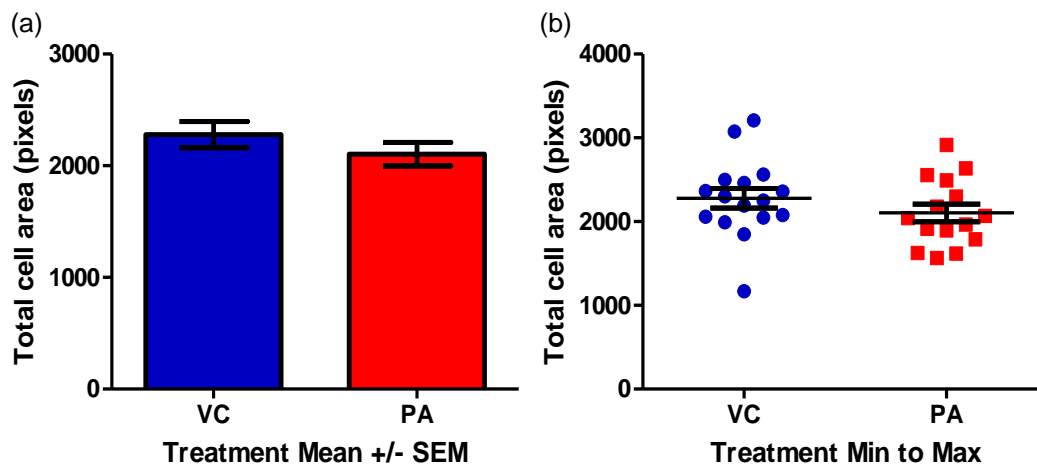
Figure 6.3 Total area of beta cells treated with palmitate for 24 hours
INS-1 cells were pre-treated with complete medium for 24 hours, then for 24 hours with serum-free medium. Vehicle control-treated cells were exposed to BSA + EtOH (VC; blue). Cells were treated with 0.125 mM palmitate (PA; red). The number of pixels corresponding to each entire cell was calculated on ImageJ after the MaxEntropy algorithm was employed. The data represent six experiments conducted where a total of 16 VC-treated cells and 15 PA-treated cells were acquired for ImageJ analysis. One-way ANOVA with Tukey's multiple comparison test. (a) Total cell area versus treatment. Mean ± SEM. (b) Total cell area versus treatment. Minimum to maximum values ± error.

Figure 6.4 Percentage of intracellular lipid in beta cells treated with palmitate for 24 hours

INS-1 cells were pre-treated with complete medium for 24 hours, then for 24 hours with serum-free medium. Vehicle control-treated cells were exposed to BSA + EtOH (VC; blue). Cells were treated with 0.125 mM palmitate (PA; red). The number of pixels corresponding to each entire cell and the lipid within each cell was calculated on ImageJ after the MaxEntropy algorithm was employed. The percentage of lipid in each cell was subsequently calculated. The data represent six experiments conducted where a total of 16 VC-treated cells and 15 PA-treated cells were acquired for ImageJ analysis. One-way ANOVA with Tukey's multiple comparison test * ($p<0.05$). (a) Lipid area versus treatment. Mean ± SEM. (b) Lipid area versus treatment. Minimum to maximum values ± error.
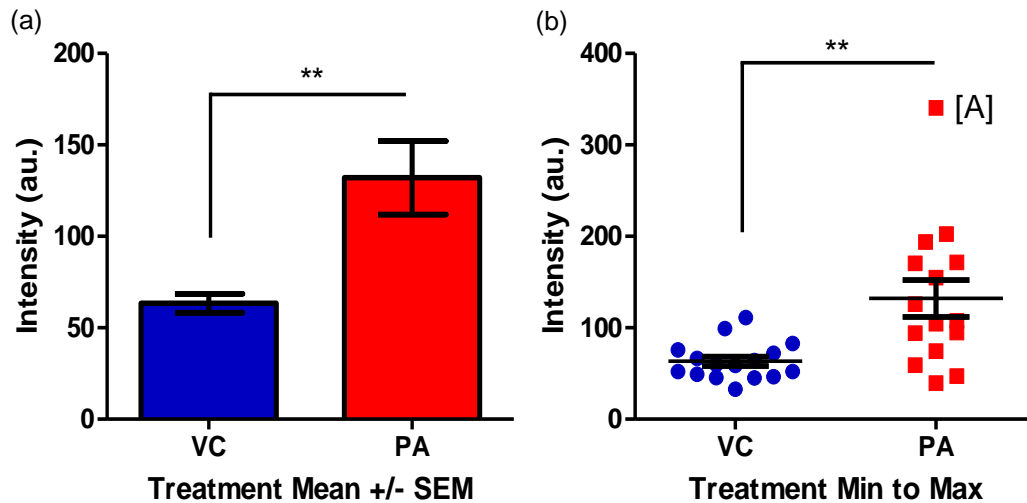
Figure 6.5 Intensity of intracellular lipid in beta cells treated with palmitate for 24 hours

INS-1 cells were pre-treated with complete medium for 24 hours, then for 24 hours with serum-free medium. Vehicle control-treated cells were exposed to BSA + EtOH (VC; blue). Cells were treated with 0.125 mM palmitate (PA; red). The intensity of the pixels corresponding to lipid within each cell was calculated on ImageJ after the MaxEntropy algorithm was employed. The data represent six experiments conducted where a total of 16 VC-treated cells and 15 PA-treated cells were acquired for ImageJ analysis. One-way ANOVA with Tukey's multiple comparison test ** ($p < 0.01$). Note that the removal of data point [A] from the scatterplot does not change statistical significance. (a) Lipid intensity versus treatment. Mean ± SEM. (b) Lipid intensity versus treatment. Minimum to maximum values ± error.

6.3.1.2 Lipid composition

6.3.1.2.1 Peak fitting

In the case for cells treated with 0.125 mM PA, equation 5.1 was employed to calculate the fold change in the AUC of the peak of interest (compare figures 6.6 and 6.7):

$$Presence\ of\ PA = \frac{AUC\ for\ 0.125\ mM\ PA\ (2882.28\ cm - 1\ curve\ centre)}{AUC\ for\ VC(1)(2885.99\ cm - 1\ curve\ centre)}$$

$$\frac{4378.84}{4214.09} = 1.04$$

$$\left(100x\frac{342}{4378.84}\right) + \left(100x\frac{314}{4214.09}\right) = 15.26\ \%$$

$$1.04x\left(\frac{15.26}{100}\right) = 0.158704 = 0.16$$

$$0.125\ mM\ PA \div VC(1) = 1.04\ \pm 0.16$$

6.3.1.2.2 Overlay of pure fatty acid spectra and cell spectra

The full spectrum of pure PA was overlaid with the INS-1 cell spectrum after treatment with 0.125 mM PA (figure 6.8). It can be seen that some areas of both spectra overlap, such as at ~ 1150 cm^{-1}, between 1400 cm^{-1} and 1500 cm^{-1}, and between 2800 cm^{-1} and 2900 cm^{-1}.

The C-H region of the cell spectrum between 2800 cm^{-1} and 3050 cm^{-1} is visible in figure 6.9. The peak at ~ 2880 cm^{-1} in the spectrum of pure PA is present in the cell spectrum, hence why this region was chosen for determining the composition of the lipid within the cells treated with PA.

In conclusion, the uni-variate analysis suggests that PA is incorporated into NLDs because the area of lipid decreases and the intensity of this lipid increases. However, the multi-variate analysis suggests that PA is not

incorporated into NLDs as the fold change of the AUC from the treatment spectrum and the VC at ~ 2880 cm^{-1} is close to 1.
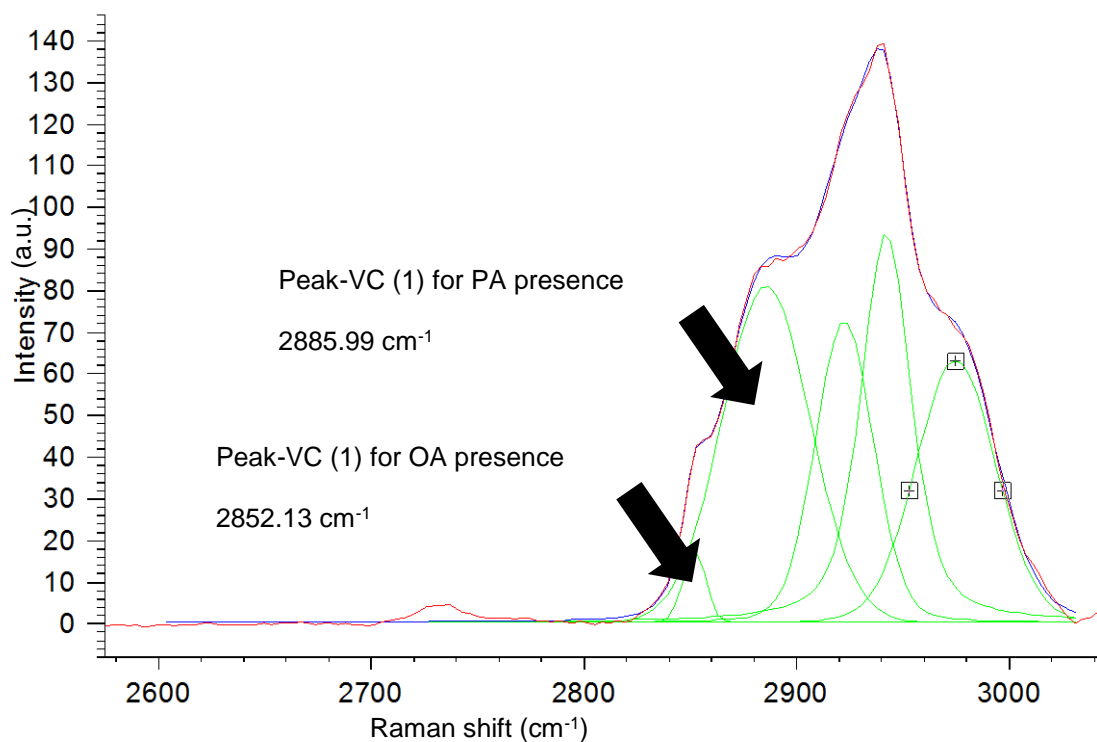
Figure 6.6 Peak fitting of spectrum representing INS-1 cells treated with the vehicle control (1)

The spectra of 16 INS-1 cells treated with the vehicle control were averaged (red line). Peak fitting was conducted (blue line) whereby six peaks were fitted to decompose the spectrum (green lines). Spectral range 2600 – 3050 cm^{-1}.
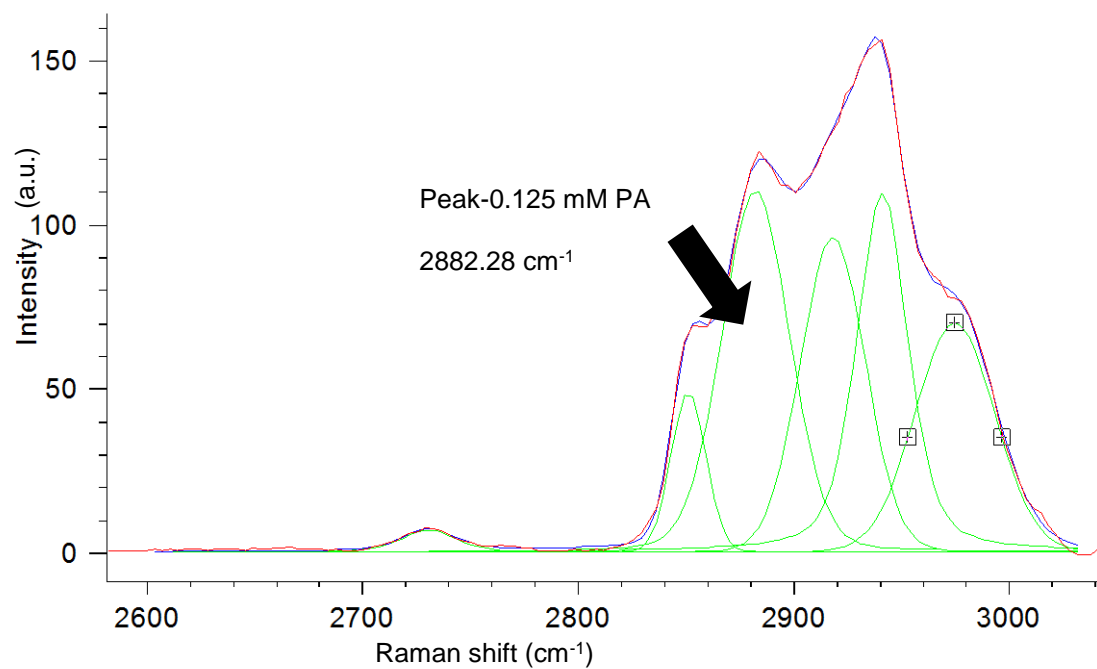
Figure 6.7 Peak fitting of spectrum representing INS-1 cells treated with 0.125 mM palmitate

The spectra of 15 INS-1 cells treated with 0.125 mM palmitate were averaged (red line). Peak fitting was conducted (blue line) whereby six peaks were fitted to decompose the spectrum (green lines). Spectral range 2600 – 3050 cm^{-1}.
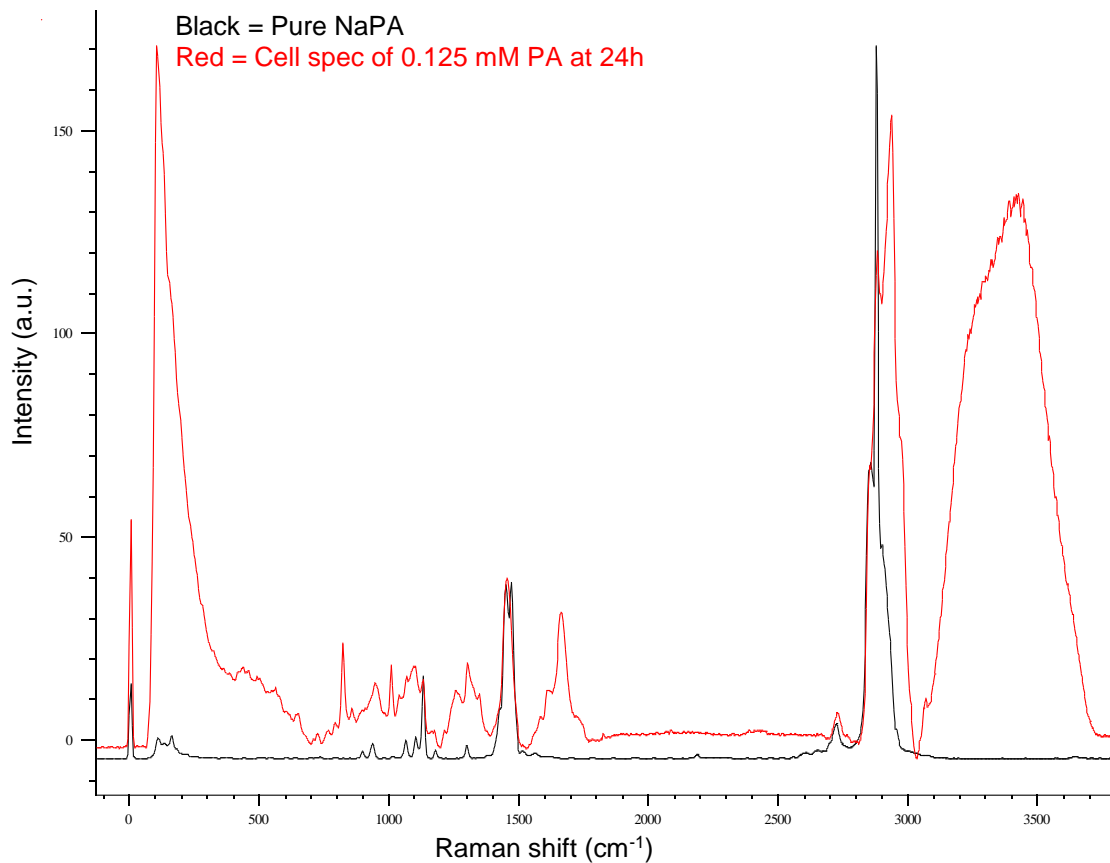
Figure 6.8 Full spectrum of pure palmitate overlaid with INS-1 cell spectrum after treatment with 0.125 mM palmitate

Black spectrum represents pure palmitate. Red spectrum represents averaged spectrum of INS-1 cells treated with 0.125 mM palmitate. Spectral range 0 – 3800 cm^{-1}.
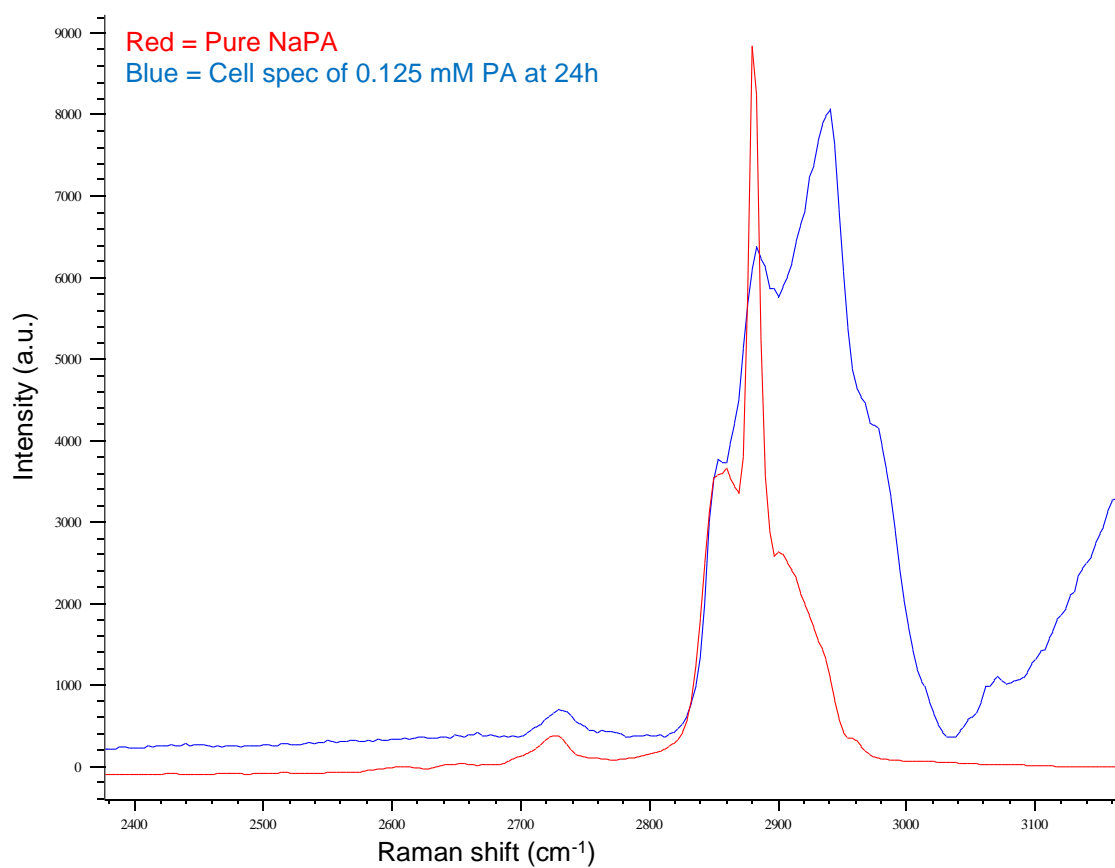
Figure 6.9 Spectrum of pure palmitate overlaid with INS-1 cell spectrum after treatment with 0.125 mM palmitate

Red spectrum represents pure palmitate. Blue spectrum represents averaged spectra of INS-1 cells treated with 0.125 mM palmitate. Spectral range 2380 – 3170 cm^{-1}.

6.3.2 Vehicle control-treated cells versus palmitate-treated cells (0.5 mM)

6.3.2.1 Lipid distribution and concentration

An experiment was conducted where four INS-1 cells exposed to the VC, and four cells exposed to 0.5 mM PA, for 24 hours, were imaged and subsequently analysed. The aim of this study was to determine whether changes in LD distribution and composition were dose-dependent. As with the cells exposed to 0.125 mM PA, the cells exposed to 0.5 mM PA were analysed using ImageJ software and the spectra of pixels corresponding to the band of interest at 2845 ± 10 cm^{-1} were subsequently averaged and normalised using cluster analysis, as described in section 5.6.1. The cells exposed to the VC showed the same lipid distribution as the cells from other data-sets (data not shown). The lipid area of cells exposed to 0.5 mM PA was less than that of VC-treated cells, similar to that of cells exposed to 0.125 mM PA, however the additional decrease was not significant (data not shown). By contrast to the cells exposed to 0.125 mM PA, a slight yet insignificant decrease in the intensity of the pixels corresponding to lipid in the cells exposed to 0.5 mM PA was observed (data not shown).

6.3.2.2 Lipid composition

6.3.2.2.1 Peak fitting

The spectra of cells exposed to 0.5 mM PA showed an interesting difference compared to the spectra of cells exposed to 0.125 mM PA. Figure 6.10 shows the averaged and normalised spectra of four cells exposed to the VC. A visual comparison of figures 6.7 and 6.11 shows differences in the relative peak heights of the three most prominent peaks: ~ 2855 cm^{-1}, ~ 2880 cm^{-1} and ~ 2940 cm^{-1}. Figure 6.11 shows the peak at 2880 cm^{-1} is relatively higher than the peak at 2940 cm^{-1}. This, however, is not the case in figure 6.7, where the peak at 2880 cm^{-1} is relatively higher than the peak at 2940 cm^{-1}.

In the case for cells treated with 0.5 mM PA, equation 5.1 was employed to calculate the fold change in the AUC of the peak of interest (compare figures 6.10 and 6.11):

$$Presence\ of\ PA = \frac{AUC\ for\ 0.5\ mM\ PA\ (2881.65\ cm-1\ curve\ centre)}{AUC\ for\ VC(2)(2881.98\ cm-1\ curve\ centre)}$$

$$\frac{2594.63}{2126.48} = 1.22$$

$$\left(100x\frac{258}{2594.63}\right) + \left(100x\frac{166}{2126.48}\right) = 17.75\ \%$$

$$1.22x\left(\frac{17.75}{100}\right) = 0.21655 = 0.22$$

$$0.5\ mM\ PA \div VC(2) = 1.22 \pm 0.22$$

In conclusion, the uni-variate analysis found that the area of lipid was not significantly different compared to the VC, and that the intensity of this lipid decreased. These data suggest that the PA was metabolised. Interestingly, the fold change was greater in the spectrum of cells treated with 0.5 mM PA (1.22) compared to the cells treated with 0.125 mM PA (1.04) suggesting that PA is dose-dependently incorporated into LDs.
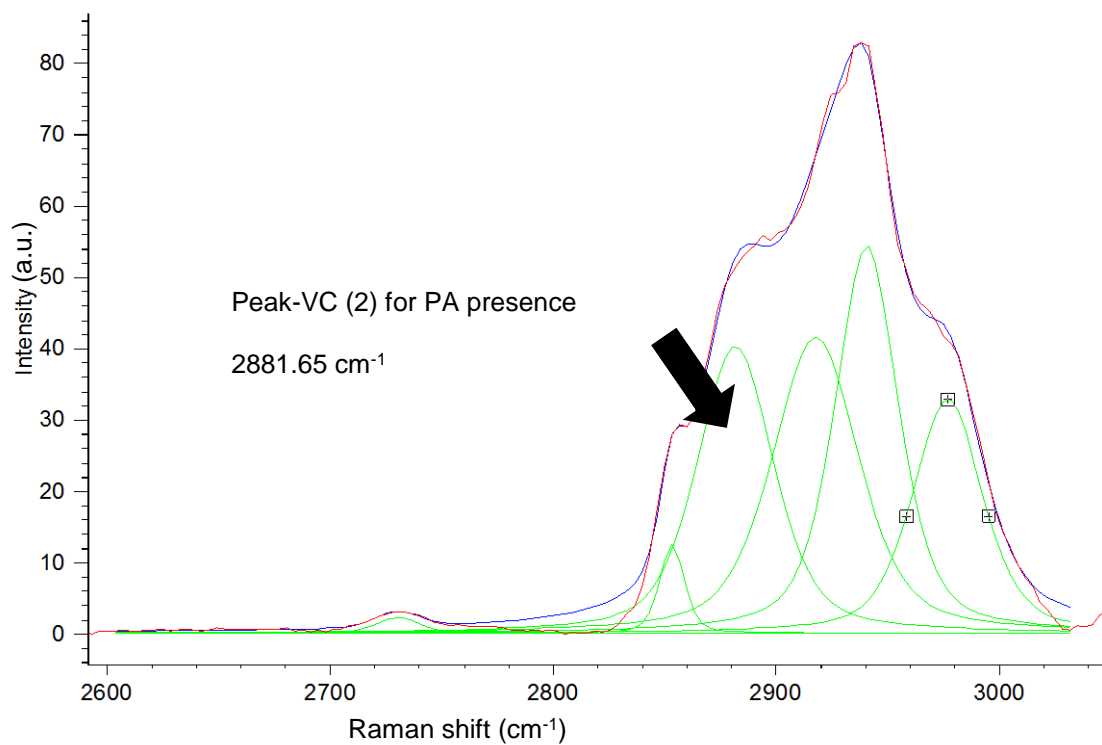
Figure 6.10 Peak fitting of spectrum representing INS-1 cells treated with the vehicle control (2)

The spectra of four INS-1 cells treated with the vehicle control were averaged (red line). Peak fitting was conducted (blue line) whereby six peaks were fitted to decompose the spectrum (green lines). Spectral range 2600 – 3050 cm^{-1}.
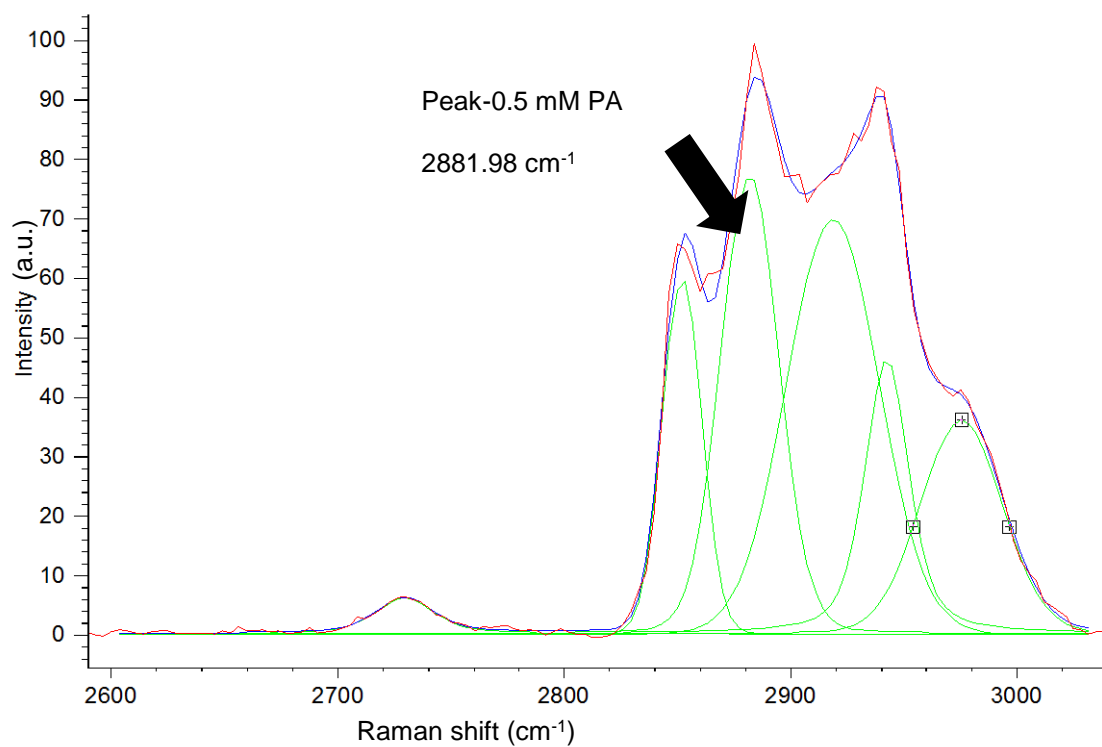
Figure 6.11 Peak fitting of spectrum representing INS-1 cells treated with 0.5 mM palmitate

The spectra of four INS-1 cells treated with 0.5 mM palmitate were averaged (red line). Peak fitting was conducted (blue line) whereby six peaks were fitted to decompose the spectrum (green lines). Spectral range $2600 - 3050$ cm^{-1}.

6.3.3 Vehicle control-treated cells versus oleic acid-treated cells (0.125 mM)

6.3.3.1 Lipid distribution and concentration

Seven cells treated with 0.125 mM OA showed comparable lipid distribution to untreated cells. However, similar to 0.125 mM PA-treated cells, four cells exhibited differential lipid distribution whereby round structures were visible (compare figures 6.2 and 6.12).

The total area of cells exposed to OA was larger compared to untreated cells, but not statistically significantly, and there were clear differences in the distribution of lipid within the cells exposed to OA (figure 6.13).

There was a slight, but insignificant, decrease in the area of lipid within OA-treated cells, and the scatterplot showed a broader distribution of data points compared to untreated cells (figure 6.14). A similar trend was observed with the 0.125 mM PA-treated cells (compare figures 6.4 and 6.14), yet the observation in the 0.125 mM PA-treated cells was statistically significant.

There was a statistically significant increase in the integrated CH_2 peak intensity in OA-treated cells despite the insignificant decrease in the area of lipid ($p<0.05$) (figure 6.15). This was similar to, but smaller than, the change seen in 0.125 mM PA-treated cells (compare figures 6.5 and 6.15).
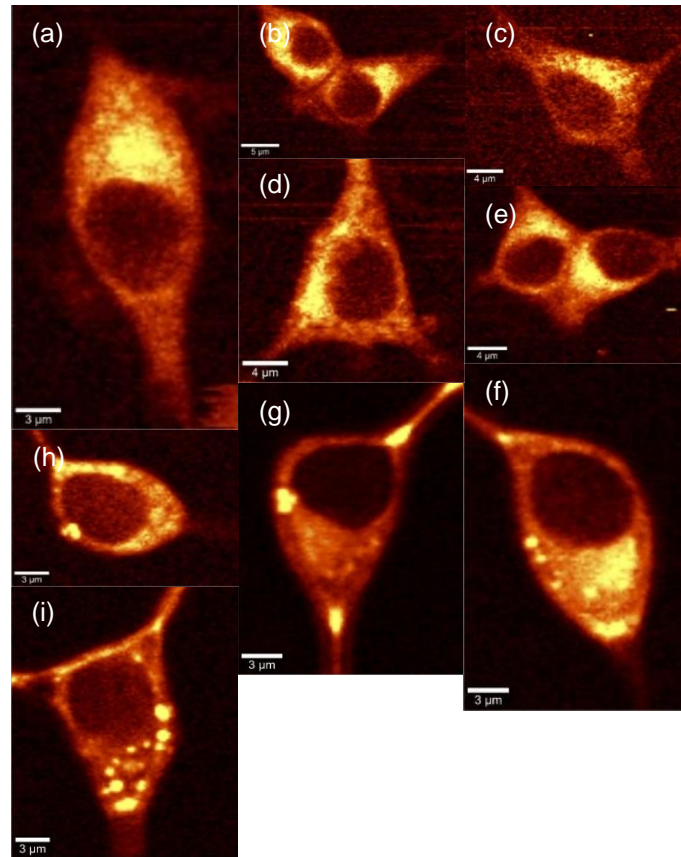
Figure 6.12 Raman maps showing distribution of lipid within oleic acid-treated beta cells

INS-1 cells were treated for 24 hours with complete medium, then treated with 0.125 mM oleic acid for 24 hours. (a – i) The data represent cells imaged from six experiments. Eleven cells were imaged and pre-processed using a WiTec 300r Raman microspectrometer. The yellow pixels correspond to lipid at the CH_2 symmetric stretch vibration mode: 2845 ± 10 cm^{-1} spectral band.
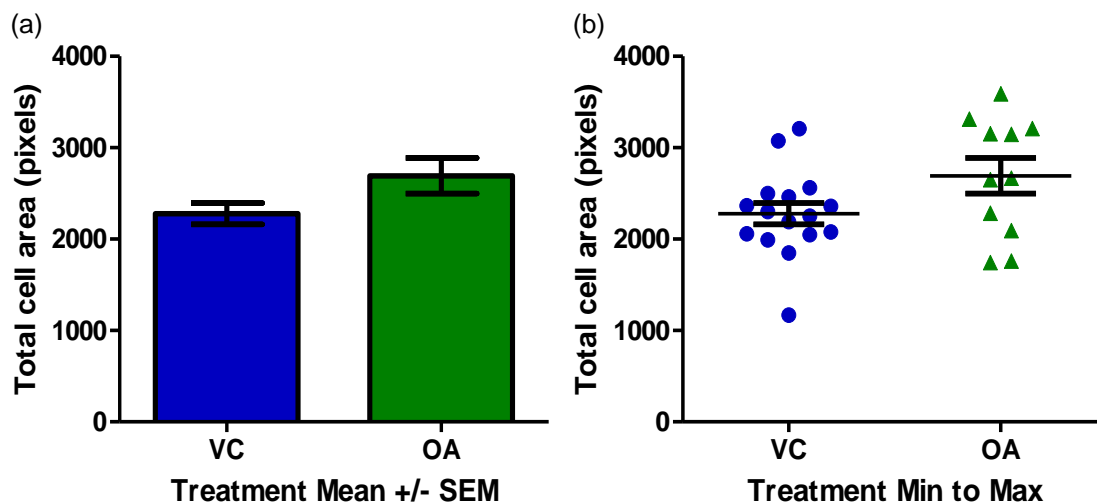
Figure 6.13 Total area of beta cells treated with oleic acid for 24 hours
INS-1 cells were pre-treated with complete medium for 24 hours, then for 24 hours with serum-free medium. Vehicle control-treated cells were exposed to BSA + EtOH (VC; blue). Cells were treated with 0.125 mM oleic acid (OA; green). The number of pixels corresponding to each entire cell was calculated on ImageJ after the MaxEntropy algorithm was employed. The data represent six experiments conducted where a total of 16 VC-treated cells and 11 OA-treated cells were acquired for ImageJ analysis. One-way ANOVA with Tukey's multiple comparison test. (a) Total cell area versus treatment. Mean ± SEM. (b) Total cell area versus treatment. Minimum to maximum values ± error.

Figure 6.14 Percentage of intracellular lipid in beta cells treated with oleic acid for 24 hours

INS-1 cells were pre-treated with complete medium for 24 hours, then for 24 hours with serum-free medium. Vehicle control-treated cells were exposed to BSA + EtOH (VC; blue). Cells were treated with 0.125 mM oleic acid (OA; green). The number of pixels corresponding to each entire cell and the lipid within each cell was calculated on ImageJ after the MaxEntropy algorithm was employed. The percentage of lipid in each cell was subsequently calculated. The data represent six experiments conducted where a total of 16 VC-treated cells and 11 OA-treated cells were acquired for ImageJ analysis. One-way ANOVA with Tukey's multiple comparison test. (a) Lipid area versus treatment. Mean ± SEM. (b) Lipid area versus treatment. Minimum to maximum values ± error.

Figure 6.15 Intensity of intracellular lipid in beta cells treated with oleic acid for 24 hours

INS-1 cells were pre-treated with complete medium for 24 hours, then for 24 hours with serum-free medium. Vehicle control-treated cells were exposed to BSA + EtOH (VC; blue). Cells were treated with 0.125 mM palmitate (OA; green). The intensity of the pixels corresponding to lipid within each cell was calculated on ImageJ after the MaxEntropy algorithm was employed. The data represent six experiments conducted where a total of 16 VC-treated cells and 11 OA-treated cells were acquired for ImageJ analysis. One-way ANOVA with Tukey's multiple comparison test * ($p<0.05$). (a) Lipid intensity versus treatment. Mean ± SEM. (b) Lipid intensity versus treatment. Minimum to maximum values ± error.

6.3.3.2 Lipid composition

6.3.3.2.1 Peak fitting

In the case for cells treated with 0.125 mM OA, equation 5.1 was employed to calculate the fold change in the AUC of the peak of interest (compare figures 6.6 and 6.16):

$$Presence\ of\ OA = \frac{AUC\ for\ 0.125\ mM\ OA\ (2853.05\ cm-1\ curve\ centre)}{AUC\ for\ VC(1)(2852.13\ cm-1\ curve\ centre)}$$

$$\frac{289.49}{232.67} = 1.24$$

$$\left(100x\frac{98}{289.49}\right) + \left(100x\frac{45}{232.67}\right) = 53.19\ \%$$

$$1.24x\left(\frac{53.19}{100}\right) = 0.659556 = 0.66$$

$$0.125\ mM\ OA \div VC(1) = 1.24 \pm 0.66$$

6.3.3.2.2 Overlay of pure fatty acid spectra and cell spectra

The full spectrum of pure OA was overlaid with the INS-1 cell spectrum after treatment with 0.125 mM OA (figure 6.17). It can be seen that some areas of both spectra overlap, as seen in figure 6.8, such as between 1400 cm^{-1} and 1500 cm^{-1}. However, other peaks overlap which are not present in figure 6.8, such as between 1250 cm^{-1} and 1350 cm^{-1}, and between 1650 cm^{-1} and 1700 cm^{-1}.

The C-H region of the cell spectrum between 2800 cm^{-1} and 3050 cm^{-1} is visible in figure 6.18. The peak at ~ 2852 cm^{-1} in the spectrum of pure OA is also present in the cell spectrum. Although the spectrum of pure PA also contains a peak at ~ 2852 cm^{-1}, and the absolute height of this peak is the same in both pure PA and OA, it seemed appropriate to use the peak at ~ 2880 cm^{-1} to represent

PA and the peak at ~ 2852 cm^{-1} to represent OA. This was because: (1) the ratio of the peaks in the spectrum of pure PA were such that the absolute peak at ~ 2880 cm^{-1} was higher than the absolute peak at ~ 2852 cm^{-1}, and (2) the ratio of the peaks in the spectrum of pure OA were such that the absolute peak at ~ 2852 cm^{-1} was higher than the absolute peak at ~ 2880 cm^{-1}. In addition, the region in the spectrum of pure OA between 2880 cm^{-1} and 2920 cm^{-1} is complex and would have been difficult to distinguish within the cell spectrum.

In conclusion the uni-variate analysis suggests that OA was not incorporated into NLDs, but instead suggests that OA partitions into lipid structures within the cell. However, the multi-variate analysis suggests that OA was present within the lipid of cells treated with 0.125 mM OA. This was based on the observed fold change value of 1.24. This suggests that OA was not metabolised but was instead incorporated into LDs.
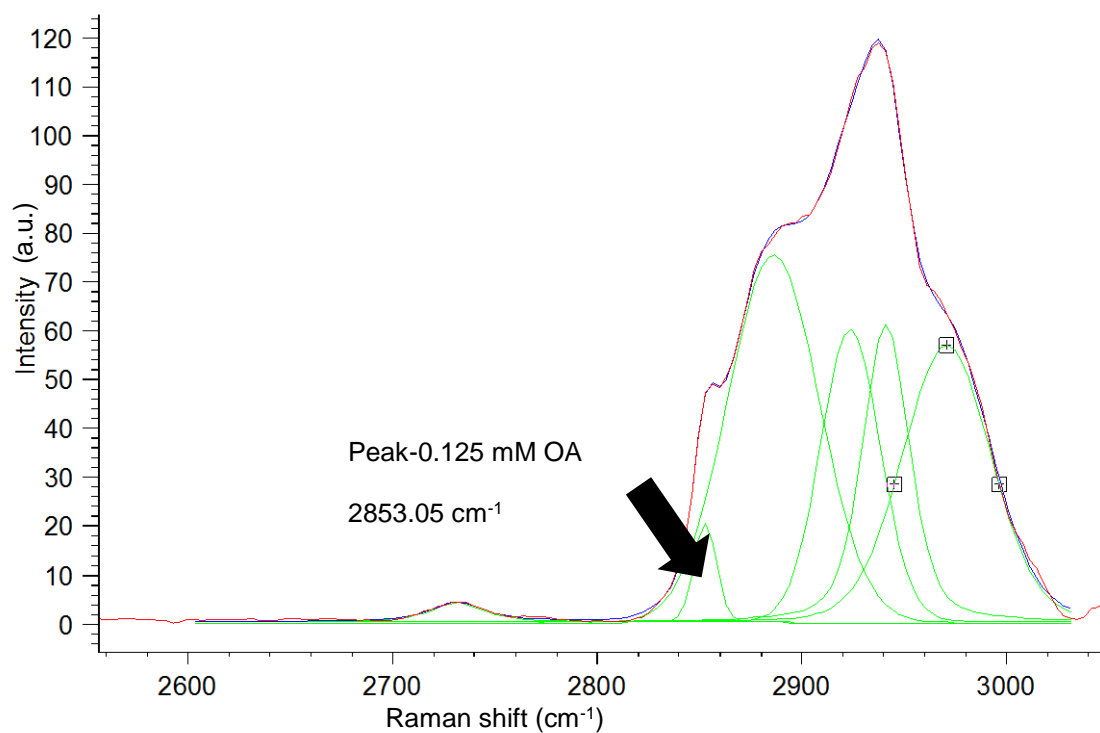
Figure 6.16 Peak fitting of spectrum representing INS-1 cells treated with 0.125 mM oleic acid

The spectra of 11 INS-1 cells treated with 0.125 mM oleic acid were averaged (red line). Peak fitting was conducted (blue line) whereby six peaks were fitted to decompose the spectrum (green lines). Spectral range 2600 – 3050 cm^{-1}.
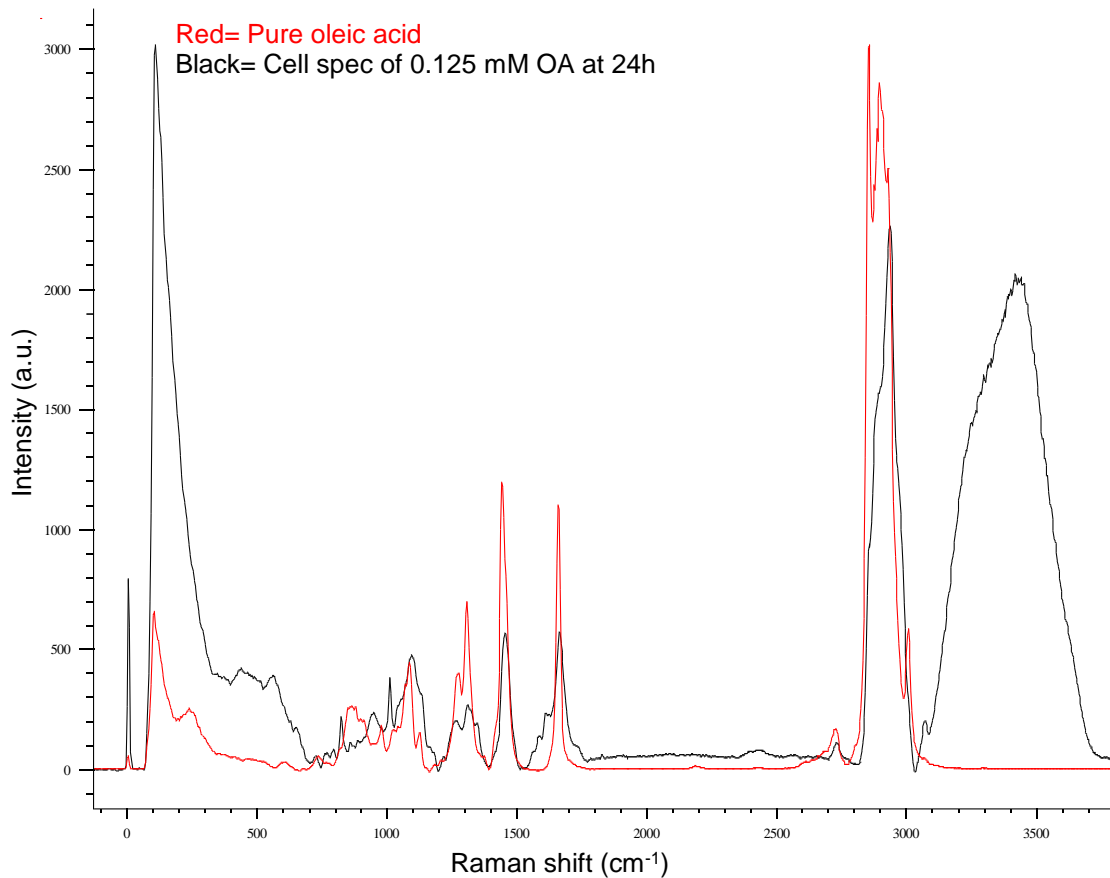
Figure 6.17 Full spectrum of pure oleic acid overlaid with cell spectrum after treatment with 0.125 mM oleic acid

Red spectrum represents pure oleic acid. Black spectrum represents averaged spectra of cells treated with 0.125 mM oleic acid. Spectral range 0 – 3800 cm^{-1}.
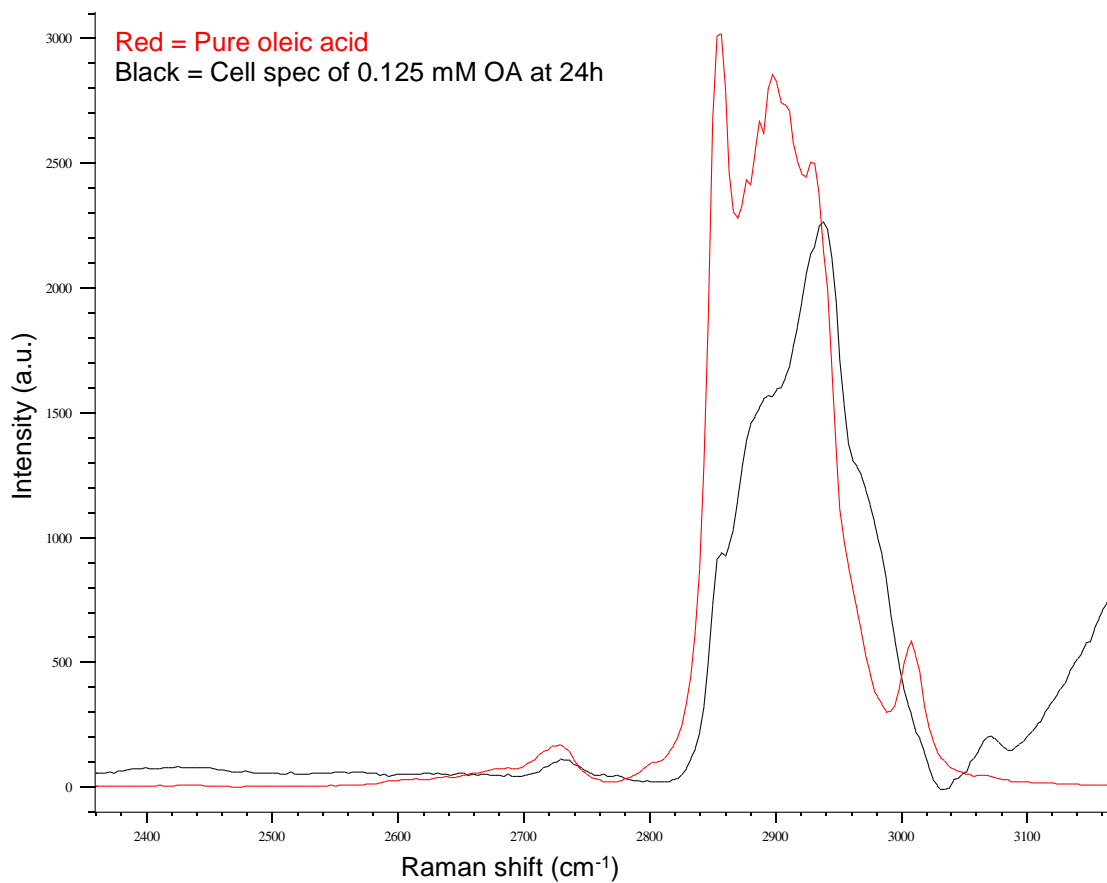
Figure 6.18 Spectrum of pure oleic acid overlaid with cell spectrum after treatment with 0.125 mM oleic acid

Red spectrum represents pure oleic acid. Black spectrum represents averaged spectra of cells treated with 0.125 mM oleic acid. Spectral range 2360 – 3170 cm^{-1}.

6.3.4 Vehicle control-treated cells versus palmitate and oleic acid-treated cells combined (0.125 mM)

6.3.4.1 Lipid distribution and concentration

Similar to the observations made in cells treated with either 0.125 mM PA or 0.125 mM OA alone, ten cells exposed to both 0.125 mM PA and 0.125 mM OA combined exhibited differential lipid distribution compared to the untreated cells. However, five cells were comparable to the untreated cells (compare figures 6.6 and 6.19).

There was a statistically significant increase in the total area of cells treated with equimolar concentrations of PA and OA ($p<0.05$) (figure 6.20). This is likely to have been due to the presence of double the concentration of lipid within the cell compared to cells only exposed to one FA.

Interestingly, even though the size of cells significantly increased of cells exposed to both PA and OA combined in equimolar concentrations, there was a statistically significant reduction in the space which the lipid occupied ($p<0.01$). These data support the hypothesis that OA shuttles PA into lipid droplets since the number of cells with lipid areas between 0 and 10 % increased from six (PA alone) (figure 6.3) to ten (figure 6.21).

The intensity of the lipid within the cells exposed to both PA and OA combined increased significantly compared to the VC ($p<0.001$) (figure 6.22). This could have been be due to the presence of double the concentration of FA within the cells. These data correlate with the data shown in figure 6.21, whereby the area of lipid decreases, suggesting that OA shuttles PA into NLDs. The hypothesis that OA shuttles PA into NLDs would be further strengthened if the composition of PA within LDs increases.

6.3.4.2 Comparison between total cell area and area of lipid (1)

The relationship between the total area of cells versus the area of lipid was compared from cells treated with non-esterified FAs and VC-treated cells (figure 6.23). The absolute values, in pixels, as opposed to percentage values, were plotted. A positive correlation was observed, whereby larger cells contain more lipid. However, outliers may skew the data. Figure 6.23 shows the data corresponding to the cells treated with 0.125 mM PA. The trend is similar to that of the VC-treated cells, however, the 0.125 mM PA-treated cells are generally smaller than the VC-treated cells. It would also seem that these smaller PA-treated cells contain less lipid. However, the single outlier may skew the data. This observation contradicts the observation in figure 6.3 which shows no significant difference between the total areas of PA- and VC-treated cells. Figure 6.23 shows the data corresponding to the cells treated with 0.125 mM OA. There is no correlation between the total area of the cell and the lipid area within the INS-1 cells. Whether there is a correlation between these two parameters, with PA and OA combined, is not clear as the data for the VC is not clear-cut either.
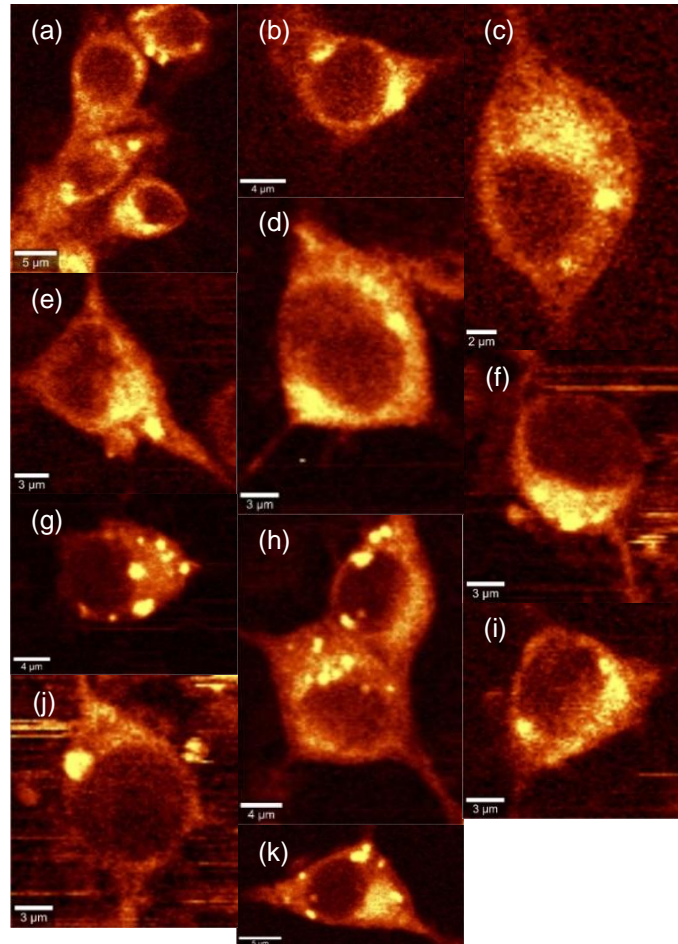
Figure 6.19 Raman maps showing distribution of lipid within palmitate- and oleic acid-treated beta cells

INS-1 cells were treated for 24 hours with complete medium, then treated with 0.125 mM palmitate and 0.125 mM oleic acid for 24 hours. (a – k) The data represent cells imaged from six experiments. Fourteen cells were imaged and pre-processed using a WiTec 300r Raman microspectrometer. The yellow pixels correspond to lipid at the CH_2 symmetric stretch vibration mode: 2845 ± 10 cm^{-1} spectral band.
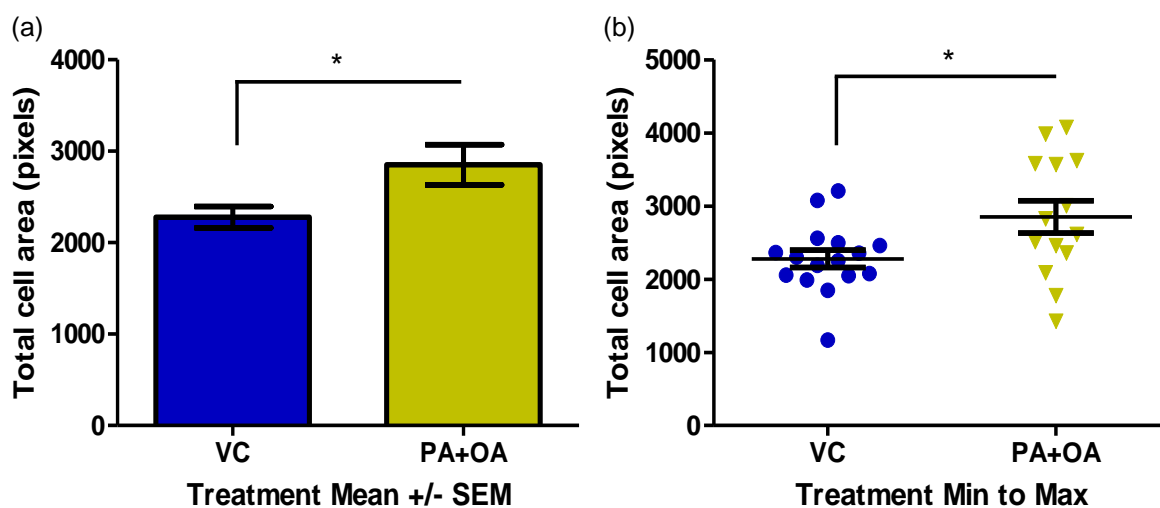
Figure 6.20 Total area of beta cells treated with palmitate and oleic acid for 24 hours

INS-1 cells were pre-treated with complete medium for 24 hours, then for 24 hours with serum-free medium. Vehicle control-treated cells were exposed to BSA + EtOH (VC; blue). Cells were treated with 0.125 mM palmitate and 0.125 mM oleic acid (PA+OA; yellow). The number of pixels corresponding to each entire cell was calculated on ImageJ after the MaxEntropy algorithm was employed. The data represent six experiments conducted where a total of 16 VC-treated cells and 14 PA+OA-treated cells were acquired for ImageJ analysis * (p<0.05). One-way ANOVA with Tukey's multiple comparison test. (a) Total cell area versus treatment. Mean ± SEM. (b) Total cell area versus treatment. Minimum to maximum values ± error.
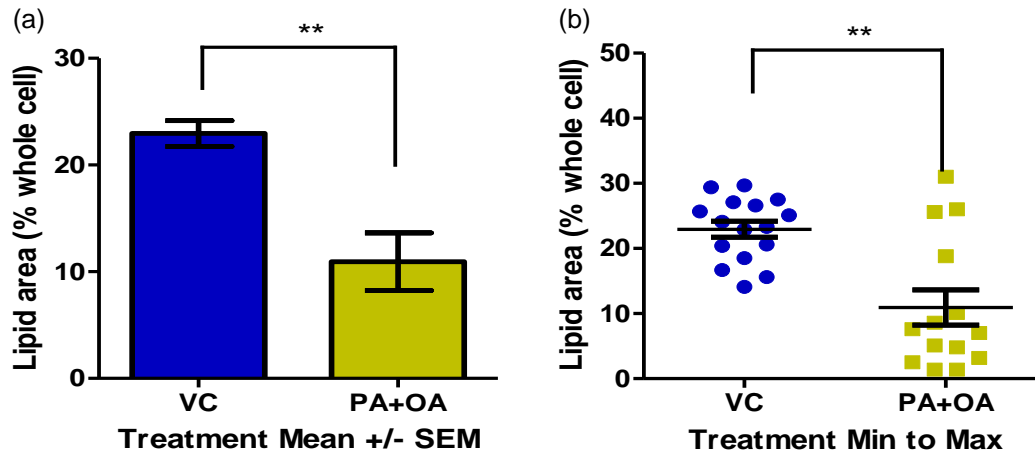
Figure 6.21 Percentage of intracellular lipid in beta cells treated with palmitate and oleic acid for 24 hours

INS-1 cells were pre-treated with complete medium for 24 hours, then for 24 hours with serum-free medium. Vehicle control-treated cells were exposed to BSA + EtOH (VC; blue). Cells were treated with 0.125 mM palmitate and 0.125 mM oleic acid (PA+OA; yellow). The number of pixels corresponding to each entire cell and the lipid within each cell was calculated on ImageJ after the MaxEntropy algorithm was employed. The percentage of lipid in each cell was subsequently calculated. The data represent six experiments conducted where a total of 16 VC-treated cells and 14 PA+OA-treated cells were acquired for ImageJ analysis. One-way ANOVA with Tukey's multiple comparison test ** ($p < 0.01$). (a) Lipid area versus treatment. Mean ± SEM. (b) Lipid area versus treatment. Minimum to maximum values ± error.
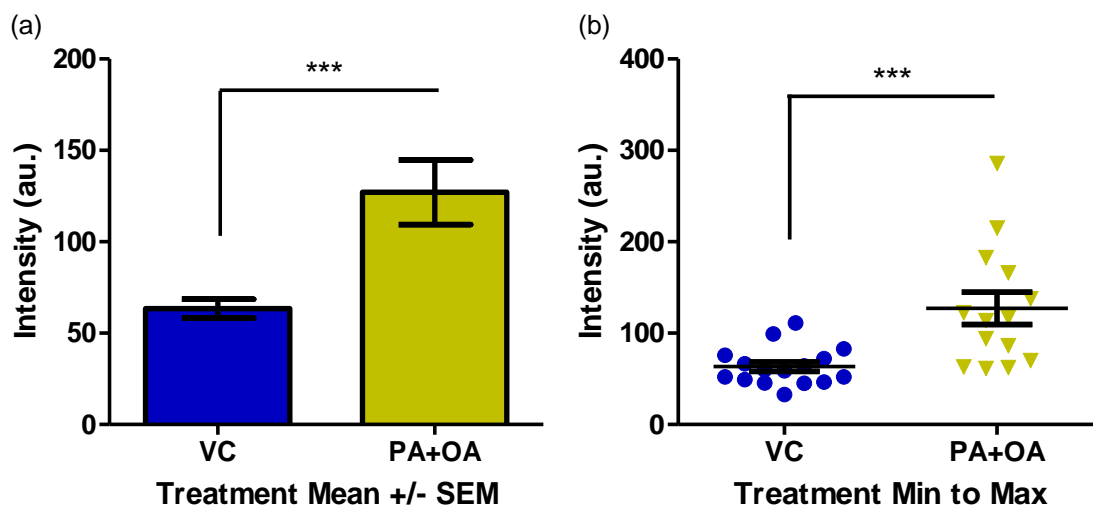
Figure 6.22 Intensity of intracellular lipid in beta cells treated with palmitate and oleic acid for 24 hours

INS-1 cells were pre-treated with complete medium for 24 hours, then for 24 hours with serum-free medium. Vehicle control-treated cells were exposed to BSA + EtOH (VC; blue). Cells were treated with 0.125 mM palmitate and 0.125 mM oleic acid (PA+OA; yellow). The intensity of the pixels corresponding to lipid within each cell was calculated on ImageJ after the MaxEntropy algorithm was employed. The data represent six experiments conducted where a total of 16 VC-treated cells and 14 PA+OA-treated cells were acquired for ImageJ analysis. One-way ANOVA with Tukey's multiple comparison test *** ($p<0.001$). (a) Lipid intensity versus treatment. Mean ± SEM. (b) Lipid intensity versus treatment. Minimum to maximum values ± error.
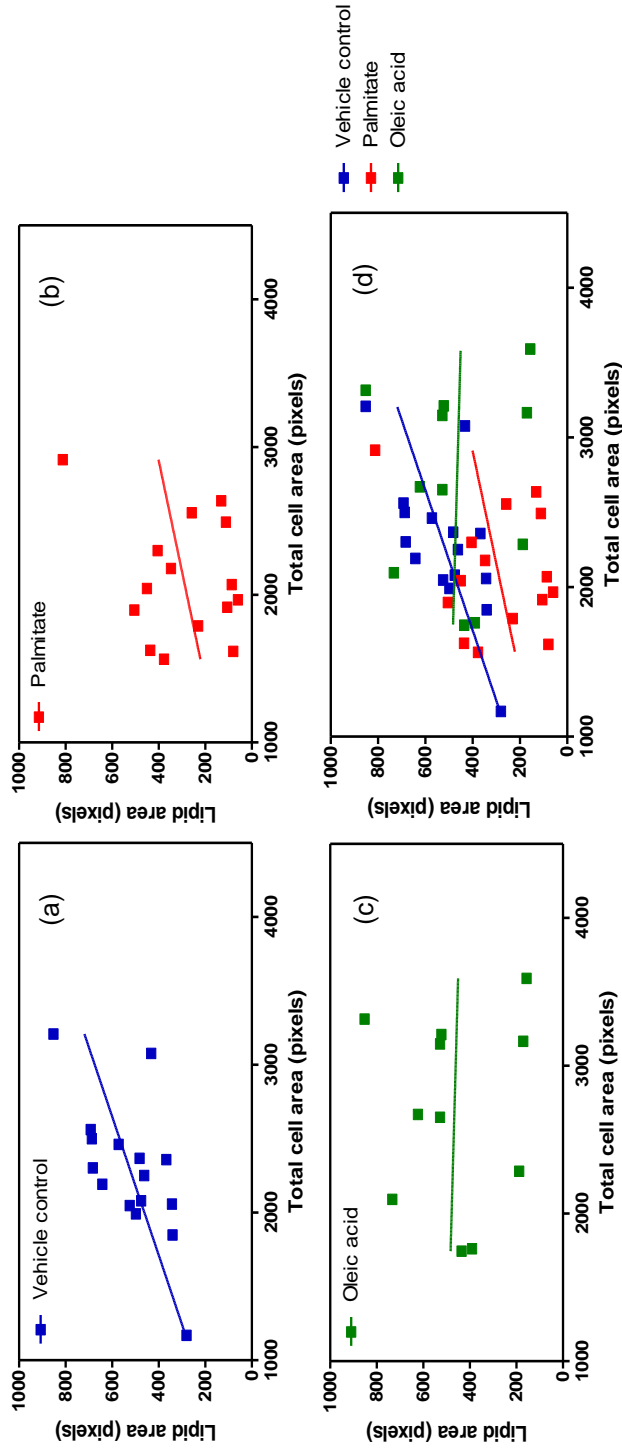
Figure 6.23 Total cell area versus lipid area in beta cells treated with non-esterified fatty acids for 24 hours

INS-1 cells were pre-treated with complete medium for 24 hours, then for 24 hours with serum-free medium and 0.125 mM fatty acid treatment: vehicle control (VC) (BSA + EtOH) (a), palmitate (PA) (b), oleic acid (OA) (c), and overlaid (d). The number of pixels corresponding to each entire cell and the area of lipid was calculated on ImageJ after the MaxEntropy algorithm was employed. The data represent six experiments conducted where a total of 16 VC-treated cells, 15 PA-treated cells and 11 OA-treated cells were acquired for ImageJ analysis. One-way ANOVA with Tukey's multiple comparison test. Mean $\pm$ SEM.

6.3.4.3 Lipid composition

6.3.4.3.1 Peak fitting

In the case for cells treated with 0.125 mM PA and 0.125 mM OA combined, equation 5.1 was employed to calculate the fold change in the AUC of the peak of interest (compare figures 6.6 and 6.24):

$$Presence\ of\ PA = \frac{AUC\ for\ 0.125\ mM\ PA\ (2883.44\ cm-1\ curve\ centre)}{AUC\ for\ VC(1)(2885.99\ cm-1\ curve\ centre)}$$

$$\frac{2900.76}{4214.09} = 0.69$$

$$\left(100x\frac{240}{2900.76}\right) + \left(100x\frac{314}{4214.09}\right) = 15.72\ \%$$

$$0.69x\left(\frac{15.72}{100}\right) = 0.108 = 0.12$$

$$0.125\ mM\ PA \div VC(1) = 0.69 \pm 0.12$$

$$Presence\ of\ OA = \frac{AUC\ for\ 0.125\ mM\ OA\ (2852.15\ cm-1\ curve\ centre)}{AUC\ for\ VC(1)(2852.13\ cm-1\ curve\ centre)}$$

$$\frac{469.71}{232.67} = 2.02$$

$$\left(100x\frac{106}{469.71}\right) + \left(100x\frac{45}{232.67}\right) = 41.91\ \%$$

$$2.02x\left(\frac{41.91}{100}\right) = 0.846 = 0.85$$

$$0.125\ mM\ OA \div VC(1) = 2.02 \pm 0.85$$

6.3.4.3.2 Overlay of pure fatty acid spectra and cell spectra

The full spectrum of pure PA was overlaid with the INS-1 cell spectrum after treatment with 0.125 mM PA and 0.125 mM OA combined (figure 6.25). It can be seen that some areas of both spectra overlap, such as at ~ 1150 cm^{-1},

between 1400 – 1500 cm^{-1}, and between 2800 cm^{-1} and 2900 cm^{-1}, similar to the observations found in figure 6.8.

The C-H region of the cell spectrum between 2800 cm^{-1} and 3050 cm^{-1} is visible in figure 6.26. The peak at ~ 2880 cm^{-1} in the spectrum of pure PA is also present in the cell spectrum.

The full spectrum of pure OA was overlaid with the INS-1 cell spectrum after treatment with 0.125 mM PA and 0.125 mM OA combined (figure 6.27). It can be seen that many areas of both spectra overlap, as seen in figure 6.17, such as between 1250 cm^{-1} and 1350 cm^{-1}, between 1400 cm^{-1} and 1500 cm^{-1}, and between 1650 cm^{-1} and 1700 cm^{-1}.

The C-H region of the cell spectrum between 2800 cm^{-1} and 3050 cm^{-1} is visible in figure 6.28. The peak at ~ 2880 cm^{-1} in the spectrum of pure PA is also present in the cell spectrum.

In conclusion, the uni-variate analysis suggests that OA shuttles PA into LDs. This was based upon the observation that the area of lipid decreases and the intensity of lipid increases. However, this effect was also found with cells treated with 0.125 mM PA alone, therefore rendering it difficult to determine whether OA is indeed able to have the effect on the cell as originally hypothesised. Therefore, the uni-variate analysis suggests that the mechanism by which OA is able to protect against PA-induced toxicity is not via the incorporation of PA into LDs, since this effect was observed with PA alone. These data suggest that the mechanism of protection of OA is via a different mechanism. Interestingly, the multi-variate analysis found that the presence of PA within LDs decreased (0.69 fold change), yet the presence of OA increased (2.02 fold change). Why this occurred is not clear, however, it could either be suggested that: (1) OA is able to induce the breakdown of PA, (2) OA is able to upregulate desaturase enzymes

which convert PA into palmitoleate and are themselves incorporated into LDs, or

(3) PA is able to shuttle OA into LDs.
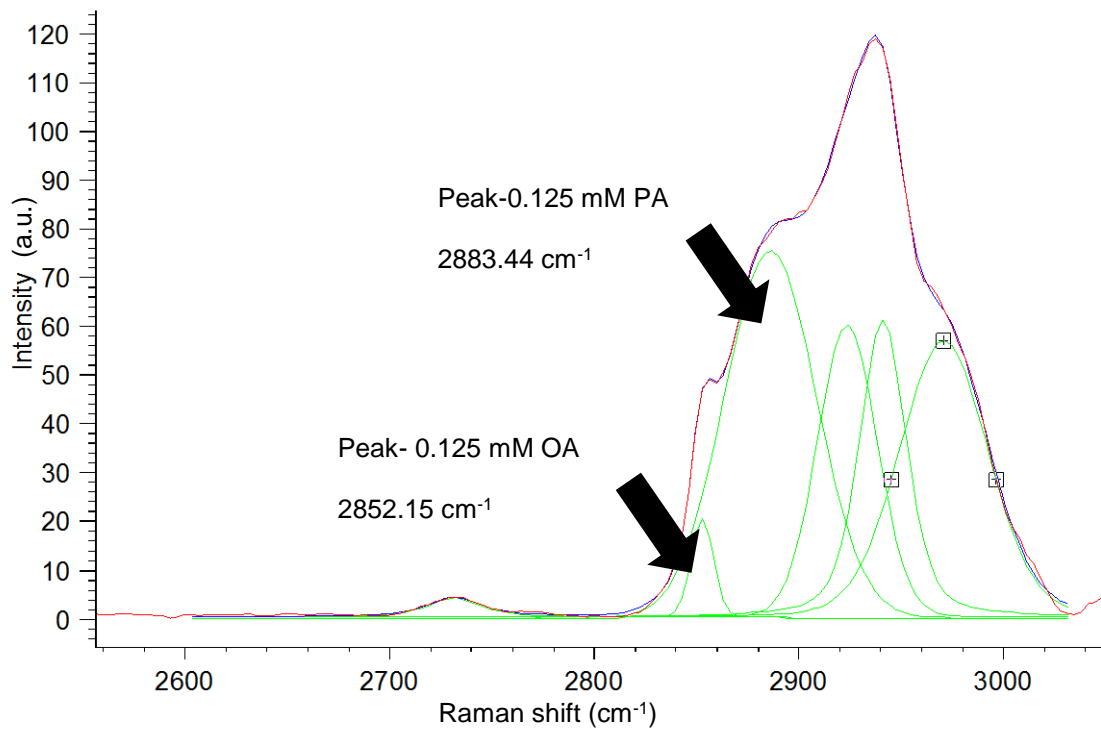
Figure 6.24 Peak fitting of spectrum representing INS-1 cells treated with 0.125 mM palmitate and 0.125 mM oleic acid

The spectra of 14 INS-1 cells treated with 0.125 mM palmitate and 0.125 mM oleic acid combined were averaged (red line). Peak fitting was conducted (blue line) whereby six peaks were fitted to decompose the spectrum (green lines). Spectral range 2600 – 3050 cm^{-1}.
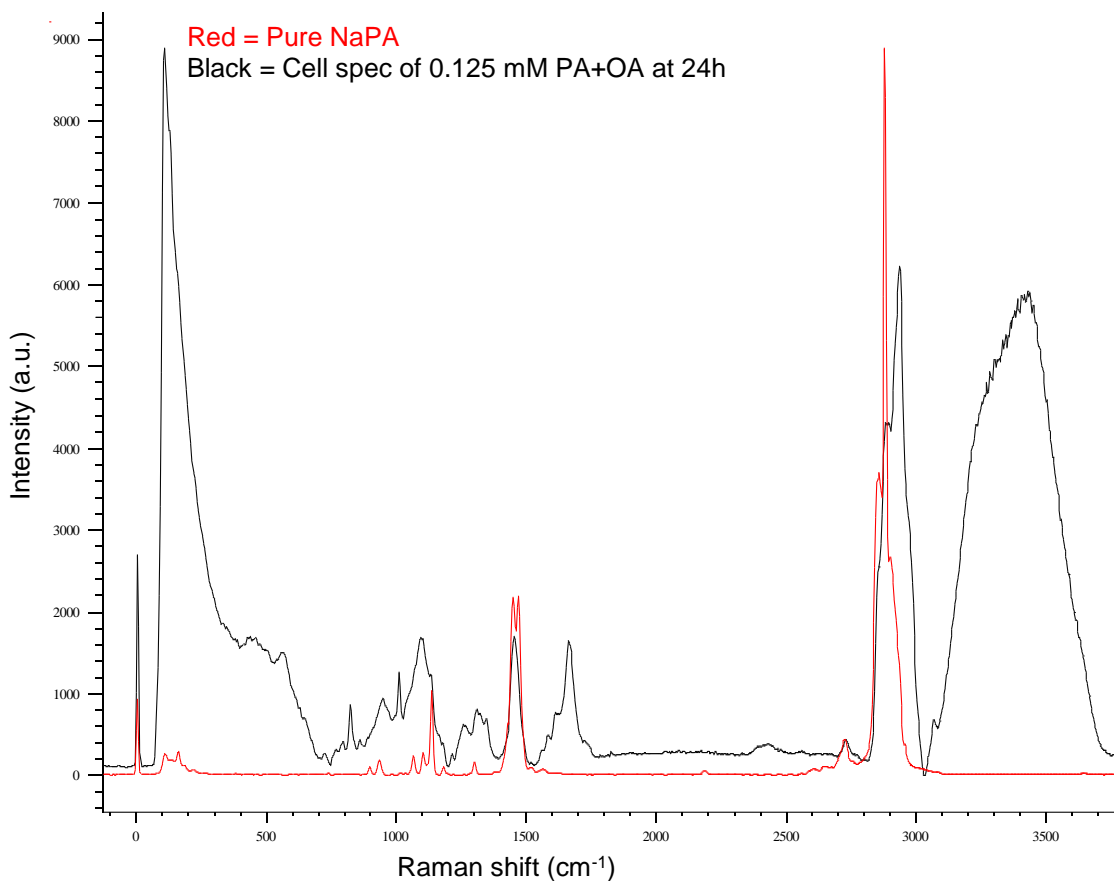
Figure 6.25 Full spectrum of pure palmitate overlaid with cell spectrum after treatment with 0.125 mM palmitate and 0.125 mM oleic acid

Red spectrum represents pure palmitate. Black spectrum represents averaged spectra of cells treated with 0.125 mM palmitate and 0.125 mM oleic acid combined. Spectral range 0 – 3800 cm^{-1}.
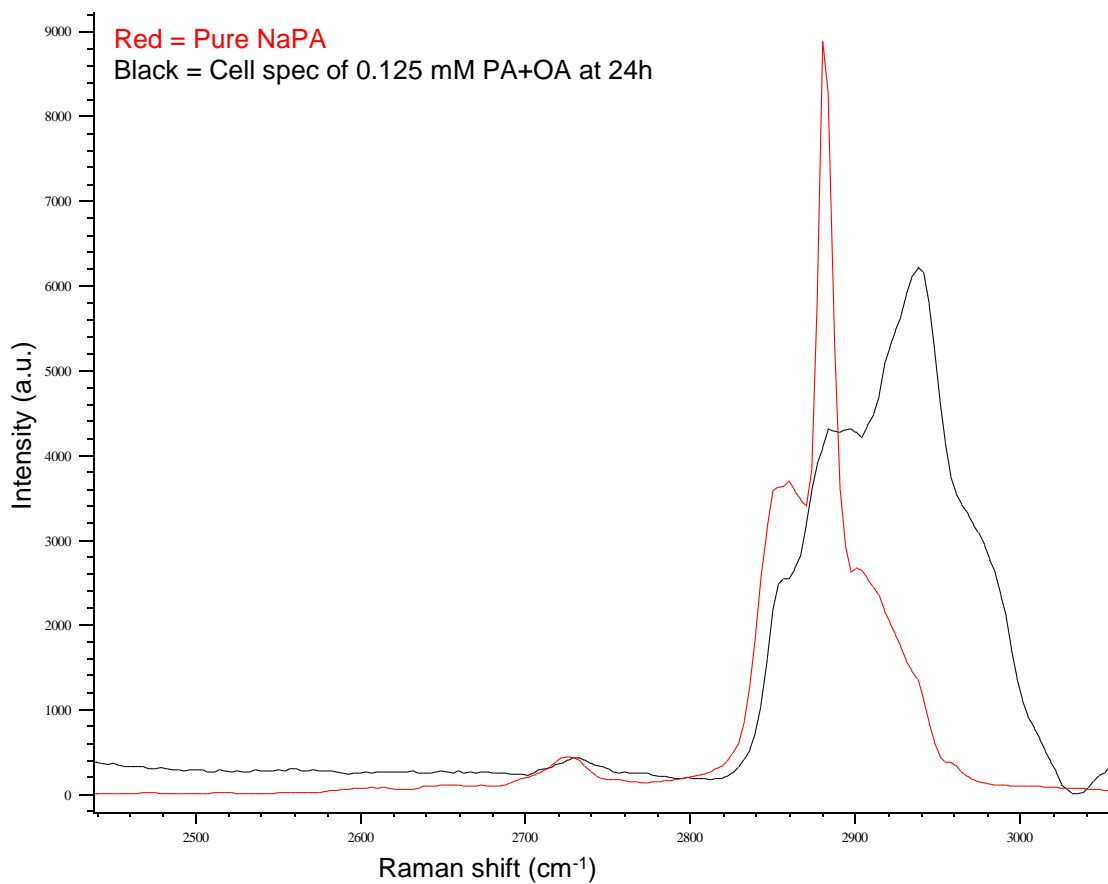
Figure 6.26 Spectrum of pure palmitate overlaid with cell spectrum after treatment with 0.125 mM palmitate and 0.125 mM oleic acid

Red spectrum represents pure palmitate. Black spectrum represents averaged spectra of cells treated with 0.125 mM palmitate and 0.125 mM oleic acid combined. Spectral range 2440 – 3060 cm^{-1}.
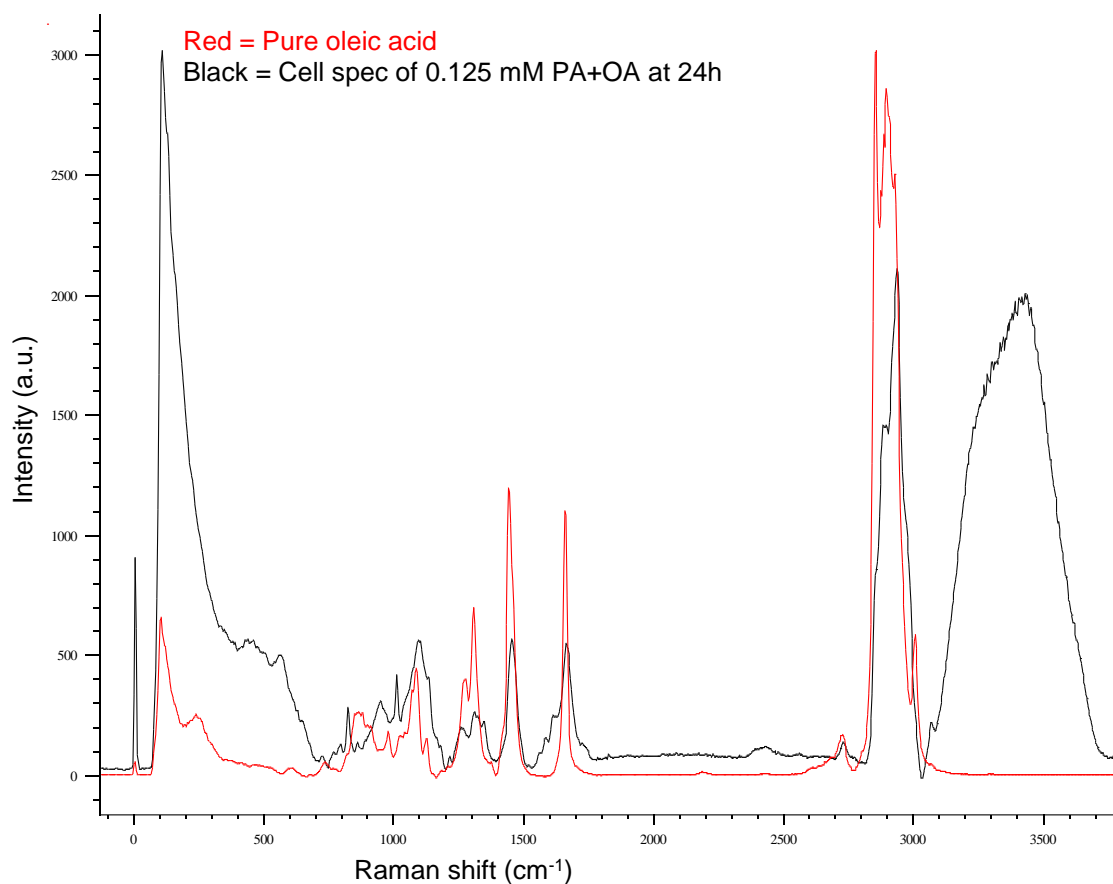
Figure 6.27 Full spectrum of pure oleic acid overlaid with cell spectrum after treatment with 0.125 mM palmitate and 0.125 mM oleic acid

Red spectrum represents pure oleic acid. Black spectrum represents averaged spectra of cells treated with 0.125 mM palmitate and 0.125 mM oleic acid combined. Spectral range 0 – 3800 cm^{-1}.
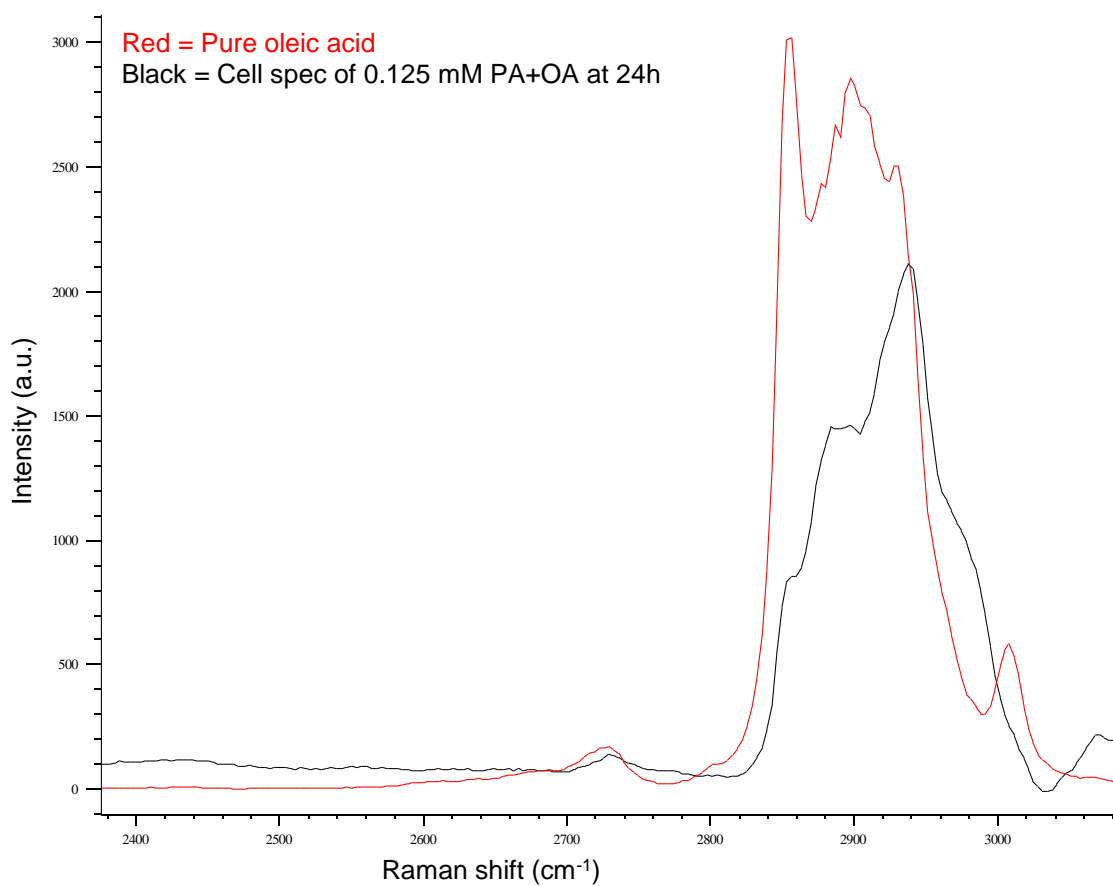
Figure 6.28 Spectrum of pure oleic acid overlaid with cell spectrum after treatment with 0.125 mM palmitate and 0.125 mM oleic acid

Red spectrum represents pure oleic acid. Black spectrum represents averaged spectra of cells treated with 0.125 mM palmitate and 0.125 mM oleic acid combined. Spectral range 2380 – 3080 cm^{-1}.

6.3.5 Vehicle control-treated cells versus esterified FA-treated cells (0.125 mM)

6.3.5.1 Lipid distribution and concentration

The VC-treated cells presented here (figure 6.29) have the same lipid distribution as the cells previously shown in figure 6.6. VC-treated maps show a consistent distribution of lipid (bonds corresponding to the CH_2 symmetric stretch vibration mode) throughout the cells.

The cells treated with 0.125 mM MePA showed the same distribution of lipid as the untreated cells (compare figures 6.29 and 6.30). In addition, the cells treated with 0.125 mM MeOA showed the same distribution of lipid as the untreated and the MePA-treated cells (compare figures 6.29, 6.30 and 6.31).

There was no statistically significant change in the total area of cells treated with esterified FAs compared to the untreated cells (figure 6.32). The range of data points of all esterified FA-treated cells was comparable to the untreated cells. These data were comparable to the cells treated with PA and OA alone (compare figures 6.3, 6.13 and 6.32).

There was no statistically significant change in the area of lipid within cells treated with esterified FAs compared to the untreated cells (figure 6.33). There was also no change in the variation of the data points of cells (i.e. different population of cells were not observed) treated with MeOA, unlike the cells treated with OA (compare figures 6.14 and 6.33). On the other hand, a significant variation in lipid area was observed with PA, but not with MePA (compare figures 6.4 and 6.33). These data suggest that esterified FAs are inert and are not incorporated into NLDs, probably due to their structural composition whereby the carboxyl oxygen atom is not biologically available for activation via CoA.

There was no significant difference in intensity values between cells treated with esterified FAs compared to the untreated cells (figure 6.34). No

significant difference between MePA-treated cells and the untreated cells was observed, unlike between PA-treated cells and the untreated cells (figure 6.4). By contrast, cells exposed to MeOA exhibited the same trend as the cells treated with OA, however, two MeOA data points in this data-set have intensity values greater than 125 au (compare figures 6.15 and 6.34). It is not clear what the biological significance of these two data points are. It is possible that cosmic rays were not removed from the pixels within the maps, causing a spike in intensity.

Since no statistical significance was observed between the lipid content of the maps esterified FA-treated cells and VC-treated cells, it can be suggested that either: (1) esterified FAs are not incorporated into NLDs, or (2) esterified FAs do not enter cells. Multi-variate data would add evidence to determine whether these hypotheses hold any truths. This would be done by determining whether peaks corresponding to pure PA and OA (peak fitting analysis) appear in the lipid of cells treated with MePA and MeOA, respectively.

6.3.5.2 Comparison between total cell area and area of lipid (2)
The relationship between the total area of cells versus the area of lipid was compared from cells treated with esterified FAs and VC-treated cells (figure 6.35). There was a positive correlation of the total cell area and the lipid area of untreated cells. Further, the VC data was comparable to all the cells exposed to esterified FAs, whereby there was no change in the range of data points. Given that the trend in data for the cells treated with the VC are identical in figures 6.23 and 6.35, these data give confidence that the data from these two separate data-sets are true. I can also be confident that the data for the non-esterified FAs (PA and OA alone) are true.

Further, these data suggest that long-chain esterified SFAs, long-chain esterified UFAs and long-chain non-esterified UFAs, alone, do not affect the

distribution of LDs within INS-1 cells. By contrast, non-esterified SFAs, do affect the distribution of lipid within INS-1 cells (compare figures 6.23 and 6.35).
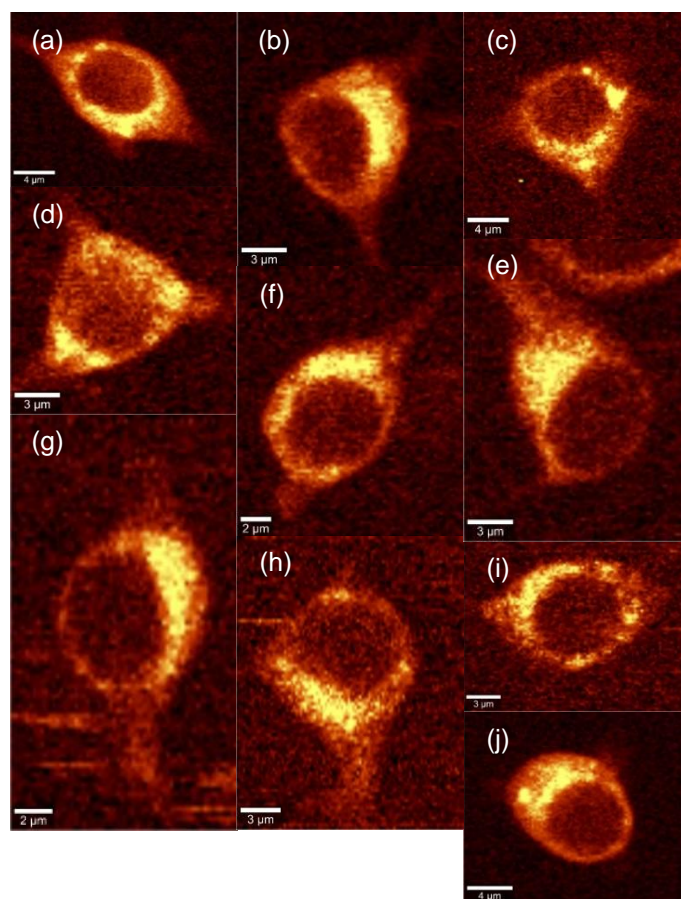
Figure 6.29 Raman maps showing distribution of lipid within untreated beta cells

INS-1 cells were treated for 24 hours with complete medium, then treated with BSA and EtOH in serum-free medium for 24 hours. (a – j) The data represent cells imaged from three experiments. Ten cells were imaged and pre-processed using a WiTec 300r Raman microspectrometer. The yellow pixels correspond to lipid at the CH_2 symmetric stretch vibration mode: 2845 ± 10 cm^{-1} spectral band.
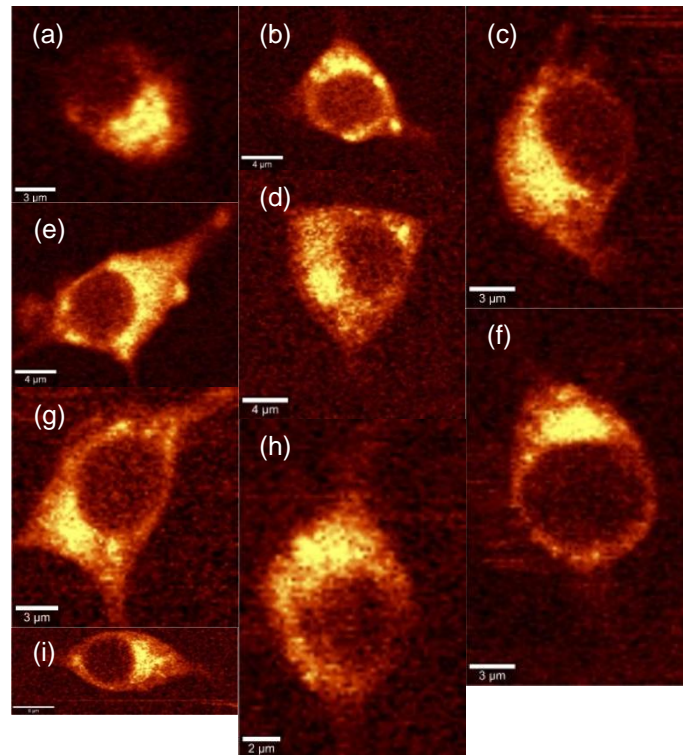
Figure 6.30 Raman maps showing distribution of lipid within methyl palmitate-treated beta cells

INS-1 cells were treated for 24 hours with complete medium, then treated with 0.125 mM methyl palmitate for 24 hours. (a – i) The data represent cells imaged from three experiments. Nine cells were imaged and pre-processed using a WiTec 300r Raman microspectrometer. The yellow pixels correspond to lipid at the CH_2 symmetric stretch vibration mode: 2845 ± 10 cm^{-1} spectral band.
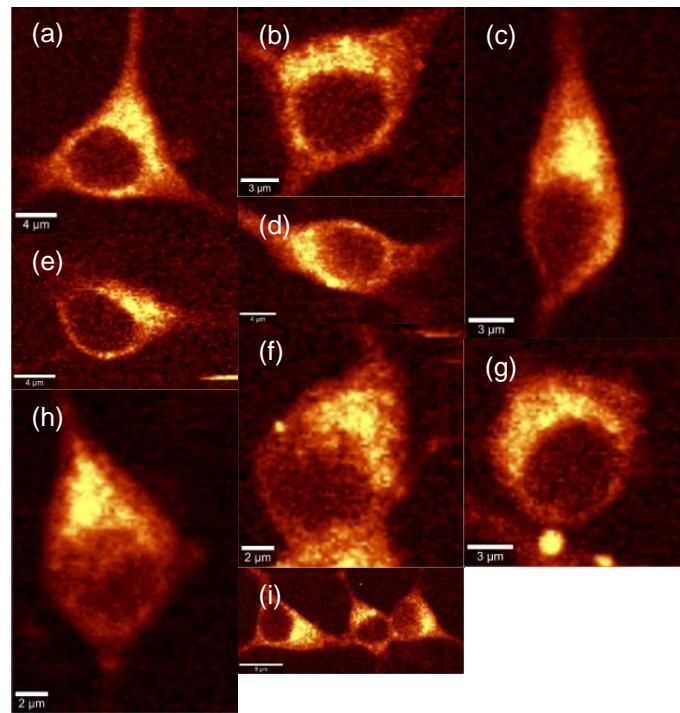
Figure 6.31 Raman maps showing distribution of lipid within methyl oleate-treated beta cells

INS-1 cells were treated for 24 hours with complete medium, then treated with 0.125 mM methyl oleate for 24 hours. (a – j) The data represent cells imaged from three experiments. Eleven cells were imaged and pre-processed using a WiTec 300r Raman microspectrometer. The yellow pixels correspond to lipid at the CH_2 symmetric stretch vibration mode: 2845 ± 10 cm^{-1} spectral band.
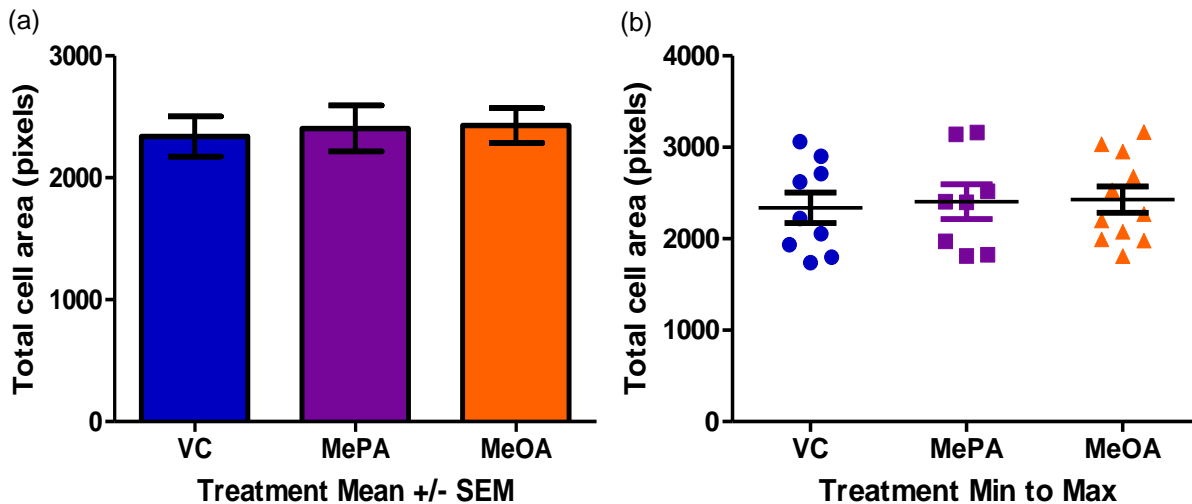
Figure 6.32 Total area of beta cells treated with esterified fatty acids for 24 hours
INS-1 cells were pre-treated with complete medium for 24 hours, then for 24 hours with serum-free medium and 0.125 mM fatty acid treatment: vehicle control (VC; BSA + EtOH; blue), methyl palmitate (MePA; purple) and methyl oleate (MeOA; orange). The number of pixels corresponding to each entire cell was calculated on ImageJ after the MaxEntropy algorithm was employed. The data represent three experiments conducted where a total of nine VC-treated cells, eight MePA-treated cells and 11 MeOA-treated cells were acquired for ImageJ analysis. One-way ANOVA with Tukey's multiple comparison test. (a) Total cell area versus treatment. Mean ± SEM. (b) Total cell area versus treatment. Minimum to maximum values ± error.

Figure 6.33 Percentage of intracellular lipid in beta cells treated with esterified fatty acids for 24 hours

INS-1 cells were pre-treated with complete medium for 24 hours, then for 24 hours with serum-free medium and 0.125 mM fatty acid treatment: vehicle control (VC; BSA + EtOH; blue), methyl palmitate (MePA; purple) and methyl oleate (MeOA; orange). The number of pixels corresponding to each entire cell and the lipid within each cell was calculated on ImageJ after the MaxEntropy algorithm was employed. The percentage of lipid in each cell was subsequently calculated. The data represent three experiments conducted where a total of nine VC-treated cells, eight MePA-treated cells and 11 MeOA-treated cells were acquired for ImageJ analysis. One-way ANOVA with Tukey's multiple comparison test. (a) Lipid area versus treatment. Mean ± SEM. (b) Lipid area versus treatment. Minimum to maximum values ± error.

Figure 6.34 Intensity of intracellular lipid in beta cells treated with esterified fatty acids for 24 hours

INS-1 cells were pre-treated with complete medium for 24 hours, then for 24 hours with serum-free medium and 0.125 mM fatty acid treatment: vehicle control (VC; BSA + EtOH; blue), methyl palmitate (MePA; purple) and methyl oleate (MeOA; orange). The intensity of the pixels corresponding to lipid within each cell was calculated on ImageJ after the MaxEntropy algorithm was employed. The data represent three experiments conducted where a total of nine VC-treated cells, eight MePA-treated cells and 11 MeOA-treated cells were acquired for ImageJ analysis. One-way ANOVA with Tukey's multiple comparison test. (a) Lipid intensity versus treatment. Mean ± SEM. (b) Lipid intensity versus treatment. Minimum to maximum values ± error.
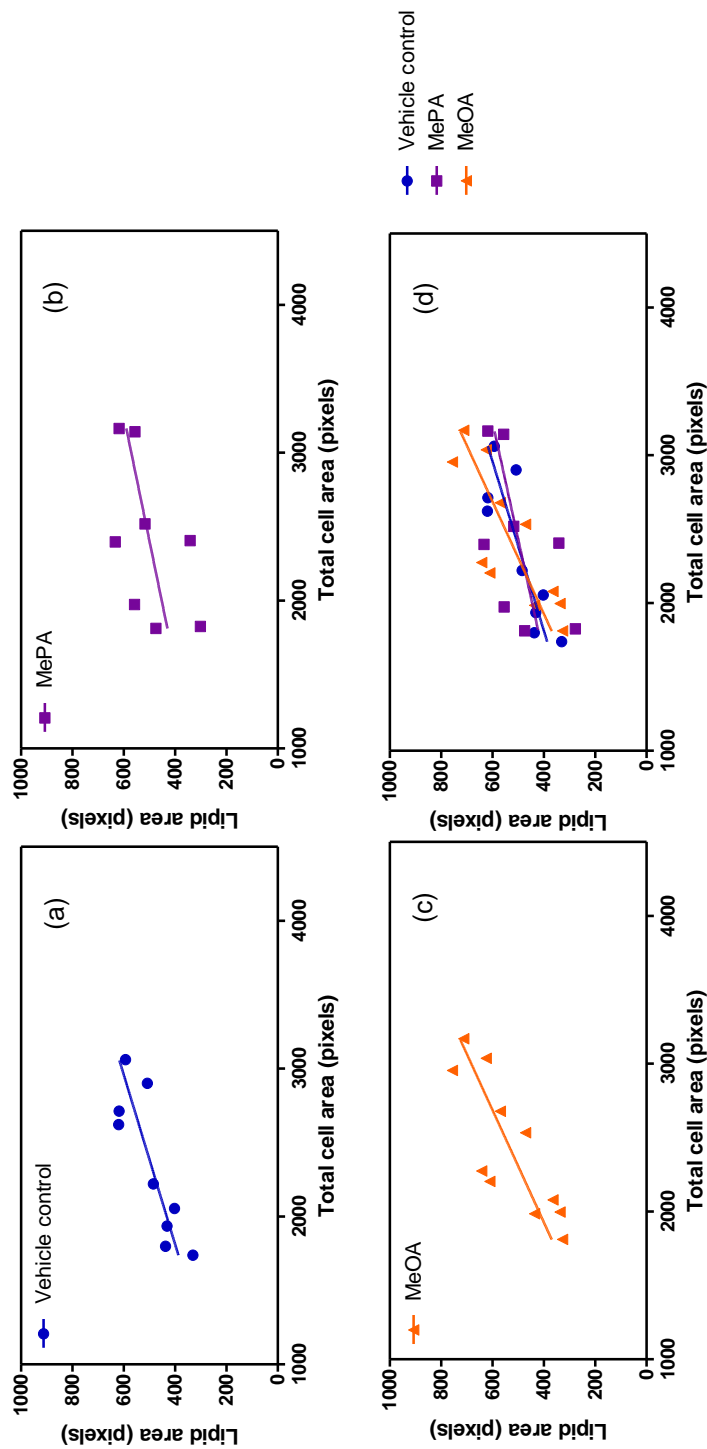
Figure 6.35 Total cell area versus lipid area in beta cells treated with esterified fatty acids for 24 hours

INS-1 cells were pre-treated with complete medium for 24 hours, then for 24 hours with serum-free medium and 0.125 mM fatty acid treatment: vehicle control (VC) (BSA + EtOH) (a), methyl palmitate (MePA) (b), methyl oleate (MeOA) (c), and overlaid (d). The number of pixels corresponding to each entire cell and the area of lipid was calculated on ImageJ after the MaxEntropy algorithm was employed. The data represent three experiments conducted where a total of nine VC-treated cells, eight MePA-treated cells and 11 MeOA-treated cells were acquired for ImageJ analysis. One-way ANOVA with Tukey's multiple comparison test. Mean ± SEM.

6.3.5.3 Lipid composition

6.3.5.3.1 Peak fitting

In the case for cells treated with 0.125 mM MePA, equation 5.1 was employed to calculate the fold change in the AUC of the peak of interest (compare figures 6.36 and 6.37):

$$Presence\ of\ PA = \frac{AUC\ for\ 0.125\ mM\ MePA\ (2880.43\ cm - 1\ curve\ centre)}{AUC\ for\ VC(3)(2880.98\ cm - 1\ curve\ centre)}$$

$$\frac{2061.87}{1890.16} = 1.09$$

$$\left(100x\frac{1030}{2061.87}\right) + \left(100x\frac{1053}{1890.16}\right) = 105.66\ \%$$

$$1.09x\left(\frac{105.66}{100}\right) = 1.15$$

$$0.125\ mM\ MePA \div VC(3) = 1.09 \pm 1.15$$

In the case for cells treated with 0.125 mM MeOA, equation 5.1 was employed to calculate the fold change in the AUC of the peak of interest (compare figures 6.36 and 6.38):

$$Presence\ of\ OA = \frac{AUC\ for\ 0.125\ mM\ MeOA\ (2853.52\ cm - 1\ curve\ centre)}{AUC\ for\ VC(3)(2853.23\ cm - 1\ curve\ centre)}$$

$$\frac{298.25}{190.27} = 1.57$$

$$\left(100x\frac{90}{298.25}\right) + \left(100x\frac{85}{190.27}\right) = 73.80\ \%$$

$$1.57x\left(\frac{73.80}{100}\right) = 1.16$$

$$0.125\ mM\ MeOA \div VC(3) = 1.57 \pm 1.16$$

A detailed comparison of the spectra of pure PA and OA with the spectra from cells exposed to MePA and MeOA was not conducted.

A summary of the peak fitting data for all treatments presented in this thesis can be found in table 6.1.

The uni-variate analysis found no change in the total cell area, lipid area or lipid intensity of cells exposed to 0.125 mM MePA compared to the untreated cells. Since no change was observed in these parameters, it can be suggested that MePA does not enter cells. To correlate with this data, the multi-variate analysis found a fold change of only 1.09 of the decomposed cell spectra corresponding to MePA and spectra corresponding to the VC suggesting that MePA does not become incorporated into LDs.

In addition, the uni-variate analysis found no change in the total cell area, lipid area or lipid intensity of cells exposed to 0.125 mM MeOA compared to the untreated cells. Because of this, these data, and the MePA data, suggest that these FAs do not become incorporated into LDs, possibly due to their chemical structures. These data have also led to the hypothesis that esterified FAs do not enter cells. This is because a displacement of the aqueous cytoplasmic content is likely to be observed when a hydrophobic structure enters the cell, even one which is not metabolised. In contrast, multi-variate analysis found a large fold increase between the decomposed peak of the cell spectrum of MeOA-treated cells and the VC-treated cells (1.57 fold change). These data suggest that OA becomes incorporated into LDs. However, whether MeOA partitions into LDs or whether endogenous OA becomes covalently incorporated into LDs is not clear. In addition, these data cannot conclude whether MeOA does or does not enter cells, however, it could be suggested that MeOA has an extracellular effect on the cell, whereby a signalling pathway initiated from outside the cell, by MeOA,

induces the intracellular production of OA, enabling OA to be subsequently incorporated into LDs.
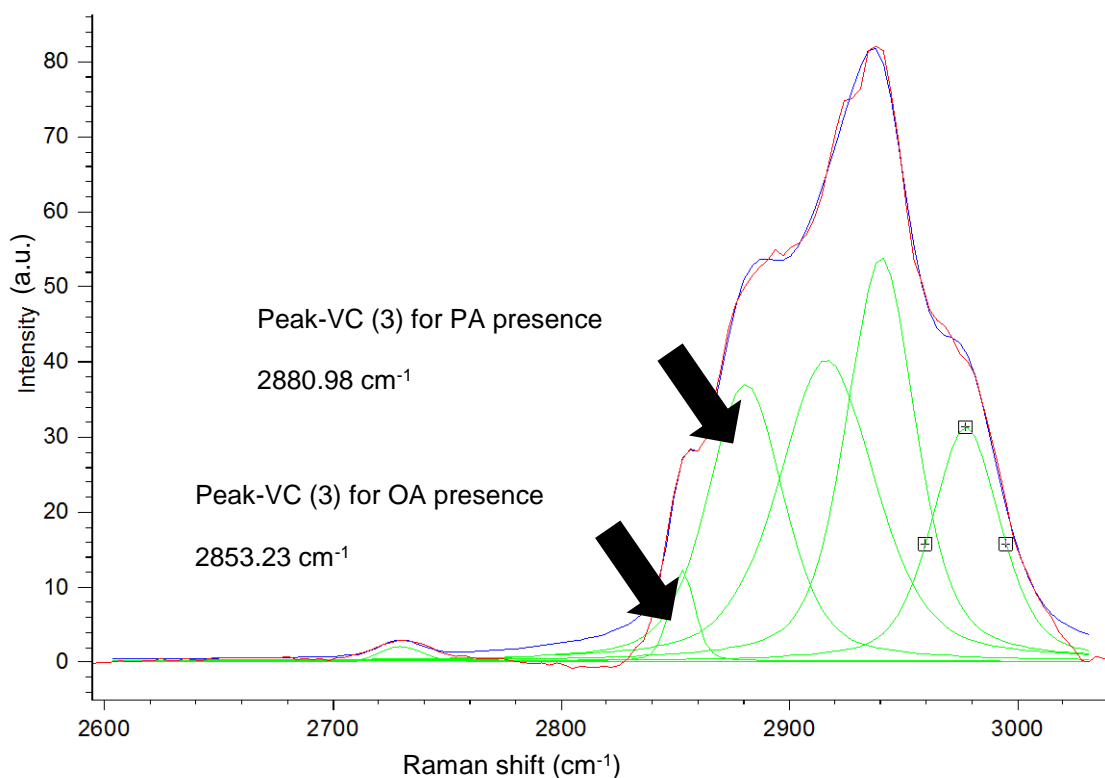
Figure 6.36 Peak fitting of spectrum representing INS-1 cells treated with the vehicle control (3)

The spectra of nine INS-1 cells treated with the vehicle control were averaged (red line). Peak fitting was conducted (blue line) whereby six peaks were fitted to decompose the spectrum (green lines). Spectral range 2600 – 3040 cm^{-1}.
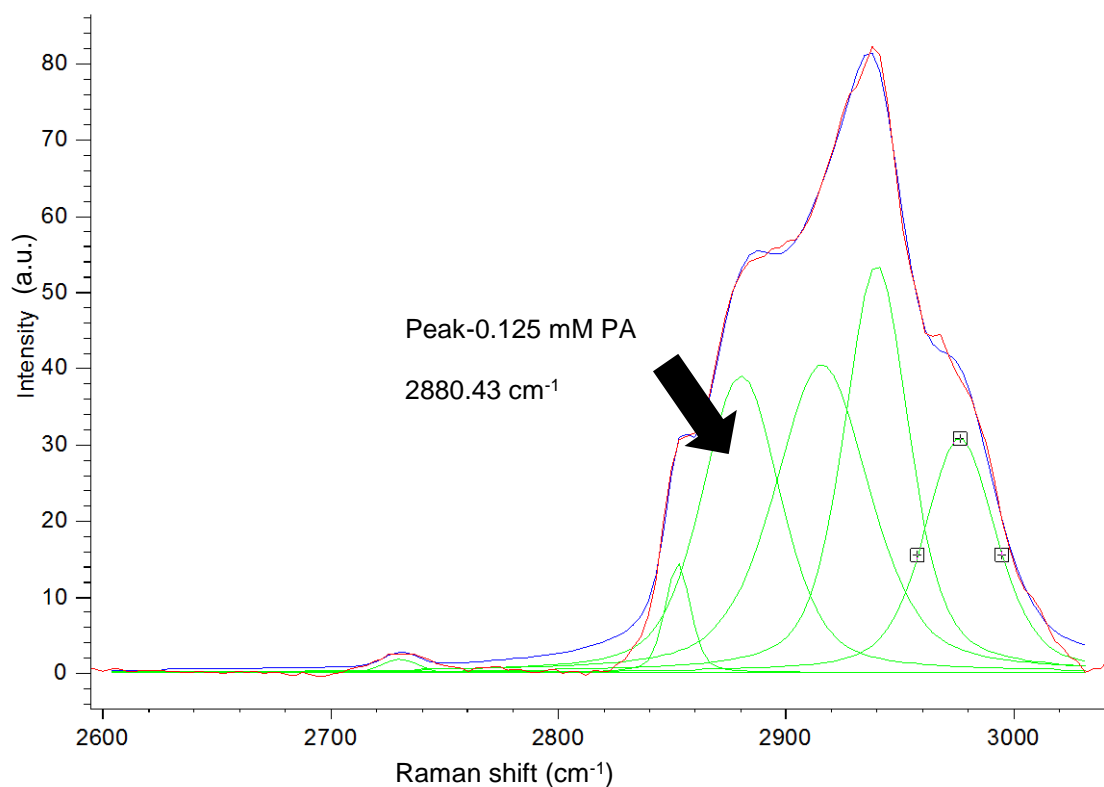
Figure 6.37 Peak fitting of spectrum representing INS-1 cells treated with 0.125 mM methyl palmitate

The spectra of eight INS-1 cells treated with 0.125 mM methyl palmitate were averaged (red line). Peak fitting was conducted (blue line) whereby six peaks were fitted to decompose the spectrum (green lines). Spectral range 2600 – 3040 cm^{-1}.
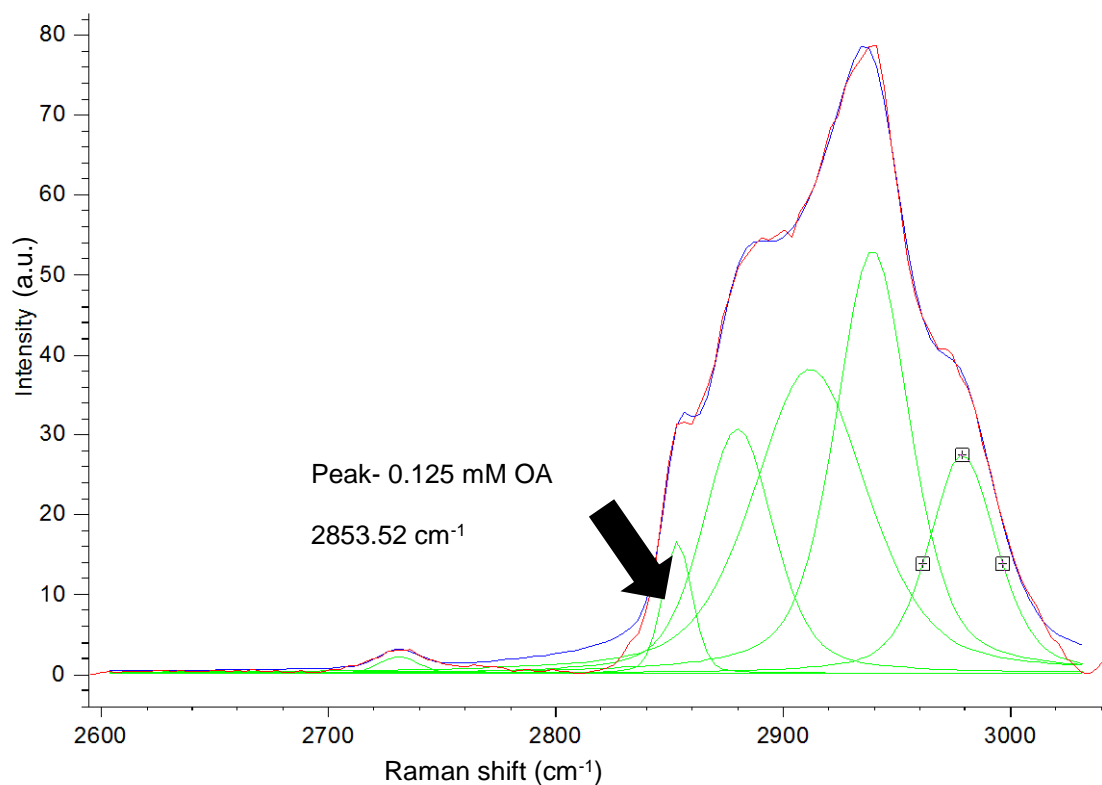
Figure 6.38 Peak fitting of spectrum representing INS-1 cells treated with 0.125 mM methyl oleate

The spectra of 11 INS-1 cells treated with 0.125 mM methyl oleate were averaged (red line). Peak fitting was conducted (blue line) whereby six peaks were fitted to decompose the spectrum (green lines). Spectral range 2600 – 3040 cm^{-1}.

Summary of fold changes AUC				
AUC of peak from FA-treatment/ AUC of peak from VC = fold change				
Peak centre of curve of interest for PA presence: ~ 2881.65 cm^{-1}				
	VC curve centre	VC area	FA curve centre	FA area
PA 0.125 mM	2885.99 cm^{-1}	4214.09	2882.28 cm^{-1}	4378.84
PA 0.5 mM	2881.65 cm^{-1}	2126.48	2881.98 cm^{-1}	2594.63
PA+OA 0.125 mM	2885.99 cm^{-1}	4214.09	2883.44 cm^{-1}	2900.76
MePA 0.125 mM	2880.98 cm^{-1}	1890.16	2852.64 cm^{-1}	2061.87
Treatment			**Fold change**	
PA 0.125 mM/ VC = 4378.84/ 4214.09			1.04 ± 0.16	
PA 0.5 mM/ VC = 2594.63/ 2126.48			1.22 ± 0.22	
PA+OA 0.125 mM/ VC = 2900.76/ 4214.09			0.69 ± 0.12	
MePA 0.125 mM/ VC = 2061.87/ 1890.16			1.09 ± 1.15	
Peak centre of curve of interest for OA presence: ~ 2853.52 cm^{-1}				
	VC curve centre	VC area	FA curve centre	FA area
OA 0.125 mM	2852.13 cm^{-1}	232.67	2853.05 cm^{-1}	289.49
PA+OA 0.125 mM	2852.13 cm^{-1}	232.67	2852.15 cm^{-1}	469.71
MeOA 0.125 mM	2853.23 cm^{-1}	190.27	2853.52 cm^{-1}	298.25
Treatment			**Fold change**	
OA 0.125 mM/ VC = 289.49/ 232.67			1.24 ± 0.66	
PA+OA 0.125 mM/ VC = 469.71/ 232.67			2.02 ± 0.85	
MeOA 0.125 mM/ VC = 298.25/ 190.27			1.57 ± 1.16	

Table 6.1 Summary of peak area changes after spectral decomposition of FA-treated spectra versus vehicle control-treated spectra

The area of each decomposed peak of interest are presented in this table. The AUC from the spectrum corresponding to a FA treatment was divided by the corresponding AUC of the VC treatment. The resulting value represents the fold change and the error as SEM.

6.4 Discussion

6.4.1 Uni-variate analysis

6.4.1.1 Total cell area

The total area of each 2D image was calculated for the purposes of determining whether the exposure of INS-1 cells to exogenous FAs (non-esterified and esterified) affected the size of the cell. These data also allowed for the determination of the relative quantity of lipid within each cell, by means of calculating the percentage of area occupied by lipid within each cell. The absolute numbers of pixels corresponding to lipid can be found in figures 6.23 and 6.35.

The total area of cells did not change upon exposure to 0.125 mM PA, OA, MePA or MeOA alone. However, there was a significant increase in the area of cells exposed to PA and OA in combination. This increase could be due to the physical presence of double the concentration of FAs within the cells. Interestingly, there was no difference in the total area of cells exposed to 0.5 mM PA compared to cells exposed to the VC. This suggests that the cause of the expanded cells exposed to PA and OA combined may not be due to the physical presence of double (or an increase in) the concentration of FAs, but may instead be due to the additional, specific presence of OA. It could otherwise be suggested that the reason why an increase in cell size was not observed of cells exposed to 0.5 mM PA was because the additional PA was metabolised. Otherwise, had an increase in total cell area been observed, this might have suggested that the PA had not been metabolised and that it had instead displaced the aqueous contents in the cytoplasm. By contrast, the slight, yet insignificant, decrease in the total cell area of cells treated with 0.5 mM PA might be interpreted as a pre-/ apoptotic state of the cell, a change that might become more pronounced with a larger data-set. It is apparent that these data are complex and can be overinterpreted.

Since the total area of cells exposed to 0.125 mM PA did not change, these data validate the chosen FA dose (0.125 mM) and time point (24 hours), and also provides confidence in the methodology. This is because cells exposed to harmful levels of PA normally reduce in size, a known characteristic of the process of apoptosis. In addition the detachment of cells from their substrate was observed when Schie *et al.* (2013) exposed HepG2 cells to 0.25 mM palmitic acid for 24 hours. This occurred because the dose of FA the cells were exposed to was too high and resulted in palmitic acid-induced cell death. This was an error I wanted to avoid; I wanted to be sure that any changes observed in the PA-treated INS-1 cells were not attributable to the cells undergoing apoptotic changes or due to any other factors. Since statistically significant cell-shrinkage was not observed in the INS-1 cells exposed to both 0.125 mM PA and 0.5 mM PA, any changes in lipid distribution cannot have been due to a result of a change in the size of the cell or due to advanced apoptotic changes. The data presented in this Chapter therefore represent changes in lipid distribution and composition that would occur in cells which are likely to be in the resting phase (G0+G1 phase) of the cell cycle. However, it should be noted, that the INS-1 cells exposed to both 0.125 mM and 0.5 mM PA may have undergone pre-apoptotic changes, and this could be investigated further, as described in section 6.4.1.2.

6.4.1.2 Lipid area

The percentage of lipid within each 2D image of the cells was calculated to determine whether differential exogenous FAs affected intracellular lipid distribution (more specifically the area which the lipid occupied).

Upon exposure to 0.125 mM PA, the percentage of lipid within cells decreased significantly. Interestingly, the scatterplot in figure 6.4 shows two populations of cells. One population, consisting of nine cells, is comparable to the

population of cells exposed to the VC. A second population of cells consists of six cells which contain significantly less lipid than the cells exposed to the VC. This observed heterogeneity of the cell population may be due to some cells (those which contain less lipid compared to the VC-treated cells) being less able to tolerate the exogenously supplied PA. However, why this might be the case is not clear as the cells with low percentages of lipid also have normal total cell areas (i.e. total cell areas which are comparable to VC-treated cells). The levels of the enzyme Δ-9-desaturase within these cells may play a role. As previously discussed in Chapter 1, these enzymes are responsible for the conversion of SFAs to UFAs. The presence of UFAs, which are preferentially metabolised over SFAs (Voet *et al.* 2000), may decrease within some cells. By contrast, some cells may have elevated levels of these enzymes, thus enabling them to convert PA into palmitoleate, thereby enabling them to tolerate the presence of elevated levels of PA and evade apoptosis. It must be noted, however, that beta-cell heterogeneity has previously been reported *in vitro* by Cao *et al.* (2016). Heterogeneity in the uptake of deuterated palmitic acid has also been observed in macrophage cells *in vitro* (Stiebing *et al.* 2014; Stiebing *et al.* 2017). The reviews by Benninger & Hodson (2018) and Pipeleers *et al.* (2017) highlight that differences in beta-cell responses *in vivo* may be due to various reasons, such as the phase of the cell cycle, and the degree to which cells are exposed to vascularisation. Although cells *in vitro* are not exposed to vasculature, other spatial factors, such as the seeding density, may affect whether some cells are exposed to more or less FAs than others. The hypothesis that the accumulation of lipid droplets might be subject to the phase of the cell cycle was suggested by Gocze & Freeman (1994). This is an interesting hypothesis since it suggests that the presence of certain FAs affects the cell cycle (as discussed in Chapter 4).

Based on the morphological requirements (cellular and nuclear) for choosing INS-1 cells to image (section 5.4) the cells imaged and analysed in this Chapter were most likely to be in the G0+G1 phase of the cell cycle. Therefore, the possibility that the two populations of cells observed when exposed to PA were due to the differential phases of the cell cycle is unlikely. In addition, it should be noted that the heterogeneity observed in the INS-1 cell population is likely to only have been observed due to the purposefully large number of cells mapped. Raman studies prior to the one presented in this thesis, for example conducted by Schie *et al*. (2013) and Stiebing *et al*. (2017) (where changes to lipid content were investigated), and Krafft *et al*. (2006) (where changes to nuclear content were investigated), did not study large number of cells.

Although it can be assumed that the cells imaged, analysed and presented in this Chapter are in the resting phase of the cell cycle, some cells may in fact be pre-apoptotic, and therefore responsible for the two populations of cells observed. Further work to determine more conclusively whether INS-1 cells might be pre-apoptotic would involve staining cells with both PI and Annexin 5, then running the cells through flow cytometry to sort the positively and negatively staining cells. The pre-apoptotic cell population would consist of PI negative cells and Annexin 5 positive cells. These cells, once sorted would be fixed in a falcon tube, then added to a coverslip for mapping, as described in section 5.3.2.

Alternatively, it may be possible to determine whether INS-1 cells were pre-apoptotic by measuring changes in the ratio of peaks specific to DNA nucleotides in Raman spectra by employing multi-variate analysis, as described by Krafft *et al*. (2006). Uni-variate analysis, as presented in this thesis to quantify the percentage of lipid within the cells, may also be employed to measure the area of nuclear material to indicate whether cells were pre-apoptotic. The area of

nuclear material would be compared to the total area of the cell. As a reduction in the size of a cell's nucleus is indicative of pre-apoptosis (Krafft *et al.* 2006), researchers will have to ensure that cells with a reduced area of nuclear material, relative to untreated cells, do not also have a reduced total cell area.

Exposing INS-1 cells to 0.125 mM OA did not change the percentage of lipid with these cells. In addition, the exposure of INS-1 cells to MePA and MeOA did not affect the percentage of intracellular lipid. Interestingly, two populations of cells were observed to OA-exposed cells, similar to the cells exposed to 0.125 mM PA. Since OA alone is not toxic to INS-1 cells, it is therefore unlikely that the two populations of cells observed here came about as a result of some cells overexpressing the Δ-9-desaturase enzyme. In fact, the population of cells consisting of small percentages of lipid after being exposed to OA may be pre-apoptotic.

It has been previously suggested that the exposure of cardiomyocytes, HeLa cells CHO cells and INS-1 cells to OA increases their content within TAG/ LDs (Akoumi *et al.* 2017; Cao *et al.* 2016; Listenberger *et al.* 2003; Plötz *et al.* 2016; Slipchenko *et al.* 2009). It has also been suggested that arachidonic acid, a polyunsaturated FA, becomes incorporated in LDs within neutrophil cells derived from PLB-985 cells (van Manen *et al.* 2005) and THP-1 macrophage cells (Stiebing *et al.* 2014). It could be suggested that the observed accumulation of lipid upon OA exposure could be due to cell-specific mechanisms. However, the results presented in this thesis using INS-1 cells do not support the results presented by Plötz *et al.* (2016) who also studied lipid accumulation in INS-1 cells exposed to OA. By contrast, in the INS-1 cells presented in this Chapter, it was observed that the lipid intensity of cells exposed to OA increased, yet the area of lipid did not change. Based on these observations, it could be suggested that

exogenously supplied OA does not change the content of LDs within INS-1 cells and therefore does not support the literature that suggests that OA induces the formation of LDs. However, whether these differences in LD formation are species-specific is unclear.

Furthermore, Raman results presented in this thesis suggest that PA accumulates within INS-1 cells, an observation which is supported by the observations made by others, whereby deuterated palmitic acid was detected within the LDs of macrophage cells (Stiebing *et al.* 2014; Stiebing *et al.* 2017) and murine fibroblast-like 3T3-L1 cells (Slipchenko *et al.* 2009).

To add an additional layer of complexity, exactly how it can be decided that a supposed cellular increase in LD content is quantified should be, in my view, be debated. For example, is an observed increase in lipid distribution a robust enough metric to study changes in LD formation? Do changes in lipid distribution necessarily have to couple with changes in lipid intensity? And to what extent is a change in lipid composition relevant? For example, could a decrease in lipid distribution and an increase in lipid intensity, as observed when INS-1 cells were exposed to 0.125 mM PA, be positively considered to correspond to an increase in intracellular LD content? Cao *et al* (2016), for example, suggest that when studying lipid accumulation in non-adipocyte cells, researchers should focus their attention to the number of LDs, not the size of LDs. By contrast, could merely a change in lipid composition constitute an increase in LD content? I believe that researchers need to come to a consensus when describing changes in intracellular LD content so as to not misinterpret findings.

Interestingly, two populations of INS-1 cells were also observed when they were exposed to OA in combination with PA. Listenberger *et al.* (2003) suggests that OA is able to protect against PA-induced cytotoxicity by shuttling PA into LDs.

The Raman data presented in this thesis might suggest that the presence of both PA and OA in combination caused a significant decrease in the percentage of lipid within the INS-1 cells, inferring that this decrease might be due to OA shuttling PA into NLDs. However, it must be noted that since PA alone also had this effect on the cells, it cannot be assumed that the decrease seen in combination with OA is due to the presence of OA. Contrary to this, the mechanism of protection may indeed be via the shuttling of PA into LDs, a process which may occur at differential time points and/ or differential FA concentrations to those chosen for this study.

Lastly it should be noted that it is difficult to distinguish between individual LDs within the INS-1 cells. Individual LDs may be present within the cells, however, due to the low resolution of the Raman technique (which is set by the diffraction limit), the LDs cannot be visualised individually.

6.4.1.3 Lipid intensity

The intensity of lipid within each cell was calculated automatically via ImageJ software and given an arbitrary value which was directly proportional to the concentration of intracellular lipid. These values were compared for each FA with which the cells were exposed to.

The intensity of the lipid within cells exposed to PA was significantly higher than the cells exposed to the VC. A decrease in the area of lipid, coupled with an increase in the intensity of this lipid might indicate the accumulation of lipid, be that from endogenous FAs or exogenously supplied FAs, within a smaller area of space.

Fluorescently labelled FAs imaged using confocal microscopy, unlike the use of Raman microspectroscopy, does not permit the evaluation of the concentration of molecules. Researchers have used BODIPY-PA to indicate

where PA might localise within the cell. BODIPY-PA is a molecule whereby PA is conjugated to BODIPY, a small molecule consisting of three ring structures which emits light at a certain wavelength when stimulated. Since this compound only acts as a proxy for visualising where PA localises within the cell, only minute (nM) concentrations are added to cells in combination with unlabelled PA. In addition, low concentrations of BODIPY-PA are employed to minimise any secondary effects from the large BODIPY molecule, such as the rate of uptake or cellular localisation, which this molecule might have on the cell. Since the fluorescence intensity of BODIPY is fixed and cannot be aggregated, changes in the concentration of BODIPY-PA cannot be calculated. Raman maps, however, depict the concentration of molecules of interest by providing a false colour representation of the intensity of the molecule of interest. As presented in this thesis, each pixel within each Raman map is coloured between black and yellow, whereby the brighter the yellow colour, the more molecules of interest there are - this is a measure of the concentration of the molecule of interest. This analysis is possible because labelled compounds are not employed in Raman microspectroscopy. Instead, the concentration of a molecule is calculated based on the vibrations detected and is measured from individual bonds within a molecule of interest - the greater the number of vibrations detected, the more profound the intensity value. Thus, the use of Raman microspectroscopy is possibly of greater benefit than the use of labelled FAs.

The lipid intensity values for cells treated with 0.125 mM OA were significantly higher than those for VC-treated cells. This is an unusual observation because no change was observed in the area of lipid. This would suggest that OA does not affect the distribution of lipid within INS-1 cells. However, the exogenously-supplied OA might be able to partition within LDs, whereby it is not

esterified to glycerol to form TAG, and might account for the observed increase in lipid intensity. Multi-variate analysis is also likely to shed some light as to whether a change in the composition of LDs occurs upon the exposure of INS-1 cells to OA.

An evaluation of the change in concentration of ester bonds, via ImageJ analysis, would further test the hypothesis that OA molecules partition into LDs. This could be determined by quantifying changes in the intensity of pixels at the 1742 cm^{-1} spectral band depicting ester bonds. No change in the intensity of the lipid at this band (versus the VC) might indicate that OA is indeed being partitioned into LDs. Alternatively, pixels in Raman maps corresponding to phosphodiester bonds (-O-P-O- moiety) at 1085 cm^{-1} or 1235 cm^{-1}, as identified by Matthäus et al. (2008), can also be studied and quantified. Since exogenous FAs can be incorporated into phospholipids as well as lipid droplets, it might be of interest to compare the number of pixels which correspond to phosphodiester bonds with those corresponding to CH$_2$ stretch vibrations within the alkyl chains of lipids. If pixels co-localise, it would suggest that the alkyl chain has been both esterified and phosphorylated. This would provide further evidence that the pixels detected in Raman maps correspond to phospholipids in LDS or membranes, and not to free FAs.

A caveat to this, however, would be that this method would not be able to differentiate between endogenous FAs and exogenously supplied FAs. This problem might be solved by employing the use of deuterated FAs, as shown by, van Manen et al. (2005), Majzner et al. (2018), Slipchenko et al. (2009), Stiebing et al. (2014) and Stiebing et al. (2017), to measure the stretch vibration of C-D bonds of FAs. This would further our understanding of the localisation of exogenously supplied FAs. This is because exogenously supplied FAs serve

many intracellular purposes, thus understanding where they localise within cells, either whole or metabolised (broken down or modified), would help elucidate the link between the intracellular localisation of different FAs and the effects which they exert. However, over extended periods of time, such as over 6 hours which is when cells begin to degrade FAs (Dhayal & Morgan, unpublished work), deuterated components of the FAs may become incorporated into other cellular organelles. For example, these components may become incorporated into mitochondria upon their degradation, or may become incorporated into proteins. Thus, the Raman maps generated from and the LDs supposedly visualised may in fact originate from cellular components other than LDs.

Further work might involve the use of deuterated FAs coupled with CARS, similar to the work conducted by Slipchenko *et al.* (2009) and Stiebing *et al.* (2017). A single vibrational frequency would be selected corresponding to C-D bonds and Raman maps generated. This would enable the visualisation of FAs over a period of seconds rather than the minutes it takes to generate a Raman map via the use of spontaneous Raman microspectroscopy, for example. In addition, the CARS maps would be of a higher resolution than the maps generated via spontaneous Raman microspectroscopy. CARS would generate uni-variate analysis, as described previously, and the analysis of these maps could be conducted with the methodology presented in this thesis (see Chapter 5). Unfortunately, CARS cannot generate multi-variate data, however CARS data could be coupled with spontaneous Raman microspectroscopy or hyper-spectral analysis to generate multi-variate data. This would allow for a more detailed analysis of the composition of the intracellular material being analysed. In addition, using CARS, cells can be analysed live, and therefore the methodology employed to do this could be a variation of the methodology presented in this thesis.

Similarly, the use of alkyne FAs, where an alkyne (carbon-carbon triple bond) is present on the terminal carbon atom of the alkyl chain, could also be employed to study the localisation of exogenous FAs, as described by Jamieson *et al.* (2018), and could be compared with their non-alkyne counterparts.

Although the use of non-labelled FAs are biologically and chemically relevant, Raman microspectroscopy cannot, at this point, determine whether a FA present within the cell was one which was there before the exogenous FA was supplied. Similarly, the use of non-labelled FAs cannot determine the localisation of exogenously supplied FAs, especially if the FAs in question are chemically identical. The use of deuterated FAs, versus the use of BODIPY dyes, however, is a technique which I would advocate the use of for furthering our understanding of intracellular lipid disposition. One step further might be to co-localise exogenously supplied FAs (perhaps deuterated) with membranes of intracellular organelles, such as the ER or mitochondria using Raman microspectroscopy. However, careful consideration would need to be taken to ensure the appropriate Raman bands are chosen to be confident that only the components of interest are measured and quantified.

As well as determining the fate of exogenously supplied FAs, it may also be of scientific interest to further investigate how endogenous LDs are synthesised. It has been suggested that LDs are synthesised from the endoplasmic reticulum (Wilfling *et al.* 2014). Although understanding where exogenous FAs are localised is important, as it can aid researchers to better understand dietary requirements to prevent the onset of certain diseases, understanding the mechanism by which endogenous LDs are synthesised would be equally important. This research may lead to the development of medicinal

drugs for people with metabolic conditions to regulate their capacity to produce excessive or faulty LDs.

The intensity of intracellular lipid within cells exposed to both 0.125 mM PA and 0.125 mM OA combined was significantly higher than the lipid within VC-treated cells. This could be because the cells had been exposed to double the quantity of FA compared to just one FA alone. However, it must also be noted that the lipid intensity values of cells exposed to PA and OA alone also increased significantly compared to the VC. Based on this observation, it is not possible to say whether an increase in lipid intensity was a result of OA shuttling PA into LDs, or whether this effect would have been expected regardless of which UFA the cells were exposed to.

The intensity of lipid within cells exposed to 0.125 mM MePA and 0.125 mM MeOA alone was comparable to the lipid of cells exposed to the VC. Since there is no evidence that cells can de-esterify the ester bond between the alkyl chain and the carboxyl oxygen, it must be assumed that this process of de-esterification does not occur. If the cell were able to de-esterify esterified FAs, MePA would cause cell death. However, as shown in figure 3.11, MePA does not cause cell death in INS-1 cells. As there was no change in the total area of the cell, the lipid within the cells and their respective intensity values of cells exposed to MePA and MeOA, it could be suggested that esterified FAs do not affect the disposition of lipid within INS-1 cells. Again, it could be suggested that these FAs do not enter cells. Since non-esterified FAs affect the total area of the cell, the distribution of lipid within cells and their relative intensity values (although differential FAs have differential effects) I find it unusual that the esterified FAs have no effect on the cell whatsoever even though it is known that esterified FAs cannot be metabolised or incorporated into LDs because the carboxyl oxygen is

covalently bound to a methyl group. This is because I would still expect the esterified FAs, if they were capable of entering cells, to alter the total area of the cell or the distribution of endogenous lipid within the cell as a result of the displacement of the aqueous solution of the cytosol due to their physical presence. Since the physical presence of these esterified FAs does not affect the size of the cell or the lipid distribution, I therefore question whether these FAs enter cells. To investigate this further, peak fitting analysis might shed some light as to whether the disposition of LDs changes upon exposure to esterified FAs. Additional work to investigate whether esterified FAs are taken up by cells might involve the direct measurement of esterified FAs into cells. Kuhl & Spector (1970) reported that radiolabelled esterified FAs were taken up by Ehrlich ascites tumour cells (murine tutor cells) and cells of the rat heart, liver and kidney. The use of radiolabelled compounds might therefore clarify whether these FAs do indeed enter INS-1 cells.

In conclusion, the data from the uni-variate analysis suggest that non-esterified FAs at 0.125 mM, at a 24-hour time point, can affect the total area of the cell, lipid distribution and concentration. The data: (a) suggest that PA is shuttled into LDs. This is based on the observation that the lipid area decreases and the intensity of this lipid increases, (b) suggest that OA partitions into lipid structures, however, further analysis is required to substantiate this hypothesis, (c) cannot suggest whether OA is able to shuttle PA into LDs because the changes observed in lipid area and intensity were also observed in cells exposed to PA alone. Therefore, the Raman data presented here do not support the hypothesis that OA protects against PA-induced cytotoxicity by shuttling PA into LDs. The data suggest that the mechanism by which OA protects against PA-induced cytotoxicity occurs via a different mechanism.

Even though the data presented in this Chapter cannot conclusively say whether OA is able to shuttle PA into NLDs, it might be of interest to investigate whether MeOA, in combination with PA, is able to affect lipid distribution and intensity. This is because it has been observed, in figure 3.11, that MeOA is able to protect against PA-induced cytotoxicity, albeit to a lesser extent than OA. If it is discovered that MeOA does not enter cells, it may be that MeOA protects against PA-induced toxicity via an extracellular mechanism.

The data from the uni-variate analysis also suggest that esterified FAs at 0.125 mM, at a 24 hour time point, do not affect the total area of the cell, lipid distribution or concentration. Although no changes in cell size, lipid distribution or lipid intensity were observed with esterified FAs, these data validate the methodology presented in Chapter 5. This is because even though these data cannot elucidate where these FAs localise within the cell and whether they can enter cells, the observation that no cellular lipid changes occur highlights the important structural requirements for the activation of FAs for their incorporation into LDs.

6.4.2 Multi-variate analysis

From the data presented in table 6.1 and from the spectra where the pure FAs were overlaid with the cell spectra, the following observations were made for each FA treatment regarding 'peak fitting' and 'pure FA spectra and cell spectra'. These data allowed for the determination of lipid composition after cells were exposed to differential FAs for 24 hours.

6.4.2.1 Peak fitting

The fold change between the decomposed spectra of cells treated with 0.125 mM PA and the VC ($\sim$ 2880 cm^{-1} peak centre) was 1.04. This is a very small change and suggests that PA was not incorporated into LDs. The fold

change between the decomposed spectra of cells treated with 0.5 mM PA and the VC (~ 2880 cm^{-1} peak centre) was 1.22. This change suggests that PA was incorporated into LDs. These data suggest that more PA was incorporated into LDs when cells were exposed to 0.5 mM PA versus 0.125 mM PA, and that the incorporation of PA into LDs is dose-dependent. This response does not correlate with the observation by Listenberger *et al.* (2013) whereby the researchers found no such effect in CHO cells exposed to 500 and 700 μM PA over a 6-hour time course.

The fold change between the decomposed spectra of cells treated with 0.125 mM OA and the VC (~ 2852 cm^{-1} peak centre) was 1.24. This change suggests that OA was incorporated into LDs.

Regarding the combined treatment of 0.125 mM PA and 0.125 mM OA, the fold change between the decomposed spectra of cells treated with 0.125 mM PA and the VC (~ 2880 cm^{-1} peak centre) was 0.69. This change suggests that PA was not incorporated into LDs and was possibly removed from the LDs. The fold change between the decomposed spectra of cells treated with 0.125 mM OA and the VC (~ 2852 cm^{-1} peak centre) was 2.02. This change suggests that large quantities of OA was incorporated into LDs. The fold changes of PA (0.69) (~ 2880 cm^{-1} peak centre) and OA (2.02) (~ 2852 cm^{-1} peak centre) are strikingly different. This is an interesting observation. These data suggest that less PA is incorporated into LDs, whereas more OA is incorporated into LDs. If this is the case, OA could be facilitating the breakdown of PA. However, why would more OA then be incorporated into LDs? What biological purpose would this serve? Alternatively, it could be suggested that PA is converted into palmitoleate via Δ-9-desaturase enzymes. This could suggest that different populations of cells, as previously discussed, have varying levels of desaturase enzymes. Even more

controversially, it could be suggested that PA shuttles OA into LDs since less PA but more OA was found to be present in the lipid.

The fold change between the decomposed spectra of cells treated with 0.125 mM MePA and the VC (~ 2880 cm^{-1} peak centre) was 1.09. This change suggests that PA was not incorporated into LDs. This would be expected since esterified FAs cannot undergo activation via ACS and thus cannot be chemically, i.e. covalently, incorporated into LDs. These data also suggest that MePA does not partition into LDs.

The fold change between the decomposed spectra of cells treated with 0.125 mM MeOA and the VC (~ 2852 cm^{-1} peak centre) was 1.57. Interestingly, this change suggests that either OA or MeOA was incorporated into LDs. As suggested with the observation made with cells treated with OA alone, it might also be possible for MeOA to partition within lipid structures within LDs.

6.4.2.1.1 Overlay of pure fatty acid spectra and cell spectra

The peak at ~ 2880 cm^{-1} from pure PA was present in the cell spectra of cells treated with 0.125 mM PA. Had this peak not been present, it could have been suggested that PA had been metabolised. However, since the peak is present, it can be suggested that PA is present within the cell, possibly in the form of LDs.

The peak at ~ 2852 cm^{-1} from pure OA was present in the cell spectra of cells treated with 0.125 mM OA. Since this peak was present in the cell spectrum, this suggests that OA was not metabolised.

Regarding the combined treatment of 0.125 mM PA and 0.125 mM OA, the peak at ~ 2880 cm^{-1} from pure PA was present in the cell spectra of cells treated with both PA and OA. Had this peak not been present, it could have been suggested that PA had been metabolised. However, since the peak is present, it

can be suggested that PA is present within the cell, possibly in the form of LDs. The peak at ~ 2852 cm^{-1} from pure OA was present in the cell spectra where the cells were treated with both PA and OA. Since this peak was present in the cell spectrum, this suggests that OA was not metabolised.

The conclusions from the multi-variate analysis suggest that: (1) PA is dose-dependently incorporated into LDs, (2) OA is incorporated into LDs, however, not via chemical incorporation, i.e. not covalently bound to glycerol, but instead might partition into lipid structures, such as LDs, (3) when cells are treated with equimolar concentrations of PA and OA in combination, the presence of PA decreases and the presence of OA increases. This suggests that OA might induce the breakdown of PA, or that OA might induce the conversion of PA into palmitoleate, or that PA might shuttle OA into LDs, and (4) MeOA but not MePA might partition into LDs.

In the study presented in this thesis, the Raman spectra were normalised against the phenylalanine peak, similar to the study conducted by Krafft *et al.* (2006). Further work could involve normalising all the Raman spectra presented in this thesis against a peak other than the phenylalanine peak, and then subsequently reanalysing the data. Slipchenko *et al.* (2009), who studied LD formation in cells *in vitro* and *in vivo*, normalised their spectra against the 1445 cm^{-1} peak in order to better understand the degree of unsaturation of the intracellular LDs. The researchers stated that the peak at 1445 cm^{-1} corresponded to C-H bonds present in SFAs, and therefore all the spectra were normalised against this peak. Had this not been done, the researchers would not have been able to compare the relative changes in the degree of unsaturation of LDs in cells. Similarly, the peak at 1440 cm^{-1} was utilised by Chan *et al.* (2005). In contrast, however, this was not done for the same reason presented by

Slipchenko *et al.* (2009). Chan *et al.* (2005) stated that the peak at 1440 cm^{-1} corresponded to bonds present in proteins. Since the researchers were focused on studying changes in the unsaturation content in LDs, the 1440 cm^{-1} peak corresponding to bonds in proteins, may have obscured any changes in the saturation content of the LDs they were studying. Despite this, the researchers compared the relative ratios of the peaks at 1654 cm^{-1} and 1445 cm^{-1} to determine whether the degree of unsaturation within intracellular LDs had increased.

Lastly, if studies similar to the one presented in this thesis are conducted in the future but with deuterated FAs, careful consideration should be taken when normalising the spectra of intracellular LDs. In the study conducted by Stiebing *et al.* (2017), the researchers normalised the spectra against the peak at 2101 cm^{-1} which corresponds to C-D bonds present within deuterated molecules. This peak was compared with the peak at 2850 cm^{-1} corresponding to C-H bonds present in lipids. This allowed for the determination of the ratio of deuterated and non-deuterated FA content within intracellular LDs. Although normalising Raman spectra does not change the absolute values within the spectra, relative differences in the heights of peaks can occur. Therefore, any conclusions drawn from Raman spectra should be carefully considered.

In conclusion, the research presented in this Chapter show the complexity of the uni- and multi-variate data, the analysis process and the interpretation of the data. The additional questions which arose from this work highlight important steps to be taken to better understand intracellular lipid changes in cells exposed to non-esterified and esterified and FAs in INS-1 cells using Raman microspectroscopy.

Chapter 7

Final discussion

7 Final discussion

The mechanism(s) by which FAs influence cell viability and function have been explored in this thesis and this has been achieved in a number of ways. Initially, well-defined biological and pharmacological methods were employed to study cell viability while, later, the possibility was explored that spontaneous Raman microspectroscopy might shed some light on these processes in novel ways. This Chapter will summarise the findings presented in this thesis, the limitations arising from the techniques used, and it will outline the gaps in the field which have been explored and those that require further work.

7.1 Structural requirements for fatty acid-mediated effects on cell viability

Chapter 3 sought to investigate whether the entry of PA into the mitochondria in INS-1 beta cells and HCMec/D3 microvascular endothelial cells would be responsible for inducing cell death. This was achieved by using several pharmacological approaches including the study of the effects of etomoxir, 2-BrPA and MePA. Etomoxir has a two-fold effect on the cell. It: (1) reduces the cytoplasmic pool of CoA, and (2) inhibits the activity of the enzyme CPT1 in the OMM. Studies employing etomoxir have reported that it can attenuate PA-induced cell death (Chen *et al*. 1994; Diakogiannaki *et al*. 2007) and suggest that PA-induced cell death is caused by the entry of PA into the mitochondria. However, the fact that etomoxir also reduces the pool of CoA available for thioesterification has been overlooked by many researchers. Thus, any cytoprotection observed with etomoxir cannot necessarily be attributed to only one of the effects that it has on the cell. I found that etomoxir, when added in the absence of PA, was unable to induce cell death in either the INS-1 or HCMec/D3

cells. In combination with etomoxir, neither cell type were rescued from PA-induced cell death.

In addition to the use of etomoxir, I employed 2-BrPA to investigate the requirement for PA activation as a mechanism to induce cell death. Interestingly (and unexpectedly), 2-BrPA induced cell death in INS-1 cells but not in HCMec/D3 cells. Even more surprisingly, when INS-1 cells were exposed to both 2-BrPA and PA, in combination, cell death was comparable to the untreated cells. These data suggest that both FAs compete for the cytoplasmic supply of CoA. When HCMec/D3 cells were exposed to both 2-BrPA and PA, in combination, 2-BrPA was able to prevent PA-induced cell death. I hypothesise that the formation of 2-BrPA-CoA might prevent the formation of palmitoyl-carnitine and this, in turn, implies that elevated levels of palmitoyl-carnitine might be one of the toxic metabolites responsible for cell death. Further work could be undertaken to detect levels of intra- and extra-cellular palmitoyl-carnitine using mass spectrometry or with the use of biomarkers to verify this hypothesis, as described by Hulme *et al.* (2017).

MePA was employed to investigate the structural requirements for PA-induced cell death. Since the activation of FAs, with CoA, requires binding to the carboxyl oxygen of the FA, I sought to covalently block this group with a methyl group. The covalent binding of the carboxyl oxygen of the FA would prevent the activation of the FA with CoA. Not only would this prevent PA-CoA from entering the mitochondria, but it would also prevent PA-CoA from mediating other cellular changes. These include: (1) the synthesis of sphingolipids in the rough endoplasmic reticulum, (2) the palmitoylation of proteins in the Golgi apparatus, and (3) the formation of LDs. Thus, any observed cytoprotection from MePA cannot solely be attributed to its inability to enter mitochondria. In both cell types,

MePA was found to be non-toxic, and when combined with PA, it was not cytoprotective. These data suggest that the free carboxyl group of PA is essential for inducing toxicity. The free carboxyl group of PA may be required for binding with CoA, and may cause cytotoxicity if the levels of PA-CoA become elevated such that the cell cannot remove this from the cell. Whether PA-CoA itself is a toxic metabolite or whether this compound facilitates downstream effects on the cell is not clear from the studies presented in this thesis. The use of labelled CoA, by radioactive labelling for example, as described by Kuhl & Spector (1970), might be a possible way to detect the cellular localisation of PA when it binds to CoA. However, due to the size of CoA, it is unlikely that PA-CoA, labelled or unlabelled, would enter the cell.

The structural requirements for OA-induced cytoprotection were investigated using the analogues RA and MeOA. MeOA, like MePA, has a methyl group covalently bound to the carboxyl oxygen, preventing OA from being activated by CoA. In both INS-1 and HCMec/D3 cells, both OA and MeOA were found to protect against PA-induced cell death. MeOA was found to be non-toxic and was also found to protect against PA-induced cell death, albeit to a lesser extent than OA. These data suggest that the activation of OA is not a requirement for inducing cytoprotection. These data also suggest that the mechanisms of OA- and MeOA-induced cytoprotection are differential.

RA, an analogue of OA with a hydroxyl group on the alkyl chain, was found to be more toxic to both INS-1 and HCMec/D3 cells than PA. This response, though unexpected, shows the importance of keeping the alkyl chain of OA free to ensure it does not induce cell death, and so it can also protect against PA-induced cell death.

7.2 Evaluation of the effects of fatty acids on the cell cycle

Chapter 4 sought to determine whether PA-induced toxicity might be a result of PA preventing cells from entering the S and G2+M phases of the cell cycle. The normalised data show that the percentage of cells exposed to PA in the S and G2+M phases of the cell cycle was comparable to untreated cells, suggesting that PA does not inhibit proliferation in either INS-1 or HCMec/D3 cells. I also sought to determine whether OA might induce cytoprotection against PA-induced cell death by eliciting a pro-proliferative response. The data was comparable to the untreated cells, suggesting that OA is not capable of inducing a pro-proliferative response in either INS-1 or HCMec/D3 cells.

Although some studies have shown OA to induce a pro-proliferative (hyperplastic) response in islets, beta cells and smooth muscle cells (Brelje *et al.* 2017; Diakogiannaki *et al.* 2007; Lamers *et al.* 2011), the methodologies are questionable. A critical review of the literature suggests that the use of BrdU, the gold standard of hyperplasia studies, has its limitations, of which the main concern is the temporal effects incurred when BrdU is applied to cells in different stages of cell growth. The method employed in this Chapter separated the percentage of cells into those in the G0+G1, S, G2+M phases as well as the non-viable cell population, an aspect not possible in other assays. Importantly, the cell cycle method presented in this thesis normalised the viable cell population against the non-viable cell population (cells with intact plasma membranes but disrupted DNA).

An alternative to the measurement of hyperplasia was suggested. Cell growth (hypertrophy) might be a more robust endpoint to study as opposed to hyperplasia. Since it has been observed *in vivo* that beta cells only replicate under certain conditions (Bonner-Weir *et al.* 2010; Nir *et al.* 2007; Wang *et al.* 2015b), I

suggest measuring hypertrophy as opposed to hyperplasia as a more robust representation of beta cell health.

7.3 Development of a methodology using Raman microspectroscopy to study intracellular lipid disposition

It has previously been shown that OA, not PA, induces the formation of lipid droplets in H9C2 cardiomyocytes (Akoumi *et al*. 2017), and that OA might be able to mitigate PA-induced cell death by shuttling PA into LDs (Diakogiannaki *et al*. 2007; Listenberger *et al*. 2003). Thus, it was important to expose the INS-1 beta cells to these two FAs alone and in combination and determine whether spontaneous Raman microspectroscopy could elucidate any changes in intracellular lipid disposition (distribution, intensity and composition). The use of labelled FAs is controversial as they do not represent the true chemical composition of biologically available FAs. In addition, they may have the capacity to disrupt normal cellular process, resulting in detrimental secondary effects. Spontaneous Raman microspectroscopy, a label-free technique, was employed to avoid such detrimental cellular effects and to further our understanding of the changes in lipid disposition that occur when cells are exposed to differential FAs. Chapter 5 described the development of a methodology to study the distribution and composition of lipid within INS-1 cells exposed to PA, OA, alone and in combination, and their esterified analogues. After careful optimisation and validation, the chosen Raman band of interest to study lipid disposition was 2845 $\pm$ 10 cm^{-1}, corresponding to the CH$_2$ symmetric stretch vibration, a stretch vibration present within the alkyl chains of FAs.

7.4 Use of Raman microspectroscopy to study the distribution and composition of lipid in beta cells

As presented in Chapter 6, uni-variate analysis of Raman maps (2D maps of cells) involved quantifying the following parameters: (1) the total area of the

cell, (2) the area of lipid within the cell, and (3) the intensity of the lipid (a measure of lipid concentration), using ImageJ software. Multi-variate analysis of the lipid at 2845 ± 10 cm^{-1} involved conducting cluster analysis which was subsequently followed by spectral decomposition of averaged spectra per FA treatment and comparing them to the spectra of untreated cells. The aim of this analysis was to determine the composition of the intracellular lipid, and more specifically, determine whether the lipid consisted of stretch vibrations corresponding to PA or OA.

INS-1 cells were exposed to 0.125 mM PA and 0.125 mM OA alone and in combination, and also their corresponding esterified analogues, for 24 hours. The employment of the corresponding esterified analogues proved important as these FAs are non-metabolisable, and hence should not, in theory, be incorporated into LDs, or any lipid structure for that matter (unless they are able to partition non-covalently within the lipid structure). No change was observed in the distribution of lipid after the INS-1 cells were exposed to esterified FAs, suggesting that these FAs were not chemically incorporated into the lipid structures, and also highlights the importance of having the carboxyl oxygen free for activation with CoA.

Unfortunately, it was not completely clear whether the lipid observed in the Raman maps were from LDs or other cellular components which also consist of FA alkly chains, such as membranes of organelles. One caveat is that the structure of LDs is still contested whereby it is not clear whether they contain a core of TAG and are surrounded by phospholipids or other types of lipids (Ohsaki Suzuki & Fujimoto 2014) and proteins (Ohsaki Suzuki & Fujimoto 2014; Welte 2007; Wilfling et al. 2014). Based on data in the literature, it was assumed that the lipid observed in the Raman maps corresponded to lipid within LDs only.

The combined uni- and multi-variate data suggest that: (1) PA is dose-dependently incorporated into LDs, (2) OA partitions into LDs, i.e. it is not covalently incorporated into LDs, (3) it is unlikely that OA is able to promote the shuttling of PA into LDs as there is only partial evidence (uni-variate data) of this, whereby the area of lipid increases within the cells exposed to both PA and OA. The multi-variate data suggest that the levels of PA decreased and the levels of OA increased within LDs, suggesting that PA might be able to shuttle OA into LDs. Based on these observations, it can be concluded that the Raman data do not support the hypothesis that OA protects against PA-induced cytotoxicity by shuttling PA into LDs, and (4) esterified FAs are not chemically incorporated into lipid droplets, and do not affect lipid distribution. In addition, MeOA, but not MePA, might partition into LDs, a suggestion based on the observation that no change in lipid distribution was observed in cells treated with these FAs, yet elevated levels of OA, but not of PA, were observed from the multi-variate analysis.

Although the uni- and multi-variate data proved complex and time consuming to analyse, it can be concluded that spontaneous Raman microspectroscopy is a useful technique for studying intracellular lipid disposition. The technique is capable of providing data which can be quantified to calculate the area of cells, the percentage of lipid and its concentration, and the composition of the lipid, albeit from 2D maps of the cells. Ideally, 3D maps of cells would be analysed to obtain a better representation of the intracellular distribution of lipid of untreated and treated cells, however, this would add a considerable amount of time to the data-analysis process.

Further work using spontaneous Raman microspectroscopy might seek to examine whether MeOA exerts similar effects on the distribution of PA when combined with OA. This would be of interest as it has been suggested in this

thesis that OA and MeOA might protect against PA-induced toxicity differentially, whereby MeOA might play an extracellular role as its ability to enter cells has been questioned.

As the methodology presented in this thesis to study intracellular lipid disposition can be applied to any other adherent cell type, it would be of interest of investigate the cellular distribution of lipid and its composition within endothelial cells, as these cells are detrimentally affected in people with T2D (Horani & Mooradian 2003; Prasad *et. al.* 2014). The use of a label-free technique would allow researchers to better understand how intracellular lipids are handled in these cells after exposure to exogenously supplied FAs.

The use of deuterated FAs in cellular systems, as described by van Manen *et al.* (2005), Majzner *et al.* (2018), Slipchenko *et al.* (2009), Stiebing *et al.* (2014) and Stiebing *et al.* (2017), or alkyne FAs, as described by Jamieson *et al.* (2018), would aid our understanding regarding the localisation of exogenously supplied FAs within cells. However, I do not believe that Raman technology is currently sufficient to visualise and quantify changes in the chemical composition of endogenous FAs upon exposure to exogenously supplied FAs, despite best-efforts by researchers to differentiate between these FAs, such as Slipchenko *et al.* (2009). In fact, none of the methodologies and technologies that currently exist can answer some pertinent questions that have arisen from the work presented in this thesis. For example, what happens to the chemical composition of endogenous FAs and exogenously supplied FAs within LDs upon exposure to exogenous FAs? Do cells synthesise FAs upon exposure to certain exogenous FAs? And if so, how are the FAs utilised? Are they degraded for the production of energy or are they incorporated into LDs? Where do exogenous FAs localise once they are inside a cell and how are they handled by the cell? Do the FAs

undergo chain elongation/ shortening, chain saturation/ unsaturation, or do they bind to macromolecules such as proteins or sugars? Until precise changes in the chemical composition of both endogenous and exogenous molecules can be detected and quantified, research into the study of cellular LD disposition will move forwards very slowly.

7.5 Final remarks

The research and discussions presented in this thesis aimed to question existing hypotheses and the use of certain experimental techniques in order to progress our understanding of how cells handle FAs *in vitro*. The work undertaken here has, I believe, added sound knowledge to furthering our understanding of beta- and endothelial-cell biology, and has raised many additional questions that require answering.

The pursuit to understand the mechanisms by which certain FAs cause cell death and how others can be cytoprotective has proven to be a difficult one, especially as the field of lipid research has been overlooked for so long. Though more work is required to progress the field, I am proud and humbled to have been able to contribute my time and thinking to this extraordinary scientific journey.

References

Aicart-Ramos, C., Valero, R. & Rodriguez-Crespo, I. *Protein palmitoylation and subcellular trafficking*, Biochimica et Biophysica Acta (BBA) – Biomembranes. Jul 2011; **1808**(12): p. 2981-2994.

Akoumi, A., Haffar, T., Mousterji, M., Kiss, R. & Bousette, N. *Palmitate mediated diacylglycerol accumulation causes endoplasmic reticulum stress, Plin2 degradation, and cell death in H9C2 cardiomyoblasts*, Experimental Cell Research. May 2017; **354**(2): p. 85-94.

Alberts, B., Johnson, A., Lewis, J., Raff, M., Roberts, K. & Walter, P. *Molecular biology of the cell*, Garland Science. Mar 2002; 4th edn, New York.

Artwohl, M., Roden, M., Waldhausl, W., Freudenthaler, A. & Baumgartner-Parzer, S. *Free fatty acids trigger apoptosis and inhibit cell cycle progression in human vascular endothelial cells*, FASEB Journal. Jan 2004; **18**(1): p. 146-148.

Asfari, M., Janjic, D., Meda, P., Li, G., Halban, P. & Wollheim, C. *Establishment of 2-mercaptoethanol-dependent differentiated insulin-secreting cell lines*, Endocrinology. Jan 1992; **130**(1): p. 167-178.

Balaban, S., Lee, L., Schreuder, M. & Hoy, A. *Obesity and cancer progression: is there a role of fatty acid metabolism?*, BioMed Research International. Nov 2015; **2015**: 17 pages.

Bartke, N. & Hannun, Y. *Bioactive sphingolipids: metabolism and function*, Journal of Lipid Research. Nov 2009; **50**: p. 91-96.

Bazylewski, P., Divigalpitiya, R. & Fanchini, G. *In situ Raman spectroscopy distinguishes between reversible and irreversible thiol modifications in l-cysteine*, The Royal Society of Chemistry. Nov 2017; **7**(5): p. 2964-2970.

Ben-Harosh, Y., Anosov, M., Salem, H., Yatchenko, Y. & Birk, R. *Pancreatic stellate cell activation is regulated by fatty acids and ER stress*, Experimental Cell Research. Oct 2017; **359**(1): p. 76-85.

Benninger R. & Hodson D. *New understanding of β-cell heterogeneity and in situ islet function*, Diabetes. Apr 2018; **67**: p. 537-547.

Bonner-Weir, S., Li, W., Ouziel-Yahalom, L., Guo, L., Weir, G. & Sharma, A. *β-cell growth and regeneration: replication is only part of the story*, Diabetes. Oct 2010; **59**(10): p. 2340-2348.

Bradley, J., Pope, I., Masia, F., Sanusi, R., Langbein, W., Swann, K. & Borri, P. *Quantitative imaging of lipids in live mouse oocytes and early embryos using CARS microscopy*, Development. Jun 2016; **143**(12): p. 2238-2247.

Baeten, V., Hourant, P. Morales, M. & Aparicio, R. *Oil and fat classification by FT-Raman spectroscopy,* Journal of Agricultural and Food Chemistry. Jun 1998; **46**(7): p. 2638–2646.

Bailey, G. & Horvat, R. *Raman spectroscopic analysis of the cis/trans composition of edible vegetable oils*, Journal of the American Oil Chemists' Society. Aug 1972; **49**(8): p. 494–498.

Brelje, T., Bhagroo, N., Stout, L. & Sorenson, R. *Prolactin and oleic acid synergistically stimulate β-cell proliferation and growth in rat islets*, Islets. Sept 2017; **9**(4): p 49–62.

Busch, A., Cordery, D., Denyer, G. & Biden, T. *Expression profiling of palmitate- and oleate-regulated genes provides novel insights into the effects of chronic lipid exposure on pancreatic β-Cell function*, Diabetes. Jan 2002; **51**(4): p. 977-987.

Busch, A., Gurisik, E., Cordery, D., Sudlow, M., Denyer, G., Laybutt, D. Hughes & W., Biden, T. *Increased fatty acid desaturation and enhanced expression of stearoyl coenzyme A desaturase protects pancreatic β-cells from lipoapoptosis*, Diabetes. Jun 2005; **54**(10): p. 2917-2924.

Cao, C., Zhou, D., Chen, T., Streets, A. & Huang, Y. *Label-free digital quantification of lipid droplets in single cells by stimulated Raman microscopy on a microfluidic platform*, Analytical Chemistry. May 2016; **88**(9): p. 4931-4939.

Cazanave, S., Elmi, N., Akazawa, Y., Bronk, S., Mott, J. & Gores, G. *CHOP and AP-1 cooperatively mediate PUMA expression during lipoapoptosis*, American Journal of Physiology - Gastrointestinal and Liver Physiology. Apr 2010; **299**(1): p. 236-243.

Cerf, M. *Beta cell dysfunction and insulin resistance*, Frontiers in Endocrinology. Mar 2013; **4**(37): p. 1-12.

Chan, J., Motton, D., Rutledge, J., Keim, N. & Huser, T. *Raman spectroscopic analysis of biochemical changes in individual triglyceride-rich lipoproteins in the pre- and postprandial state*, Analytical Chemistry. Aug 2005; **77**(18): p. 5870-5876.

Chase, J. & Tubbs, P. *Specific inhibition of mitochondrial fatty acid oxidation by 2-bromopalmitate and its coenzyme A and carnitine esters*, Biochemical Journal. Aug 1972; **129**(1): p. 55-65.

Chen, S, Ogawa, A, Ohneda, M, Unger, R, Foster, D. & McGarry, J. *More direct evidence for a malonyl-CoA-carnitine palmitoyltransferase I interaction as a key event in pancreatic beta-cell signalling*, Diabetes. Jul 1994; **43**(7): p. 878–883.

Chen, X., Gasecka, P., Formanek, F., Galey, J., & Rigneault, H. *In vivo single human sweat gland activity monitoring using coherent anti-Stokes Raman scattering and two-photon excited autofluorescence microscopy, British Journal of Dermatology*. Nov 2015; **174**: p. 803-812.

Chien, C., Chen, W., Wu, J. & Chang, T. *Investigation of lipid homeostasis in living Drosophila by coherent anti-Stokes Raman scattering microscopy*, Journal of Biomedical Optics. Dec 2012; **17**(12): p. 126001.

Çimen, I., Kocatürk, B., Koyuncu, S., Tufanlı, Ö., Onat, U., Yıldırım, A., Apaydın, O., Demirsoy, Ş., Aykut, Z., Nguyen, U., Watkins, S., Hotamışlıgil, G. & Erbay, E. *Prevention of atherosclerosis by bioactive palmitoleate through suppression of organelle stress and inflammasome activation*, Science Translational Medicine. Sep 2016; **8**(358): 14 pages.

Cunha, D., Hekerman, P., Ladriere, L., Bazarra-Castro, A., Ortis, F., Wakeham, M., Moore, F., Rasschaert, J., Cardozo, A., Bellomo, E., Overbergh, L., Mathieu, C., Lupi, R., Hai, T., Herchuelz, A., Marchetti, P., Rutter, G., Eizirik, D. & Cnop, M. *Initiation and execution of lipotoxic ER stress in pancreatic beta-cells*, Journal of Cell Science. Jul 2008; **121**(14): p. 2308-2318.

Czamara, K., Majzner, K., Pacia, M., Kochan, K., Kaczor, A. & Baranska, M. *Raman spectroscopy of lipids: a review*, Journal of Raman Spectroscopy. Oct 2014; **46**(1): p. 4-20.

Diabetes UK: facts and figures, 2018, Accessed on 23/09/18, https://www.diabetes.org.uk/professionals/position-statements-reports/statistics

Dhayal, S., Welters, H. & Morgan, N. *Structural requirements for the cytoprotective actions of mono-unsaturated fatty acids in the pancreatic beta-cell line, BRIN-BD11*, British Journal of Pharmacology. Jan 2008; **153**: p. 1718–1727.

Dhayal, S. & Morgan, N. *Structure-activity relationships influencing lipid-induced changes in eIF2alpha phosphorylation and cell viability in BRIN-BD11 cells*, FEBS Letters. Jul 2011; **585**(14): p. 2243-2248.

Diakogiannaki, E., Dhayal, S., Childs, C., Calder, P., Welters, H. & Morgan, N. *Mechanisms involved in the cytotoxic and cytoprotective actions of saturated versus monounsaturated long-chain fatty acids in pancreatic beta-cells*, Journal of Endocrinology. Aug 2007; **194**(2): p. 283-291.

Diakogiannaki, E., Welters, H. & Morgan, N. *Differential regulation of the endoplasmic reticulum stress response in pancreatic beta-cells exposed to long-chain saturated and monounsaturated fatty acids*, Journal of Endocrinology. Mar 2008; **197**(3): p. 553-563.

Draux, F., Jeannesson, P., Beljebbar, A., Tfayli, A., Fourre, N., Manfait, M., Sule-Suso, J. & Sockalingum, G. *Raman spectral imaging of single living cancer cells: a preliminary study*, The Royal Society of Chemistry. Nov 2008; **134**(3): p. 542-548.

Emmelot, P. & van Hoeven, R. *Phospholipid unsaturation and plasma membrane organisation*, Chemistry and Physics of Lipids. Aug 1974; **14**(1975): p. 236-246.

Eynard, A. *Does chronic essential fatty acid deficiency constitute a pro-tumorigenic condition?*, Medical Hypotheses. Apr 1997; **48**(1): p. 55-62.

Featherstone, H. & Whitham, L. *The Cost of Cancer*, 2010, Policy Exchange. Accessed on 21/11/16, http://www.policyexchange.org.uk/images/publications/pdfs/The_cost_of_cancer_FINAL.pdf

Frank, C., Redd, D., Gansler, T. & McCreery, R. *Characterization of human breast biopsy specimens with near-IR Raman spectroscopy*, Analytical Chemistry. Feb 1994; **66**(3): p. 319–326.

Friedrichsen, B., Neubauer, N., Lee, Y., Gram, V., Blume, N., Petersen, J., Nielsen, J. & Møldrup, A. *Stimulation of pancreatic β-cell replication by incretins involves transcriptional induction of cyclin D1 via multiple signalling pathways*, Journal of Endocrinology. Mar 2006; **188**(3): p. 481-492.

Galadari, S., Rahman, A., Pallichankandy, S., Galadari, A. & Thayyullathil, F. *Role of ceramide in diabetes mellitus: evidence and mechanisms*, Lipids in Health and Disease. Jul 2013; **12**(1): p. 98-112.

Gehrmann, W., Würdemann, W., Plötz, T., Jörns, A., Lenzen, S. & Elsner, M. *Antagonism between saturated and unsaturated fatty acids in ROS mediated lipotoxicity in rat insulin-producing cells*, Cellular Physiology and Biochemistry. Apr 2015; **36**: p. 852-865.

Gilbert, S. *A small dose of toxicology: the health effects of common chemicals*, Healthy World Press. Jan 2012; 2nd edn, Seattle, WA.

Gjoni, E., Brioschi, L., Cinque, A., Coant, N., Islam, M., Ng, C., Verderio, C., Magnan, C., Riboni, L., Viani, P., Le Stunff, H. & Giussani, P. *Glucolipotoxicity impairs ceramide flow from the endoplasmic reticulum to the golgi apparatus in INS-1 β-cells*, PLoS ONE. Oct 2014; **9**(10): p. e110875.

Goodman, D. *The interaction of human serum albumin with long-chain fatty acid anions*, Journal of the American Chemical Society. Aug 1958; **80**(15): p. 3892-3898.

Gocze, P. & Freeman, M. *Factors underlying the variability of lipid droplet fluorescence in MA-10 leydig tutor cell*, Cytometry. Apr 1994; **17**(2): p. 151-158.

Greene, J., Newman, J., Williamson, K. & Hammock, B. *Toxicity of epoxy fatty acids and related compounds to cells expressing human soluble epoxide hydrolase*, Chemical Research in Toxicology. Apr 2000, **13**(4): p. 217-226.

Gunaratnam, K., Vidal, C., Boadle, R., Thekkedam, C. & Duque, G. *Mechanisms of palmitate-induced cell death in human osteoblasts*, Biology Open. Oct 2013; **2**(12): p. 1382-1389.

Guo, J., Qian, Y., Xi, X., Hu, X., Zhu, J. & Han, X. *Blockage of ceramide metabolism exacerbates palmitate inhibition of pro-insulin gene expression in pancreatic β-cells*, Molecular and Cellular Biochemistry. Dec 2010; **338**(1): p. 283-290.

Hagve, T. & Christophersen, B. *In vitro effects of α-bromopalmitate on metabolism of essential fatty acids studied in isolated rat hepatocytes: sex differences*, Biochimica et Biophysica Acta (BBA) - Lipids and Lipid Metabolism. Feb 1987, **917**(2): p. 333-336.

Hardy, S., El-Assaad, W., Przybytkowski, E., Joly, E., Prentki, M. & Langelier, Y. *Saturated fatty acid-induced apoptosis in MDA-MB-231 breast cancer cells*, Journal of Biological Chemistry. Jun 2003, **278**(34): p. 31861-31870.

Harvey, K., Walker, C., Pavlina, T., Xu, Z., Zaloga, G. & Siddiqui, R. *Long-chain saturated fatty acids induce pro-inflammatory responses and impact endothelial cell growth*, Clinical Nutrition. Oct 2009, **29**(4): p. 492-500.

Hayes, D., Mannam, V., Ye, R., Zhao, H., Ortega, S. & Montiel, M. *Modification of oligo-ricinoleic acid and its derivatives with 10-undecenoic acid via lipase-catalyzed esterification*, Polymers. Apr 2012, **4**(2): p. 1037-1055.

Henique, C., Mansouri, A., Fumey, G., Lenoir, V., Girard, J., Bouillaud, F., Prip-Buus, C. & Cohen, I. *Increased mitochondrial fatty acid oxidation is sufficient to protect skeletal muscle cells from palmitate-induced apoptosis*, Journal of Biological Chemistry. Nov 2010; **285**(47): p. 36818-36827.

Hex, N., Bartlett, C., Wright, D., Taylor, M. & Varley, D. *Estimating the current and future costs of Type 1 and Type 2 diabetes in the UK, including direct health costs and indirect societal and productivity costs*, Diabetic Medicine. Jul 2012; **29**(7): p. 855-862.

Horani, M. & Mooradian, A. *Effect of diabetes on the blood brain barrier*, Current Pharmaceutical Design. 2003 Apr; **9**(10): p. 833-840.

Hulme, H., Meikle, L., Wessel, H., Strittmatter, N., Swales, J., Thomson, C., Nilsson, A., Nibbs, R., Milling, S., Andren, P., Mackay, C., Dexter, A., Bunch, J., Goodwin, R., Burchmore, R. & Wall, D. *Mass spectrometry imaging identifies palmitoylcarnitine as an immunological mediator during Salmonella Typhimurium infection*, Scientific Reports. Jun 2017; **7**(2786): p. 1-13.

Ibarguren, M., López, D. & Escribá, P. *The effect of natural and synthetic fatty acids on membrane structure, microdomain organization, cellular functions and human health*, Biochimica et Biophysica Acta. Jun 2014; **1838**(6): p. 1518-1528.

Jamieson, L., Greaves, J., McLellan, J., Munro, K., Tomkinson, N., Chamberlain, L., Faulds, K. & Graham, D. *Tracking intracellular uptake and localisation of alkyne tagged fatty acids using Raman spectroscopy*, Spectrochimica Acta Part A: Molecular and Biomolecular Spectroscopy. May 2018; **197**: p. 30–36

Kim, H-S. & Lee, M-K. *β-cell regeneration through the transdifferentiation of pancreatic cells: pancreatic progenitor cells in the pancreas*, Journal of Diabetes Investigation. Mar 2016; **7**(3): p. 286-296.

Kim, K. & Sederstrom, J. *Assaying cell cycle status using flow cytometry*, Current Protocols in Molecular Biology. Jul 2015; **111**: p. 28.6.1-28.6.11.

Klein, K., Gigler, A., Aschenbrenner, T., Monetti, R., Bunk, W., Jamitzky, F., Morfill, G., Stark, R. & Schlegel, J. *Label-free live-cell imaging with confocal Raman microscopy*, Biophysical Journal. Jan 2012; **102**(2): p. 360-368.

Kochan, K., Marzec, K., Chruszcz-Lipska, K., Jasztal, A., Maslak, E., Musiolik, H., Chlopicki, S. & Baranska, M. *Pathological changes in the biochemical profile of the liver in atherosclerosis and diabetes assessed by Raman spectroscopy*, Analyst. Jul 2013a; **138**(14): p. 3885-3890.

Kochan, K., Maslak, E., Kostogrys, R., Chlopicki, S. & Baranska, M. *A comprehensive approach to study liver tissue: spectroscopic imaging and histochemical staining*, Biomedical Spectroscopy and Imaging. Nov 2013b; **2**: p. 331-337.

Kochan, K., Maslak, E., Krafft, C., Kostogrys, R., Chlopicki, S. & Baranska, M. *Raman spectroscopy analysis of lipid droplets content, distribution and saturation level in non-alcoholic fatty liver disease in mice*, Journal of Biophotonics. Jul 2015; **8**(7): p. 597-609.

Krafft, C., Knetschke, T., Funk, R. & Salzer, R. *Studies on stress-induced changes at the subcellular level by Raman microspectroscopic mapping*, Analytical Chemistry. July 2006; **78**(13): p. 4424-4429.

Kuda, O., Brezinova, M., Silhavy, J., Landa, V., Zidek, V., Dodia, C., Kreuchwig, F., Vrbacky, M., Balas, L., Durand, T., Hubner, N., Fisher, A., Kopecky, J. & Pravenec, M. *Nrf2-mediated antioxidant defense and peroxiredoxin 6 are linked to biosynthesis of palmitic acid ester of 9-hydroxystearic acid*, Diabetes. Jun 2018; **67**(6): p. 1190-1199.

Kuhl, W. & Spector, A. *Uptake of long-chain fatty acid methyl esters by mammalian cells*, Journal of Lipid Research. Sep 1970; **11**(5): p. 458-465.

Lamers, D., Schlich, R., Greulich, S., Sasson, S., Sell, H. & Eckel, J. *Oleic acid and adipokines synergize in inducing proliferation and inflammatory signalling in human vascular smooth muscle cells*, Journal of Cellular and Molecular Medicine. May 2011; **15**(5): p. 1177-1188.

Legrand, P. & Rioux, V. *Specific roles of saturated fatty acids: beyond epidemiological data*, European Journal of Lipid Science and Technology. Jun 2015; **117**(10): p. 1489-1499.

Li-Chan, E. *Developments in the detection of adulteration of olive oil*, Trends in Food Science and Technology. Jan 1994; **5**(1): p. 3-11.

Li-Chan, E. *The application of Raman spectroscopy in food science*, Trends in Food Science and Technology. Nov 1996; **7**(11): p. 361-370.

Listenberger, L., Ory, D. & Schaffer, J. *Palmitate-induced apoptosis can occur through a ceramide-independent pathway*, Journal of Biological Chemistry. Feb 2001; **276**(18): p. 14890-14895.

Listenberger, L., Han, X., Lewis, S., Cases, S., Farese, R., Ory, Daniel S. & Schaffer, J. *Triglyceride accumulation protects against fatty acid-induced lipotoxicity*, Proceedings of the National Academy of Sciences. Mar 2003; **100**(6): p. 3077-3082.

Maedler, K., Spinas, G., Dyntar, D., Moritz, W., Kaiser, N. & Donath, M. *Distinct effects of saturated and monounsaturated fatty acids on beta-cell turnover and function*, Diabetes. Jan 2001; **50**(1): p. 69-76.

Majzner, K., Kochan, K., Kachamakova-Trojanowska, N., Maslak, E., Chlopicki, S. & Baranska, M. *Raman imaging providing insights into chemical composition of lipid droplets of different size and origin: in hepatocytes and endothelium*, Analytical Chemistry. Jul 2014; **86**(13): p. 6666-6674.

Majzner, K., Chlopicki, S. & Baranska, M. *Lipid droplets formation in human endothelial cells in response to polyunsaturated fatty acids and 1-methyl-nicotinamide (MNA); confocal Raman imaging and fluorescence microscopy studies*, Journal of Biophotonics. Apr 2016; **9**(4): p. 396-405.

Majzner, K., Tott, S., Roussille, L., Deckert, V., Chlopickiae, S. & Baranska, M. *Uptake of fatty acids by a single endothelial cell investigated by Raman spectroscopy supported by AFM*, Analyst. Jan 2018; **143**: p. 970-980.

Mansfield, J. & Winlove, C. *Lipid distribution, composition and uptake in bovine articular cartilage studied using Raman micro-spectrometry and confocal microscopy*, Journal of Anatomy. Jul 2017; **231**(1): p. 156-166.

Martin, S., Reutelingsperger, C., McGahon, A., Rader, J., van Schie, R., LaFace, D. & Green, D. *Early redistribution of plasma membrane phosphatidylserine is a general feature of apoptosis regardless of the initiating stimulus: inhibition by*

overexpression of Bcl-2 and Abl, Journal of Experimental Medicine. Nov 1995; **182**(5): p. 1545-1556.

Matthäus, C., Bird, B., Miliković, M., Chernenko, T. & Romeo, M. *Infrared and Raman microscopy in cell biology*, Methods in Cell Biology. Mar 2008; **89**: p. 275-308.

McMahon, H. & Boucrot, E. *Membrane curvature at a glance*, Journal of Cell Science. Mar 2015; **128**(6): p. 1065-1070.

Mead, T. & Lefebvre, V. *Proliferation assays (BrdU and EdU) on skeletal tissue sections*, Methods in Molecular Biology. Jun 2014; **1130**: p. 233-243.

Mishra, R. & Simonson, M. *Saturated free fatty acids and apoptosis in microvascular mesangial cells: palmitate activates pro-apoptotic signaling involving caspase 9 and mitochondrial release of endonuclease G*, Cardiovascular Diabetology. Jan 2005; **4**(2): 12 pages.

Morgan, N. *Fatty acids and beta-cell toxicity*, Current Opinion in Clinical Nutrition and Metabolic Care. Mar 2009; **12**(2): p.117-122.

Morgan, N., Dhayal, S., Diakogiannaki, E. & Welters, H. *The cytoprotective actions of long-chain mono-unsaturated fatty acids in pancreatic β-cells*, Biochemical Society Transactions. Apr 2008, **36**(5): p. 905-908.

Newsholme, P., Haber, E., Hirabara, S., Rebelato, E., Procopio, J. & Morgan, D. *Diabetes associated cell stress and dysfunction: role of mitochondrial and non-mitochondrial ROS production and activity*, Journal of Physiology. 2007; **583**(1): p. 9-24.

Nikolova N. & Jaworska J. *Approaches to measure chemical similarity – a review*, QSAR & Combinatorial Science. Jul 2003; **22**(9-10): p. 1006-1026.

Nir, T., Melton, D. & Dor, Y. *Recovery from diabetes in mice by beta cell regeneration*, Journal of Clinical Investigation. Sept 2007; **117**(9): p 2553-2561.

Nolan, C., Madiraju, M., Delghingaro-Augusto, V., Peyot M. & Prentki, M. *Fatty acid signaling in the beta-cell and insulin secretion*, Diabetes. Dec 2006; **55**(Suppl 2): S16-23.

Ohanian, J. & Ohanian, V. *Sphingolipids in mammalian cell signalling*, Cellular and Molecular Life Sciences. Dec 2001; **58**(14): p. 2053-2068.

Ohsaki, Y., Suzuki, M. & Fujimoto, T. *Open questions in lipid droplet biology*, Chemistry & Biology. Jan 2014; **21**(1): p. 86-96.

Oliveira, A., Cunha, D., Ladriere, L., Igoillo-Esteve, M., Bugliani, M., Marchetti, P. & Cnop, M. *In vitro use of free fatty acids bound to albumin: A comparison of protocols*, Biotechniques. May 2015; **58**(5): p. 228-233.

Paradies, G., Paradies, V., De Benedictis, V., Ruggiero, F. & Petrosillo, G. *Functional role of cardiolipin in mitochondrial bioenergetics*, Biochimica et Biophysica Acta (BBA) – Bioenergetics. Oct 2014; **1837**(4):p. 408-417.

Paris, S., Samuel, D., Jacques, Y., Gache, C., Franchi, A. & Ailhaud, G. *The role of serum albumin in the uptake of fatty acids by cultured cardiac cells from chick embryo*, European Journal of Biochemistry. Feb 1978; **83**(1): p. 235-243.

Pascoe, J., Hollern, D., Stamateris, R., Abbasi, M., Romano, L., Zou, B., O'Donnell, C., Garcia-Ocana, A. & Alonso, L. *Free fatty acids block glucose-induced β-cell proliferation in mice by inducing cell cycle inhibitors p16 and p18*, Diabetes. Oct 2012; **61**(3): p 632-641.

Patella, F., Schug, Z., Persi, E., Neilson, L., Erami, Z., Avanzato, D., Maione, F., Hernandez-Fernaud, J., Mackay, G., Zheng, L., Reid, S., Frezza, C., Giraudo, E., Fiorio Pla, A., Anderson, K., Ruppin, E., Gottlieb, E., Zanivan, S. *Proteomics-based metabolic modeling reveals that fatty acid oxidation (FAO) controls endothelial cell (EC) permeability*, Molecular and Cellular Proteomics. Mar 2015; **14**(3): p. 621–634.

Patková, J., Anděl, M. & Trnka, J. *Palmitate-induced cell death and mitochondrial respiratory dysfunction in myoblasts are not prevented by mitochondria-targeted antioxidants*, Cellular Physiology and Biochemstry. Nov 2014; **33**(5): p. 1439-1451.

Pilon, M. *Revisiting the membrane-centric view of diabetes*, Lipids in Health and Disease. Sep 2016; **15**(1): 6 pages.

Pipeleers D., Mesaeker I., Robert T. & Hulle F. *Heterogeneity in the beta-cell population: a guided search into its significance in pancreas and in implants*, Current Diabetes Report. Aug 2017; **17**(10): p. 86.

Plötz, T., Hartmann, M., Lenzen, S. & Elsner, M. *The role of lipid droplet formation in the protection of unsaturated fatty acids against palmitic acid induced lipotoxicity to rat insulin-producing cells*, Nutrition & Metabolism. Feb 2016; **13**: 16.

Prasad, S., Sajja R., Naik P. & Cucullo, L. *Diabetes mellitus and blood-brain barrier dysfunction: an overview*, Journal of Pharmacovigilance. Jun 2014; **2**(2): 25 pages.

Rawicz, W., Olbrich, K., McIntosh, T., Needham, D. & Evans, E. *Effect of chain length and unsaturation on elasticity of lipid bilayers*, Biophysical Journal. Jul 2000; **79**(1): p. 328-339.

Reaven, G. *Role of insulin resistance in human disease*, Diabetes. Dec 1988; **37**(12): p. 1595-1607.

Rho, M., Ah, L., Mi, K., Sik, L., Jeong, J. & Kook, K. *Sensitization of vascular smooth muscle cell to TNF-alpha-mediated death in the presence of palmitate*, Toxicology and Applied Pharmacology. May 2007; **220**(3): p. 311-319.

Robblee, M, Kim, C, Abate, J., Valdearcos, M., Sandlund, K., Shenoy, M., Volmer, R., Iwawaki, T. & Koliwad, S. *Saturated fatty acids engage an IRE1alpha;-dependent pathway to activate the NLRP3 inflammasome in myeloid cells*, Cell Reports. Mar 2016; **14**(11): p. 2611-2623.

Russell, M. *Characterisation of FTO and cGMP signalling in clonal pancreatic β-cells*, 2010; PhD thesis, Peninsula College of Medicine & Dentistry.

Rygula A., Majzner K., Marzec K., Kaczor A., Pilarczyk M. & Baranska M. *Raman spectroscopy of proteins: a review*, Journal of Raman Spectroscopy. May 2013; **44**(8): p. 1061-1076.

Sadeghi-Jorabchi, H., Hendra, P., Wilson, R. & Belton, P. *Determination of the total unsaturation in oils and margarines by fourier transform Raman spectroscopy*, Journal of the American Oil Chemists' Society. Aug 1990; **67**(8): p. 483–486.

Sargsyan, E., Artemenko, K., Manukyan, L., Bergquist, J. & Bergsten, P. *Oleate protects beta-cells from the toxic effect of palmitate by activating pro-survival pathways of the ER stress response*, Biochimica et Biophysica Acta. Sep 2016; **9**(1861): p. 1151-1160.

Sassa, T. & Kihara, A. *Metabolism of very long-chain fatty acids: genes and pathophysiology*, Biomol Ther. Mar 2014; **22**(2): p. 83-92.

Schie, I., Nolte, L., Pedersen, T., Smith, Z., Wu, J., Yahiatene, I., Newman, J. & Huser, T. *Direct comparison of fatty acid ratios in single cellular lipid droplets as determined by comparative Raman spectroscopy and gas chromatography*, Analyst. Nov 2013; **138**(21): p. 6662-6670.

Schönfeld, P. & Wojtczak, L. *Short- and medium-chain fatty acids in the energy metabolism - the cellular perspective*, Journal of Lipid Research. Jun 2016; **57**(6): p. 943-954.

Schoors, S., Bruning, U., Missiaen, R., Queiroz, K., Borgers, G., Elia, I., Zecchin, A., Cantelmo, A., Christen, S., Goveia, J., Heggermont, W., Godde, L., Vinckier, S., Van Veldhoven, P., Eelen, G., Schoonjans, L., Gerhardt, H., Dewerchin, M., Baes, M., De Bock, K., Ghesquiere, B., Lunt, S., Fendt, S. & Carmeliet, P. *Fatty acid carbon is essential for dNTP synthesis in endothelial cells*, Nature. Apr 2015; **520**(7546): p. 192-197.

Shimabukuro, M., Higa, M., Zhou, Y., Wang, M., Newgard, C. & Unger, R. *Lipoapoptosis in beta-cells of obese prediabetic fa/fa rats. Role of serine palmitoyltransferase overexpression*, Journal of Biological Chemistry. Dec 1998; **273**(49): p. 32487-32490.

Slipchenko, M., Le, T., Chen, H. & Cheng, J. *High-speed vibrational imaging and spectral analysis of lipid bodies by compound Raman microscopy*, Journal of Physical Chemistry B. May 2009; **113**(21): p. 7681-7686.

Slivniak, R. & Domb, A. *Macrolactones and polyesters from ricinoleic acid,* Biomacromolecules. Mar 2005; **6**(3): p. 1679-1688.

Smith, R., Wright, K. & Ashton, L. *Raman spectroscopy: an evolving technique for live cell studies*, The Royal Society of Chemistry. Mar 2016; **141**(12): p. 3590-3600.

Staiger, K., Staiger, H., Weigert, C., Haas, C., Häring, H. & Kellerer, M. *Saturated, but not unsaturated, fatty acids induce apoptosis of human coronary artery endothelial cells via nuclear factor-κB activation*, Diabetes. Nov 2006; **55**(11): p. 3121-3126.

Stiebing, C., Matthäus, C., Krafft, C., Keller, A., Weber, K., Lorkowski, S. & Popp, J. *Complexity of fatty acid distribution inside human macrophages on single cell level using Raman micro-spectroscopy*, Analytical and Bioanalytical Chemistry. Nov 2014; **406**(27): p. 7037-7046.

Stiebing, C., Matthäus, C., Krafft, C., Keller, A., Weber, K., Lorkowski, S. & Popp, J. *Real-time Raman and SRS imaging of living human macrophages reveals cell-to-cell heterogeneity and dynamics of lipid uptake*, Journal of Biophotonics. Sept 2017; **10**(9): p. 1217-1226.

Su, T. & O'Farrell, P. *Size control: cell proliferation does not equal growth*, Current Biology. Sept 1998; **8**(19): p. 687-689.

Sun, Q. *The Raman OH stretching bands of liquid water*, Vibrational Spectroscopy. Nov 2009; **51**(2): p. 213-217.

Tannock, I. & Hayashi, S. *The proliferation of capillary endothelial cells*, Cancer Research. Jan 1972; **33**: p. 77-82.

Tipping, W., Lee, M., Serrels, A., Brunton, V. & Hulme, A. *Stimulated Raman scattering microscopy: an emerging tool for drug discovery*, Chemical Society Reviews. Apr 2016; **45**(8): p. 2075-2089.

Toporski, J., Dieing, T. & Hollricher, O. *Confocal Raman Microscopy*, Springer International Publishing AG. Jan 2018; 2nd edn, Switzerland.

Tschen, S., Dhawan, S., Gurlo, T. & Bhushan, A. *Age-dependent decline in beta-cell proliferation restricts the capacity of beta-cell regeneration in mice*, Diabetes. Jun 2009; **58**(6): p. 1312-1320.

Ubhayasekera, S., Staaf, J., Forslund, A., Bergsten, P. & Bergquist, J. *Free fatty acid determination in plasma by GC-MS after conversion to weinreb amides*, Analytical and Bioanalytical Chemistry. Feb 2013; **405**(6): p. 1929-1935.

Ulloth, J., Casiano, C. & De Leon, M. *Palmitic and stearic fatty acids induce caspase-dependent and -independent cell death in nerve growth factor differentiated PC12 cells*, Journal of Neurochemistry. Feb 2003; **84**(4): p. 655-668.

van der Vusse, G. *Albumin as fatty acid transporter*, Drug Metabolism and Pharmacokinetics. Sep 2009; **24**(4): p. 300-307.

van Manen, H-J., Kraan, y.,Roos, D & Otto, C. *Single-cell Raman and fluorescence microscopy reveal the association of lipid bodies with phagosomes in leukocytes*, Proceedings of the National Academy of Sciences of the United States of America. Jul 2005; **102**(29): p. 10159-10164.

Voet, D., Voet, J. & Pratt, C. *Fundamentals of biochemistry*, John Wiley & Sons. 2000; 4th edn, Hoboken, NJ.

Wakil, S. & Abu-Elheiga, L. Fatty acid metabolism: target for metabolic syndrome, Journal of Lipid Research. Apr 2009; **50**(Suppl): S138-143.

Wang, T., Liu, M., Portincasa, P. & Wang, D. *New insights into the molecular mechanism of intestinal fatty acid absorption*, European Journal of Clinical Investigation. Nov 2013; **43**(11): p. 1203-1223.

Wang, P., Alvarez-Perez, J., Felsenfeld, D., Liu, H., Sivendran, S., Bender, A., Kumar, A., Sanchez, R., Scott, D., Garcia-Ocana, A. & Stewart, A. *A high-throughput chemical screen reveals that harmine-mediated inhibition of DYRK1A increases human pancreatic beta cell replication*, Nature Medicine. Apr 2015a; **21**(4): p. 383-388.

Wang, P., Fiaschi-Taesch, N., Vasavada, R., Scott, D., Garcia-Ocana, A. & Stewart, A. *Diabetes mellitus--advances and challenges in human beta-cell proliferation*, Nature Reviews Endocrinology. Apr 2015b; **11**(4): p. 201-212.

Waterham, H., Ferdinandusse, S. & Wanders, R. *Human disorders of peroxisome metabolism and biogenesis*, Biochimica et Biophysica Acta (BBA) - Molecular Cell Research. Nov 2015; **1863**(5): p. 922-933.

Webb, Y., Hermida-Matsumoto, L. & Resh, M. *Inhibition of protein palmitoylation, raft localization, and T cell signaling by 2-bromopalmitate and polyunsaturated fatty acids*, Journal of Biological Chemistry. Jan 2000; **275**(1): p. 261-270.

Weksler, B., Subileau, E., Perriere, N., Charneau, P., Holloway, K., Leveque, M., Tricoire-Leignel, H., Nicotra, A., Bourdoulous, S., Turowski, P., Male, D., Roux, F., Greenwood, J., Romero, I. & Couraud, P. *Blood-brain barrier-specific properties of a human adult brain endothelial cell line*, The FASEB Journal. Nov 2005; **19**(13): p. 1872-1874.

Welte, M. *Proteins under new management: lipid droplets deliver*, Trends in Cell Biology. Aug 2007; **17**(8): p. 363-369.

Welters, H., Tadayyon, M., Scarpello, J., Smith, S. & Morgan, N. *Mono-unsaturated fatty acids protect against beta-cell apoptosis induced by saturated fatty acids, serum withdrawal or cytokine exposure*, FEBS Letters. Feb 2004; **560**(1-3): p. 103-108.

Weng, Y-M., Weng, R-H., Tzeng, C-Y. & Chen, W. *Structural analysis of triacylglycerols and edible oils by near-infrared fourier transform Raman spectroscopy*, Applied Spectroscopy. Apr 2003; **57**(4): p. 413-418.

Wilfling, F., Haas, J., Walther, T. & Farese R. Lipid droplet biogenesis, Current Opinion in Cell Biology. Aug 2014; **29**: p. 39-45.

Yli-Jama, P., Meyer, H., Ringstad, J. & Pedersen, J. *Serum free fatty acid pattern and risk of myocardial infarction: a case-control study*, Journal of Internal Medicine. Jan 2002; **251**(1): p. 19-28.

Yue, S., Cardenas-Mora, J., Chaboub, L., Lelievre, S. & Cheng, J. *Label-free analysis of breast tissue polarity by Raman imaging of lipid phase*, Biophysical Journal. Mar 2012; **102**(5): p. 1215-1223.

Yousef, E., Furrer, D., Laperriere, D., Tahir, M., Mader, S., Diorio, C. & Gaboury, L. *MCM2: an alternative to Ki-67 for measuring breast cancer cell proliferation*, Modern Pathology. May 2017; **30**(5): p. 682-697.